Aspects of the Electroweak Phase Transition and Baryogenesis

Kevin E.C. Benson
Wadham College

Department of Physics · Theoretical Physics
University of Oxford

A thesis submitted for the degree of
Doctor of Philosophy at the University of Oxford

Trinity 1993

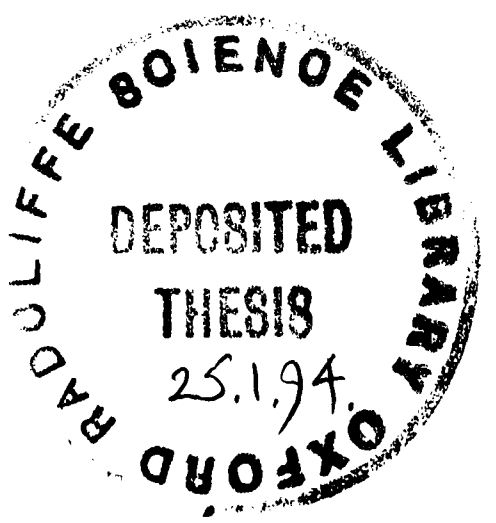

Aspects of the Electroweak Phase Transition and Baryogenesis

Kevin E.C. Benson
Wadham College

Department of Physics · Theoretical Physics
University of Oxford

Abstract

In this thesis we study aspects of the cosmological electroweak phase transition which are relevant to the possibility of baryogenesis at this epoch. We focus on two issues: first, requiring that the observed baryon number be of electroweak origin places strong constraints on electroweak physics, and second, baryogenesis at the electroweak scale may be driven by an asymmetry generated at the GUT scale.

We use the effective potential at finite temperature as a means of analyzing phase transitions associated with spontaneous symmetry breaking. We develop the theory with two basic examples: the scalar and Abelian Higgs models. Infrared divergences near the phase transition make the one-loop description unreliable, and indeed invalidate conventional perturbation theory. Borrowing a method from studies of QCD at high temperatures, we demonstrate that the summation of ring diagrams cures the leading infrared divergences and achieves a more reliable perturbative expansion.

We then apply this formalism to the minimal Standard Model, following previous work, and confirm weak first-order behavior at the phase transition. We show that requiring the baryon number not be erased by sphaleron processes after the phase transition places a stringent bound on the Higgs mass, which is incompatible with experiment. This cosmological bound, however, may be relaxed by extending the scalar sector of the Standard Model. We consider the two simplest such extensions, the addition of a gauge singlet and of a second doublet. We demonstrate that ring-improvement in the singlet extension alters previous arguments at the one-loop level and yields a more restrictive bound on the Higgs mass. While ring-improvement in the two-doublet model, in principle, also reduces the Higgs mass bound found earlier at one loop, the multitude of new couplings in this model does not permit a definitive statement.

We then investigate a mechanism for generating the observed baryon asymmetry ($n_B/s \sim 10^{-10}$) at the electroweak phase transition from a pre-existing leptonic asymmetry ($L_\tau/s \sim 10^{-5}$) produced at the GUT scale. This mechanism works by charge transport in a strongly first-order phase transition and avoids the need for large CP-violation at the electroweak scale.

A thesis submitted for the degree of
Doctor of Philosophy at the University of Oxford

Trinity 1993

For my mother and in memory of my father

Acknowledgements

It is a pleasure to thank my supervisor Subir Sarkar for guidance and encouragement during my time as a research student. I am very grateful to him for stimulating my interest in cosmology and for many enlightening discussions.

I would like to thank Steve Abel for proposing the work of Chapter 8 and for fruitful discussions and criticism thoughout its completion. Also I would like to thank Mike Teper for supervision during my first year of studies.

I acknowledge the financial support of the Marshall Aid Commemoration Commission and appreciate funds made available for travel and conferences. I am also grateful to Wadham College for the award of a Senior Scholarship and for travel grants from the Pollard Fund.

Special thanks go to Frank Hoogeveen and Hunter Monroe for proofreading, to Boom Kanjanarat for emergency assistance, and to friends who made the department a wonderful place to work: I. Adjali, F. Anton, L. da Mota, A. de la Macorra, M. Klein, S. Lola, T. Moretto, L. O'Donnell, D. Philippides, A. Rau, G. Tabor, R. Thorne, K. Wanelik, and J. Watson.

Finally I would like to thank Kirsti-Pirsti Viking Queen for keeping me human during a rather inhumane time, and for being such a good friend.

Contents

List of Figures

List of Tables

Chapter 1

Introduction

Particle cosmology describes physical phenomena in the early universe. It links physics on the smallest and largest scales, by revealing the intrinsic relationship manifest at high energy between particle physics and cosmology — the fundamental constituents of matter and their interactions determine both the contents of the early universe and the dynamics of its evolution.

The standard cosmology, or Hot Big Bang Model, integrates the Standard Model of particle physics with the Friedmann-Robertson-Walker cosmology. It is the first and indeed simplest theory that successfully describes the salient features of our universe: the Hubble expansion, the cosmic microwave background at 2.73 K, and the abundances of the primordially synthesized light elements. In addition it provides the framework for a meaningful exchange between particle physics and cosmology, with the power to probe unknown sectors in both fields. For instance, calculations of primordial nucleosynthesis compared with observation first indicated that the number of neutrino flavors is limited to four or less, long before accelerator experiments gave any direct evidence. Also, new stable particles which are contained in extensions of physics beyond the Standard Model may constitute the cosmological dark matter. Paradoxically, it is much harder to understand the cosmological origin of ordinary (baryonic) matter, specifically, the observed excess of matter over antimatter in the universe.

1.1 The Baryon Asymmetry Problem

The matter content in the observable universe has two striking features. The first is the scarcity of matter relative to radiation; observationally, the ratio of number densities is only $\eta = n_b/n_\gamma \sim 10^{-10}$, i.e., there are about ten billion photons for every baryon. The second is the predominance of matter over antimatter. We have direct evidence from planetary probes that our solar system is composed primarily of matter, and from cosmic rays, that our galaxy is as well. On larger scales, such as clusters of galaxies, we have indirect evidence from the absence of γ-ray emission characteristic of baryon-antibaryon annihilations from the intracluster gas. The recent observation by

COBE that the spectrum of the relic radiation is Planckian to an accuracy of $\sim 0.03\%$ also demonstrates that there could not have been any significant matter-antimatter annihilation in the early universe below a temperature of $\mathcal{O}(1\ \mathrm{keV})$ [1]. All the evidence suggests that our observed universe is made of matter, and that antimatter is very rare [2]. This observation alone is the most visible manifestation of baryon and CP violation, reflecting such violation either in the dynamics of the universe's evolution or in its initial conditions.

The baryon asymmetry is quantified by the baryon-to-entropy ratio

$$B \equiv \frac{n_b - n_{\bar{b}}}{s} \approx \frac{n_b - n_{\bar{b}}}{g_* n_\gamma} \sim 10^{-10} ,$$

where n_b ($n_{\bar{b}}$, n_γ) is the density of baryons (antibaryons, photons), $s \approx 1.80 g_* n_\gamma$ is the entropy density, [1] and g_* counts the number of effective relativistic degrees of freedom in equilibrium. B gives the scaled number of baryons per comoving volume, and remains constant as long as entropy and baryon number are conserved [2] — that is, most of cosmic evolution. Today the asymmetry is maximal, $B \approx n_b/s \sim 10^{-10}$, i.e., there is essentially no antimatter. The baryon density is determined by direct astrophysical measurements of the amount of luminous (nucleonic) matter in the universe, while the entropy density includes contributions both from the cosmic background of 2.73 K microwave photons and from the neutrino species ν_e, ν_μ, ν_τ.

Instead of assuming that the presently observed B is simply an initial condition for baryon-conserving cosmic evolution, models of baryogenesis attempt to provide a dynamical means for generating the excess of matter over antimatter. The question of the origin of B and its evolution form the Baryon Asymmetry Problem. Two aspects of the problem are the sign and magnitude of B. In other words, *Why is the B-asymmetry maximal? (Why is there so much more matter than antimatter?)* and *Why is B so small? (Why is there so little matter compared with photons?).* Baryogenesis provides the framework for understanding and investigating the B-asymmetry, and it highlights the crucial role of microphysics (e.g., B and CP violation) in explaining cosmological phenomena. By requiring that the observed B be of some particular origin, it may also be used to constrain particle theories.

Why not consider a universe that is baryon symmetric on scales larger than our observable universe? If the universe at some early point were locally baryon symmetric, baryons and antibaryons would remain in equilibrium annihilating each other as the universe cools, until the annihilation interactions freeze out at a temperature of ~ 20 MeV, leaving residual baryon and antibaryon numbers of $n_b/s = n_{\bar{b}}/s \sim 10^{-19}$. This is nine orders of magnitude too small, even if some mechanism could then separate matter from antimatter. To avoid this "annihilation catastrophe" of the baryon symmetric universe, some mechanism would have to segregate matter and antimatter

[1] See Appendix A for a review of thermodynamics in the standard cosmology.

[2] Unlike B, the baryon-to-photon number η decreases whenever a particle species (most recently, the electron) falls out of equilibrium and annihilates to produce photons.

on large scales, at a temperature greater than 40 MeV, when $n_b/s = n_{\bar{b}}/s \sim 10^{-10}$. At such an early time, however, the horizon only contained $\sim 10^{-7}$ solar masses. This invalidates causal processes of the standard cosmology as a means of large-scale segregation of matter and antimatter, and thus eliminates the possibility of any reasonable baryon-symmetric cosmology. It appears most natural to assume the symmetric initial condition of $B_{\rm initial} = 0$ and to attempt to develop a *dynamical* mechanism for generating the value of B observed today.

1.2 The Conditions for Baryogenesis

In 1967 Sakharov [3] identified the three prerequisites for dynamically generating the observed baryon number:

- **Baryon violation:** Without it, the present baryon asymmetry would only reflect asymmetric initial conditions. This implies the existence of an interaction $X \to Y$ in which the baryon number of X does not equal that of Y.

- **C and CP violation:** Since B is odd under C and CP transformations, their invariance would require that $B = 0$. Their violation allows a distinction between baryons and anti-baryons in C- and CP-conjugate reactions. Hence the reaction rate of $X \to Y$ may differ from the rates of $\bar{X} \to \bar{Y}$ and $\bar{X}$(helicity flip) $\to$ $\bar{Y}$(helicity flip). Note that CP violation (which implies T violation by CPT invariance) guarantees a different rate for the reverse reaction of opposite net B, $Y \to X$. [3]

- **Departure from equilibrium:** In equilibrium, the B-violating interactions ensure that the baryon chemical potentials vanish, $\mu_b = -\mu_{\bar{b}} = 0$; and by CPT invariance, $m_b = m_{\bar{b}}$. Hence in equilibrium, baryons and antibaryons have identical distribution functions, $f_b(\vec{p}) = f_{\bar{b}}(\vec{p}) = [\exp(\sqrt{\vec{p}^2 + m_b^2}/T) + 1]^{-1}$, and consequently, equal number densities.

Although a plausible scheme of baryogenesis was nonexistent at the time these criteria were proposed, they served a useful purpose in providing constraints on physics at the primordial epoch: processes must occur which violate B, C, and CP, and which eventually cease to be in equilibrium. A variety of theoretical models have emerged since then that naturally fulfill these requirements. Baryon number, though perturbatively conserved in the Standard Model, is not protected by any gauge symmetry (in the manner that $U(1)_{\rm EM}$ guarantees charge conservation), and Grand Unified Theories predict its violation. C transformation is not a symmetry of the fermion representation in the Standard Model and is violated in the weak interactions; and CP violation has

[3] This example is misleading in its suggestion that B, C, and CP violation should all occur in the same process; as we demonstrate in Chapter 8, separation of these processes may yield efficient schemes of baryogenesis.

been experimentally observed in the neutral kaon system. Moreover the degree of CP violation can be enhanced in theoretically favored, modest extensions of the Standard Model. Finally, the universe may have undergone several departures from equilibrium during its evolution, particularly during phase transitions associated with spontaneous symmetry breaking in gauge theories. Such a departure is determined by comparing the reaction rate Γ of the interactions maintaining equilibrium with the Hubble expansion rate of the universe, $H = \dot{R}/R = -\dot{T}/T$.

1.3 Baryogenesis in Grand Unified Theories

The first scenario for baryogenesis emerged in the context of Grand Unified Theories. GUTs attempt to unify the non-gravitational forces of nature — the strong and weak nuclear forces and electromagnetism — by embedding the $SU(3)_C \otimes SU(2)_L \otimes U(1)_Y$ symmetry of the Standard Model into a larger simple symmetry group with a single coupling. The matter fields are arranged into irreducible fermion representations that include both leptons and baryons, which are transformed into each other by the gauge bosons of the theory. In this way, GUTs naturally accommodate B violation. Such B-violating reactions may be potent at the GUT scale $T \sim 10^{14}$ GeV, with rates that may be calculated perturbatively. GUTs also incorporate C and CP violation explicitly, which may be enhanced to a degree greater than that observed in the Standard Model. Finally, a departure from equilibrium may occur when the heavy gauge bosons fall out of equilibrium, as the temperature cools below the GUT scale; at such early times the universe is expanding so rapidly that many interactions are not in equilibrium ($\Gamma_{\rm rxn} \ll H$). Thus GUTs satisfy the Sakharov conditions for baryogenesis.

The standard picture that evolved is the so-called "drift and decay" scenario [4]. The basic idea of this picture is the production of baryon number by the B-violating decays of particles falling out of equilibrium. For instance, consider some GUT in which a supermassive gauge boson X mediates B-violating reactions. In the early universe, at temperatures $T > m_X$, the numbers of X and $\bar{X}$ are equal to the number of photons (neglecting statistical factors): $n_X \approx n_{\bar{X}} \sim n_\gamma$. In the presence of CP violation, the decay of an X added to the decay of an $\bar{X}$ produces a net baryon number ε, which is proportional to the CP parameter that measures the difference between the rates for the decay reaction and its CP conjugate. [4]

The sequence of events is as follows:

1. For $T \gg m_X$, thermal abundances of X and $\bar{X}$ are maintained in equilibrium, so that $n_X^{\rm EQ} = n_{\bar{X}}^{\rm EQ} \sim n_\gamma$.

2. For $T \lesssim m_X$, X and $\bar{X}$ become overabundant as the reactions that change the

[4] Although the total decay rates of X and $\bar{X}$ are equal by CPT invariance, their partial decay rates for the various channels differ; it is this difference between the branching ratios for the individual decay channels and their CP conjugates which is relevant here.

number density n_X fall out of equilibrium (provided m_X is massive enough); $n_X \gg n_X^{\rm EQ}$.

3. For $T \ll m_X$, the X and $\bar{X}$ freely decay; inverse decays and other B-violating reactions are suppressed by the low temperature. This results in a baryon number

$$B = \frac{n_B - n_{\bar{B}}}{s} \sim \frac{\varepsilon n_X}{g_* n_\gamma} \sim \frac{\varepsilon}{g_*} .$$

This scenario, though simple and appealing, raises further questions: What are the potential effects of a baryon asymmetry generated at the Planck scale, $T_{\rm Planck} \sim 10^{19}$ GeV? Which GUT describes the physics of baryogenesis, and which superheavy particles drop out of equilibrium, producing B by their eventual decays? Is the GUT-generated baryon number influenced by subsequent events? B might be significantly diluted or amplified, for instance, by entropy generation or by further baryogenesis at a lower scale.

1.4 Electroweak Baryogenesis

Although various GUT models of primordial baryogenesis were found capable, in principle, of dynamically generating an acceptable value of B, subsequent research brought to light several problems with the GUT scenario. First was the lack of experimental evidence or motivation for any particular GUT; the failure to observe proton decay has severely restricted, and in some cases eliminated, the simplest GUTs. Further, it was discovered that GUTs generically produce an unacceptably high relic abundance of stable massive magnetic monopoles, and of gravitinos in the case of supersymmetric GUTs. The solution to this problem was provided by inflation, which dilutes the abundances of these unwanted relics by a period of exponential expansion of the universe. But this process also diminishes the primordial B to a negligible value, which is unlikely to be regenerated by GUT processes since the reheat temperature is typically orders of magnitude below the GUT scale.

The advent of baryon violation at high temperature, via anomalous electroweak processes, was decisive in casting doubt on the ability of primordial baryogenesis to survive down to the electroweak scale. Although it was known that baryon violation mediated by instantons occurs in the Standard Model, the rate, like that for any tunneling process, is exponentially small. It was subsequently realized that such anomalous processes could in fact occur *without* suppression, at temperatures of order the electroweak scale. This development raised the specter of equilibrating the primordial baryon number to zero, at temperatures $\sim$ 100 GeV, unless a component of B were protected by some symmetry immune to electroweak processes.

Along with the possibility of depleting the primordial B-asymmetry came the prospect of baryon production at the electroweak scale. Indeed, electroweak physics may feasibly fulfill the Sakharov conditions for dynamical baryogenesis:

- Baryon violation is mediated by instantons at zero temperature and by sphalerons in equilibrium at high temperature.
- CP violation is explicit in the Standard Model and may be enhanced in modest extensions.
- If electroweak physics undergoes a first-order phase transition, as suggested by preliminary studies in the 1970s, disequilibrium may result from the separation of different phases and their respective particle interactions.

There emerged a promising opportunity to explain the baryon asymmetry in terms of low-energy physics — physics that is either known or experimentally accessible. As an added bonus, by requiring that the observed B-asymmetry be of electroweak origin, baryogenesis could provide a powerful probe of particle physics. For instance, despite our familiarity with electroweak physics, the origins of spontaneous symmetry breaking (the scalar sector) and of CP violation remain unknown; electroweak baryogenesis could place constraints on the Higgs mass and the CP-violating parameter.

In summary, electroweak baryogenesis has two chief advantages:

- it involves physics that is experimentally accessible (rather than conjectured physics at the GUT scale);
- it may place useful constraints on particle physics.

1.5 Review of the Literature

The possibility of generating the cosmological baryon asymmetry at the electroweak phase transition has aroused considerable interest. A comprehensive survey of the abundant literature may be found in the review by Cohen, Kaplan, and Nelson [5]; here we note only the work relevant to this thesis. Corresponding to the three Sakharov conditions, research in electroweak baryogenesis has focused on calculating detailed rates of baryon violation, investigating the role of C and CP violation and ways to enhance it, and determining the nature of the phase transition for different electroweak models. In connection with this, different mechanisms of baryogenesis have been proposed and studied, and various authors have obtained baryogenesis constraints on the Higgs sector.

The possibility that anomalous baryon violation within electroweak theory may have implications for baryogenesis was first suggested by Linde and by Dimopoulos and Susskind [6]. Manton and Klinkhamer [7] explicitly computed the specific field configuration (the so-called sphaleron) which could mediate thermal fluctuations between different topological vacua of the electroweak theory; because of the electroweak anomaly, such transitions mediate violation of baryon number. The connection to baryogenesis was realized in the work of Kuzmin, Rubakov, and Shaposhnikov [8], who argued that sphaleron-mediated transitions should occur unsuppressed at high enough

temperatures and estimated the rate of baryon violation in the broken phase. They considered the equilibrating effects of sphalerons on a primordially generated baryon number, and even further, proposed that the electroweak phase transition might itself be the origin of baryogenesis. The work of Arnold and McLerran [9] achieved more refined calculations of the sphaleron rate and a resolution of the apparent paradox between suppression of baryon violation at zero temperature and its enhancement at high temperature.

The role of C and CP violation has been investigated in various mechanisms of baryogenesis. Apart from the observed violation of CP in the K^0–$\bar{K}^0$ system of the Standard Model, there are new sources of CP violation in extensions of the Standard Model. Turok and Zadrozny [10] proposed CP violation in the new couplings of an extended scalar sector (e.g., the two-doublet model), which bias topological fluctuations and thereby baryon production. Cohen, Kaplan, and Nelson studied baryogenesis occurring in the adiabatic regime near slowly moving bubble walls, where CP violation in the scalar sector (e.g., the two-doublet model [11] and supersymmetric models [12]) induces an effective chemical potential that drives the generation of baryons. Cohen, Kaplan, and Nelson also proposed a charge-transport mechanism that operates under strongly non-equilibrium conditions, in which the CP-violating reflection of fermions off the bubble wall creates a net charge flux that triggers baryon production in the symmetric phase. CP violation resides in the scalar (e.g., the two-doublet model [13]) or leptonic (e.g., Majorana neutrino masses [14]) sectors. There have been further attempts within the Standard Model to amplify the existing source of CP violation in the CKM fermion mixing matrix to a level relevant in electroweak baryogenesis [15]. Along these lines, Farrar and Shaposhnikov [16] very recently suggested that baryogenesis may occur within the minimal Standard Model at a strongly first-order phase transition. CP violation in this case arises through dynamical effects associated with the reflection of fermionic plasma modes off the bubble wall.

1.6 Outline

Owing to the intense research activity in the last decade, baryogenesis via electroweak processes has emerged as a credible candidate to explain the cosmological generation of baryon number. Many uncertainties remain, however, and must be resolved before any conclusions are reached. First, despite the plausibility of baryogenesis in the Standard Model, several difficulties have prevented the construction of a compelling scenario: CP violation in the Kobayashi-Maskawa matrix is unacceptably small, and it is unknown whether the phase transition is sufficiently first-order to ensure efficient baryon production. Related to this last point is the need to protect the freshly generated B from erasure by sphalerons, which might still exist in equilibrium following the phase transition. A second question addresses the possibility of transforming a primordial asymmetry other than B into the baryon asymmetry, by anomalous processes at the electroweak phase transition. If some protection mechanism exists, e.g., a symmetry

like $B - L$ which is immune to anomalous baryon violation, a primordially generated asymmetry may survive to the electroweak scale to play some role in generating the observed baryon number. These concerns have motivated the work of this thesis.

This thesis therefore addresses two aspects of baryogenesis at the electroweak scale: determining the nature of the phase transition and the associated baryogenesis bounds on the Higgs mass, and investigating the possibility of a (CP-conserving) mechanism for converting some pre-existing leptonic asymmetry into B. First, the phase transition is analyzed by means of the effective potential at finite temperature. The effective potential at one loop suggests a first order phase transition; an accurate analysis, however, is complicated by infrared divergences, which reflect the appearance of massless modes near the phase transition, where the Higgs field has zero thermal average. We therefore treat these modes by including the effects of large thermal fluctuations, in the form of thermal self-energies or plasma masses. This achieves a resummation of perturbation theory at high temperature, which more reliably describes the phase transition. Because of the wide variety of mechanisms suggested in the literature, and the lack of any compelling scenario among them, this analysis (and the associated baryon-washout bounds on the Higgs boson mass) is made as general as possible; it is independent of any particular scheme of baryogenesis, and depends only on the electroweak model under consideration. We apply this analysis to modest extensions of the Standard Model.

Secondly, we consider a scenario in which anomalous electroweak processing converts a pre-existing $B/3 - L_\tau$ asymmetry into the baryon asymmetry. Rather than imagining exotic ways to enhance CP violation in the minimal Standard Model, or incorporating new sources of CP violation in its extensions, this mechanism demonstrates that one need not automatically invoke a large degree of electroweak CP violation in order to produce B. Instead CP violation is assumed to reside in physics at the GUT scale, which generates the initial leptonic asymmetry. Furthermore, it is investigated how charge transport in a strongly first-order phase transition might enhance the effect to produce a cosmologically acceptable baryon number.

The outline of this thesis follows. Chapters 2, 3, and 4 review the background essential to a study of baryogenesis at the electroweak scale. Chapter 2 introduces the methods and basic results of finite-temperature field theory. Chapter 3 develops the theory of symmetry restoration and illustrates the theory with two basic examples: the scalar and the Abelian Higgs models. It emphasizes their analogies and makes their relation to the Standard Model apparent. This chapter also shows how to cure the leading infrared divergences by the method of summing ring diagrams, a technique borrowed from studies of QCD at high temperature [17]. Chapter 4 reviews baryon violation and its enhancement at high temperature. Chapter 5 describes the behavior of the phase transition in the minimal Standard Model, and it demonstrates in detail that the requirement of avoiding baryon washout leads to an upper bound on the Higgs mass inconsistent with present experiment. It supplements the analyses of Dine, Leigh, Linde, et. al. [18] and of Carrington [19] by including scalar loops in the effective potential. One way to relax the constraint on the Higgs boson mass is to extend the scalar

sector of the Standard Model, and in Chapters 6 and 7 we consider the two simplest such extensions, the addition of a gauge singlet and of a second doublet. The one-loop analyses of Anderson and Hall [20] and of Bochkarev, Kuzmin, and Shaposhnikov [21] are refined by ring improvement, and original results are presented. It is shown how a singlet can relax the Higgs bound, and bounds for the two-doublet model are also considered. In Chapter 8 we address the second topic of this thesis, by proposing and investigating a specific mechanism for generating B through electroweak processing of a primordial lepton asymmetry. [5] This work combines the ideas of Nelson, Kaplan, and Cohen [13] for the enhancing effect of charge transport via fermion reflection off an expanding bubble wall during the phase transition, and the methods of Farrar and Shaposhnikov [16] for describing the fermionic collective modes of a relativistic plasma. It is found that this mechanism yields a baryon number consistent with observation, without the restrictive assumption of large CP violation at the electroweak scale. Chapter 9 concludes the thesis with a summary and discussion of results, and gives suggestions for further work.

[5] This work was done in collaboration with Dr. S. Abel.

Chapter 2

Field Theory at High Temperature

The physical effects of high temperature and density, characteristic of the early universe, require modification to the quantum field theory description of elementary particles. In order to calculate the effective potential at high temperature, as a means of studying the electroweak phase transition and its implications for baryogenesis, we first review the principles and methods of finite-temperature field theory.

Starting from the basic principles of statistical mechanics and field theory, we develop relativistic quantum field theory at high temperature and density. We use the functional integral approach to display the analogy between the time evolution operator e^{-iHt} and the partition function $\mathrm{Tr}\, e^{-H/T}$, rendered by analytic continuation to imaginary time. Once we have the path-integral representation of the partition function, we derive the Feynman rules and note that thermal effects are ultraviolet finite. We then construct the generating functionals and conclude with a technique for computing the effective potential. Throughout, we will emphasize the physical interpretation of the formalism, and describe the similarities and differences of field theories at zero and high temperatures. This chapter covers only the material relevant to the work of this thesis; comprehensive treatments may be found in References [22, 23, 24].

2.1 Path-Integral Representation and Feynman Rules

The equilibrium behavior of a field theory at non-zero temperature is specified by the partition function,

$$Z^T = \mathrm{Tr}\, e^{-\widehat{H}/T} ,$$

and the thermal expectation of physical observables (the Green functions),

$$\langle \widehat{\mathcal{O}} \rangle = \frac{1}{Z^T}\, \mathrm{Tr}\, e^{-\widehat{H}/T} \widehat{\mathcal{O}} ,$$

where the trace is taken over the physical states of the system and operators are described in the Heisenberg picture. Thermodynamic properties can be derived from the partition function, perturbation theory from the Green functions.

We use the imaginary-time formalism, which makes explicit the mathematical resemblance between field theory at zero and finite temperatures. [1] For motivation, let us consider a field theory at zero temperature and analytically continue to imaginary time, $\tau = it$. First notice that, for $\tau = T^{-1}$, the time-evolution operator $e^{-i\widehat{H}t}$ transforms into the density operator $\widehat{\rho} = e^{-\widehat{H}/T}$ of thermodynamics, and the Green functions into

$$\langle \widehat{A}(\vec{x}_1,\tau_1)\widehat{B}(\vec{x}_2,\tau_2)\cdots\rangle = \frac{1}{Z^T}\,\mathrm{Tr}\; e^{-\widehat{H}/T}\, T_\tau \left\{ \widehat{A}(\vec{x}_1,\tau_1)\widehat{B}(\vec{x}_2,\tau_2)\cdots \right\} ,$$

where T_τ is the (imaginary-time) τ-ordering operation. Secondly, by exploiting the relation between the density and the time evolution operators, we notice that the Green functions are periodic or anti-periodic for bose or fermi fields, on the interval $[0, T^{-1}]$:

$$\begin{aligned}
\langle \widehat{A}(\vec{x}_1,T^{-1})\widehat{B}(\vec{x}_2,\tau_2)\cdots\rangle &= \frac{1}{Z^T}\,\mathrm{Tr}\;\widehat{\rho}\, T_\tau \left\{ \widehat{A}(\vec{x}_1,T^{-1})\widehat{B}(\vec{x}_2,\tau_2)\cdots \right\} \\
&= \frac{1}{Z^T}\,\mathrm{Tr}\; e^{-\widehat{H}/T}\,\widehat{A}(\vec{x}_1,T^{-1})\widehat{B}(\vec{x}_2,\tau_2)\cdots \\
&= \frac{1}{Z^T}\,\mathrm{Tr}\; e^{-\widehat{H}/T}\; e^{\widehat{H}/T}\,\widehat{A}(\vec{x}_1,0)\, e^{-\widehat{H}/T}\widehat{B}(\vec{x}_2,\tau_2)\cdots \\
&= \frac{1}{Z^T}\,\mathrm{Tr}\;\widehat{A}(\vec{x}_1,0)\, e^{-\widehat{H}/T}\widehat{B}(\vec{x}_2,\tau_2)\cdots \\
&= \frac{1}{Z^T}\,\mathrm{Tr}\; e^{-\widehat{H}/T}\widehat{B}(\vec{x}_2,\tau_2)\cdots\widehat{A}(\vec{x}_1,0) \\
&= \pm\frac{1}{Z^T}\,\mathrm{Tr}\;\widehat{\rho}\, T_\tau \left\{ \widehat{A}(\vec{x}_1,0)\widehat{B}(\vec{x}_2,\tau_2)\cdots \right\} \\
&= \pm\langle \widehat{A}(\vec{x}_1,0)\widehat{B}(\vec{x}_2,\tau_2)\cdots\rangle ,
\end{aligned}$$

and hence the fields themselves may be taken to be periodic or anti-periodic. Above we have used the cyclic property of the trace, the definition of τ-ordering for bose and fermi fields, and the fact that fermionic Green functions are composed of bilinear combinations (and hence an even number) of spinor fields. Finally the transition amplitude from the state $|\Psi_0\rangle$ at $t = 0$ to the state $|\Psi_1\rangle$ at $t = t_1$,

$$\langle \Psi_1|e^{-i\widehat{H}t_1}|\Psi_0\rangle \propto \int \mathcal{D}\Psi\;\; \exp\left\{ i\int_0^{t_1} dt \int d^3\vec{x}\;\; \mathcal{L}\left(\Psi, \frac{\partial\Psi}{\partial t}, \vec{\nabla}\Psi\right)\right\} ,$$

[1] And we neglect the real-time formalism, which makes explicit, in their contributions to physical observables, the distinction between quantum and thermal fluctuations. While the real-time formulation preserves manifest Lorentz covariance, we find it inconvenient for the purposes of this thesis; the imaginary-time formulation, however, allows an immediate interpretation of the ring diagrams as an infrared effect (Chapter 3).

is transformed into

$$\langle \pm\Psi_0 | e^{-\widehat{H}/T} | \Psi_0 \rangle \propto \int_{\substack{\text{(anti-)}\\ \text{periodic}}} \mathcal{D}\Psi \ \exp\left\{ - \int_0^{T^{-1}} d\tau \int d^3\vec{x} \ \mathcal{L}_{\mathrm{E}}\left(\Psi, \frac{\partial\Psi}{\partial\tau}, \vec{\nabla}\Psi\right) \right\} ,$$

where we have imposed the (anti-) periodicity condition on Ψ over $[0, T^{-1}]$ and $\mathcal{L}_{\mathrm{E}}$ is the Euclidean Lagrangian. We see that, by analytically continuing to imaginary time, the quantum transition amplitude has been transformed into the Boltzmann probability of statistical mechanics, thereby relating the evolution of a quantum field theory to the behavior of a thermal ensemble in static equilibrium.

In analogy with the zero-temperature generating functional $Z[J]$, the partition function may now be expressed as a functional integral solution to the finite-temperature equations of motion. Thus, we transform Z^T from a trace over all states,

$$Z^T = \sum_{|\Psi\rangle} \langle \pm\Psi | e^{-\widehat{H}/T} | \Psi \rangle ,$$

into a Euclidean path integral over all periodic bose fields and anti-periodic fermi fields, defined on the imaginary-time interval $[0, T^{-1}]$. Because of the (anti-) periodic boundary conditions, the Fourier-transformed fields have discrete Matsubara frequencies, $\omega_n = 2n\pi T$ for bose fields and $(2n+1)\pi T$ for fermi fields. Adding an external source J results in the generating functional $Z^T[J]$, from which the Green functions may be obtained by taking the appropriate derivatives. Thus

$$Z^T[J] = N \int_{\substack{\text{(anti-)}\\ \text{periodic}}} \mathcal{D}\Psi \ \exp\left\{ - \int_0^{T^{-1}} d\tau \int d^3\vec{x} \ \mathcal{L}_{\mathrm{E}}\left(\Psi, \frac{\partial\Psi}{\partial\tau}, \vec{\nabla}\Psi\right) - J\Psi \right\} , \tag{2.1}$$

and the analogy is explicit: to get $Z^T[J]$ from $Z[J]$, we merely continue to Euclidean time, impose the appropriate boundary conditions, and convert Fourier integrals over continuous energies to Fourier sums over discrete frequencies.

Because the Green functions at finite temperature satisfy the same equations of motion as their counterparts at zero temperature and differ only in their boundary conditions, we may appropriate the entire framework of zero-temperature perturbation theory and the corresponding Feynman rules. We need only make the following modifications:

$$\begin{aligned} t &\rightarrow -i\tau \\ \int d^4x &\rightarrow -i \int_0^{T^{-1}} d\tau \int d^3\vec{x} \end{aligned}$$

$$
\begin{aligned}
k^0 &\to i\omega_n = \begin{cases} i2n\pi T & \text{bose} \\ i(2n+1)\pi T & \text{fermi} \end{cases} \\
\int \frac{d^4k}{(2\pi)^4} &\to iT \sum_{n=-\infty}^{\infty} \int \frac{d^3\vec{k}}{(2\pi)^3} \\
(2\pi)^4 \delta^4(k) &\to (iT)^{-1} \delta_{n,0}\, (2\pi)^3 \delta^3(\vec{k}) \,.
\end{aligned} \tag{2.2}
$$

Additional modifications apply to gauge theories. Here we define the partition function in the space of physical states,

$$
Z^T = \mathrm{Tr}\, e^{-\widehat{H}/T}\Big|_{\text{physical gauge}} \,, \tag{2.3}
$$

thus excluding the unphysical degrees of freedom, such as ghost fields or unphysical polarization states of gauge fields, which cannot come into equilibrium with a physical heat bath. The partition function is then generalized to arbitrary gauges via the Fadeev-Popov procedure. Ghost fields, although anti-commuting, have bose-like Matsubara frequencies since they represent the effects of a determinant defined in the function space of gauge fields.

In the calculation of Green functions, we encounter expressions involving sums over Matsubara frequencies; for instance, taking f and g to be the integrands of a bosonic and fermionic loop integral, respectively, we have from the integrals' zero components

$$
\begin{aligned}
&\text{Bose:} && T \sum_n f(k^0 = i2n\pi T) \\
&\text{Fermi:} && T \sum_n g(p^0 = i(2n+1)\pi T) \,.
\end{aligned} \tag{2.4}
$$

We evaluate these sums in the standard way by expressing them as contour integrals and then separating the zero-temperature and thermal contributions:

$$
\begin{aligned}
T \sum_n f(k^0 = i2n\pi T) &= \frac{T}{2\pi i} \oint_{C_\mathrm{B}} dk^0\, f(k^0)\, \frac{1}{2T} \coth(\frac{k^0}{2T}) \\
&= \int_{-\infty}^{\infty} \frac{dk^0}{2\pi}\, f(ik^0) + \frac{1}{2\pi i} \int_{-i\infty+\varepsilon}^{i\infty+\varepsilon} dk^0\, \frac{2f(k^0)}{\mathrm{e}^{k^0/T} - 1}
\end{aligned} \tag{2.5}
$$

for bosonic loops and

$$
\begin{aligned}
T \sum_n g(p^0 = i(2n+1)\pi T) &= \frac{T}{2\pi i} \oint_{C_\mathrm{F}} dp^0\, g(p^0)\, \frac{1}{2T} \tanh(\frac{p^0}{2T}) \\
&= \int_{-\infty}^{\infty} \frac{dp^0}{2\pi}\, g(ip^0) - \frac{1}{2\pi i} \int_{-i\infty+\varepsilon}^{i\infty+\varepsilon} dp^0\, \frac{2g(p^0)}{\mathrm{e}^{p^0/T} + 1} \,.
\end{aligned} \tag{2.6}
$$

for fermionic loops. The contours $C_{\rm B}$ and $C_{\rm F}$ are given in Figure 2.1. The contributions

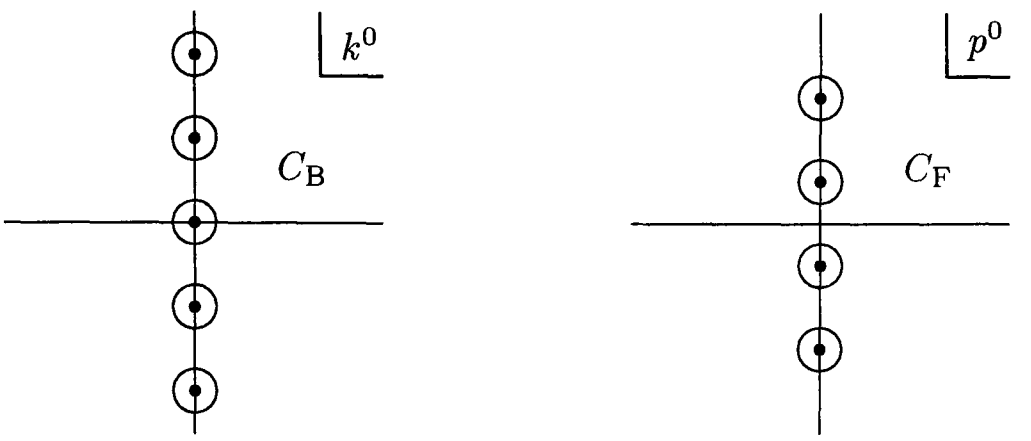

Figure 2.1: The integration contours for evaluating Bose and Fermi thermal sums, with poles at $\omega_n = 2n\pi T$ and $\omega_n = (2n+1)\pi T$ respectively.

from the vacuum and non-zero temperature naturally separate; the physical interpretation is that, because physical particles interact with the thermal bath, there are indistinguishable contributions within the loop from virtual particles (quantum fluctuations of the vacuum) and from physical particles in the ambient distribution (thermal fluctuations due to the heat bath). Note that because the thermal distribution acts as an exponential cutoff (i.e., the temperature effectively serves as a high-momentum cutoff), only the zero-temperature piece requires ultraviolet renormalization. Thus finite temperature introduces no new UV divergences; *renormalization performed at zero temperature is sufficient at finite temperature.* Physically, finite-temperature effects do not change the short-distance behavior of the theory.

It should be mentioned for completeness that this formalism may be extended to include the case of high density effects. Denoting by μ_i the chemical potentials associated with the independent conserved charges $\widehat{Q}_i$, the density operator is then $\widehat{\rho} = e^{-(\widehat{H}-\mu_i\widehat{Q}_i)/T}$, and the partition function and Green functions become

$$\begin{aligned} Z^T &= \mathrm{Tr}\, e^{-(\widehat{H}-\mu_i\widehat{Q}_i)/T} \,, \\ \langle \widehat{A}(x_1)\widehat{B}(x_2)\cdots\rangle &= \frac{1}{Z^T}\,\mathrm{Tr}\, e^{-(\widehat{H}-\mu_i\widehat{Q}_i)/T}\, T_\tau\left\{\widehat{A}(x_1)\widehat{B}(x_2)\cdots\right\} . \end{aligned}$$

The functional integral may be derived analogously to (2.1), with the only exception that the Euclidean time derivative for the field with conserved charges q_i is now $\partial/\partial\tau \to \partial/\partial\tau - q_i\mu_i$:

$$Z^T[J] = N \int\limits_{\substack{\text{(anti-)}\\ \text{periodic}}} \mathcal{D}\Psi \;\; \exp\left\{ -\int_0^{T^{-1}} d\tau \int d^3\vec{x} \;\; \mathcal{L}_{\rm E}\left(\Psi; \frac{\partial\Psi}{\partial\tau} - q_i\mu_i\Psi; \vec{\nabla}\Psi\right) - J\Psi \right\} . \qquad (2.7)$$

Consequently, in the Feynman rules, the time-component of the momentum becomes $k^0 \to i\omega_n - q_i\mu_i$, and the loop integrals corresponding to (2.5) and (2.6) are modified to reflect the separate contributions due to a finite density of particles and antiparticles.

For most of our discussion, we will assume that all chemical potentials vanish. When we require chemical potentials in Chapter 8, they will be small enough, $|\mu|/T \ll 1$, that only the lowest order (linear) contribution will be needed, which we extract using the distribution functions $f_{B,F}(\vec{k}) = [\exp{(\sqrt{\vec{k}^2 + m^2} - q_i\mu_i)/T} \mp 1]^{-1}$.

2.2 Generating Functionals and the Effective Potential

The thermal generating functionals are constructed by analogy to their counterparts at zero temperature. Connected thermal Green functions are generated by $W^T[J] = -\log Z^T[J]$. Defining the classical field ψ,

$$\psi(\bar{x}) = \frac{\delta W^T}{\delta J(\bar{x})}[J] = \langle \Psi(\bar{x}) \rangle \ ,$$

the effective action is obtained from $W^T[J]$ by Legendre transform:

$$\Gamma^T[\psi] = W^T[J] - \int d^4\bar{x}\ J\psi \ ,$$

where we denote Euclidean coordinates by $\bar{x}$. The effective action generates proper (1PI) vertices,

$$\Gamma^T[\psi] = \sum_{n=1}^{\infty} \frac{1}{n!} \int d^4\bar{x}_1 \cdots d^4\bar{x}_n\ \Gamma^{(n)}(\bar{x}_1 \cdots \bar{x}_n)\ \psi(\bar{x}_1) \cdots \psi(\bar{x}_n) \ .$$

The effective potential V^T is then defined as the first term in a derivative expansion for the effective action,

$$\Gamma^T[\psi] = \int d^4\bar{x} \left[-V^T(\psi) + \frac{1}{2} Z^T(\psi)(\bar{\partial}^\mu\psi)(\bar{\partial}_\mu\psi) + \cdots \right] ,$$

and for constant ψ, may be expressed in terms of zero-momentum 1PI Green functions:

$$V^T(\psi) = -\sum_{n=1}^{\infty} \frac{1}{n!}\ \tilde{\Gamma}^{(n)}(\omega_j = 0, \vec{k}_j = 0)\ \psi^n \ . \tag{2.8}$$

The effective potential at finite temperature is the free-energy density associated with the field ψ; more precisely, it measures the free energy density of the field theory coupled to the heat bath, a system which is characterized by its average field ψ and its temperature T. It contains thermodynamic information through the relations

$$\begin{aligned} &\text{Pressure density:} && p(\psi) = -V^T(\psi) \\ &\text{Entropy density:} && s(\psi) = -\frac{\partial V^T}{\partial T}(\psi) \\ &\text{Energy density:} && \rho(\psi) = V^T(\psi) + Ts(\psi) \ . \end{aligned} \tag{2.9}$$

Because the ground state of the system minimizes the free energy, the effective potential serves as a useful tool to investigate symmetry breaking and its thermal restoration. In this thesis we use $V^T(\psi)$ exclusively for this purpose.

We employ the tadpole method for calculating the effective potential, which avoids the combinatorics encountered in a direct calculation of $V^T(\psi)$ via (2.8). The method requires only computing the 1PI tadpole and integrating. To see this, we simply expand the effective potential about $\psi = \theta$; this is equivalent to shifting the field $\psi \to \psi + \theta$, so that the effective potential is expressed in terms of zero-momentum proper vertices in the *shifted* theory:

$$V^T(\psi) = -\sum_{n=1}^{\infty} \frac{1}{n!} \widetilde{\Gamma}_{\theta}^{(n)}(\omega_j = 0, \vec{k}_j = 0)\,(\psi - \theta)^n \,. \tag{2.10}$$

Taking the first derivative at $\psi = \theta$ and comparing with the unshifted theory in (2.8),

$$\left.\frac{dV^T}{d\psi}\right|_{\psi=\theta} = -\widetilde{\Gamma}_{\theta}^{(1)}(k=0) = -\sum_{n=1}^{\infty} \frac{1}{(n-1)!} \widetilde{\Gamma}^{(n)}(k=0)\,\theta^{n-1} = \frac{dV^T}{d\theta}(\theta) \,.$$

Integration yields $V^T(\theta)$.

Further differentiation of the effective potential (2.10) yields proper vertices of the shifted theory (at zero external momenta), in a form useful for our later analysis:

$$\widetilde{\Gamma}_{\theta}^{(n)}(k=0) = -\frac{d^n V^T}{d\theta^n}(\theta) \,. \tag{2.11}$$

For non-zero external momenta, the analogous relation may be derived similarly from the effective action $\Gamma^T[\psi]$:

$$\widetilde{\Gamma}_{\theta}^{(n)}(p_1, \ldots, p_{n-1}, 0) = \frac{d}{d\theta} \widetilde{\Gamma}_{\theta}^{(n-1)}(p_1, \ldots, p_{n-1}) \,. \tag{2.12}$$

These relations for $n = 2$ will be used to find convenient expressions for the scalar self-energy.

Chapter 3

Restoration of Symmetry at High Temperature

Symmetry restoration is an important feature of finite temperature field theory: thermal effects at high temperature may restore a symmetry that is spontaneously broken at zero temperature [23, 25]. To motivate our study of this phenomenon, consider the free energy of a physical system, described by a chosen field theory that induces spontaneous breakdown of symmetry (with thermal expectation $\langle\Phi\rangle$) coupled to a heat bath (at temperature T). The system occupies the state that minimizes its free energy, which at zero temperature occurs at the minimum of the tree-level potential: $\langle\Phi\rangle \neq 0$. At high temperature, the thermal distribution of ambient particles increases the cost in energy terms of a non-zero value of $\langle\Phi\rangle$, as free energy must be added to the ambient particles that are gaining mass. Thus the scalar condensate that forms at zero temperature becomes increasingly unstable as the temperature rises, and as it gradually melts away, the system undergoes a phase transition in the order parameter $\langle\Phi\rangle$: $\langle\Phi\rangle \to 0$. This process of symmetry restoration occurs as the system seeks to minimize its free energy in the presence of an ambient thermal distribution.

Consider this phenomenon from another point of view. At low temperature, a classical determination of the vacuum, and hence a classical picture of spontaneous symmetry breaking, is sufficient as long as perturbation theory is valid; quantum effects at higher orders in the coupling parameters are perturbative, so they do not alter our tree-level description to any significance. At high temperature, however, conventional perturbation theory fails — a large temperature may compensate for small coupling parameters. Thus a classical description is insufficient, and one must go to higher orders to reliably determine the vacuum state. In physical terms, at high enough temperature, *thermal fluctuations may change the nature of the vacuum.*

In this chapter, it is shown how a symmetry-restoring phase transition may be described by means of the effective potential at finite temperature. To motivate our treatment of the electroweak phase transition in Chapters 5, 6, and 7, we first choose to analyze the scalar and the Abelian Higgs models as our prototypes. We compute

the effective potential at one loop and find that the phase transition is apparently first-order. This description, however, is misleading, and in fact inconsistent, because of infrared divergences that invalidate the loop expansion. Perturbation theory at finite temperature will then be considered in general, and it will be seen how the effective expansion parameter is altered from the usual case at zero temperature, thus permitting us to easily identify the source of the leading infrared divergences. These divergences may be cured by taking into account, via thermal masses and dressed propagators, the effect of large thermal fluctuations on the infrared modes characteristic of the phase transition. In other words, because of long-range collective modes in the plasma, there are contributions that are non-analytic in the couplings (the plasmon effect), which should be included in the effective potential. This will be done to leading order in the temperature by summing ring diagrams. We will find at this point that we have a reliable and consistent description of the phase transition, to lowest order (viz. cubic) in the coupling parameters, and we will conclude by considering the validity of our new perturbative expansion. Our results confirm weak first-order behavior at the phase transition.

3.1 The Scalar Model

Notation

We first consider symmetry restoration in the simplest context, the scalar model with spontaneous symmetry breaking. It has the Z_2-invariant Lagrangian

$$\mathcal{L}_{\text{scalar}} = \frac{1}{2}\partial_\mu\Phi\partial^\mu\Phi - U(\Phi) + \mathcal{L}_{\text{c.t.}}\,, \tag{3.1}$$

where the classical potential and counter-term Lagrangian are given by

$$U(\Phi) = -\frac{\mu^2}{2}\Phi^2 + \frac{\lambda}{4}\Phi^4 \tag{3.2}$$

and

$$\mathcal{L}_{\text{c.t.}} = \frac{A}{2}\partial_\mu\Phi\partial^\mu\Phi + \frac{B}{2}\Phi^2 + \frac{C}{4}\Phi^4 + D\,. \tag{3.3}$$

The mass parameter μ^2 is positive, so that the minimum of $U(\Phi)$ occurs at $|\Phi|^2 = \mu^2/\lambda \equiv v^2$, where $d^2U/d|\Phi|^2 = 2\mu^2$ (see Figure 3.1). At zero temperature, the system minimizes its energy by choosing one of the classical minima, and because this choice of vacuum does not respect the Z_2 symmetry of the field dynamics ($\Phi \to -\Phi$), a spontaneous breakdown of symmetry is said to occur.

At finite temperature, the physical system favors the state that minimizes its free energy density V^T. If this minimum-energy state develops a thermal average $\langle\Phi\rangle \neq 0$, the Z_2 symmetry is broken; otherwise we say that the symmetry is restored. Choosing $\langle\Phi\rangle$ to be non-negative, we denote it by $\langle\Phi\rangle = \phi$ and expand the field Φ about its

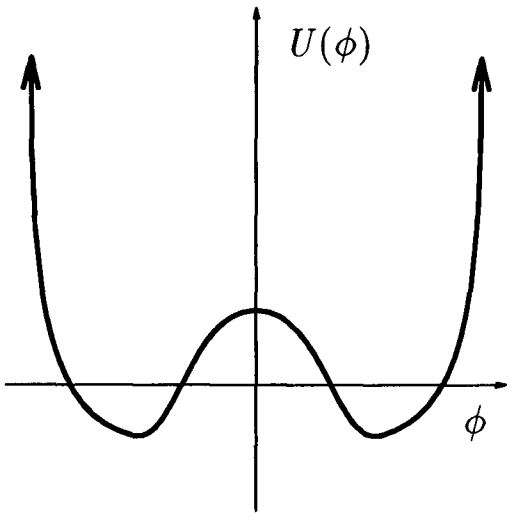

Figure 3.1: The classical potential for the scalar model.

Poincaré-invariant [1] thermal average:

$$\Phi = \phi + \sigma \tag{3.4}$$

where $\langle\sigma\rangle = 0$. This is analogous to the analysis of Bose-Einstein condensation, in which one isolates the static infrared part of the field. Shifting by ϕ in $U(\phi)$ yields the scalar mass $m^2(\phi) = -\mu^2 + 3\lambda\phi^2 = \lambda(3\phi^2 - v^2)$. The thermal average $\langle\Phi\rangle$ will be found as a function of temperature T by minimizing the effective potential $V^T(\phi)$.

Performing the shift (3.4) and neglecting constants and total divergences, we express the Lagrangian as the sum of a quadratic part and an interacting part:

$$\mathcal{L} = \mathcal{L}_0 + \mathcal{L}_{\rm I}\,, \tag{3.5}$$

where

$$\mathcal{L}_0 = \frac{1}{2}\partial_\mu\sigma\partial^\mu\sigma - \frac{m^2(\phi)}{2}\sigma^2 \tag{3.6}$$

and

$$\mathcal{L}_{\rm I} = -\lambda\phi\sigma^3 - \frac{\lambda}{4}\sigma^4 + (\mu^2\phi - \lambda\phi^3)\,\sigma + (\text{counter-terms})\,. \tag{3.7}$$

Effective Potential at One Loop

We compute the effective potential by the method of tadpoles. At lowest order we get the tree-level contributions from the classical potential and the counter-term Lagrangian:

$$U(\phi) = -\frac{\mu^2}{2}\phi^2 + \frac{\lambda}{4}\phi^4 \tag{3.8}$$

[1] We know from thermodynamics that the pressure density ($= -V^T$) is spatially uniform in equilibrium; local fluctuations are unstable.

and

$$V_{\text{c.t.}}(\phi) = -\frac{B}{2}\phi^2 - \frac{C}{4}\phi^4 - D\ . \tag{3.9}$$

At next order, we obtain a contribution from the scalar loop of Figure 3.2, which has the form

$$\begin{aligned}\frac{dV}{d\phi}(\phi) &= 3\lambda\phi \int \frac{d^4k}{(2\pi)^4}\, \frac{i}{k^2 - m^2(\phi) + i\varepsilon} \\ &= \frac{1}{2}\frac{dm^2}{d\phi}(\phi)\, T \sum_n \int \frac{d^3\vec{k}}{(2\pi)^3}\, \frac{1}{(2\pi n T)^2 + \vec{k}^2 + m^2(\phi)}\ .\end{aligned} \tag{3.10}$$

We express this as a contour integral (in the manner used to derive (2.5)), arriving at

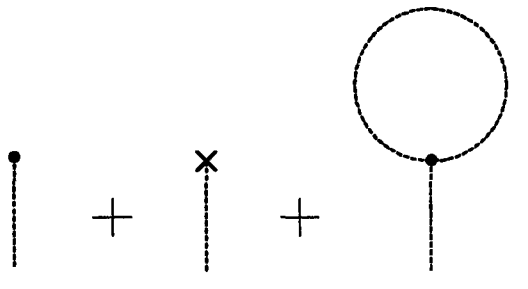

Figure 3.2: The tadpole graphs for the one-loop effective potential in the scalar model.

the standard expression

$$V(\phi) = \frac{1}{2}\int \frac{d^4k_{\text{E}}}{(2\pi)^4}\, \log\left(k_{\text{E}}^2 + m^2(\phi)\right) + T^4 I_B\left(\frac{m(\phi)}{T}\right)\ . \tag{3.11}$$

Notice that the zero- and finite-temperature pieces separate. The zero-temperature integral is taken over Euclidean momenta, while the convergent integral I_B embodies the thermal effects at one loop of the ambient boson field. It possesses the high-temperature expansion

$$\begin{aligned}I_B(y) &\equiv +\frac{1}{2\pi^2}\int_0^\infty dx\ x^2 \log\left(1 - \exp\left(-\sqrt{x^2 + y^2}\right)\right) \\ &= \text{constant} + \frac{y^2}{24} - \frac{y^3}{12\pi} - \frac{y^4}{64\pi^2}\log\left(\frac{y^2}{c_B}\right) + \mathcal{O}\left(y^6, y^6 \log y^2\right)\ ,\end{aligned} \tag{3.12}$$

where $\log c_B = \frac{3}{2} + 2\log 4\pi - 2\gamma \approx 5.41$. As we will see below, $T \sim v = \mu/\sqrt{\lambda}$ near the phase transition, and the high-temperature expansion gives a valid approximation to the effective potential.

Although formally a function of y^2, notice that $I_B(y)$ is non-analytic in y^2; hence the cubic term in the expansion (3.12). This cubic term is crucial to the first-order behavior of the phase transition, and will be examined in detail below. Here we see from integration that it derives directly from the zero mode in the one-loop tadpole

(3.10). Thus infrared effects will be important in assessing the first-order nature of the phase transition.

We obtain the unrenormalized one-loop effective potential:

$$V^T_{1\,\mathrm{loop}}(\phi) = V^0(\phi) + \Delta V^T(\phi) \tag{3.13}$$

where

$$V^0(\phi) = U(\phi) + V_{\mathrm{c.t.}}(\phi) + \frac{1}{2}\int \frac{d^4k_{\mathrm{E}}}{(2\pi)^4} \log\left(k_{\mathrm{E}}^2 + m^2(\phi)\right) \tag{3.14}$$

and

$$\Delta V^T(\phi) = T^4 I_B\left(\frac{m_1(\phi)}{T}\right) . \tag{3.15}$$

$V^T_{1\,\mathrm{loop}}(\phi)$ is the free energy of a (non-interacting) ideal gas of scalar particles. Because finite temperature effects introduce no new ultraviolet divergences, we need only renormalize the zero-temperature piece V^0. For convenience, we choose a renormalization prescription that preserves at one loop the tree-level relations for the location of the minimum (at $v = \mu/\sqrt{\lambda}$) as well as the Higgs mass ($M^2 = 2\lambda v^2$) at this minimum:

$$\left.\frac{dV^0}{d\phi}\right|_{\phi=v} = 0 \tag{3.16}$$

$$\left.\frac{d^2V^0}{d\phi^2}\right|_{\phi=v} = M^2 . \tag{3.17}$$

These conditions determine the renormalization constants B and C of (3.9); D is chosen to cancel the constant part of V^0, and A of (3.3), which is superfluous for the purpose of computing V^0, is determined by requiring that the thermal propagator have unit residue.

Renormalization yields the final expression for the zero-temperature effective potential at one loop:

$$V^0(\phi) = -\frac{\mu^2}{2}\left(1 - \frac{21\lambda}{32\pi^2}\right)\phi^2 + \frac{\lambda}{4}\left(1 - \frac{27\lambda}{32\pi^2}\right)\phi^4 + \frac{m^4(\phi)}{64\pi^2}\log\left(\frac{m^2(\phi)}{M^2}\right) . \tag{3.18}$$

Adding the finite-temperature piece (3.15) and using the high-temperature expansion for I_B (3.12), the effective potential at one loop may now be approximated as

$$\begin{aligned} V^T_{1\,\mathrm{loop}}(\phi) = {} & \frac{\phi^2}{2}\left[-\mu^2 + \frac{\lambda}{4}T^2 + \frac{3\lambda M^2}{32\pi^2}\log\left(\frac{M^2}{a'_B T^2}\right)\right] \\ & + \frac{\phi^4}{4}\left[\lambda - \frac{9\lambda^2}{16\pi^2}\log\left(\frac{M^2}{a_B T^2}\right)\right] - \frac{T}{12\pi}\lambda^{3/2}\left[3\phi^2 - v^2\right]^{3/2} . \end{aligned} \tag{3.19}$$

$\log a_B = \log c_B - 3/2 \approx 3.91$ and $\log a'_B = \log c_B - 7/2 \approx 1.91$. Notice the cancelation of the $m^4(\phi)\log m^2(\phi)$ terms from the thermal and zero-temperature pieces, ΔV^T and

V^0. Here, and throughout this thesis, terms that are independent of ϕ (i.e., constant or depending only on the temperature) are discarded from the effective potential; that is, we renormalize to zero the vacuum pressure and energy densities. One may obtain the effective potential valid at lower temperature, by numerically evaluating the integral I_B, (3.12).

The Phase Transition

To gain some insight into the phase transition, let us first approximate V^T by including only the leading thermal contribution, i.e., only the $m^2(\phi)/T^2$ term of the expansion (3.12). In this case, the effective potential becomes

$$\begin{aligned} V^T_{\rm approx}(\phi) &= U(\phi) + \frac{\phi^2}{2}\frac{\lambda}{4}T^2 \\ &= \frac{\phi^2}{2}\left(-\mu^2 + \frac{\lambda}{4}T^2\right) + \frac{\lambda}{4}\phi^4 \,. \end{aligned} \tag{3.20}$$

Scaling V^T and ϕ by the temperature, $x \equiv \phi/T$ and $f(x) = V^T_{\rm approx}/T^4$, we have

$$f(x) = \frac{\lambda}{8}\left(1 - \frac{T_0^2}{T^2}\right)x^2 + \frac{\lambda}{4}x^4 \,, \tag{3.21}$$

where $T_0^2 = 4\mu^2/\lambda$. This can be written as $f(x) = a(T)x^2 + c(T)x^4$, with the temperature-dependent coefficients such that the quartic term is always positive, while the quadratic term is positive for $T > T_0$ and negative for $T < T_0$. $V^T_{\rm approx}(\phi)$ is plotted in Figure 3.3.

Defining $T_{\rm c}$ to be the critical temperature at which the origin of $V^T(\phi)$ has vanishing curvature, $f''(0) = 0$, we see that $T_{\rm c} = T_0$. This definition of $T_{\rm c}$ is suitable for describing a second-order phase transition, or the end of a first-order one. For a first-order phase transition, one may also define the critical temperature $\widetilde{T}$, at which two degenerate minima (the coexisting phases of symmetric and broken vacua) exist. For the purposes of this thesis, we will be interested almost exclusively in the critical temperature $T_{\rm c}$, which may be used to distinguish first-order behavior from second-order:

$$\left(\frac{\phi}{T}\right)_{\rm crit} \begin{cases} = 0 & \text{if second-order} \\ \neq 0 & \text{if first-order} \\ \gtrsim 1 & \text{if strongly first-order} \end{cases} . \tag{3.22}$$

In addition, $T_{\rm c}$ is the more appropriate definition when considering the survival of baryon number freshly generated during the phase transition, as in the analyses of Chapters 5, 6, and 7, since it describes conditions at the *end* of the phase transition.

We obtain the vacuum state and scalar mass from the first and second derivatives

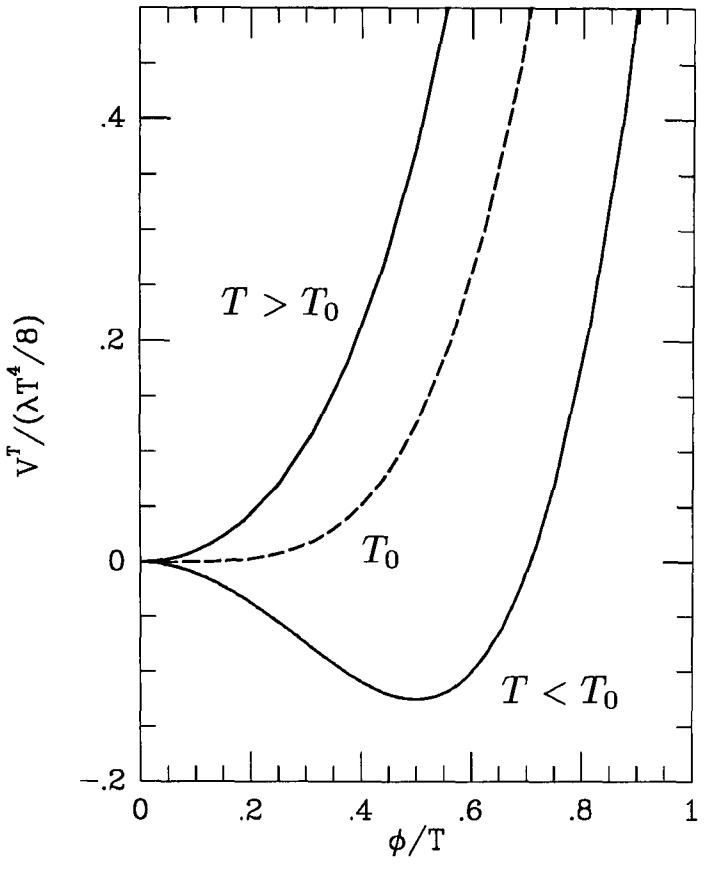

Figure 3.3: The effective potential in the scalar model, approximated to leading order in the temperature.

of $f(x)$:

$$f'(x) = \frac{\lambda}{4}x\left[\left(1-\frac{T_0^2}{T^2}\right)+4x^2\right] \tag{3.23}$$

$$f''(x) = \frac{\lambda}{4}\left(1-\frac{T_0^2}{T^2}\right)+3\lambda x^2\,. \tag{3.24}$$

Recall from (2.11) that $d^2V^T/d\phi^2$ gives the zero-momentum mass $\tilde{m}^2$ at finite temperature; this is the vacuum mass $m^2(\phi) = 3\lambda\phi^2 - \mu^2$ plus thermal corrections due to interactions (at one loop) with the heat bath, which we will later calculate explicitly. The resulting minima as functions of temperature and their related masses are as follows:

Symmetric minimum: $T > T_0$	Broken minimum: $T < T_0$
$x = 0$	$x_+^2 = \frac{1}{4}\left(T_0^2/T^2 - 1\right)$
$\tilde{m}^2 = \frac{\lambda}{4}\left(T^2 - T_0^2\right)$	$\tilde{m}^2 = \frac{\lambda}{2}\left(T_0^2 - T^2\right)$

(3.25)

The minimum $\phi/T(T)$ and mass $\tilde{m}^2(T)$ are shown in Figures 3.4 and 3.5. The broken minimum x_+ goes continuously into the symmetric minimum at $T = T_0$, at which point symmetry is restored and the mass vanishes. This approximation describes a second-order phase transition — at the critical point T_c, $\phi/T = 0$.

Let us continue the analysis and see whether this second-order behavior persists,

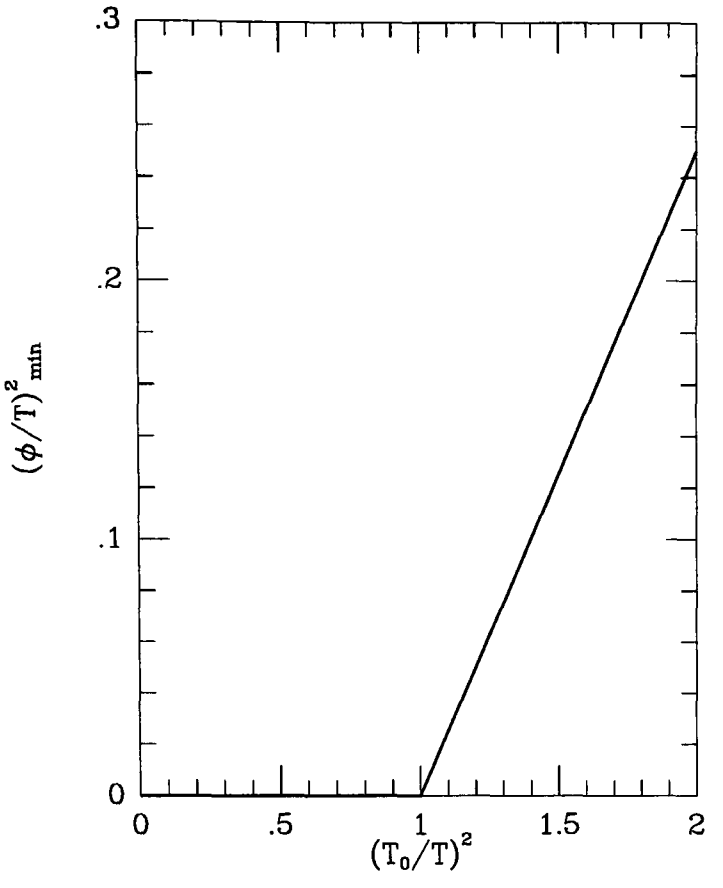

Figure 3.4: The minimum of the effective potential in the scalar model, approximated to leading order in the temperature.

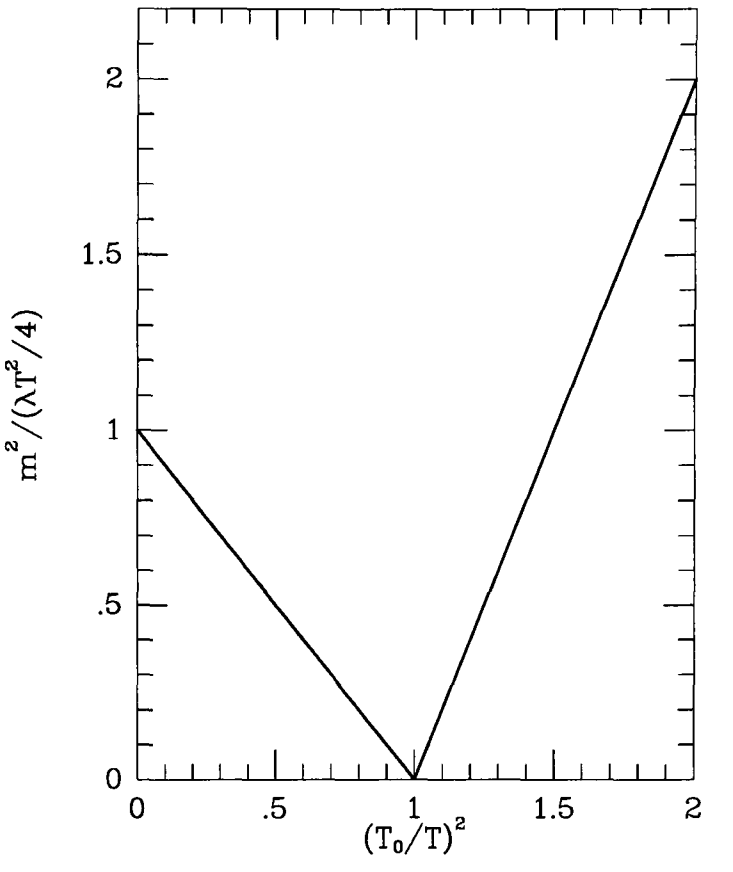

Figure 3.5: The mass squared at the minimum of the effective potential in the scalar model, approximated to leading order in the temperature.

by using the full effective potential at one loop in (3.19):

$$\begin{aligned} g(x) &\equiv \frac{V^T_{1\,\mathrm{loop}}}{T^4}\left(\frac{\phi}{T}\right) \\ &= \frac{\lambda}{8}\left[1-\frac{T_0^2}{T^2}+\frac{3M^2}{8\pi^2T^2}\log\left(\frac{M^2}{a'_BT^2}\right)\right]x^2 \\ &\quad +\frac{\lambda}{4}\left[1-\frac{9\lambda}{16\pi^2}\log\left(\frac{M^2}{a_BT^2}\right)\right]x^4-\frac{\lambda^{3/2}}{12\pi}\left[3x^2-\frac{v^2}{T^2}\right]^{3/2}. \end{aligned} \tag{3.26}$$

The first and second derivatives are then

$$\begin{aligned} g'(x) &= x\left\{\frac{\lambda}{4}\left[1-\frac{T_0^2}{T^2}+\frac{3M^2}{8\pi^2T^2}\log\left(\frac{M^2}{a'_BT^2}\right)\right]+\lambda\left[1-\frac{9\lambda}{16\pi^2}\log\left(\frac{M^2}{a_BT^2}\right)\right]x^2\right. \\ &\quad \left.-\frac{3\lambda^{3/2}}{4\pi}\left[3x^2-\frac{v^2}{T^2}\right]^{1/2}\right\} \end{aligned} \tag{3.27}$$

$$\begin{aligned} g''(x) &= \frac{\lambda}{4}\left[1-\frac{T_0^2}{T^2}+\frac{3M^2}{8\pi^2T^2}\log\left(\frac{M^2}{a'_BT^2}\right)\right]+3\lambda\left[1-\frac{9\lambda}{16\pi^2}\log\left(\frac{M^2}{a_BT^2}\right)\right]x^2 \\ &\quad -\frac{3\lambda^{3/2}}{4\pi}\left[3x^2-\frac{v^2}{T^2}\right]^{1/2}-\frac{9\lambda^{3/2}}{4\pi}\frac{x^2}{\left[3x^2-\frac{v^2}{T^2}\right]^{1/2}}. \end{aligned} \tag{3.28}$$

The critical temperature, defined by $g''(0) = 0$, is given implicitly by the relation

$$\frac{\lambda}{4}\left[1 - \frac{T_0^2}{T_c^2} + \frac{3M^2}{8\pi^2 T_c^2}\log\left(\frac{M^2}{a'_B T_c^2}\right)\right] = \frac{3\lambda^{3/2}}{4\pi}\left[-\frac{v^2}{T_c^2}\right]^{1/2} , \tag{3.29}$$

which may be approximated as

$$T_c^2 \approx T_0^2 - \frac{3M^2}{8\pi^2}\log\left(\frac{M^2}{a'_B T_0^2}\right) , \tag{3.30}$$

where we have neglected the imaginary term.

Notice that the piece $m^3(\phi)/T^3 \sim \lambda^{3/2}\left[3x^2 - v^2/T^2\right]^{3/2}$ leads to imaginary terms in the effective potential and physical quantities obtained from it. It has been shown [26] that the emergence of imaginary terms in the perturbative effective potential indicates a physical instability, and in fact, the imaginary part of V^T is simply half the rate per unit volume of vacuum decay by perturbative processes; the real part is the usual expectation value of the energy density, which can be used to diagnose the nature of the phase transition. Henceforth all physical quantities (e.g., the critical temperature and scalar mass) will be extracted from the real part of V^T.

$V^T_{1\,\mathrm{loop}}$ can be written as $g(x) = a(T)x^2 + c(T)x^4 - (\lambda^{3/2}/12\pi)[3x^2 - v^2/T^2]^{3/2}$. As in our previous approximation $f(x)$, the quartic term is positive, and the quadratic term is positive or negative depending on whether T is greater or less than T_c. Here, however, the cubic term leads to an energy barrier at the critical point. We plot $V^T_{1\,\mathrm{loop}}(\phi)$ in Figure 3.6 and observe first-order behavior at the phase transition. Thus, the second-order behavior of $f(x)$ was simply an artifact of the approximation used.

The minimum and the corresponding mass, as functions of the temperature, are given by the following expressions:

Symmetric minimum: $T > \widetilde{T}$ (3.31)

$$\begin{aligned} x &= 0 \\ \frac{\widetilde{m}^2}{T^2} &= \frac{\lambda}{4}\left[1 - \frac{T_0^2}{T^2} + \frac{3M^2}{8\pi^2 T^2}\log\left(\frac{M^2}{a'_B T^2}\right)\right] - \frac{3\lambda^{3/2}}{4\pi}\left[-\frac{v^2}{T^2}\right]^{1/2} \end{aligned}$$

Broken minimum: $T < \widetilde{T}$ (3.32)

$$\begin{aligned} \frac{\lambda}{4}\left[1 - \frac{T_0^2}{T^2} + \frac{3M^2}{8\pi^2 T^2}\log\left(\frac{M^2}{a'_B T^2}\right)\right] + \lambda\left[1 - \frac{9\lambda}{16\pi^2}\log\left(\frac{M^2}{a_B T^2}\right)\right] x_+^2 \\ = \frac{3\lambda^{3/2}}{4\pi}\left[3x_+^2 - \frac{v^2}{T^2}\right]^{1/2} \\ \frac{\widetilde{m}^2}{T^2} = -\frac{\lambda}{2}\left[1 - \frac{T_0^2}{T^2} + \frac{3M^2}{8\pi^2 T^2}\log\left(\frac{M^2}{a'_B T^2}\right)\right] \end{aligned}$$

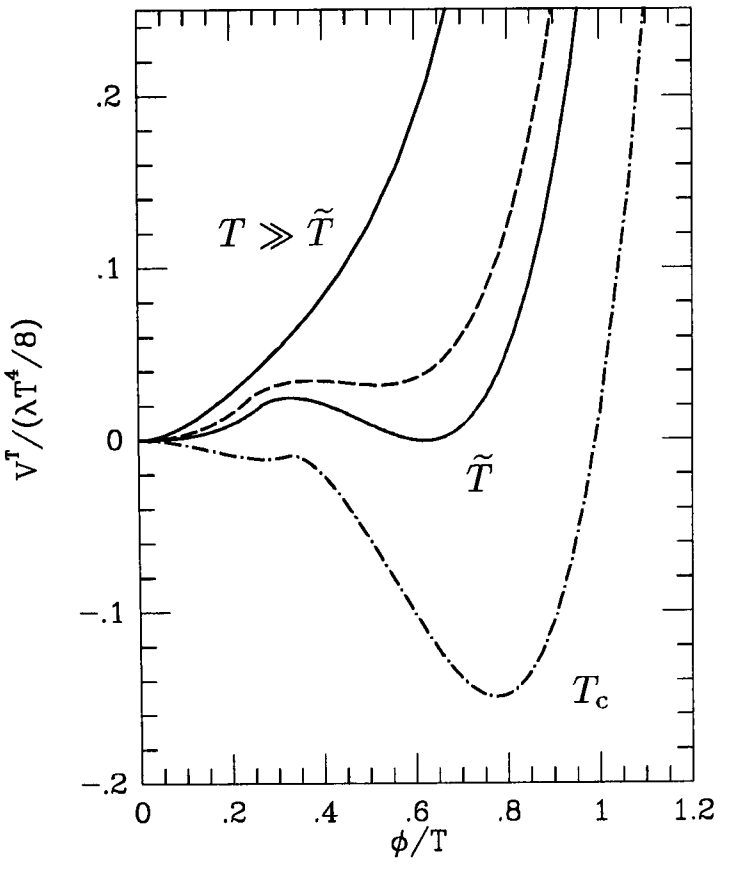

Figure 3.6: The effective potential at one loop in the scalar model.

$$+\frac{3\lambda^{3/2}}{2\pi}\left[3x_+^2-\frac{v^2}{T^2}\right]^{1/2}-\frac{9\lambda^{3/2}}{4\pi}\frac{x_+^2}{\left[3x_+^2-\frac{v^2}{T^2}\right]^{1/2}}$$

$$=\ x_+^2\left\{2\lambda\left[1-\frac{9\lambda}{16\pi^2}\log\left(\frac{M^2}{a_BT^2}\right)\right]-\frac{9\lambda^{3/2}}{4\pi}\left[3x_+^2-\frac{v^2}{T^2}\right]^{-1/2}\right\}\ .$$

$\tilde{m}^2$ here includes the one-loop corrections due to vacuum and thermal interactions, whereas our previous $\tilde{m}^2$, computed from $f(x)$ in (3.25), only included the leading thermal corrections $\propto T^2$. The minimum $\phi/T(T)$ and mass $\tilde{m}^2(T)$ are shown in Figures 3.7 and 3.8. The broken minimum jumps discontinuously to the symmetric minimum at $T=\tilde{T}$, at which point symmetry is restored, although the mass remains greater than zero.

We examine the critical point in greater detail. At T_c, the asymmetric minimum $x_{\rm crit}=(\phi/T)_{\rm crit}$ is given by

$$\lambda\left[1-\frac{9\lambda}{16\pi^2}\log\left(\frac{M^2}{a_BT_c^2}\right)\right]x_{\rm crit}=\frac{3\lambda^{3/2}}{4\pi x_{\rm crit}}\left[\left(3x_{\rm crit}^2-\frac{v^2}{T_c^2}\right)^{1/2}-\left(-\frac{v^2}{T_c^2}\right)^{1/2}\right]\ , \quad (3.33)$$

where the mass is

$$\frac{\tilde{m}^2}{T^2}=\frac{3\lambda^{3/2}}{2\pi}\left[\left(3x_{\rm crit}^2-\frac{v^2}{T_c^2}\right)^{1/2}-\left(-\frac{v^2}{T_c^2}\right)^{1/2}\right]-\frac{9\lambda^{3/2}}{4\pi}\frac{x_{\rm crit}^2}{\left[3x_{\rm crit}^2-\frac{v^2}{T_c^2}\right]^{1/2}}\ . \quad (3.34)$$

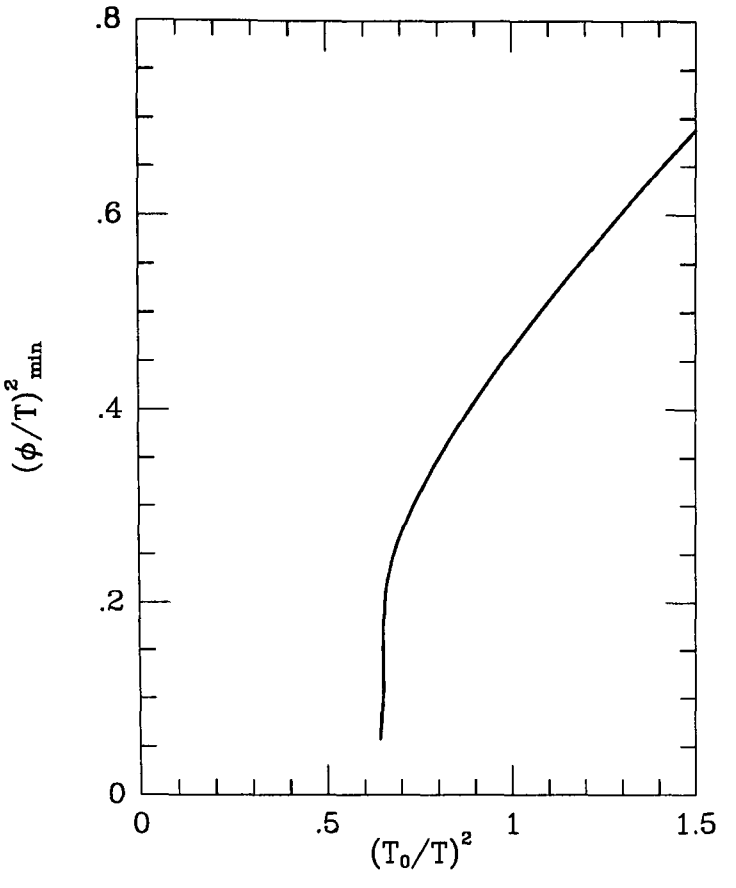

Figure 3.7: The minimum of the one-loop effective potential in the scalar model.

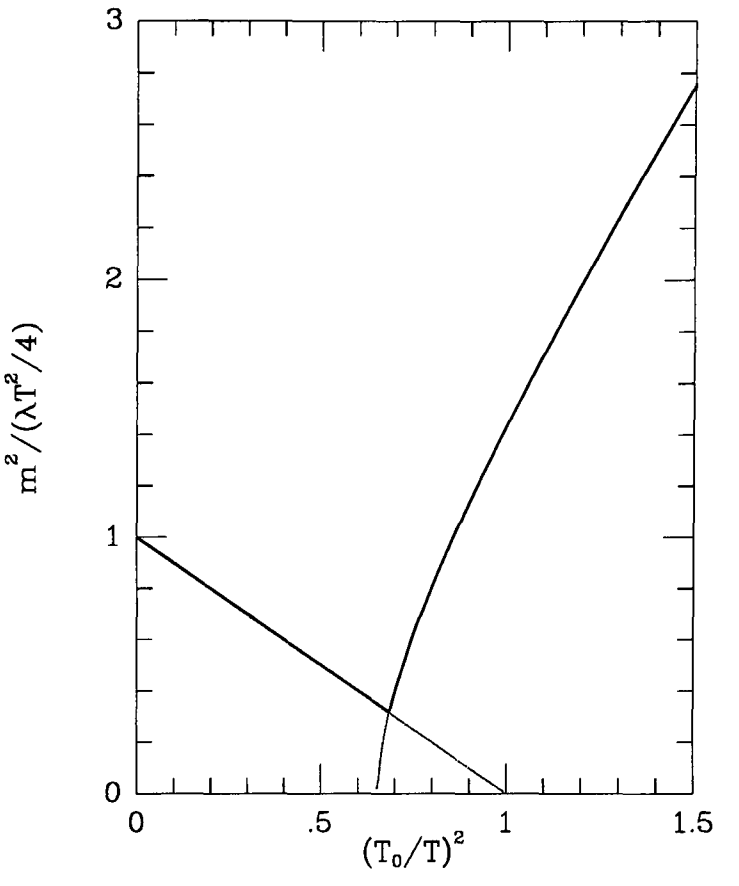

Figure 3.8: The mass squared at the minimum of the one-loop effective potential in the scalar model.

If $x_{\rm crit} > 0$ is a solution to (3.33) (hence implying first-order behavior), then the mass is necessarily positive: $g''(x_{\rm crit}) > 0$. Even without explicitly solving for $x_{\rm crit}$ as a function of the parameters λ and M, we may obtain a stability bound from (3.34) by requiring that the curvature be real and positive. It is clear by inspection that the solution does not exist (and the mass is imaginary) for $(\phi/T)^2_{\rm crit} < v^2/(3T_c^2)$. Expanding $g''(x_{\rm crit})$ for small and large values of $x_{\rm crit}$, we see that

$$x^2_{\rm crit} \ll v^2/T_c^2 :$$

$$g''(x_{\rm crit}) \approx \frac{27}{16\pi}\lambda^{3/2}x^4_{\rm crit}\left(-\frac{v^2}{T_c^2}\right)^{-3/2} \tag{3.35}$$

$$x^2_{\rm crit} \gg v^2/T_c^2 :$$

$$g''(x_{\rm crit}) \approx \frac{3\sqrt{3}}{4\pi}\lambda^{3/2}x_{\rm crit} \, . \tag{3.36}$$

The mass is positive for large $x_{\rm crit}$, and therefore $(\phi/T)_{\rm crit}$ must satisfy $x^2_{\rm crit} \gtrsim v^2/3T_c^2 \approx 1/12$ for all values of λ and M. Expressions of the type (3.33) and (3.34) may be employed to obtain constraints on the parameters by requiring that the phase transition be strongly first-order ($(\phi/T)_{\rm crit} \gtrsim 1$), as we will see later.

This analysis depicts a phase transition that proceeds as follows. At extremely high temperatures, $T \gg v$, the symmetry is unbroken and $\langle\Phi\rangle = 0$ is the unique vacuum.

As the system cools down to a temperature $T \gtrsim \widetilde{T} > T_c$, an asymmetric (local) minimum appears, which becomes degenerate with the symmetric minimum when $T = \widetilde{T}$, at which point vacuum tunneling commences in earnest. There is supercooling of the metastable symmetric minimum until $T \sim T_c < \widetilde{T}$, during which time it gradually decays to the stable broken minimum. The decay process occurs as bubbles of true vacuum nucleate in the sea of false vacuum, at a rate that can be computed using the theory of vacuum tunneling at finite temperature [27, 28]. The bubbles of $\langle\Phi\rangle \neq 0$ propagate and percolate through the sea of false vacuum, and eventually coalesce to fill all space. And if the phase transition is sufficiently strongly first-order, entropy is generated. As the temperature falls below $T \sim v$, thermal effects become negligible, conventional perturbation theory becomes valid (and our high-temperature approximation invalid), and $\langle\Phi\rangle$ seeks the minimum of $V^T \sim V_{\text{tree}}$. A condensate of zero-momentum bosons forms, reflecting an inherent ordering in the vacuum.

There remain serious problems with the description just portrayed, however, and as we will see in Section 3.3, a more reliable description of the phase transition must account for infrared divergences.

3.2 The Abelian Higgs Model

Before delving into infrared divergences in the next section, let us consider a phase transition in another simple context. We choose the Abelian Higgs model because it illustrates the generic features — to be encountered later in the Standard Model — of infrared divergences due to both scalar and gauge fields. The treatment builds on that developed for the scalar model.

Notation

The Abelian Higgs model is scalar electrodynamics with spontaneous symmetry breaking. It is defined by the following $U(1)$-invariant Lagrangian:

$$\mathcal{L} = \mathcal{L}_{\text{gauge}} + \mathcal{L}_{\text{Higgs}} + \mathcal{L}_{\text{gauge-fixing}} + \mathcal{L}_{\text{ghost}} + \mathcal{L}_{\text{c.t.}} \,. \tag{3.37}$$

The gauge kinetic term is given by

$$\mathcal{L}_{\text{gauge}} = -\frac{1}{4} F_{\mu\nu} F^{\mu\nu}, \tag{3.38}$$

with the field-strength tensor $F_{\mu\nu} = \partial_\mu A_\nu - \partial_\nu A_\mu$. The Higgs field Lagrangian is

$$\mathcal{L}_{\text{Higgs}} = (D_\mu \Phi)^\dagger (D^\mu \Phi) - U(\Phi) \,, \tag{3.39}$$

where the covariant derivative $D_\mu\Phi$ and the classical potential $U(\Phi)$ are given by

$$D_\mu \Phi = (\partial_\mu + ieA_\mu)\Phi \tag{3.40}$$

and

$$U(\Phi) = -\mu^2 \Phi^\dagger \Phi + \lambda (\Phi^\dagger \Phi)^2 \, . \tag{3.41}$$

The mass parameter $\mu^2 > 0$, so that the classical potential $U(\Phi)$ describes a spontaneous breakdown of the $U(1)$ symmetry at zero temperature; the minimum of $U(\Phi)$ occurs at $|\Phi|^2 = \mu^2/2\lambda \equiv v^2/2$, where $d^2U/d|\Phi|^2 = 4\mu^2$ (Figure 3.9).

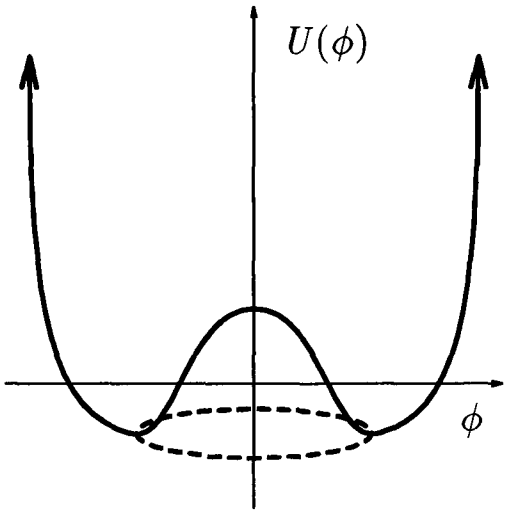

Figure 3.9: The classical potential for the Abelian Higgs model.

At finite temperature, the physical system favors the state that minimizes its free energy density V^T. If this minimum-energy state develops a non-zero thermal average, $\langle \Phi \rangle \neq 0$, the $U(1)$ symmetry is spontaneously broken; otherwise it is restored. Choosing $\langle \Phi \rangle$ to be real, we denote it by $\langle \Phi \rangle = \phi/\sqrt{2}$ and expand the field Φ about its Poincaré-invariant thermal average:

$$\Phi = \frac{1}{\sqrt{2}}(\phi + \chi_1 + i\chi_2) \tag{3.42}$$

where $\langle \chi_1 \rangle = \langle \chi_2 \rangle = 0$. The thermal average as a function of the temperature, $\langle \Phi \rangle(T)$, is to be determined by minimizing the effective potential $V^T(\phi)$. Shifting by ϕ in $\mathcal{L}_{\text{Higgs}}$ gives rise to masses $m_1^2(\phi) = -\mu^2 + 3\lambda\phi^2 = \lambda(3\phi^2 - v^2)$ for the Higgs field χ_1, $m_2^2(\phi) = -\mu^2 + \lambda\phi^2 = \lambda(\phi^2 - v^2)$ for the Goldstone field χ_2, and $m_A^2(\phi) = e^2\phi^2$ for the photon field.

We eliminate mixing of the Goldstone and photon fields in the shifted $\mathcal{L}_{\text{Higgs}}$ (from the cross term $e\phi\partial_\mu\chi_2 A^\mu$ in $|D_\mu\Phi|^2$) by choosing the R_ξ class of renormalizable gauges, where the gauge-fixing Lagrangian is

$$\mathcal{L}_{\text{gauge-fixing}} = -\frac{1}{2\xi}(\partial_\mu A^\mu - \xi e\phi\chi_2)^2 .$$

In analogy with our later analysis of the Standard Model, we work in Landau gauge, $\xi \to 0$, so that

$$\mathcal{L}_{\text{gauge-fixing}} \longrightarrow -\frac{1}{2\xi}(\partial_\mu A^\mu)^2 + e\phi\chi_2\partial_\mu A^\mu \, , \tag{3.43}$$

ensuring that only gauge configurations with $\partial_\mu A^\mu = 0$ contribute to the functional integral. The cross term combines with that from $|D_\mu \Phi|^2$ in $\mathcal{L}_{\text{Higgs}}$ to produce a total divergence that vanishes upon integration. The effective potential will depend on the gauge, but the physical quantities we obtain from it will not. As in quantum electrodynamics,

$$\mathcal{L}_{\text{ghost}} = -\overline{\omega}\partial^2\omega \ ; \tag{3.44}$$

Abelian ghost fields are non-interacting, decoupling from the effective potential, and henceforth will be ignored. Finally we take a counter-term Lagrangian of the form

$$\mathcal{L}_{\text{c.t.}} = A(\partial_\mu\Phi)^\dagger(\partial^\mu\Phi) + B\Phi^\dagger\Phi + C(\Phi^\dagger\Phi)^2 + D \ , \tag{3.45}$$

since computation of the effective potential requires only that we renormalize Φ explicitly.

Performing the shift (3.42) and neglecting constants and total divergences, we express the Lagrangian as the sum of a quadratic part and an interacting part:

$$\mathcal{L} = \mathcal{L}_0 + \mathcal{L}_{\text{I}} \ , \tag{3.46}$$

where

$$\begin{aligned} \mathcal{L}_0 \ = \ & -\frac{1}{4}F_{\mu\nu}F^{\mu\nu} - \frac{1}{2\xi}(\partial_\mu A^\mu)^2 + \frac{m_A^2(\phi)}{2}A_\mu A^\mu \\ & + \frac{1}{2}(\partial_\mu\chi_1)(\partial^\mu\chi_1) - \frac{m_1^2(\phi)}{2}\chi_1^2 + \frac{1}{2}(\partial_\mu\chi_2)(\partial^\mu\chi_2) - \frac{m_2^2(\phi)}{2}\chi_2^2 \end{aligned} \tag{3.47}$$

and

$$\begin{aligned} \mathcal{L}_{\text{I}} \ = \ & -\lambda\phi\,\chi_1\left(\chi_1^2+\chi_2^2\right) - \frac{\lambda}{4}\left(\chi_1^4+\chi_2^4+2\,\chi_1^2\chi_2^2\right) + (\mu^2\phi - \lambda\phi^3)\,\chi_1 \\ & + e^2\phi\,\chi_1 A_\mu A^\mu + \frac{e^2}{2}\left(\chi_1^2+\chi_2^2\right)A_\mu A^\mu \\ & + e\,(\chi_1\partial_\mu\chi_2 - \chi_2\partial_\mu\chi_1)\,A^\mu + (\text{counter-terms}) \ . \end{aligned} \tag{3.48}$$

Effective Potential at One Loop

We compute the effective potential by the method of tadpoles. At lowest order we get the tree-level contributions from the classical potential and the counter-term Lagrangian:

$$U(\phi) = -\frac{\mu^2}{2}\phi^2 + \frac{\lambda}{4}\phi^4 \tag{3.49}$$

and

$$V_{\text{c.t.}}(\phi) = -\frac{B}{2}\phi^2 - \frac{C}{4}\phi^4 - D \ . \tag{3.50}$$

At next order, we obtain terms from scalar and gauge loops, depicted in Figure 3.10. The scalar contributions are identical to that computed for the scalar model in the

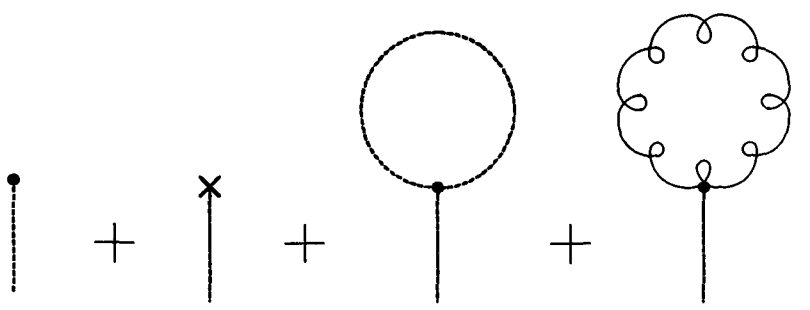

Figure 3.10: The tadpole graphs for the one-loop effective potential in the Abelian Higgs model.

previous section, so we need only compute explicitly the gauge contribution, which has the form

$$\begin{aligned}\frac{dV}{d\phi}(\phi) &= -e^2\phi g^{\mu\nu}\int\frac{d^4k}{(2\pi)^4}\,\frac{-i(g_{\mu\nu}-k_\mu k_\nu/k^2)}{k^2-m_A^2(\phi)+i\varepsilon} \\ &= \frac{3}{2}\frac{dm_A^2}{d\phi}(\phi)\,T\sum_n\int\frac{d^3\vec{k}}{(2\pi)^3}\,\frac{1}{(2\pi nT)^2+\vec{k}^2+m_A^2(\phi)}\,. \end{aligned} \tag{3.51}$$

We express this as a contour integral, separate the zero- and finite-temperature pieces, and integrate, to derive the standard expression

$$V(\phi) = \frac{3}{2}\int\frac{d^4k_{\rm E}}{(2\pi)^4}\,\log\left(k_{\rm E}^2+m_1^2(\phi)\right) + 3T^4 I_B\left(\frac{m_1(\phi)}{T}\right). \tag{3.52}$$

Near the phase transition, $T\sim\mu/\sqrt{\lambda}$ or μ/e, and the high-temperature expansion (3.12) gives a valid approximation to the effective potential.

Combining the Higgs, Goldstone, and photon contributions at one loop, we obtain the unrenormalized one-loop effective potential:

$$V_{1\,\rm loop}^T(\phi) = V^0(\phi) + \Delta V^T(\phi) \tag{3.53}$$

where

$$\begin{aligned}V^0(\phi) &= U(\phi)+V_{\rm c.t.}(\phi) \\ &\quad+\frac{1}{2}\int\frac{d^4k_{\rm E}}{(2\pi)^4}\,\log\left(k_{\rm E}^2+m_1^2(\phi)\right)+\frac{1}{2}\int\frac{d^4k_{\rm E}}{(2\pi)^4}\,\log\left(k_{\rm E}^2+m_2^2(\phi)\right) \\ &\quad+\frac{3}{2}\int\frac{d^4k_{\rm E}}{(2\pi)^4}\,\log\left(k_{\rm E}^2+m_A^2(\phi)\right)\end{aligned} \tag{3.54}$$

and

$$\Delta V^T(\phi) = T^4 I_B\left(\frac{m_1(\phi)}{T}\right)+T^4 I_B\left(\frac{m_2(\phi)}{T}\right)+3\,T^4 I_B\left(\frac{m_A(\phi)}{T}\right). \tag{3.55}$$

$V_{1\,\rm loop}^T(\phi)$ is the free energy of an ideal gas of scalar and gauge particles in the background field ϕ. Because finite temperature effects introduce no new ultraviolet diver-

gences, we need only renormalize the zero-temperature piece V^0. For convenience, we choose a renormalization prescription that preserves the tree-level values for the location of the minimum (at $v = \mu/\sqrt{\lambda}$) as well as the Higgs mass ($M_1^2 = 2\lambda v^2$) at this minimum:

$$\left.\frac{dV^0}{d\phi}\right|_{\phi=v} = 0 \tag{3.56}$$

$$\left.\frac{d^2V^0}{d\phi^2}\right|_{\phi=v} = M_1^2 \,. \tag{3.57}$$

These conditions determine B and C; D is chosen to cancel the constant part of V^0, and A, which is superfluous for the purpose of computing V^0, is determined by requiring that the thermal propagator have unit residue.

Renormalization results in the final expression for the zero-temperature effective potential at one loop:

$$\begin{aligned} V^0(\phi) = & -\frac{\mu^2}{2}\left(1 - \frac{3\lambda}{4\pi^2} - \frac{3e^4}{16\pi^2\lambda}\right)\phi^2 + \frac{1}{4}\left(\lambda - \frac{15\lambda^2}{16\pi^2} - \frac{9e^4}{32\pi^2}\right)\phi^4 \\ & + \frac{m_1^4(\phi)}{64\pi^2}\log\left(\frac{m_1^2(\phi)}{M_1^2}\right) + \frac{m_2^4(\phi)}{64\pi^2}\log\left(\frac{m_2^2(\phi)}{M_2^2}\right) + \frac{3m_A^4(\phi)}{64\pi^2}\log\left(\frac{m_A^2(\phi)}{M_A^2}\right) . \end{aligned} \tag{3.58}$$

Here and in the following, M_j denotes the zero-temperature mass, $M_j^2 = m_j^2(v)$. Also, because $M_2^2 = 0$, $\log M_2^2$ leads to an infinity that reflects the running of the physical mass off-shell to zero momentum, which we neglect [29]. Adding the finite-temperature piece (3.55) and using the high-temperature expansion for I_B (3.12), the effective potential at one loop may be approximated as

$$\begin{aligned} V_{1\,\mathrm{loop}}^T(\phi) = & \frac{\phi^2}{2}\left[-\mu^2 + \left(\frac{\lambda}{4} + \frac{\lambda}{12} + \frac{e^2}{4}\right)T^2 + \frac{3\lambda M_1^2}{32\pi^2}\log\left(\frac{M_1^2}{a_B' T^2}\right)\right. \\ & \left. + \frac{\lambda M_2^2}{16\pi^2} + \frac{\lambda\mu^2}{16\pi^2}\log\left(\frac{M_2^2}{a_B T^2}\right) + \frac{3e^2 M_A^2}{16\pi^2}\right] \\ & + \frac{\phi^4}{4}\left[\lambda - \frac{9\lambda^2}{16\pi^2}\log\left(\frac{M_1^2}{a_B T^2}\right) - \frac{\lambda^2}{16\pi^2}\log\left(\frac{M_2^2}{a_B T^2}\right) - \frac{3e^4}{16\pi^2}\log\left(\frac{M_A^2}{a_B T^2}\right)\right] \\ & - \frac{T}{12\pi}\left\{\lambda^{3/2}\left(3\phi^2 - v^2\right)^{3/2} + \lambda^{3/2}\left(\phi^2 - v^2\right)^{3/2} + 3e^3\phi^3\right\} . \end{aligned} \tag{3.59}$$

This expression has been written in a form that separates the contributions due to scalar, Goldstone, and gauge fields (compare to the scalar result of (3.19) and note the cancelation of the $m_j^4 \log m_j^2$ terms). One may obtain the effective potential valid at lower temperature, by numerically evaluating the integral I_B, (3.12).

We note that the nature of the phase transition depends highly on the relation between the couplings λ and e [30]. Interesting effects may occur for large or small

values of e^2/λ. For instance, the quadratic term of V^0 in (3.58) becomes positive for $\lambda \lesssim 3e^4/(16\pi^2) \ll e^2$, so that the spontaneously broken symmetry may be restored by quantum effects even at zero temperature. These cases, however, obtain only for certain ranges of parameter space and will be irrelevant for our purposes, since we take $e^4 \ll \lambda \sim e^2$ as in the Standard Model.

The Phase Transition

To gain some insight into the phase transition, let us first approximate V^T, as in the scalar model previously, by including only the leading thermal contributions ($\propto m_i^2/T^2$) in the expansion (3.12). In this case, the effective potential becomes

$$\begin{aligned} V^T_{\text{approx}}(\phi) &= V_{\text{tree}} + \frac{\phi^2}{2}\left(\frac{\lambda}{3} + \frac{e^2}{4}\right)T^2 \\ &= \frac{\phi^2}{2}\left[-\mu^2 + \left(\frac{\lambda}{3} + \frac{e^2}{4}\right)T^2\right] + \frac{\lambda}{4}\phi^4 \,. \end{aligned} \tag{3.60}$$

Scaling V^T and ϕ by the temperature, $x \equiv \phi/T$ and $f(x) = V^T_{\text{approx}}/T^4$, we have

$$f(x) = \frac{1}{2}\left(\frac{\lambda}{3} + \frac{e^2}{4}\right)\left[1 - \frac{T_0^2}{T^2}\right]x^2 + \frac{\lambda}{4}x^4 \,, \tag{3.61}$$

where $T_0^2 = 12\mu^2/(4\lambda + 3e^2)$. This can be written as $f(x) = a(T)x^2 + c(T)x^4$, with the temperature-dependent coefficients such that the quartic term is always positive, while the quadratic term is positive or negative for $T > T_0$ or $T < T_0$. The effective potential $V^T_{\text{approx}}(\phi)$ resembles that of the scalar model, depicted in Figure 3.3. Defining the critical temperature T_c as the temperature when the origin of $V^T(\phi)$ has vanishing curvature, $T_c = T_0$.

We find the vacuum state and scalar mass from the first and second derivatives of $f(x)$:

$$f'(x) = x\left[\left(\frac{\lambda}{3} + \frac{e^2}{4}\right)\left(1 - \frac{T_0^2}{T^2}\right) + \lambda x^2\right] \tag{3.62}$$

$$f''(x) = \left(\frac{\lambda}{3} + \frac{e^2}{4}\right)\left(1 - \frac{T_0^2}{T^2}\right) + 3\lambda x^2 \,. \tag{3.63}$$

Recall from (2.11) that $d^2V^T/d\phi^2$ gives the zero-momentum mass $\tilde{m}_1^2$ at finite temperature; this is the vacuum mass plus thermal corrections due to interactions (at one loop) with the heat bath, which we calculate in the next section. The resulting minima

as functions of temperature and their related masses are as follows:

Symmetric minimum: $T > T_0$	Broken minimum: $T < T_0$
$x = 0$	$x_+^2 = \left(\frac{1}{3} + \frac{e^2}{4\lambda}\right)(T_0^2/T^2 - 1)$
$\tilde{m}_1^2 = \left(\frac{\lambda}{3} + \frac{e^2}{4}\right)(T^2 - T_0^2)$	$\tilde{m}_1^2 = 2\left(\frac{\lambda}{3} + \frac{e^2}{4}\right)(T_0^2 - T^2)$

(3.64)

The minimum $\phi/T(T)$ and mass $\tilde{m}_1^2(T)$ take the forms shown in Figures 3.4 and 3.5 for the scalar model. The broken minimum goes continuously into the symmetric minimum at $T = T_0$, at which point symmetry is restored and the mass vanishes. This approximation describes a second-order phase transition: $(\phi/T)_{\text{crit}} = 0$.

It should be mentioned for completeness that the thermally-corrected masses for the Goldstone and gauge modes can be calculated as well: [2]

Symmetric minimum: $T > T_0$	Broken minimum: $T < T_0$
$\tilde{m}_2^2 = \left(\frac{\lambda}{3} + \frac{e^2}{4}\right)(T^2 - T_0^2)$	$\tilde{m}_2^2 = 0$
$\tilde{m}_A^2(00) = \frac{e^2}{3}T^2$	$\tilde{m}_A^2(00) = e^2\left(\frac{1}{3} + \frac{e^2}{4\lambda}\right)(T_0^2 - T^2) + \frac{e^2}{3}T^2$
$\tilde{m}_A^2(jj) = 0$	$\tilde{m}_A^2(jj) = e^2\left(\frac{1}{3} + \frac{e^2}{4\lambda}\right)(T_0^2 - T^2)$

(3.65)

We see that, with thermal corrections taken into account, the Goldstone mode is massless when the symmetry is broken, as we know from the Goldstone theorem at finite temperature. Also, the longitudinal ($\tilde{m}_A^2(00)$) and transverse ($\tilde{m}_A^2(jj)$) components of the gauge field have different thermal masses, owing to the lack of a magnetic mass Π_A^{jj} at one loop; we will see this in more detail later.

Thus we have the following picture of a second-order phase transition:

- $T < T_c$: the symmetry is spontaneously broken and the system occupies the asymmetric vacuum $x_+ > 0$; the scalar mass $\tilde{m}_1^2 > 0$, the gauge mass $\tilde{m}_A^2 > 0$, while the Goldstone mode is massless, $\tilde{m}_2^2 = 0$.

- $T = T_c$: the scalar and Goldstone modes are both massless (a characteristic feature of second-order phase transitions, in which correlation lengths diverge); the gauge masses $\tilde{m}_A^2(00) = e^2T^2/3$, $\tilde{m}_A^2(jj) = 0$. [3]

- $T > T_c$: the symmetry is restored and the system assumes the symmetric vacuum $x = 0$; the scalar and Goldstone masses are identical, $\tilde{m}_1^2 = \tilde{m}_2^2 > 0$, and the gauge field has just the plasma mass $\tilde{m}_A^2(00) = e^2T^2/3$.

To see whether this second-order behavior is simply an artifact of our approxima-

[2] In general, $\tilde{m}_i^2 = m_i^2 + \Pi_i(0)$, where $m_i^2(\phi)$ is the mass at zero temperature and $\Pi_i(0)$ the thermal self-energy at zero momentum. $\Pi_i(0)$ at one loop will be computed in Section 3.3.

[3] This is at one loop; at two loops, however, $\tilde{m}_A^2(jj) \propto e^4T^2$. See Section 3.3.

tion, let us now employ the full effective potential at one loop, (3.59):

$$\begin{aligned} g(x) &\equiv \frac{V_{1\,\mathrm{loop}}^{T}}{T^4}\left(\frac{\phi}{T}\right) \\ &= \frac{1}{2}\left[\left(\frac{\lambda}{3}+\frac{e^2}{4}\right)\left(1-\frac{T_0^2}{T^2}\right)+\frac{3\lambda M_1^2}{32\pi^2T^2}\log\left(\frac{M_1^2}{a_B'T^2}\right)\right. \\ &\qquad \left.+\frac{\lambda M_2^2}{16\pi^2T^2}+\frac{3e^2M_A^2}{16\pi^2T^2}+\frac{\lambda\mu^2}{16\pi^2T^2}\log\left(\frac{M_2^2}{a_BT^2}\right)\right]x^2 \\ &\quad +\frac{1}{4}\left[\lambda-\frac{9\lambda^2}{16\pi^2}\log\left(\frac{M_1^2}{a_BT^2}\right)-\frac{\lambda^2}{16\pi^2}\log\left(\frac{M_2^2}{a_BT^2}\right)-\frac{3e^4}{16\pi^2}\log\left(\frac{M_A^2}{a_BT^2}\right)\right]x^4 \\ &\quad -\frac{1}{12\pi}\left[\lambda^{3/2}\left(3x^2-\frac{v^2}{T^2}\right)^{3/2}+\lambda^{3/2}\left(x^2-\frac{v^2}{T^2}\right)^{3/2}+3e^3x^3\right]. \end{aligned} \tag{3.66}$$

For convenience, we cast this in the form

$$\begin{aligned} g(x) &= \frac{1}{2}a(T)x^2+\frac{1}{4}c(T)x^4 \\ &\quad -\frac{1}{12\pi}\left[\lambda^{3/2}\left(3x^2-\frac{v^2}{T^2}\right)^{3/2}+\lambda^{3/2}\left(x^2-\frac{v^2}{T^2}\right)^{3/2}+3e^3x^3\right]. \end{aligned} \tag{3.67}$$

The first and second derivatives are then

$$\begin{aligned} g'(x) &= x\left\{a(T)+c(T)x^2\right. \\ &\quad \left.-\frac{1}{4\pi}\left[3\lambda^{3/2}\left(3x^2-\frac{v^2}{T^2}\right)^{1/2}+\lambda^{3/2}\left(x^2-\frac{v^2}{T^2}\right)^{1/2}+3e^3x\right]\right\} \end{aligned} \tag{3.68}$$

$$\begin{aligned} g''(x) &= a(T)+3c(T)x^2 \\ &\quad -\frac{1}{4\pi}\left[3\lambda^{3/2}\left(3x^2-\frac{v^2}{T^2}\right)^{1/2}+\lambda^{3/2}\left(x^2-\frac{v^2}{T^2}\right)^{1/2}+3e^3x\right] \\ &\quad -\frac{x}{4\pi}\left[9\lambda^{3/2}x\left(3x^2-\frac{v^2}{T^2}\right)^{-1/2}+\lambda^{3/2}x\left(x^2-\frac{v^2}{T^2}\right)^{-1/2}+3e^3\right]. \end{aligned} \tag{3.69}$$

The critical temperature, defined by $g''(0)=0$, is given implicitly by the relation

$$a(T_c)=\frac{\lambda^{3/2}}{\pi}\left(-\frac{v^2}{T_c^2}\right)^{1/2}, \tag{3.70}$$

which may be approximated by

$$T_c^2 \approx T_0^2-\frac{T_0^2}{\mu^2}\left[\frac{3\lambda M_1^2}{32\pi^2}\log\left(\frac{M_1^2}{a_B'T_0^2}\right)+\frac{\lambda M_2^2}{16\pi^2}+\frac{3e^2M_A^2}{16\pi^2}+\frac{\lambda\mu^2}{16\pi^2}\log\left(\frac{M_2^2}{a_BT_0^2}\right)\right], \tag{3.71}$$

again neglecting the imaginary term. Notice the reappearance of imaginary terms in the effective potential and related quantities, due to the cubic terms $\propto m^3_{\rm scalar}$; the gauge fields do not contribute such terms. Throughout this thesis, physical quantities will be obtained from the real part of V^T, and since we are not interested in vacuum decay rates, imaginary terms will be ignored. [4] In the abbreviated form for $g(x)$ above, the quartic term is positive, and the quadratic term is positive for $T > T_{\rm c}$ and negative for $T < T_{\rm c}$, as in the previous approximation $f(x)$. Here, however, the cubic terms lead to an energy barrier at the critical point. $V^T_{1\,\rm loop}(\phi)$ is similar to that of the scalar model shown in Figure 3.6, and first-order behavior is evident.

The minimum and the corresponding mass, as functions of the temperature, are given by the following expressions:

Symmetric minimum: $T > \widetilde{T}$ (3.72)

$$\begin{aligned} x &= 0 \\ \frac{\widetilde{m}^2}{T^2} &= a(T) - \frac{\lambda^{3/2}}{\pi}\left(-\frac{v^2}{T^2}\right)^{1/2} \end{aligned}$$

Broken minimum: $T < \widetilde{T}$ (3.73)

$$\begin{aligned} a(T) + c(T)x_+^2 &= \frac{1}{4\pi}\left[3\lambda^{3/2}\left(3x_+^2 - \frac{v^2}{T^2}\right)^{1/2} + \lambda^{3/2}\left(x_+^2 - \frac{v^2}{T^2}\right)^{1/2} + 3e^3 x_+\right] \\ \frac{\widetilde{m}^2}{T^2} &= -2a(T) \\ &\quad + \frac{1}{2\pi}\left[3\lambda^{3/2}\left(3x_+^2 - \frac{v^2}{T^2}\right)^{1/2} + \lambda^{3/2}\left(x_+^2 - \frac{v^2}{T^2}\right)^{1/2} + 3e^3 x_+\right] \\ &\quad - \frac{x_+}{4\pi}\left[9\lambda^{3/2}\frac{x_+}{\sqrt{3x_+^2 - \frac{v^2}{T^2}}} + \lambda^{3/2}\frac{x_+}{\sqrt{x_+^2 - \frac{v^2}{T^2}}} + 3e^3\right] \\ &= x_+\left\{2c(T)x_+ - \frac{1}{4\pi}\left[9\lambda^{3/2}\frac{x_+}{\sqrt{3x_+^2 - \frac{v^2}{T^2}}} + \lambda^{3/2}\frac{x_+}{\sqrt{x_+^2 - \frac{v^2}{T^2}}} + 3e^3\right]\right\}. \end{aligned}$$

$\widetilde{m}^2$ now includes the one-loop corrections due to vacuum and thermal interactions, whereas previously it only included the leading thermal corrections $\propto T^2$, as calculated from $f(x)$. The minimum $\phi/T(T)$ and mass $\widetilde{m}^2(T)$ resemble those of the scalar model shown in Figures 3.4 and 3.5. The broken minimum jumps discontinuously to the symmetric minimum at $T = \widetilde{T}$, at which point symmetry is restored, although the mass remains positive.

We now examine the critical point in greater detail. At the critical point, $T_{\rm c}$, the

[4] E.g., $m^3_{\rm scalar}$ in expressions for physical quantities implicitly means $\mathcal{R}e\left(m^3_{\rm scalar}\right)$.

asymmetric minimum $x_{\rm crit} = (\phi/T)_{\rm crit}$ is given by

$$c(T_{\rm c})x_{\rm crit} = \frac{1}{4\pi x_{\rm crit}}\left\{3\lambda^{3/2}\left[\left(3x_{\rm crit}^2 - \frac{v^2}{T_{\rm c}^2}\right)^{1/2} - \left(-\frac{v^2}{T_{\rm c}^2}\right)^{1/2}\right] + \lambda^{3/2}\left[\left(x_{\rm crit}^2 - \frac{v^2}{T_{\rm c}^2}\right)^{1/2} - \left(-\frac{v^2}{T_{\rm c}^2}\right)^{1/2}\right] + 3e^3 x_{\rm crit}\right\} , \quad (3.74)$$

where the mass is

$$\frac{\widetilde{m}^2}{T^2} = \frac{1}{2\pi}\left\{3\lambda^{3/2}\left[\left(3x_{\rm crit}^2 - \frac{v^2}{T_{\rm c}^2}\right)^{1/2} - \left(-\frac{v^2}{T_{\rm c}^2}\right)^{1/2}\right] + \lambda^{3/2}\left[\left(x_{\rm crit}^2 - \frac{v^2}{T_{\rm c}^2}\right)^{1/2} - \left(-\frac{v^2}{T_{\rm c}^2}\right)^{1/2}\right] + 3e^3 x_{\rm crit}\right\} - \frac{x_{\rm crit}}{4\pi}\left[9\lambda^{3/2}\frac{x_{\rm crit}}{\sqrt{3x_{\rm crit}^2 - \frac{v^2}{T_{\rm c}^2}}} + \lambda^{3/2}\frac{x_{\rm crit}}{\sqrt{x_{\rm crit}^2 - \frac{v^2}{T_{\rm c}^2}}} + 3e^3\right] . \quad (3.75)$$

Unlike the case for the scalar model, there is no simple stability bound to be obtained here. Indeed, expanding $g''(x_{\rm crit})$ for small and large values of $x_{\rm crit}$,

$x_{\rm crit}^2 \ll v^2/T_{\rm c}^2$:

$$g''(x_{\rm crit}) \approx \frac{3}{4\pi}e^3 x_{\rm crit} + \frac{7}{4\pi}\lambda^{3/2}x_{\rm crit}^4\left(-\frac{v^2}{T_{\rm c}^2}\right)^{-3/2} \quad (3.76)$$

$x_{\rm crit}^2 \gg v^2/T_{\rm c}^2$:

$$g''(x_{\rm crit}) \approx \frac{1}{4\pi}\left[\left(3\sqrt{3}+1\right)\lambda^{3/2} + 3e^3\right]x_{\rm crit} , \quad (3.77)$$

so that the solution is not restricted to large values. The effect of the gauge field is to strengthen the first-order behavior of the phase transition relative to that of the scalar model. We will use similar expressions for $(\phi/T)_{\rm crit}$ in our analysis of the electroweak phase transition (Chapters 5, 6, and 7) to place constraints on the parameters, by requiring that $(\phi/T)_{\rm crit} \gtrsim 1$. We will thus obtain upper bounds on the Higgs mass from the condition that the universe undergo a sufficiently strongly first-order phase transition, to ensure successful baryogenesis.

3.3 Infrared Divergences and Ring Improvement

The effective potential at one loop suggests a first-order phase transition, because of the negative terms cubic in ϕ. Before drawing any conclusion, however, we must decide whether our result is to be trusted — that is, we must see whether it survives the inclusion of higher-order terms in the loop expansion. Indeed, at the very least, we must include higher-loop terms contributing at the same order in λ and e, i.e., at

$\mathcal{O}(\lambda^{3/2})$ and $\mathcal{O}(e^3)$. Recalling that the cubic terms derive from the infrared behavior of the theory, we are led to analyze infrared divergences in higher-loop graphs. It is well known that the leading IR divergences occur in the ring diagrams of Figure 3.11 (also known as daisy or plasmon diagrams), whose summation contributes terms proportional

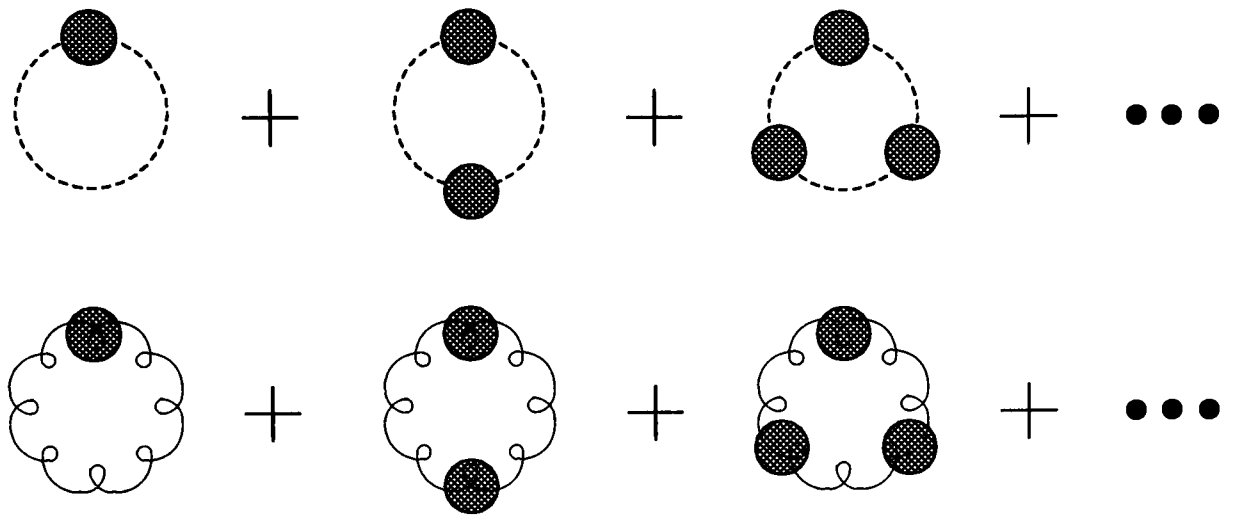

Figure 3.11: The contributions of scalar and gauge ring diagrams to the effective potential; blobs represent the scalar self-energy and the gauge polarization tensor, respectively.

to $\lambda^{3/2}\phi^3$ and $e^3\phi^3$.

Another reason to consider ring diagrams is provided by the scalar terms $\propto m_j^{3/2}(\phi)$ in the effective potential. These are responsible for the energy barrier between the symmetric and broken minima and become imaginary near the phase transition, precisely the region of interest. Thus it is not obvious how reliable the one-loop description is of first-order behavior. Summing the ring diagrams will enable us to make the substitution $m_j^2(\phi) \longrightarrow m_j^2(\phi) + \Pi_j(0)$ in such terms, resulting in terms that are real near the phase transition. $\Pi_j(k)$ is the thermal self-energy in the presence of the field ϕ, and $\Pi_j(0)$ denotes its static infrared limit ($\omega_n = 0, \vec{k} \to 0$).

More fundamentally, perturbation theory at finite temperature *requires* us to sum ring diagrams. In contrast to the case at zero temperature, perturbation theory at finite temperature is an expansion in the parameters $e^2T^2/\mathcal{M}_{\text{eff}}^2$ and $e^2T/\mathcal{M}_{\text{eff}}$, where $\mathcal{M}_{\text{eff}}$ is an effective mass scale of the theory and e is the coupling constant e or $\lambda^{1/2}$ [25, 31]. The first parameter corresponds to quadratically divergent loops, the second to all other loops in the expansion. Near the phase transition, $\mathcal{M}_{\text{eff}} \to 0$, so that our lowest-order description of the phase transition is no longer reliable; higher-order effects then must be taken into account. For example, we will see below that the graphs of Figure 3.12 (in which the zero mode of the large loop is taken) contribute to the effective potential terms proportional to $\left(e^2T^2/m_A^2(\phi)\right)^N = (T/\phi)^{2N}$, which are significant at high temperature ($T \gtrsim v$) near the phase transition. Summing up such terms will yield an improved perturbative expansion.

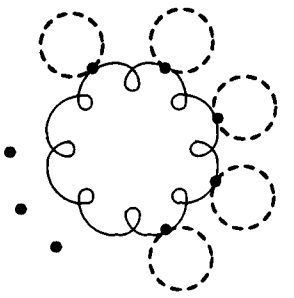

Figure 3.12: A typical graph that is infrared divergent near the phase transition; $\omega = 0$ in the gauge loop.

Summation of Ring Diagrams to Leading Order

We proceed to higher orders of perturbation theory in the Abelian Higgs model; the scalar model is similar and is omitted for brevity. In this subsection, we will work to third order in e and $\sqrt{\lambda}$, and we will compute only the leading-order result in the high-temperature expansion.

At two loops, we encounter the tadpole graphs of Figure 3.13. These diagrams (their

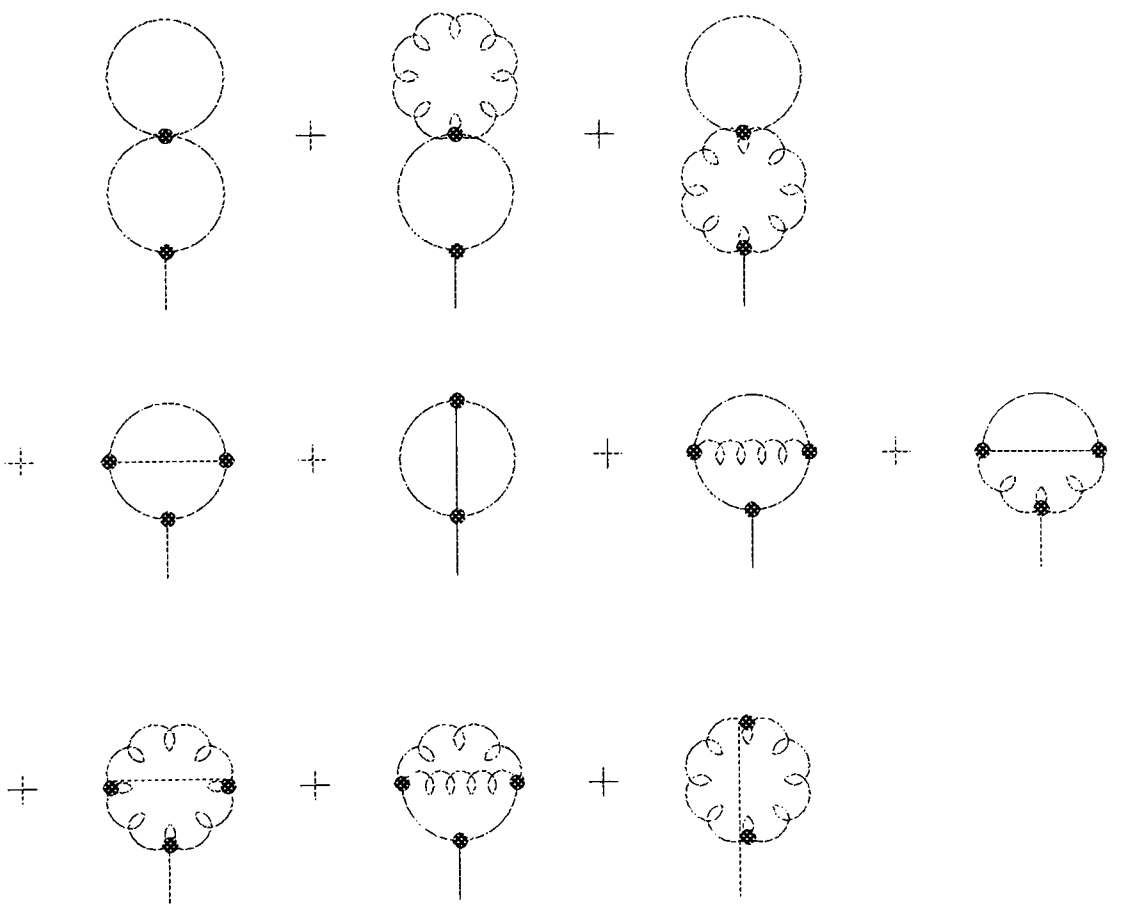

Figure 3.13: The two-loop tadpole graphs for the effective potential in the Abelian Higgs model.

contribution to V^T is denoted $\Delta V_{2\,\mathrm{loop}}^T$) will be evaluated later with similar terms from the ring diagrams.

The next higher-order terms contribute at order $\mathcal{O}(\lambda^{3/2})$ and $\mathcal{O}(e^3)$, rather than $\mathcal{O}(\lambda^2)$ and $\mathcal{O}(e^4)$. These are the ring diagrams shown in Figure 3.11, excluding the

first, which is included in the two-loop graphs of Figure 3.13. The $\lambda^{3/2}$ and e^3 terms arise solely from the zero modes of the diagrams. The other modes are analytic in λ and e, and hence contribute to the effective potential V^T at $\mathcal{O}(\lambda^2)$ and $\mathcal{O}(e^4)$. We first calculate the scalar ring diagrams; the gauge ring diagrams will be analyzed later in a similar fashion after discussing new complications arising from the thermodynamics of gauge fields.

We isolate the zero mode of the scalar χ_1 ring diagrams:

$$\begin{aligned}\frac{d\Delta V^{(1)}_{\text{ring}}}{d\phi} &= 3\lambda\phi\, T\sum_n \int\frac{d^3\vec{k}}{(2\pi)^3}\,\frac{1}{\omega_n^2+\vec{k}^2+m_1^2(\phi)}\sum_{N=2}^{\infty}\left(\frac{-\mathrm{H}^{(1)}(\omega_n,\vec{k})}{\omega_n^2+\vec{k}^2+m_1^2(\phi)}\right)^N \\ &\longrightarrow 3\lambda\phi\, T\int\frac{d^3\vec{k}}{(2\pi)^3}\,\frac{1}{\vec{k}^2+m_1^2(\phi)}\sum_{N=2}^{\infty}\left(\frac{-\Pi^{(1)}(0)}{\vec{k}^2+m_1^2(\phi)}\right)^N . \qquad (3.78)\end{aligned}$$

Note that we are computing only those ring diagrams with two or more self-energy insertions; the ring diagram with one Π-insertion is included in the two loop diagrams of $\Delta V^T_{2\,\text{loop}}$. We have approximated $\Pi^{(1)}(0,\vec{k}) \approx \Pi^{(1)}(0,\vec{k}=0)$ in the last line because the loop is dominated by its infrared behavior (i.e., for $N \geq 2$, the corresponding integral in $\Delta V^{(1)}_{\text{ring}}$ receives its dominant contribution from the region $\vec{k}^2 \lesssim m_1^2(\phi)$). Summing the series and integrating,

$$\begin{aligned}\frac{d\Delta V^{(1)}_{\text{ring}}}{d\phi} &= \frac{T}{2}\frac{dm_1^2}{d\phi}(\phi)\int\frac{d^3\vec{k}}{(2\pi)^3}\left[\frac{1}{\vec{k}^2+m_1^2(\phi)+\Pi^{(1)}(0)}-\frac{1}{\vec{k}^2+m_1^2(\phi)}\right. \\ &\qquad\left.+\frac{\Pi^{(1)}(0)}{\left(\vec{k}^2+m_1^2(\phi)\right)^2}\right] \\ \Longrightarrow\quad \Delta V^{(1)}_{\text{ring}}(\phi) &= -\frac{T}{12\pi}\left\{\left[m_1^2(\phi)+\Pi^{(1)}(0)\right]^{3/2}-m_1^3(\phi)\right\} \\ &\qquad+\frac{T}{2}\int\frac{d^3\vec{k}}{(2\pi)^3}\,\frac{-\Pi^{(1)}(0)}{\vec{k}^2+m_1^2(\phi)} . \qquad (3.79)\end{aligned}$$

The ring diagrams represent long-distance effects, as reflected in the infrared self-energy. The scalar χ_2 ring diagrams yield a similar expression. Note that because we are only interested in the leading-order result, all ϕ-dependence in the self-energies has been ignored.

The self-energies will be computed to one loop, and only their leading (quadratic) temperature dependence will be kept here. The scalar self-energies $\Pi^{(1)}$ and $\Pi^{(2)}$ at one loop are represented by the graphs of Figure 3.14; because T effectively acts as a physical high-momentum cutoff, $\Pi \propto T^2$ simply arises from the (first two) quadratically divergent graphs. $\Pi^{(1)}$ may be calculated either explicitly using the finite-temperature Feynman rules, or more simply by taking the second derivative of the one-loop effective

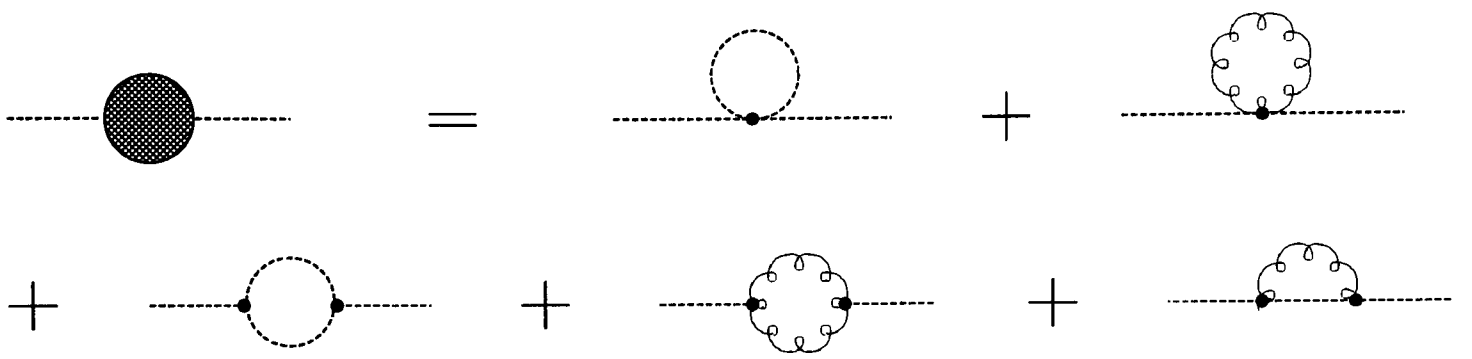

Figure 3.14: The scalar self-energy at one loop in the Abelian Higgs model.

potential (3.59). From relation (2.11), we have

$$\begin{aligned} \frac{d^2 V^T_{1\,\mathrm{loop}}}{d\phi^2}(\phi) &= m_1^2(\phi) + \Pi^{(1)}(0) \\ \Longrightarrow \quad \Pi^{(1)}(0) &= \frac{\lambda}{3}T^2 + \frac{e^2}{4}T^2 + \lambda T^2 \cdot \mathcal{O}\left(m_1(\phi)/T\,,\, m_2(\phi)/T\right) \\ &\quad + e^2 T^2 \cdot \mathcal{O}\left(m_A(\phi)/T\right)\,. \end{aligned} \tag{3.80}$$

In this expression, the perturbative terms of the zero-temperature self-energy have been neglected. The self-energy $\Pi^{(2)}$ for χ_2 has the same leading temperature dependence, since $\Pi^{(1)} = \Pi^{(2)}$ in the limit $m_{\mathrm{scalar}} \to 0$, or as may be seen from explicit computation of the diagrams.

We now turn to the gauge field ring diagrams. Denoting by $\Pi^{\alpha\beta}(k)$ the polarization tensor of the gauge field A^μ, the gauge ring diagrams give a tadpole contribution similar to that of the scalar case (3.78):

$$\begin{aligned} \frac{d\Delta V^A_{\mathrm{ring}}}{d\phi} &= -e^2\phi \int \frac{d^4k}{(2\pi)^4}\,\mathrm{Tr}\left\{ \frac{-i(g_{\mu\nu} - k_\mu k_\nu/k^2)}{k^2 - m_A^2(\phi) + i\varepsilon} \right. \\ &\qquad \left. \cdot \sum_{N=2}^{\infty} \left[\frac{\Pi^{\alpha\beta}(k)(g_{\mu\nu} - k_\mu k_\nu/k^2)}{k^2 - m_A^2(\phi) + i\varepsilon} \right]^N \right\}\,, \end{aligned} \tag{3.81}$$

where the Wick rotation to Euclidean space has not been performed yet, nor has the zero-mode been isolated. An additional complication arises here due to the thermodynamics of gauge fields. At finite temperature, not all components of A^μ gain screening masses at lowest order; in other words, $\Pi^{\alpha\beta}(0)$ will vanish for some components, to the order in which we are working. As a result, only those components of A^μ that *do* gain screening masses will contribute nonvanishing ring diagrams. We will see that the time component of the field acquires an electric mass $\Pi^{00}(0) \sim e^2T^2$ at one loop; the spatial components remain massless until two loops, when the magnetic mass becomes $\Pi^{jj}(0) \sim e^4T^2$.

We proceed by analogy to finite temperature QCD [17]. We decompose the four-dimensional transverse operator $g_{\mu\nu} - k_\mu k_\nu/k^2$ into the sum of three-dimensional trans-

verse and longitudinal operators:

$$T_{\mu\nu} + L_{\mu\nu} = k_\mu k_\nu / k^2 - g_{\mu\nu} \ . \tag{3.82}$$

As projection operators, T and L satisfy the relations $TT = -T$, $LL = -L$, and $LT = 0$; and because they are four-dimensionally transverse, $kT = 0 = kL$. T has the explicit form

$$\begin{aligned} T_{00} &= T_{0i} = T_{i0} = 0 \\ T_{ij} &= \delta_{ij} + k_i k_j / \vec{k}^2 \ . \end{aligned} \tag{3.83}$$

Then $\Pi^{\alpha\beta}$ can be decomposed as $\Pi_{\mu\nu} = \Pi^T T_{\mu\nu} + \Pi^L L_{\mu\nu}$. In the infrared limit ($k_0 = 0$, $\vec{k} \to 0$), $T_{00} = 0$, $L_{00} = -1$, $T^i{}_i = -2$, and $L^i{}_i = 0$. Thus the screening mass is given by

$$\Pi_{\mu\nu}(0) = \frac{1}{2}\Pi_{jj}(0)\, T_{\mu\nu}(0) - \Pi_{00}(0)\, L_{\mu\nu}(0) \ . \tag{3.84}$$

We will see below that at one loop, $\Pi_{00}(0) \sim e^2T^2$, while $\Pi_{jj}(0) = 0$; the magnetic mass vanishes at one loop. At two loops, one can show that the magnetic mass is $\Pi_{jj}(0) \sim e^4T^2$. Hence, at lowest order, the longitudinal component of A^μ acquires an electric mass, while the transverse components remain massless. Neglecting $\Pi_{jj}(0)$, the polarization tensor takes the form $\Pi_{\mu\nu}(0) = -\Pi_{00}(0)L_{\mu\nu}(0)$.

We return to the gauge ring diagrams (3.81), isolate the zero mode, and use $\mathrm{H}^{\alpha\beta}\,(g_{\beta\gamma} - k_\beta k_\gamma / k^2) \longrightarrow -\Pi_{00} L^\alpha{}_\gamma$ in the infrared limit, to obtain

$$\begin{aligned} \frac{d\Delta V^A_{\rm ring}}{d\phi} &= -e^2\phi\, T \int \frac{d^3\vec{k}}{(2\pi)^3}\, \mathrm{Tr} \left\{ \frac{T+L}{\vec{k}^2 + m_A^2(\phi)} \sum_{N=2}^{\infty} \left[\frac{\Pi_{00}(0) L}{\vec{k}^2 + m_A^2(\phi)} \right]^N \right\} \\ &= e^2\phi\, T \int \frac{d^3\vec{k}}{(2\pi)^3} \frac{1}{\vec{k}^2 + m_A^2(\phi)} \sum_{N=2}^{\infty} \left(\frac{-\Pi_{00}(0)}{\vec{k}^2 + m_A^2(\phi)} \right)^N \ . \end{aligned} \tag{3.85}$$

Summing the series and integrating,

$$\begin{aligned} \Delta V^A_{\rm ring}(\phi) &= -\frac{T}{12\pi} \left\{ \left[m_A^2(\phi) + \Pi_{00}(0) \right]^{3/2} - m_A^3(\phi) \right\} \\ &\qquad + \frac{T}{2} \int \frac{d^3\vec{k}}{(2\pi)^3} \frac{-\Pi_{00}(0)}{\vec{k}^2 + m_1^2(\phi)} \ . \end{aligned} \tag{3.86}$$

The effect of the gauge ring diagrams has been expressed in terms of the electric mass, which we now compute.

The polarization tensor at one loop is given by the diagrams in Figure 3.15. We calculate the individual diagrams to find the leading (quadratic) temperature dependence of the components $\Pi_{00}(0)$ and $\Pi_{jj}(0)$. Using the Feynman rules and the integrals of

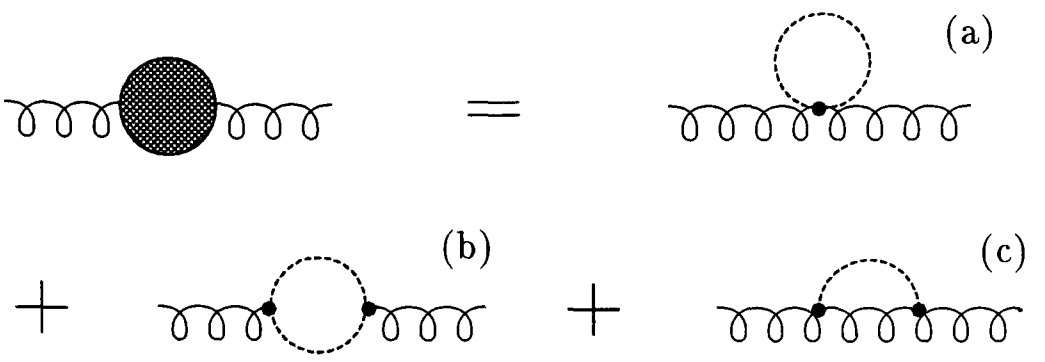

Figure 3.15: The gauge polarization tensor at one loop in the Abelian Higgs model.

Appendix C, we find the first graph results in

$$\text{Graph (a):} \qquad \begin{aligned} \Pi_{00}^{(a)}(0) &= \frac{e^2T^2}{6} \\ \Pi_{jj}^{(a)}(0) &= -\frac{e^2T^2}{2}\,, \end{aligned}$$

while the second graph gives

$$\text{Graph (b):} \qquad \begin{aligned} \Pi_{00}^{(b)}(0) &= \frac{e^2T^2}{6} \\ \Pi_{jj}^{(b)}(0) &= \frac{e^2T^2}{2}\,. \end{aligned}$$

The third graph is $\propto e^4T\phi^2$, and we ignore it relative to graphs (a) and (b); furthermore, it is negligible in the interesting region near the phase transition ($\phi \sim 0$). Thus at one loop,

$$\begin{aligned} \Pi_{00}(0) &= \frac{e^2T^2}{3} \\ \Pi_{jj}(0) &= 0\,, \end{aligned} \tag{3.87}$$

confirming the claims made earlier.

Now add the two-loop and ring contributions to the one-loop effective potential. We note that the last terms of both the gauge and scalar ring diagrams cancel the zero modes of the two-loop graphs. The remaining modes in the two-loop graphs contribute perturbative terms analytic in λ and e, which may be neglected to lowest order. Thus we arrive at our final expression for the ring-improved effective potential, at leading order in the temperature:

$$\begin{aligned} V_{\text{ring}}^T(\phi) &= V_{1\,\text{loop}}^T(\phi) + \Delta V_{2\,\text{loop}}^T(\phi) + \Delta V_{\text{ring}}^{(1)}(\phi) + \Delta V_{\text{ring}}^{(2)}(\phi) + \Delta V_{\text{ring}}^{A}(\phi) \\ &= V_{1\,\text{loop}}^T(\phi) - \frac{T}{12\pi}\left\{\left[m_1^2(\phi) + \Pi^{(1)}(0)\right]^{3/2} - m_1^3(\phi)\right\} \end{aligned}$$

$$- \frac{T}{12\pi} \left\{ \left[m_2^2(\phi) + \Pi^{(2)}(0) \right]^{3/2} - m_2^3(\phi) \right\}$$
$$- \frac{T}{12\pi} \left\{ \left[m_A^2(\phi) + \Pi_{00}(0) \right]^{3/2} - m_A^3(\phi) \right\} . \qquad (3.88)$$

Note that the effect of summing ring diagrams is to replace $m_j^2(\phi)$ by thermal masses $m_j^2(\phi) + \Pi_j(0)$ in the infrared terms. Because this substitution occurs for only one of the three gauge degrees of freedom, the cubic gauge term in the one-loop effective potential (3.59) is effectively reduced by a factor of 2/3. As we will see, this effect — found in the context of the Standard Model by Dine, Leigh, Huet, et.al. [18] — weakens the first-order behavior of the phase transition.

3.4 Discussion

Let us summarize the analysis of this chapter, as we will offer a similar treatment for the Standard Model and its simplest extensions in later chapters. We first compute the effective potential at one loop and find that the phase transition displays first-order behavior, essentially due to the negative cubic term in the effective potential. This term, central to what follows, is non-analytic in m^2/T^2 and arises solely from the zero-frequency mode of the one-loop graph; hence it reflects the infrared regime of the theory. Our description of the phase transition, however, is unreliable, for we have neglected terms corresponding to higher loops that contribute to this cubic term at the same order in λ. These terms are the ring diagrams (Figure 3.11), which sum the leading infrared divergences in the theory. Note that only the zero modes are relevant here; other modes are analytic in m^2/T^2 and do not contribute to the cubic term.

Summing the ring diagrams gives

$$\Delta V_{\rm ring}^T(v) = -\frac{T}{12\pi} \left\{ \left[m^2(v) + \Pi(0) \right]^{3/2} - m^3(v) \right\} \qquad (3.89)$$

for each mode that gains a plasma mass. Here $\Pi(0)$ is a scalar self-energy (or the longitudinal component of a gauge polarization tensor) at zero momentum (Figures 3.14 and 3.15); to leading order in the temperature, $\Pi(0) \propto \lambda T^2$ (or e^2T^2) and is given by the quadratically-divergent graphs. Including these ring diagrams in $V^T(v)$ effectively dampens the cubic term responsible for first-order behavior. The ring-improved effective potential, $V_{\rm ring}^T = V_{\rm 1\,loop}^T + \Delta V_{\rm ring}^T$, thus shows a more weakly first-order phase transition. We will see a similar effect later in Chapters 5, 6, and 7.

To have any confidence in our results, we must still question the validity of the effective potential. In view of the shortcomings suffered by the one-loop result, we have "improved" $V^T(\phi)$ by summing ring diagrams. Yet how is the new effective potential better than the old? We address this question from the same points of view considered earlier. First, we have at least computed to leading order the cubic terms that are crucial for ensuring a first-order phase transition. Higher loops contribute to this cubic

term perturbatively. Secondly, our summation of ring diagrams guarantees that the effective potential (3.88) remains real for all values of ϕ (including the critical region between degenerate minima), provided that the temperature is higher than T_0, where

$$T_0^2 = \frac{12\mu^2}{4\lambda + 3e^2} \,. \tag{3.90}$$

At temperatures lower than T_0, the ring-improved effective potential develops imaginary terms for small ϕ, signaling the physical instability near the origin that we expect.

Finally, we have to determine the validity of our new perturbative expansion. By summing ring diagrams, we have accounted for quadratically divergent loop corrections to the one-loop result. All diagrams we have neglected are suppressed by factors of $\lambda T/\mathcal{M}_{\rm eff}$ and $e^2 T/\mathcal{M}_{\rm eff}$, where the effective mass scale is now $\mathcal{M}_{\rm eff}^2 = m^2(\phi) + \Pi(0)$ for the relevant degree of freedom. Requiring these parameters to be $\lesssim 1$ in the perturbative domain, we see that our new perturbative expansion will be valid everywhere outside the region $|T - T_{\rm c}| \lesssim \lambda T_{\rm c}$ and $e^2 T_{\rm c}$. Within these limits, we can reliably predict weak first-order behavior at the phase transition.

It is possible to consider $V_{\rm ring}^T$ from another point of view. Because interactions of the system with the heat bath become significant at high temperature, it is natural to construct perturbation theory in terms of thermal masses and dressed propagators, which reflect the *physical* (rather than elementary) degrees of freedom in the plasma. Thus we are lead to a thermal resummation of perturbation theory [32, 33], which is achieved in a self-consistent manner via the Schwinger-Dyson equations at finite temperature. Our calculation of plasma masses $\propto T^2$ is a (leading-order) approximate solution of the Schwinger-Dyson equation, and our summation of ring diagrams is simply the lowest-order result of a self-consistent treatment of infrared divergences.

Chapter 4

Baryon Violation at High Temperature

This chapter summarizes basic results pertaining to the anomalous violation of fermion number in the electroweak model, at both zero and high temperatures. We briefly review the literature, stressing the results that we use later.

4.1 Anomalous Violation of Fermion Number

The electroweak Lagrangian conserves baryon and lepton number at the classical level; that is, $\mathcal{L}_{\rm EW}$ is invariant under the global $U(1)$ transformations $e^{iB\alpha}$ and $e^{iL\beta}$. In constructing the quantum field theory, however, the global B and L symmetries are broken by the process of quantization and regularization; B and L are said to be broken anomalously. This non-conservation of B and L currents is described by the Adler-Bell-Jackiw-Bardeen anomaly [34]:

$$\partial_\mu j^\mu_B = \partial_\mu j^\mu_L = N\left(\frac{g^2}{32\pi^2}G\tilde{G} - \frac{g'^2}{32\pi^2}F\tilde{F}\right) . \tag{4.1}$$

G and F are the respective $SU(2)_L$ and $U(1)_Y$ field-strength tensors, tilde denotes dual, and N is the number of fermion generations. The anomalous violation of B and L is an inherently non-perturbative phenomenon; for instance, scattering amplitudes computed in perturbation theory conserve B and L. Notice that while B, L, and $B+L$ are anomalous, $B-L$ is strictly conserved; in fact, $B/N - L_j$ is separately conserved for each generation.

We express $G\tilde{G}$ and $F\tilde{F}$ in terms of the $SU(2)_L$ and $U(1)_Y$ Chern-Simons currents:

$$\begin{aligned} \partial_\mu K^\mu &= \frac{g^2}{32\pi^2}G\tilde{G} \\ \partial_\mu k^\mu &= \frac{g'^2}{32\pi^2}F\tilde{F} , \end{aligned}$$

where

$$\begin{aligned} K^\mu &= \varepsilon^{\mu\nu\alpha\beta}\left(G^a_{\nu\alpha}W^a_\beta - \frac{1}{3}g\varepsilon_{abc}W^a_\nu W^b_\alpha W^c_\beta\right) \\ k^\mu &= \varepsilon^{\mu\nu\alpha\beta}F_{\nu\alpha}B_\beta \ , \end{aligned}$$

and W^a_μ and B_μ are the respective $SU(2)$ and $U(1)$ fields. Integration of the anomaly equation gives the change in total baryon and lepton numbers between initial and final field configurations:

$$\Delta B = \Delta L = N\Delta N_{\rm CS} + N\Delta n_{\rm CS} \ . \tag{4.2}$$

The charges $N_{\rm CS}$ and $n_{\rm CS}$ are topologically invariant (although not gauge-invariant) properties of a field configuration; however the differences $\Delta N_{\rm CS}$ and $\Delta n_{\rm CS}$ are both topologically and gauge-invariant. Hence we use them to describe the topology of the vacuum manifold in electroweak theory.

A vacuum configuration of gauge fields has zero field strength by definition; and because the $U(1)_Y$ topological charge is proportional to the field strength, the vacuum manifold is specified simply by the $SU(2)_L$ charge $\Delta N_{\rm CS}$. In the absence of fermions, we find that the vacuum manifold of gauge and scalar fields is infinitely degenerate, with inequivalent vacua related by topologically non-trivial $SU(2)_L$ gauge transformations. The vacua are specified by the Chern-Simons number n, [1] which takes on integer values, and the gauge transformation that relates different vacua of charges m and n has charge $n-m$. The inclusion of fermions lifts this degeneracy, and by the integrated anomaly equation (4.2), gives different baryon and lepton numbers to inequivalent vacua. As we will see later, this also creates a bias for equilibrium B and L violation.

't Hooft first considered the possibility of tunneling between inequivalent vacua at zero temperature, using semi-classical weak coupling methods [35]. Such transitions, accompanied by baryon and lepton violation, are mediated by extremal solutions of the Euclidean action, termed instantons [36]. 't Hooft computed the rate of instanton-induced baryon violation, and found the interaction rate (per unit volume) to be

$$\Gamma \propto e^{-4\pi/\alpha_{\rm W}} \sim 10^{-173} \ ,$$

which implies that fermion number is accurately conserved in the universe today; in fact, this also implies a vanishing probability that such instanton-mediated processes have ever occurred in the history of the universe.

Subsequently Kuzmin, Rubakov, and Shaposhnikov pointed out that the rate of anomalous baryon violation may be enhanced at high temperature [8]. Their idea was that, at sufficiently high temperatures, large thermal fluctuations give rise (as described by the thermal ensemble) to configurations that can mediate diffusion over the energy barrier, rather than penetration through the barrier. Thus the rate of baryon violation

[1] n denotes the integer value of $\Delta N_{\rm CS}$, the topological charge relative to a chosen standard (which ensures a gauge- and topologically invariant description).

is determined by a thermal Boltzmann factor $e^{-E/T}$, which may be appreciable at high temperatures, rather than the prohibitively small WKB factor $e^{-4\pi/\alpha_W}$ at zero temperature.

Klinkhamer and Manton had earlier found such configurations, called sphalerons, as static solutions that extremize the three-dimensional action [7]. The sphaleron is a saddle-point solution in the functional space of field configurations, and it represents the lowest barrier point, with half-integer topological charge $n+1/2$, intermediate between vacua with charges n and $n+1$. A semiclassical analysis in the broken phase yields the equilibrium rate for sphaleron interactions [9]:

$$\text{Broken phase:} \qquad \Gamma^{\rm b} = \gamma \frac{M_W^7}{(\alpha_W T)^3} e^{-E_{\rm sph}/T} , \tag{4.3}$$

where the pre-exponential factor is given by the determinant of fluctuations around the sphaleron solution and the energy of the sphaleron by

$$E_{\rm sph}(T) = \frac{2M_W(T)}{\alpha_W(T)} B\left(\frac{\lambda(T)}{g^2(T)}\right) . \tag{4.4}$$

The temperature dependence of the parameters is shown explicitly, and the numerical coefficient B ranges monotonically from $B(0) = 1.56$ to $B(\infty) = 2.72$. As a semi-classical result in the high-temperature limit, this expression for $\Gamma^{\rm b}$ is valid below the phase transition only for $m_W(T) < T < m_W(T)/\alpha_W(T)$. The sphaleron mediates a process that can be visualized as creating out of the vacuum one color-singlet $SU(2)_L$-singlet neutral hydrogen-like state from each fermion generation: $\prod_j (u_L d_L u_L e_L^-)_j$. Note that $\Delta B = \Delta L = 3$, although $B - L = 0 = B/N - L_j$.

The sphaleron solution was first constructed for the electroweak theory with one scalar doublet and electromagnetism ignored ($\sin^2\theta_W = 0$), and was later generalized to non-zero $\sin^2\theta_W$. The sphaleron solution was also found for the electroweak model with two scalar doublets; the energy in this case is identical in form to that for the Standard Model:

$$\tilde{E}_{\rm sph}(T) = \frac{2M_W(T)}{\alpha_W(T)} B(\lambda^{\rm eff}(T)) , \tag{4.5}$$

although $\lambda^{\rm eff}$, the argument of B, is a complicated combination of the scalar and gauge couplings [37].

Above the phase transition, infrared divergences at high temperature complicate the analysis considerably. A scaling argument, however, allows a simple estimate for the rate of baryon-violating transitions [38]. Because classical equilibrium statistical mechanics describes the plasma above the phase transition, the fields may be rescaled so that the partition function is Tr exp $-H/(\alpha_W T)$; the coupling appears only outside the classical Hamiltonian in the combination $\alpha_W T$. The plasma generates a magnetic screening mass that cuts off the infrared divergences, and for dimensional reasons, this

mass must be $\propto \alpha_W T$. [2] The rate of anomalous fermion-number violation is then

$$\text{Symmetric phase:} \qquad \Gamma^s = \kappa(\alpha_W T)^4 \ , \tag{4.6}$$

where attempts to numerically evaluate the parameter κ suggest the bounds $0.1 \lesssim \kappa \lesssim 1.0$ [39].

Analyses in both the symmetric and broken phases thus permit the possibility of baryon- and lepton-number violation, mediated by thermal — as opposed to quantum — tunneling between topologically distinct vacua.

4.2 Interaction Rates

As Cohen, Kaplan, and Nelson have emphasized [5], there are several distinct timescales at the electroweak phase transition that are crucial in determining equilibrium during baryogenesis:

- $\tau_{\rm sph}^{-1} \sim \alpha_W^4 T \approx 1.3 \cdot 10^{-6} T$ is the rate of baryon violation in the symmetric phase.
- The thermalization rate for quarks is $\tau_T^{-1} \sim 0.25\,T$ due to the strong interactions and that for leptons and weak gauge bosons is $\tau_T^{-1} \sim 0.08\,T$ due to the weak interactions.
- The Higgs timescale is $\tau_H^{-1} = \dot{\phi}/\phi \sim u/\delta$ where u is the wall velocity and δ the wall thickness. For the cases of interest in this thesis, the phase separation boundary will be taken to be thin compared to particle mean free paths, $\tau_T \gg \tau_H$, so that particles reflect off the bubble wall with calculable reflection coefficients.
- The expansion rate $H = -\dot{T}/T$ is orders of magnitude smaller than the other rates at the electroweak scale and is irrelevant for baryogenesis.

We see that the rate for anomalous violation of fermion number is much slower than the rates of Standard Model interactions, in both the broken and symmetric phases. Hence, in studying baryogenesis at the electroweak scale, we must use the rate equation to describe the approach of baryon number to equilibrium in the symmetric phase. The authors of [38] find this rate by a simple detailed-balance argument, as follows. The net rate of baryon production is given by $\dot{n}_B = 3(\Gamma_+ - \Gamma_-)$ where $\Gamma_\pm$ is the rate of anomalous processes that produce or destroy baryons, respectively. In the absence of bias, the rates cancel, leaving zero net baryon production; however, the presence of fermions contributes free energy to the system which lifts the degeneracy between inequivalent vacua, and thereby creates a bias. [3] Assuming this bias is small, $\dot{n}_B = -3\Gamma\Delta F/T$, where Γ is the rate of fluctuations between neighboring vacua in

[2] No reliable means of perturbatively computing the magnetic mass is known [17].

[3] For a sufficiently dilute system this is simply the energy of a free Fermi gas with fixed baryon and lepton numbers.

the absence of fermions and ΔF is the change in free energy between them. Because $\Delta F = 3\partial F/\partial B$ ($\partial F/\partial B$ is taken with baryon and lepton numbers held fixed), the final rate equation is

$$\dot{n}_B = -9\frac{\Gamma^s}{T}\frac{\partial F}{\partial B} \,. \tag{4.7}$$

We may use the interaction rate of anomalous baryon violation to constrain the value of $(\phi/T)_{\rm crit}$ following the phase transition, by requiring that the observed baryon number be of electroweak origin; hence the baryon number generated at the phase transition must not be diluted beyond the observed value. Integration of the kinetic Boltzmann equations with sphaleron interactions in equilibrium gives the surviving baryon number as a fraction of the generated baryon number [21]:

$$\frac{B_{\rm final}}{B_{\rm init}} = \exp\left(-\Omega\left(\frac{E_{\rm sph}}{T}\right)^6 \exp\left(-\frac{E_{\rm sph}}{T}\right)\right) \,,$$

where

$$\Omega = \frac{2\cdot 10^{-5}}{B^7}\cdot\frac{M_{\rm Pl}}{T_{\rm c}}$$

and the largest value of n_B/n_γ that may be generated within the Standard Model (assuming maximal CP violation) is 10^{-5} to 10^{-6}. The ratio $B_{\rm final}/B_{\rm init}$ is exponentially sensitive to $E_{\rm sph}/T$, and it therefore gives an upper bound to good accuracy:

$$\frac{E_{\rm sph}}{T_{\rm c}} \geq 45 \,,$$

which means conservatively that

$$\left(\frac{\phi}{T}\right) \gtrsim 1.3 \,. \tag{4.8}$$

As we will see in later chapters, the value of $(\phi/T)_{\rm crit}$ is inversely proportional to the Higgs boson mass M_H, so the requirement that sphaleron interactions *not* be in equilibrium to ensure the survival of B, following the phase transition, places an upper bound on M_H. We use $(\phi/T)_{\rm crit} \gtrsim 1$ as a general criterion to avoid baryon washout and thus obtain a cosmological constraint on the Higgs boson mass.

Chapter 5

The Minimal Standard Model

There has been much interest in the possibility that the observed baryon asymmetry of the universe is generated at the cosmological phase transition associated with $SU(2)_L \otimes U(1)_Y$ symmetry breaking [40]. The exact nature of this phase transition plays a crucial role in such considerations: strong first-order behavior ensures that B-violating reactions are out of equilibrium both during and after the phase transition. The former condition is required to allow baryogenesis to occur, while the latter is necessary for the baryon asymmetry thus created not to be erased subsequently. The basic tool employed to study this question is the effective potential at finite temperature [41].

Recently, Anderson and Hall [20] analyzed the effective potential of the Standard Model at one loop and concluded that the phase transition is indeed first-order, but only weakly so. Requiring that B-violating reactions not be in equilibrium following the transition places an upper bound on the mass of the Standard Model Higgs boson, which is barely consistent with the bound from LEP [42].

More recently, Carrington [19] and Dine, Leigh, Huet, et. al. [18] have shown that a consistent computation of the effective potential requires that additional terms, viz. ring diagrams, be considered beyond one loop. The result of including these terms is to reduce the strength of the phase transition by a factor of 2/3, and consequently the Higgs mass bound by $\sqrt{2/3}$. This, of course, exacerbates the conflict with experiment and *eliminates* the possibility of electroweak baryogenesis within the minimal Standard Model.

This chapter analyzes the electroweak phase transition in the Standard Model. After a brief review of notation, two cases are considered: light scalars ($M_H \lesssim M_W$), as studied by Carrington [19] and Dine, Leigh, Huet, et. al. [18], and heavy scalars ($M_H \gtrsim M_W$). In both cases, the one-loop effective potential will be used to determine the critical temperature T_c and critical point $(\phi/T)_{\rm crit}$ as functions of the parameters M_H and M_t. The method of summing ring diagrams will then be applied to derive an improved effective potential, which will be done to leading order in the temperature, and it will be found that the first-order nature of the phase transition is considerably weaker than in the one-loop description. This is reflected in the more stringent cosmological

bound on the Higgs boson mass required for a strongly first-order phase transition.

5.1 Notation

The minimal Standard Model is defined by the Lagrangian

$$\mathcal{L} = \mathcal{L}_{\text{gauge}} + \mathcal{L}_{\text{fermion}} + \mathcal{L}_{\text{Higgs}} + \mathcal{L}_{\text{Yukawa}} + \mathcal{L}_{\text{gauge-fixing}} + \mathcal{L}_{\text{ghost}} + \mathcal{L}_{\text{c.t.}} \,. \tag{5.1}$$

It is invariant under the gauged symmetry $SU(2)_L \otimes U(1)_Y$, that is, left-handed weak isospin and weak hypercharge, which is spontaneously broken at zero temperature to the $U(1)_{\text{EM}}$ of electromagnetism. The gauge kinetic term is

$$\mathcal{L}_{\text{gauge}} = -\frac{1}{4} G^j_{\mu\nu} G^{\mu\nu}_j - \frac{1}{4} F_{\mu\nu} F^{\mu\nu} \tag{5.2}$$

where $G^j_{\mu\nu} = \partial_\mu W^j_\nu - \partial_\nu W^j_\mu - g\varepsilon^{jkl} W^k_\mu W^l_\nu$ and $F_{\mu\nu} = \partial_\mu B_\nu - \partial_\nu B_\mu$ are the respective $SU(2)_L$ and $U(1)_Y$ field-strength tensors.

The fermion Lagrangian reads

$$\mathcal{L}_{\text{fermion}} = \sum_a \left(\overline{Q}^a_L \, i\not{D} Q^a_L + \overline{L}^a_L \, i\not{D} L^a_L + \overline{u}^a_R \, i\not{D} u^a_R + \overline{d'}^a_R \, i\not{D} d'^a_R + \overline{e}^a_R \, i\not{D} e^a_R \right) \,, \tag{5.3}$$

where the summation is over families (and $SU(3)_C$ color for quarks) and the covariant derivative is

$$D_\mu \Psi = \left(\partial_\mu + igT^j W^j_\mu + ig' \frac{Y}{2} B_\mu \right) \Psi \,. \tag{5.4}$$

T^j is the appropriate $SU(2)_L$ representation ($T^j = \frac{1}{2}\tau^j$ for left-handed doublets and zero for right-handed singlets) and Y is the hypercharge, normalized such that $Q = Y/2 + T_3$. Chiral fermion fields are defined by $\Psi_{L,R} \equiv \frac{1}{2}(1 \mp \gamma_5)\Psi$, and d'_L denotes weak eigenstate, related to the mass eigenstate d_L by the Kobayashi-Maskawa mixing matrix; u_L and d'_L form the quark doublet Q_L, ν_L and e_L the lepton doublet L_L.

The Higgs field Φ is an $SU(2)_L$ doublet with weak hypercharge $Y/2 = 1/2$; we denote its components by

$$\Phi = \begin{pmatrix} \chi^+ \\ \chi^0 \end{pmatrix} = \frac{1}{\sqrt{2}} \begin{pmatrix} \chi_3 + i\chi_4 \\ \chi_1 + i\chi_2 \end{pmatrix} \,. \tag{5.5}$$

Its dynamics is described by the Lagrangian

$$\mathcal{L}_{\text{Higgs}} = (D_\mu \Phi)^\dagger (D^\mu \Phi) - U(\Phi) \,, \tag{5.6}$$

with the covariant derivative

$$D_\mu \Phi = \left(\partial_\mu + ig \frac{\tau^k}{2} W^k_\mu + i \frac{g'}{2} B_\mu \right) \Phi \tag{5.7}$$

and classical potential

$$U(\Phi) = -\mu^2 \Phi^\dagger \Phi + \lambda (\Phi^\dagger \Phi)^2 \; . \tag{5.8}$$

τ^k are the Pauli matrices, and g and g' are the weak and hypercharge couplings. Upon spontaneous symmetry breaking, $SU(2)_L \otimes U(1)_Y \rightarrow U(1)_{\rm EM}$ and Φ develops a thermal average in the real part of its neutral component:

$$\langle \Phi \rangle = \frac{1}{\sqrt{2}} \begin{pmatrix} 0 \\ \phi \end{pmatrix} \; ; \tag{5.9}$$

in making this choice of vacuum, we have assumed that the universe is electrically neutral and preserves the CP invariance of the vacuum during its evolution. Expanding Φ about its thermal average,

$$\Phi = \frac{1}{\sqrt{2}} \begin{pmatrix} \chi_3 + i\chi_4 \\ \phi + \chi_1 + i\chi_2 \end{pmatrix} = \frac{1}{\sqrt{2}} \begin{pmatrix} 0 \\ \phi \end{pmatrix} + \begin{pmatrix} \chi^+ \\ H \end{pmatrix} \; , \tag{5.10}$$

and substituting into $\mathcal{L}_{\rm Higgs}$ results in masses (see Table 5.1) for the Higgs field χ_1, the Goldstone fields χ_2 and $\chi^\pm$, and the gauge fields $W_\mu^\pm$ and Z_μ, while the electromagnetic field A_μ remains massless. (The gauge fields $W_\mu^\pm$, Z_μ, and A_μ, as well as the mixing angle $\theta_{\rm W}$ and electromagnetic coupling e, are defined in the usual way.) The thermal average as a function of temperature, $\langle \Phi \rangle (T)$, minimizes the effective potential $V^T(\phi)$; at zero temperature, the classical minimum as determined by $U(\Phi)$ occurs at $\phi = v \equiv \mu/\sqrt{\lambda} = 246$ GeV.

Yukawa interactions are described by the Lagrangian

$$\mathcal{L}_{\rm Yukawa} = \sum_{a,b} \left(-f^{ab}\, \overline{Q}_L^a \Phi\, d_R'^b - g^{ab}\, \overline{Q}_L^a \widetilde{\Phi}\, u_R^b - h^{ab}\, \overline{L}_L^a \Phi\, e_R^b + \text{h.c.} \right) \; , \tag{5.11}$$

where $\widetilde{\Phi} = i\tau_2 \Phi^\dagger$ is the Higgs conjugate with hypercharge $Y/2 = -1/2$. We make the approximation that only the top quark has non-vanishing Yukawa coupling, i.e., that all other quarks have negligible masses. Shifting by the thermal average (5.10) in $\mathcal{L}_{\rm Yukawa}$ produces a mass term for the top quark (Table 5.1).

The gauge is fixed in the R_ξ class of renormalizable gauges, which eliminates mixing of the Goldstone and gauge fields in $\mathcal{L}_{\rm Higgs}$ (arising from the cross terms of $|D_\mu \Phi|^2 = \cdots + i m_W [W_\mu^+ \partial^\mu \chi^- - W_\mu^- \partial^\mu \chi^+] - m_Z Z_\mu \partial^\mu \chi_2$). The gauge-fixing Lagrangian is

$$\begin{aligned} \mathcal{L}_{\text{gauge-fixing}} \;=\; & -\frac{1}{2\xi} \left(\partial^\mu W_\mu^1 - \frac{\xi g \phi}{2} \chi_4 \right)^2 - \frac{1}{2\xi} \left(\partial^\mu W_\mu^2 - \frac{\xi g \phi}{2} \chi_3 \right)^2 \\ & - \frac{1}{2\xi} \left(\partial^\mu W_\mu^3 - \frac{\xi g \phi}{2} \chi_2 \right)^2 - \frac{1}{2\xi} \left(\partial^\mu B_\mu - \frac{\xi g' \phi}{2} \chi_2 \right)^2 \; . \end{aligned} \tag{5.12}$$

We choose to work in Landau gauge, $\xi \rightarrow 0$, so that

$$\mathcal{L}_{\text{gauge-fixing}} \;=\; -\frac{1}{2\xi} \left[\left(\partial^\mu W_\mu^1 \right)^2 + \left(\partial^\mu W_\mu^2 \right)^2 + \left(\partial^\mu W_\mu^3 \right)^2 + (\partial^\mu B_\mu)^2 \right]$$

Field		Mass
Gauge	$W^{\pm}$	$m_W^2 = \frac{1}{4}g^2\phi^2$
	Z	$m_Z^2 = \frac{1}{4}(g^2+g'^2)\phi^2$
	A	$m_A^2 = 0$
Ghost	ω_j, ζ	$m^2 = 0$
Fermion	t	$m_t^2 = \frac{1}{2}g_t^2\phi^2$
	other quarks	$m^2 = 0$
	leptons	$m^2 = 0$
Scalar	χ_1	$m_H^2 = \lambda(3\phi^2 - v^2)$
	$\chi_2, \chi^{\pm}$	$m_G^2 = \lambda(\phi^2 - v^2)$

Table 5.1: Summary of the fields and masses in the Standard Model, as approximated in this chapter.

$$+\frac{\phi}{2}\left(g\chi_4\partial^\mu W_\mu^1 + g\chi_3\partial^\mu W_\mu^2 + g\chi_2\partial^\mu W_\mu^3 + g'\chi_2\partial^\mu B_\mu\right) , \quad (5.13)$$

ensuring that only gauge configurations with $\partial^\mu W_\mu^k = 0$ and $\partial^\mu B_\mu = 0$ contribute to the functional integral. The cross terms combine with those from $|D_\mu\Phi|^2$ in $\mathcal{L}_{\text{Higgs}}$ to produce a total divergence that vanishes upon integration. In this gauge ghost fields are massless and do not couple to Φ, facilitating computation of the effective potential. Although the effective potential will be gauge-dependent, the physical quantities we extract from it must be gauge-*in*dependent. Denoting the $SU(2)_L$ and $U(1)_Y$ ghosts by ω_j and ζ, respectively, the ghost-field Lagrangian is then

$$\mathcal{L}_{\text{ghost}} = -\overline{\omega}_j\partial^2\omega_j - \overline{\zeta}\partial^2\zeta + g\varepsilon^{jkl}(\partial_\mu\overline{\omega}_j)\omega_k W_l^\mu , \quad (5.14)$$

so that the ghosts couple only to the W. We take the counter-term Lagrangian

$$\mathcal{L}_{\text{c.t.}} = A(\partial_\mu\Phi)^\dagger(\partial^\mu\Phi) + B\Phi^\dagger\Phi + C(\Phi^\dagger\Phi)^2 + D , \quad (5.15)$$

as we will renormalize only Φ explicitly.

Shifting Φ by its thermal average (5.10) in the spontaneously broken theory, the Standard Model gives mass to the gauge bosons, fermions, and scalars, and yet remains renormalizable. The degrees of freedom in our approximate Standard Model are summarized in Table 5.1. Neglecting constants and total divergences, the Lagrangian may be expressed as a kinetic part plus an interacting part:

$$\mathcal{L} = \mathcal{L}_0 + \mathcal{L}^{\text{I}}_{\text{gauge}} + \mathcal{L}^{\text{I}}_{\text{fermion}} + \mathcal{L}^{\text{I}}_{\text{Higgs}} + \mathcal{L}^{\text{I}}_{\text{Yukawa}} + \mathcal{L}_{\text{c.t.}} , \quad (5.16)$$

where

$$\begin{aligned}\mathcal{L}_0 \;=\; & -W_\mu^+\left[g^{\mu\nu}\left(-\partial^2 - m_W^2(\phi)\right) + (1-1/\xi)\,\partial^\mu\partial^\nu\right]W_\nu^- \\ & -\frac{1}{2}Z_\mu\left[g^{\mu\nu}\left(-\partial^2 - m_Z^2(\phi)\right) + (1-1/\xi)\,\partial^\mu\partial^\nu\right]Z_\nu \\ & -\frac{1}{2}A_\mu\left[-g^{\mu\nu}\partial^2 + (1-1/\xi)\,\partial^\mu\partial^\nu\right]A_\nu\end{aligned}$$

$$
\begin{aligned}
&- \overline{\omega}_j \partial^2 \omega_j - \overline{\zeta} \partial^2 \zeta \\
&+ \sum_a \left(\overline{u}^a \, i\partial\!\!\!/ u^a + \overline{d}^a \, i\partial\!\!\!/ d^a + \overline{\nu}^a \, i\partial\!\!\!/ \nu^a + \overline{e}^a \, i\partial\!\!\!/ e^a \right) - m_t(\phi)\, \overline{t}\, t \\
&+ \frac{1}{2}\chi_1 \left(-\partial^2 - m_H^2(\phi) \right) \chi_1 + \frac{1}{2}\chi_2 \left(-\partial^2 - m_G^2(\phi) \right) \chi_2 \\
&+ \chi^+ \left(-\partial^2 - m_G^2(\phi) \right) \chi^- \, .
\end{aligned} \tag{5.17}
$$

We list for reference the following interaction terms:

$$
\begin{aligned}
\mathcal{L}^{\mathrm{I}}_{\mathrm{gauge}} &= g\varepsilon^{jkl} \left(\partial_\mu W^j_\nu \right) W^\mu_k W^\nu_l + g^2 \left(\delta_{km}\delta_{ln} - \delta_{kn}\delta_{lm} \right) W^k_\mu W^l_\nu W^\mu_m W^\nu_n \\
&\quad + g\varepsilon^{jkl} (\partial_\mu \overline{\omega}_j) \omega_k W^\mu_l
\end{aligned} \tag{5.18}
$$

$$
\begin{aligned}
\mathcal{L}^{\mathrm{I}}_{\mathrm{fermion}} &= \sum_a -\frac{g}{2\sqrt{2}} W^+_\mu \left[\overline{u}\gamma^\mu (1-\gamma_5)\, d' + \overline{\nu}\gamma^\mu (1-\gamma_5)\, e \right] \\
&\quad - \frac{g}{2\sqrt{2}} W^-_\mu \left[\overline{d'}\gamma^\mu (1-\gamma_5)\, u + \overline{e}\gamma^\mu (1-\gamma_5)\, \nu \right] \\
&\quad + \frac{g}{4} W^3_\mu \left[-\overline{u}\gamma^\mu (1-\gamma_5)\, u + \overline{d}\gamma^\mu (1-\gamma_5)\, d \right. \\
&\qquad \left. - \overline{\nu}\gamma^\mu (1-\gamma_5)\, \nu + \overline{e}\gamma^\mu (1-\gamma_5)\, e \right] \\
&\quad + \frac{g'}{4} B_\mu \left[-\overline{u}\gamma^\mu \left(\frac{5}{3} + \gamma_5 \right) u + \overline{d}\gamma^\mu \left(\frac{1}{3} + \gamma_5 \right) d \right. \\
&\qquad \left. - \overline{\nu}\gamma^\mu (-1+\gamma_5)\, \nu + \overline{e}\gamma^\mu (3+\gamma_5)\, e \right]
\end{aligned} \tag{5.19}
$$

$$
\begin{aligned}
\mathcal{L}^{\mathrm{I}}_{\mathrm{Higgs}} &= (\mu^2\phi - \lambda\phi^3)\, \chi_1 - \lambda\phi\, \chi_1 \left(\chi_1^2 + \chi_2^2 + 2\,\chi^+\chi^- \right) \\
&\quad - \frac{\lambda}{4} \left(\chi_1^4 + \chi_2^4 + 2\,\chi_1^2\chi_2^2 \right) - \lambda \left(\chi_1^2 + \chi_2^2 \right) \chi^+\chi^- - \lambda \left(\chi^+\chi^- \right)^2 \\
&\quad + g m_W(\phi)\, \chi_1 W^+_\mu W^{-\,\mu} + \frac{g m_Z(\phi)}{2\cos\theta}\, \chi_1 Z_\mu Z^\mu \\
&\quad + \left(\chi^- W^+_\mu + \chi^+ W^-_\mu \right) \left[e m_W(\phi)\, A^\mu - g m_Z(\phi) \sin^2\theta\, Z^\mu \right] \\
&\quad + \frac{g^2}{4} \left(\chi_1^2 + \chi_2^2 + 2\,\chi^+\chi^- \right) W^+_\mu W^{-\,\mu} + \frac{g^2}{8\cos^2\theta} \left(\chi_1^2 + \chi_2^2 \right) Z_\mu Z^\mu \\
&\quad + \frac{g^2}{4\cos^2\theta}\, \chi^+\chi^- \left[\sin^2 2\theta\, A_\mu A^\mu + \cos^2 2\theta\, Z_\mu Z^\mu + \sin 4\theta\, A_\mu Z^\mu \right] \\
&\quad + \frac{ge}{\sqrt{2}} \left(H\chi^- W^+_\mu + H^\dagger \chi^+ W^-_\mu \right) \left[A^\mu - \tan\theta\, Z^\mu \right] \\
&\quad - \frac{g}{2\cos\theta} \left(\chi_1 \partial_\mu \chi_2 - \chi_2 \partial_\mu \chi_1 \right) Z^\mu \\
&\quad + \frac{g}{\cos\theta} \frac{1}{2i} \left(\chi^- \partial_\mu \chi^+ - \chi^+ \partial_\mu \chi^- \right) \left[\cos 2\theta\, Z^\mu + \sin 2\theta\, A^\mu \right] \\
&\quad + \frac{ig}{\sqrt{2}} \left[H(\partial^\mu \chi^-) W^+_\mu - H^\dagger (\partial^\mu \chi^+) W^-_\mu \right. \\
&\qquad \left. - (\partial^\mu H) \chi^- W^+_\mu + (\partial^\mu H)^\dagger \chi^+ W^-_\mu \right]
\end{aligned} \tag{5.20}
$$

$$
\mathcal{L}^{\mathrm{I}}_{\mathrm{Yukawa}} = -\frac{g_t}{\sqrt{2}} \left(\chi_1\, \overline{t}\, t - i\chi_2\, \overline{t}\, \gamma_5 t \right)
$$

$$+\frac{g_t}{2}\left(\chi^-\,\overline{b'}\,(1+\gamma_5)\,t+\chi^+\,\bar{t}\,(1-\gamma_5)\,b'\right)\ . \tag{5.21}$$

5.2 Effective Potential

Having established our notation, we now turn to computing the effective potential and deriving the baryogenesis bound on the Higgs boson mass. In general the effective potential may be written as the sum of a vacuum part and a thermal part:

$$V^T(\phi)=V^0(\phi)+\Delta V^T(\phi)\ . \tag{5.22}$$

Using the standard expressions derived in Appendix B, we may sum over the various particle species to obtain the effective potential for the Standard Model at one loop, subject to our usual renormalization conditions:

$$\begin{aligned} V^0_{1\,\mathrm{loop}}(\phi) &= V(\phi)+\sum_{j=B,F}\frac{\pm g_j}{64\pi^2}\left[m_j^4(\phi)\log\left(\frac{m_j^2(\phi)}{M_j^2}\right)-\frac{3}{2}m_j^4(\phi)+2M_j^2m_j^2(\phi)\right] \\ \Delta V^T_{1\,\mathrm{loop}}(\phi) &= T^4\sum_B g_B I_B\left(\frac{m_B(\phi)}{T}\right)+T^4\sum_F g_F I_F\left(\frac{m_F(\phi)}{T}\right)\ , \end{aligned} \tag{5.23}$$

where

$$V(\phi)=\frac{M_H^2}{8v^2}\left(\phi^2-v^2\right)^2\ . \tag{5.24}$$

The conditions

$$\begin{aligned} \left.\frac{dV^0}{d\phi}\right|_{\phi=v} &= 0 \\ \left.\frac{d^2V^0}{d\phi^2}\right|_{\phi=v} &= M_H^2 \end{aligned} \tag{5.25}$$

preserve at one loop the tree-level expressions for the minimum and corresponding mass, g_j counts the degrees of freedom, $\pm$ is for bosons or fermions, and the temperature integrals $I_{B,F}$ are given in (B.5) and (B.6). At high temperature, $M_j \lesssim T$, the integrals $I_{B,F}$ may be approximated as

$$\begin{aligned} I_B(y) &= \frac{y^2}{24}-\frac{y^3}{12\pi}-\frac{y^4}{64\pi^2}\log\left(y^2/c_B\right)+\mathcal{O}\left(y^6,y^6\log y^2\right) \\ I_F(y) &= \frac{y^2}{48}+\frac{y^4}{64\pi^2}\log\left(y^2/c_F\right)+\mathcal{O}\left(y^6,y^6\log y^2\right)\ , \end{aligned}$$

yielding the following expression:

$$\begin{aligned} V^T_{1\,\mathrm{loop}}(\phi) &= V(\phi) \\ &\quad+\sum_B g_B\left\{\left(\frac{M_B^2}{32\pi^2}+\frac{T^2}{24}\right)m_B^2(\phi)-\frac{T}{12\pi}m_B^3(\phi)-\frac{m_B^4(\phi)}{64\pi^2}\log\left(\frac{M_B^2}{a_BT^2}\right)\right\} \end{aligned}$$

$$-\sum_F g_F \left\{ \left(\frac{M_F^2}{32\pi^2} - \frac{T^2}{48} \right) m_F^2(\phi) - \frac{m_F^4(\phi)}{64\pi^2} \log \left(\frac{M_F^2}{a_F T^2} \right) \right\} . \qquad (5.26)$$

We will divide our analysis below into two cases, depending on the relative masses of the scalar and gauge bosons. In the case of light scalars, $M_{\rm scalar} \lesssim M_W$, scalar loops may be neglected from the one-loop effective potential and the analysis is greatly simplified. For heavy scalars, $M_{\rm scalar} \gtrsim M_W$, scalar loops must be included.

As we have seen in Chapter 3, an accurate analysis demands that we sum the ring diagrams to account for the leading infrared effects, which contribute to the cubic term in V^T at the same order as the one-loop graphs. Fermion ring diagrams need not be considered since they do not contribute to the cubic terms $\sim T m_j^3(\phi)$. The scalar modes all receive cubic contributions from the ring summation, while only the longitudinal components do so for the massive gauge fields:

$$\begin{aligned} \Delta V^T_{\rm ring}(\phi) \;=\; & -\frac{T}{12\pi} \sum_{j={\rm scalar}} \left\{ \left[m_j^2(\phi) + \Pi_j(0) \right]^{3/2} - m_j^3(\phi) \right\} \\ & -\frac{T}{12\pi} \sum_{\substack{j={\rm long.} \\ {\rm gauge}}} \left\{ \left[m_j^2(\phi) + \Pi_j^{00}(0) \right]^{3/2} - m_j^3(\phi) \right\} . \end{aligned} \qquad (5.27)$$

$\Pi(0)$ and $\Pi^{00}(0)$ are the scalar self-energy and longitudinal component of the polarization tensor at zero momentum.

In the following sections, we will determine the critical temperature $T_{\rm crit}$, the order parameter at the critical point $(\phi/T)_{\rm crit}$, and the nature of the phase transition, as functions of the parameters M_H and M_t. By requiring that sphaleron-mediated effects not be in equilibrium at the end of the phase transition, in order for a net baryon number to survive, we will obtain a cosmological mass bound on the Higgs boson. This will be done first for light scalars and then for heavy scalars.

5.3 Light Scalars

First we assume light scalar modes, $M_{\rm scalar} \lesssim M_W$, [1] and neglect scalar loops in the effective potential. This case, at one loop and with ring improvement, has been analyzed in [18, 19]; we give the details of the calculation below.

[1] Or equivalently, $\lambda \lesssim g^2$. It is only the scalar self-interactions (and non-top Yukawa interactions in our approximation) that are neglected; gauge couplings to scalars (and fermions) *are* included when computing polarization tensors in the later treatment of gauge ring diagrams.

One Loop

The one-loop effective potential is given by (5.26), with $B = W^{\pm}, Z$ and $F = t$. The result may be written at high temperature in the form [43, 20]

$$V_{1\,\mathrm{loop}}^{T}(\phi) = D\left(T^2 - T_0^2\right)\phi^2 - ET\phi^3 + \frac{\lambda_T}{4}\phi^4\,, \tag{5.28}$$

where

$$\begin{aligned}
D &= \frac{1}{24v^2}\left(6M_W^2 + 3M_Z^2 + 6M_t^2\right)\\
T_0^2 &= \frac{1}{D}\left(\frac{M_H^2}{4} - \frac{1}{32\pi^2 v^2}\left[6M_W^4 + 3M_Z^4 - 12M_t^4\right]\right)\\
E &= \frac{1}{12\pi v^3}\left(6M_W^3 + 3M_Z^3\right)\\
\lambda_T &= \lambda - \frac{1}{16\pi^2 v^4}\left[6M_W^4 \log\left(\frac{M_W^2}{a_B T^2}\right)\right.\\
&\qquad \left. + 3M_Z^4 \log\left(\frac{M_Z^2}{a_B T^2}\right) - 12M_t^4 \log\left(\frac{M_t^2}{a_F T^2}\right)\right]\,.
\end{aligned} \tag{5.29}$$

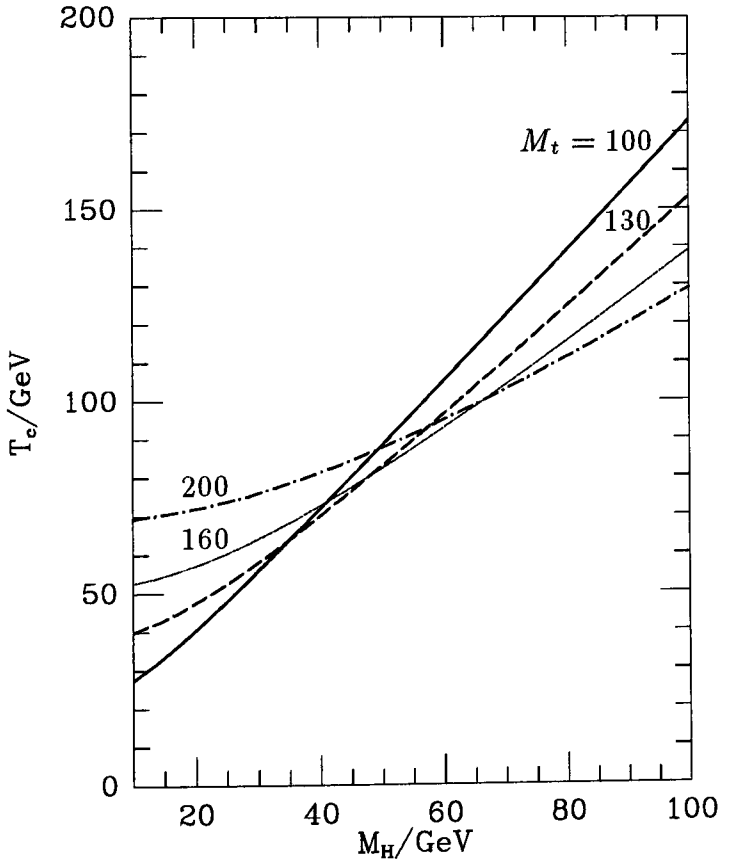

Figure 5.1: The critical temperature at one loop in the Standard Model with light scalars; the top mass in GeV labels the lines.

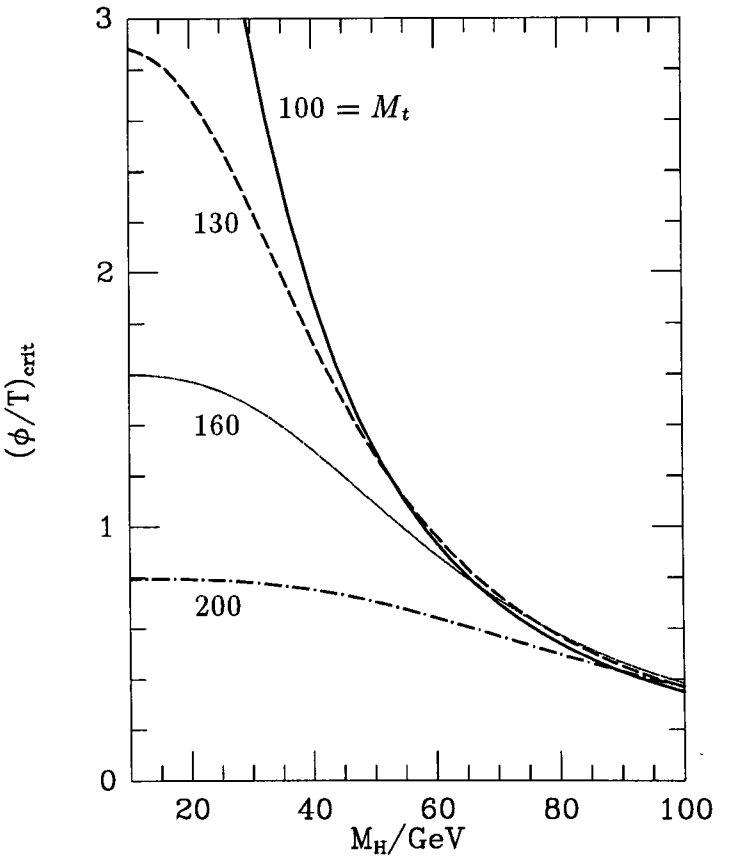

Figure 5.2: The critical point at one loop in the Standard Model with light scalars.

We define T_c to be the critical temperature where the curvature of V^T at the origin vanishes, which equals T_0 given above for the Standard Model (but differs for

its ring-improvement and extensions). [2] At the critical temperature, the asymmetric minimum is $(\phi/T)_{\rm crit} = 3E/\lambda_{T_0}$. The values of T_c and $(\phi/T)_{\rm crit}$ as functions of the Higgs mass M_H are displayed in Figures 5.1 and 5.2, for four choices of the top quark mass in the phenomenologically restricted range $M_t \sim 100$ to 200 GeV [42]. Requiring $(\phi/T)_{\rm crit} \gtrsim 1$ — necessary to avoid baryon washout — yields the Higgs mass bound $M_H \lesssim 55$ GeV. This is barely consistent with the individual limits set by the four LEP experiments, which when combined yield the even stricter bound $M_H \gtrsim 60$ GeV [42].

Thus, at one loop, first-order behavior is observed at the phase transition, provided that $M_H \lesssim 55$ GeV. However, for the reasons enumerated in our analysis of the scalar and Higgs models in Section 3.3, we now include the ring diagrams.

Ring Improvement

The negative cubic term in the effective potential arises from the zero modes of the massive gauge loops, and just as in the scalar and Higgs theories, gauge ring diagrams — which contribute to E at the same order in coupling constants — must be included for consistency. However, as we compute below, it is only the longitudinal component of $W^{\pm}$ or Z that gains a thermal mass ($\Pi^{00} \sim g^2T^2,\ g'^2T^2$) at one loop; the two transverse components do not, and hence their ring diagrams vanish. Consequently, summing the gauge ring diagrams cancels only 1/3 of the cubic term, i.e., E is reduced by a factor 2/3. The resulting effective potential is

$$\begin{aligned} V^T_{\rm ring}(\phi) &= D\left(T^2 - T_0^2\right)\phi^2 - \frac{2}{3}ET\phi^3 + \frac{\lambda_T}{4}\phi^4 \\ &\quad - \frac{T}{12\pi}\left\{2\left[m_W^2(\phi) + \Pi_W^{00}(0)\right]^{3/2} + \left[m_Z^2(\phi) + \Pi_Z^{00}(0)\right]^{3/2}\right\} . \quad (5.30) \end{aligned}$$

The gauge polarization tensors are given by the graphs of Figure 5.3, where gauge, fermionic, and scalar contributions are separated, and may be computed in analogy to Section 3.3 for the Abelian Higgs model. $\Pi^{\mu\nu}(0)$ is calculated to leading order in the temperature, and is simply given by the quadratically divergent graphs. Decomposing the four-dimensionally transverse polarization tensors into three-dimensionally longitudinal and transverse components, $\Pi_j^{\mu\nu} = -\Pi_j^{00}L^{\mu\nu} + \frac{1}{2}\Pi_j^{kk}T^{\mu\nu}$, and using the integrals

[2] One may also define the critical temperature to occur when the origin and asymmetric minimum are degenerate, i.e., when $V^T(0) = V^T(\phi_{\rm min})$. We choose our definition as the more appropriate one for considering baryon washout at the end of the phase transition; this choice, however, is immaterial to our results, since the Higgs mass bounds we derive are consistent with (indeed, more conservative than) those obtained with the alternative definition.

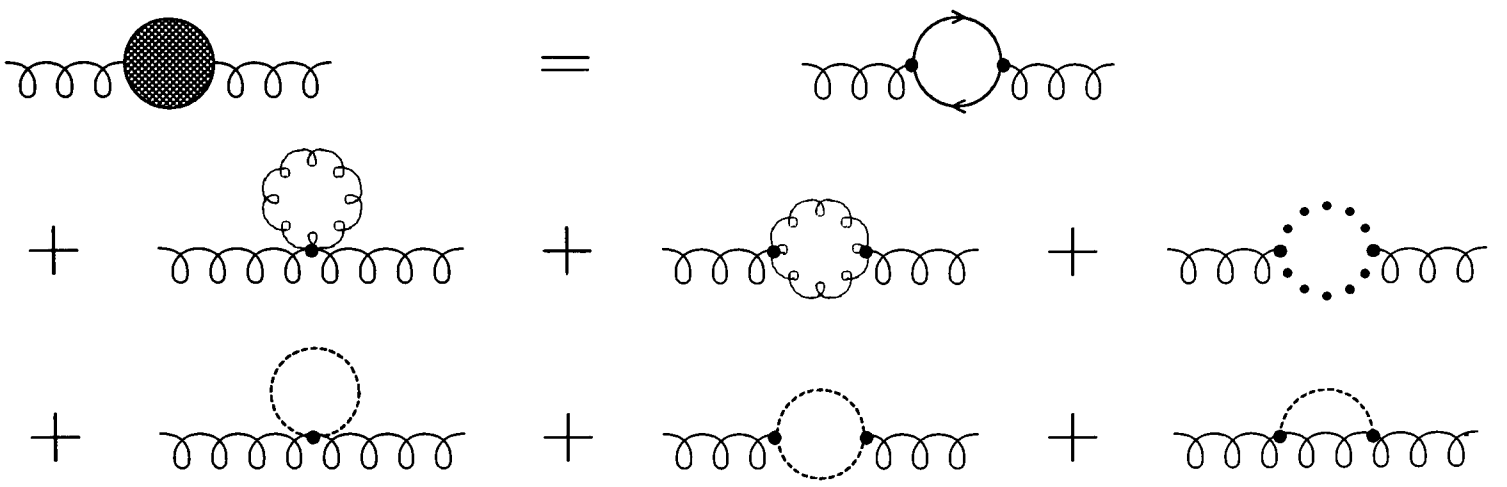

Figure 5.3: The gauge polarization tensor at one loop in the Standard Model.

tabulated in Appendix C, our final result at one loop is

$$\begin{aligned}
& & \boxed{\text{gauge}} & & \boxed{\text{fermionic}} & & \boxed{\text{scalar}} \\
\Pi_W^{00}(0) = & & g^2T^2 & + & \tfrac{1}{6}g^2T^2 & + & \tfrac{2}{3}g^2T^2 \\
\Pi_Z^{00}(0) = & & \left(g^2\cos^2\theta_{\rm W} + \tfrac{5}{3}g'^2\sin^2\theta_{\rm W}\right)T^2 & + & \tfrac{1+\cos^2 2\theta_{\rm W}}{12\cos^2\theta_{\rm W}}g^2T^2 & + & \tfrac{2}{3}g^2\cos^2\theta_{\rm W}T^2 \\
\Pi_A^{00}(0) = & & \tfrac{8}{3}e^2T^2 & + & \tfrac{1}{3}e^2T^2 & + & \tfrac{2}{3}e^2T^2\,,
\end{aligned} \tag{5.31}$$

while the transverse component vanishes at one loop, for all gauge fields: $\Pi_j^{kk}(0) = 0$. We parametrize the longitudinal components by $\Pi_W^{00}(0) \equiv wT^2$ and $\Pi_Z^{00}(0) \equiv zT^2$.

The critical point is now characterized by

Critical temperature: (5.32)

$$T_{\rm c}^2 = \frac{T_0^2}{1 - \frac{1}{32\pi D}\left[2g^2\sqrt{w} + \frac{g^2}{\cos^2\theta_{\rm W}}\sqrt{z}\right]}$$

Asymmetric minimum: (5.33)

$$\begin{aligned}
\lambda_{T_{\rm c}}\left(\frac{\phi}{T}\right)_{\rm crit} - 2E = & \frac{1}{4\pi\left(\frac{\phi}{T}\right)_{\rm crit}}\left\{2\frac{g^2}{4}\left(\sqrt{\frac{g^2}{4}\left(\frac{\phi}{T}\right)_{\rm crit}^2 + w} - \sqrt{w}\right)\right. \\
& \left. + \frac{g^2}{4\cos^2\theta_{\rm W}}\left(\sqrt{\frac{g^2}{4\cos^2\theta_{\rm W}}\left(\frac{\phi}{T}\right)_{\rm crit}^2 + z} - \sqrt{z}\right)\right\}.
\end{aligned}$$

$T_{\rm c}$ and $(\phi/T)_{\rm crit}$ versus M_H are plotted in Figures 5.4 and 5.5.

Because the contribution of ring diagrams dampens the negative cubic term present at one loop, $V_{\rm ring}^T$ displays more weakly first-order behavior at the phase transition; the one-loop and ring-improved results are compared for $M_t = 130$ GeV in Figures 5.6 and 5.7. The condition for avoiding baryon washout, $(\phi/T)_{\rm crit} \gtrsim 1$, now places an upper bound of 45 GeV on the Higgs mass, which clearly violates the bound from LEP [42].

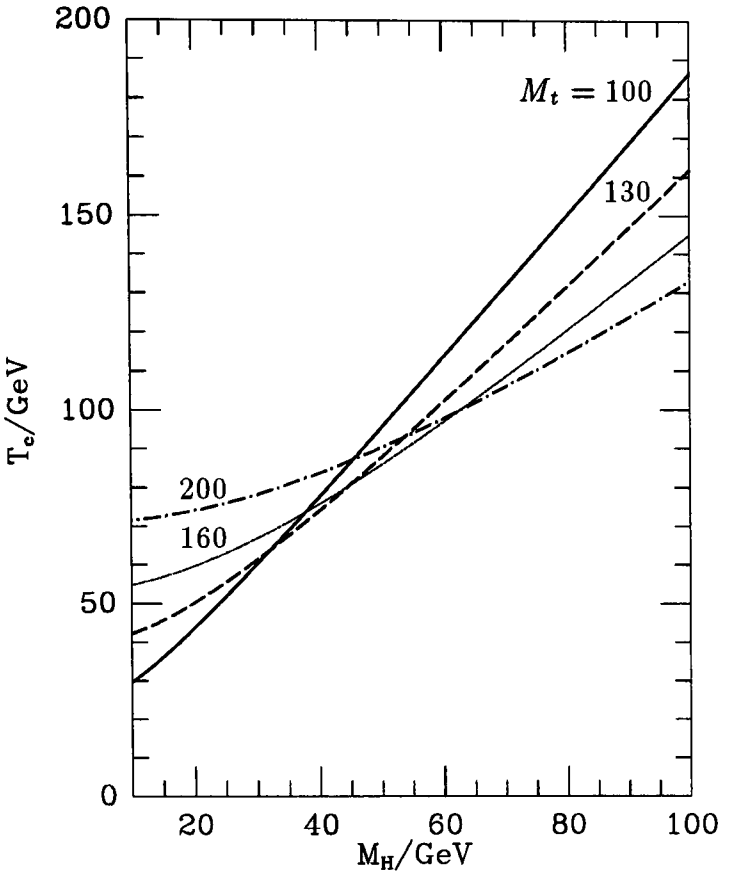

Figure 5.4: The critical temperature with ring improvement in the Standard Model with light scalars; the top mass in GeV labels the lines.

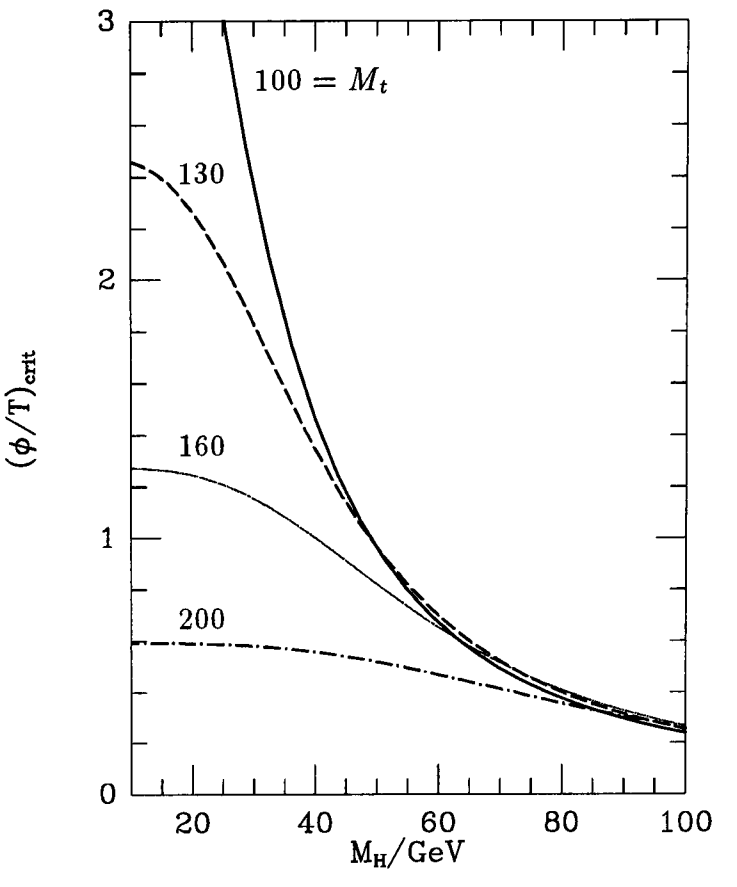

Figure 5.5: The critical point with ring improvement in the Standard Model with light scalars.

5.4 Heavy Scalars

The results of the previous section for the critical temperature and critical point (Figures 5.1, 5.2, 5.4, and 5.5) may be questioned, however, for they lead to a mass bound on the Higgs boson (50 – 60 GeV) that is near the range where scalar loops must be included in the effective potential. This section considers the more general case of heavy scalars ($M_H \sim M_W$), and shows explicitly, through calculations first at one loop and then with ring improvement, that such fears are groundless; the cosmological mass bound on the Higgs boson remains unchanged.

One Loop

To (5.28) we must add the scalar loops due to the Higgs field χ_1 and Goldstone fields χ_2, and $\chi^{\pm}$. Using (5.26), we arrive at the following expression:

$$\begin{aligned} V^T_{1\,\mathrm{loop}}(\phi) &= D'\left(T^2 - T_0'^2\right)\phi^2 - ET\phi^3 + \frac{\lambda'_T}{4}\phi^4 \\ &\quad - \frac{T}{12\pi}\left(\frac{M_H^2}{2v^2}\right)^{3/2}\left[(3\phi^2 - v^2)^{3/2} + 3(\phi^2 - v^2)^{3/2}\right], \end{aligned} \tag{5.34}$$

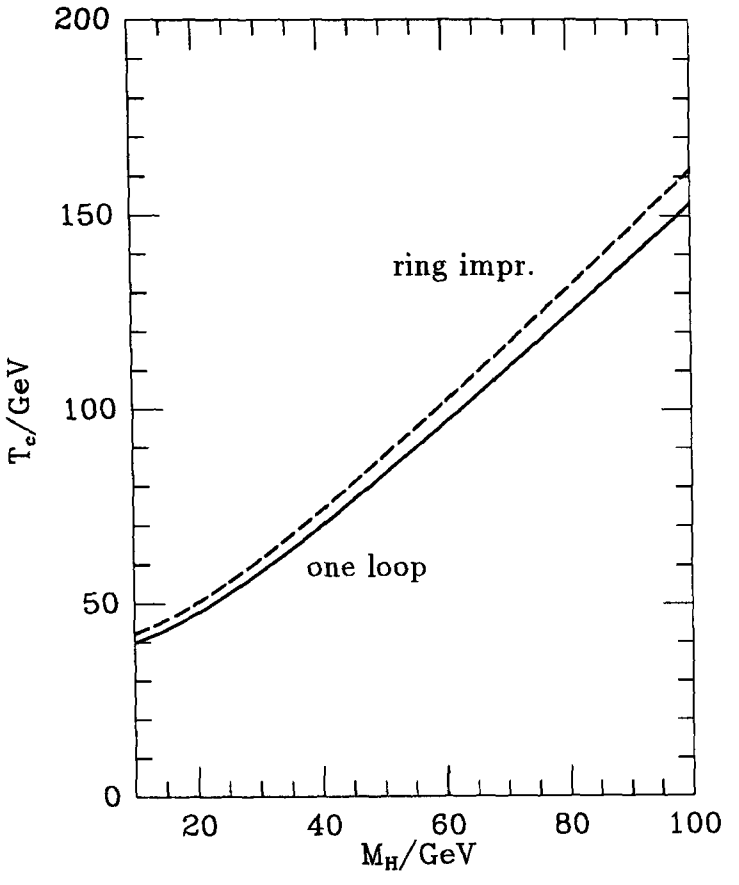

Figure 5.6: The critical temperature at one loop and with ring improvement in the Standard Model with light scalars; $M_t = 130$ GeV.

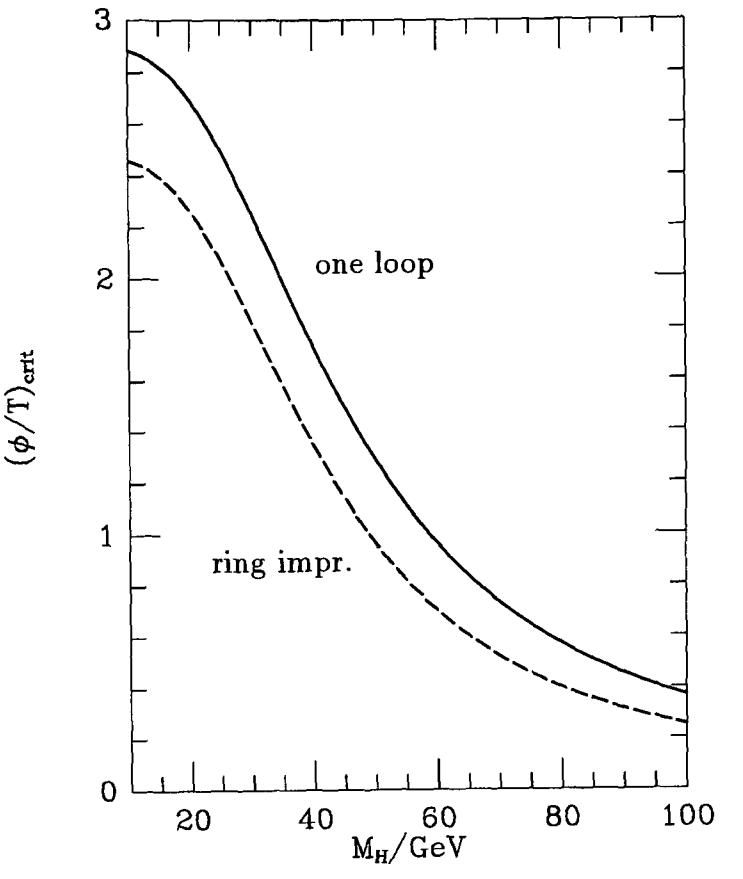

Figure 5.7: The critical point at one loop and with ring improvement in the Standard Model with light scalars; $M_t = 130$ GeV.

where

$$
\begin{aligned}
D' &= D + \frac{M_H^2}{8v^2} = \frac{1}{24v^2}\left(6M_W^2 + 3M_Z^2 + 6M_t^2 + 3M_H^2\right) \\
T_0'^2 &= \frac{1}{D'}\left[DT_0^2 - \frac{3M_H^4}{64\pi^2v^2} - \frac{3M_H^4}{128\pi^2v^2}\log\left(\frac{M_H^2}{a_B T^2}\right)\right] \\
&= \frac{1}{D'}\left[\frac{M_H^2}{4} - \frac{1}{32\pi^2v^2}\left(6M_W^4 + 3M_Z^4 - 12M_t^4 + \frac{3}{2}M_H^4\right) - \frac{3M_H^4}{128\pi^2v^2}\log\left(\frac{M_H^2}{a_B T^2}\right)\right] \\
\lambda_T' &= \lambda_T - \frac{9M_H^4}{64\pi^2v^4}\log\left(\frac{M_H^2}{a_B T^2}\right) \\
&= \frac{M_H^2}{2v^2} - \frac{1}{16\pi^2v^4}\left[6M_W^4\log\left(\frac{M_W^2}{a_B T^2}\right) + 3M_Z^4\log\left(\frac{M_Z^2}{a_B T^2}\right)\right. \\
&\qquad \left. - 12M_t^4\log\left(\frac{M_t^2}{a_F T^2}\right) + \frac{9}{4}M_H^4\log\left(\frac{M_H^2}{a_B T^2}\right)\right] .
\end{aligned}
\tag{5.35}
$$

The critical point is now characterized by

Critical temperature: (5.36)

$$
T_c^2 = T_0'^2(T_c) = \frac{1}{D'}\left[\frac{M_H^2}{4} - \frac{1}{32\pi^2v^2}\left(6M_W^4 + 3M_Z^4 - 12M_t^4 + \frac{3}{2}M_H^4\right)\right.
$$

$$- \frac{3M_H^4}{128\pi^2 v^2} \log\left(\frac{M_H^2}{a_B T_c^2}\right)\Bigg]$$

Asymmetric minimum:

$$\lambda'_{T_c}\left(\frac{\phi}{T}\right)_{\text{crit}} - 3E = \frac{3}{4\pi\left(\frac{\phi}{T}\right)_{\text{crit}}}\left(\frac{M_H^2}{2v^2}\right)^{3/2} \mathcal{R}e\left\{\sqrt{\left(\frac{\phi}{T}\right)^2_{\text{crit}} - \frac{v^2}{T_c^2}} - \sqrt{-\frac{v^2}{T_c^2}} + \sqrt{3\left(\frac{\phi}{T}\right)^2_{\text{crit}} - \frac{v^2}{T_c^2}} - \sqrt{-\frac{v^2}{T_c^2}}\right\} . \tag{5.37}$$

T_c and $(\phi/T)_{\text{crit}}$ as functions of M_H are plotted in Figures 5.8 and 5.9. While the values

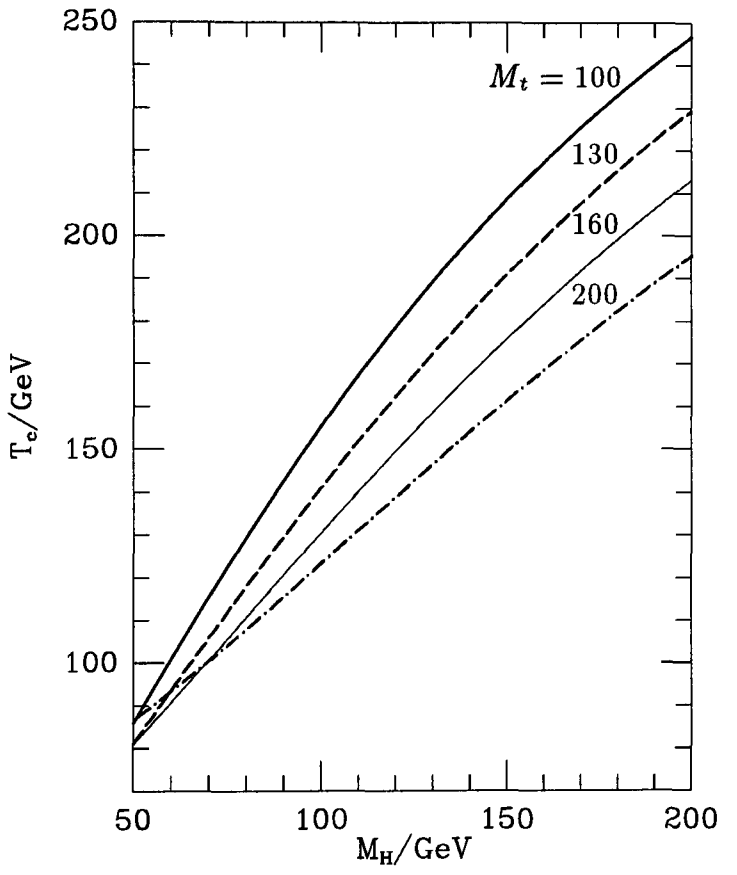

Figure 5.8: The critical temperature at one loop in the Standard Model with heavy scalars; the top mass in GeV labels the lines.

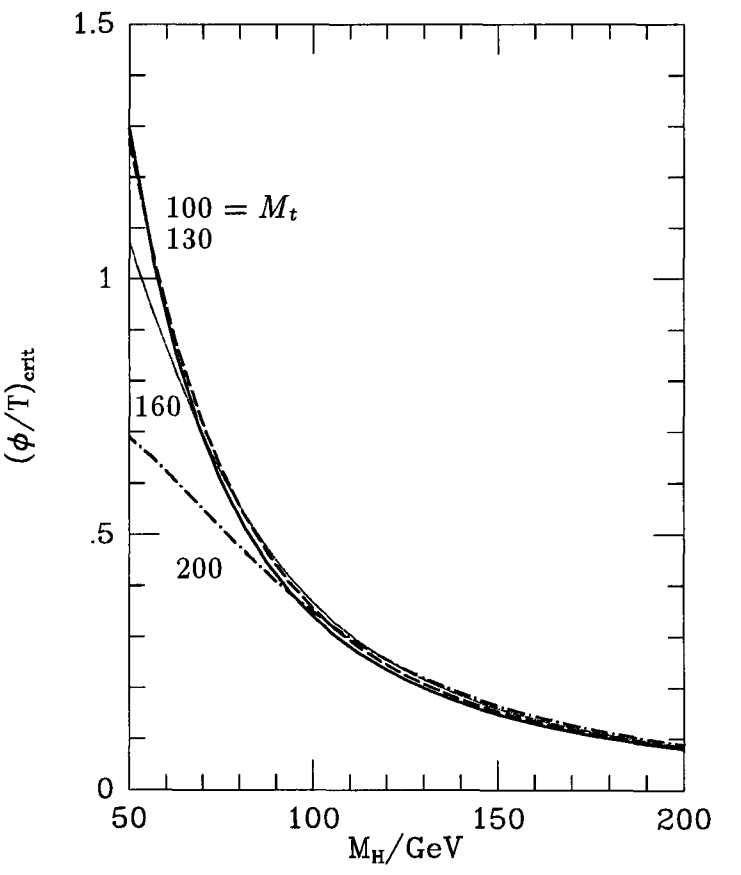

Figure 5.9: The critical point at one loop in the Standard Model with heavy scalars.

of T_c and $(\phi/T)_{\text{crit}}$ at large M_H are indeed different from those of the previous case for light scalars, first-order behavior ($(\phi/T)_{\text{crit}} \gtrsim 1$) obtains precisely in the region of low $M_H \lesssim M_W$ where neglecting scalar loops is a valid approximation. Hence we have the same mass bound at one loop: $M_H \lesssim 50$ GeV.

Ring Improvement

Summing ring diagrams for both the gauge and scalar modes results in the expression

$$\begin{aligned} V^T_{\text{ring}}(\phi) &= D'\left(T^2 - T_0'^2\right)\phi^2 - \frac{2}{3}ET\phi^3 + \frac{\lambda'_T}{4}\phi^4 \\ &\quad - \frac{T}{12\pi}\left\{2\left[m_W^2(\phi) + \Pi_W^{00}(0)\right]^{3/2} + \left[m_Z^2(\phi) + \Pi_Z^{00}(0)\right]^{3/2}\right. \\ &\quad \left. + \left[m_H^2(\phi) + \Pi(0)\right]^{3/2} + 3\left[m_G^2(\phi) + \Pi(0)\right]^{3/2}\right\} . \end{aligned} \tag{5.38}$$

The scalar self-energy may be computed from the Feynman diagrams of Figure 5.10 and the integrals of Appendix C; the result is

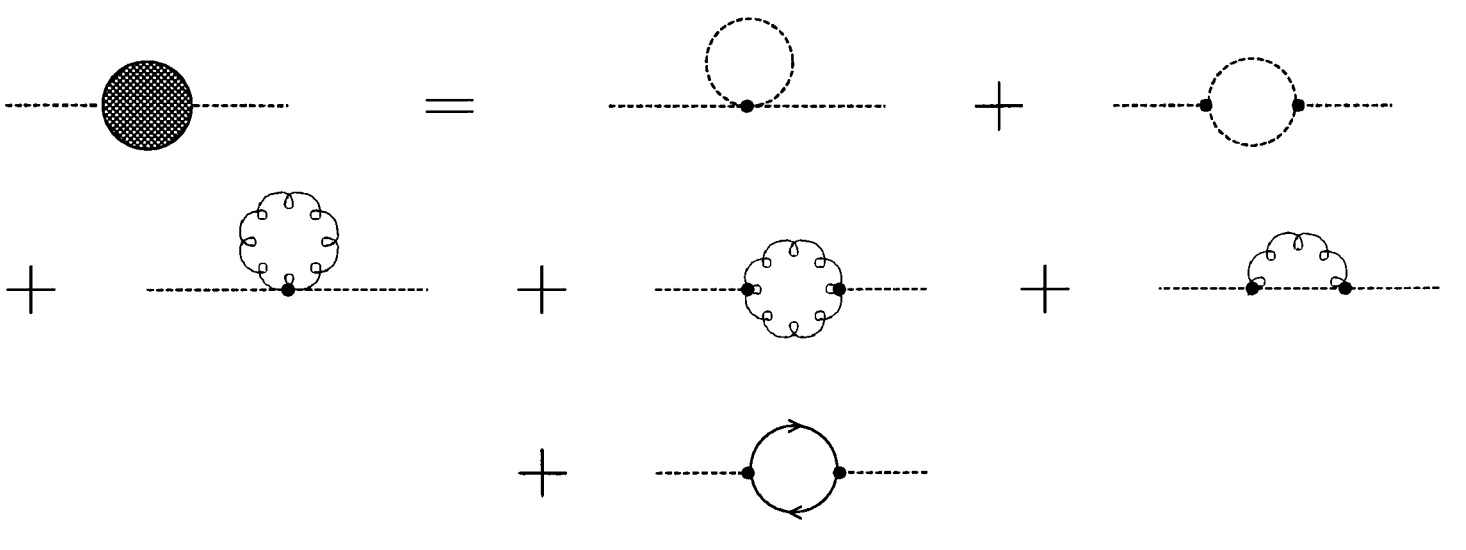

Figure 5.10: The scalar self-energy at one loop in the Standard Model.

$$\Pi(0) = \frac{1}{2}\lambda T^2 + \left(\frac{1}{8} + \frac{1}{16\cos^2\theta_{\text{W}}}\right) g^2T^2 + \frac{1}{4}g_t^2T^2 , \tag{5.39}$$

where the individual pieces correspond to the scalar, gauge, and fermionic contributions, respectively. We parametrize the scalar self-energy by $\Pi(0) \equiv hT^2$.

The critical point is now characterized by

Critical temperature: (5.40)

$$T_{\text{c}}^2 = T_0'^2(T_{\text{c}}) + \frac{T_{\text{c}}}{8\pi D'}\left\{2\frac{g^2}{4}\sqrt{wT_{\text{c}}^2} + \frac{g^2}{4\cos^2\theta_{\text{W}}}\sqrt{zT_{\text{c}}^2} + 3\frac{M_H^2}{2v^2}2\sqrt{\frac{-M_H^2}{2} + hT_{\text{c}}^2}\right\}$$

Asymmetric minimum: (5.41)

$$\begin{aligned} \lambda'_{T_{\text{c}}}\left(\frac{\phi}{T}\right)_{\text{crit}} - 2E &= \frac{1}{4\pi\left(\frac{\phi}{T}\right)_{\text{crit}}}\left\{2\frac{g^2}{4}\left(\sqrt{\frac{g^2}{4}\left(\frac{\phi}{T}\right)_{\text{crit}}^2 + w} - \sqrt{w}\right)\right. \\ &\quad \left. + \frac{g^2}{4\cos^2\theta_{\text{W}}}\left(\sqrt{\frac{g^2}{4\cos^2\theta_{\text{W}}}\left(\frac{\phi}{T}\right)_{\text{crit}}^2 + z} - \sqrt{z}\right)\right. \end{aligned}$$

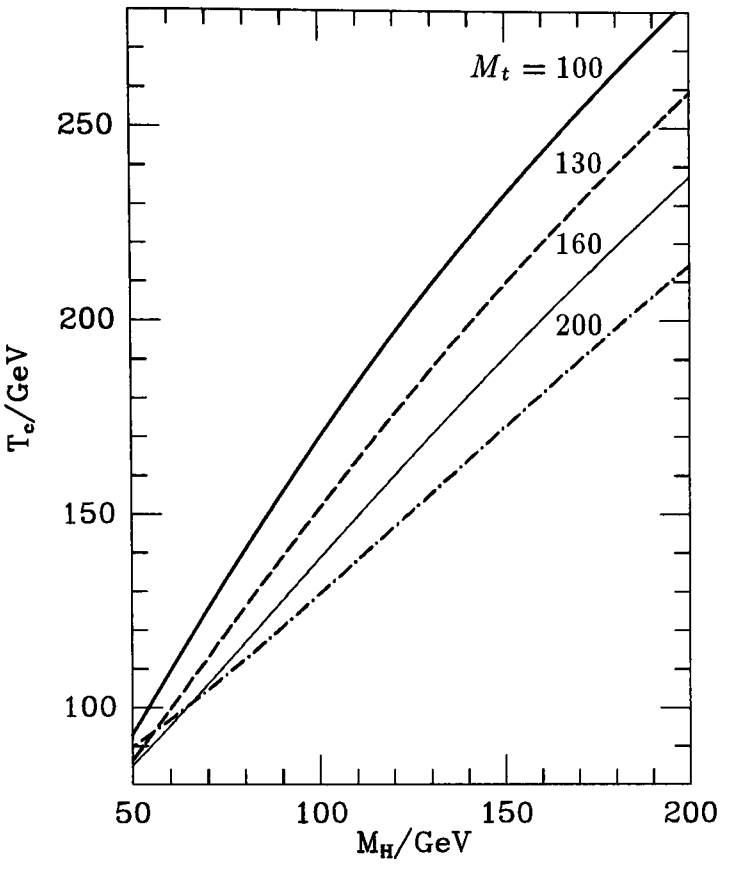

Figure 5.11: The critical temperature with ring improvement in the Standard Model with heavy scalars; the top mass in GeV labels the lines.

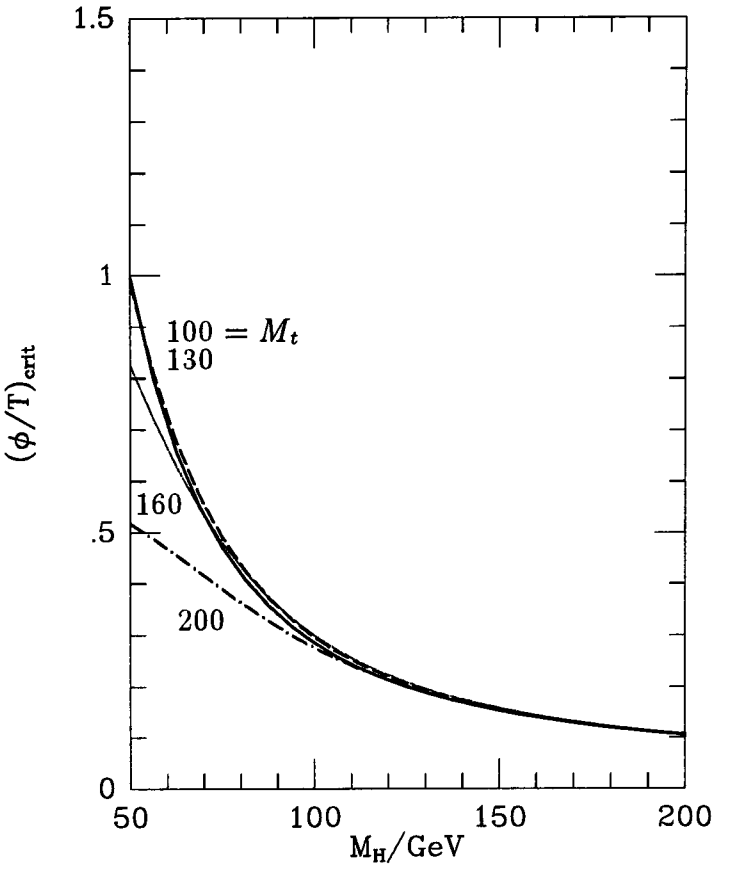

Figure 5.12: The critical point with ring improvement in the Standard Model with heavy scalars.

$$+ 3\frac{M_H^2}{2v^2}\left[\sqrt{\frac{M_H^2}{2v^2}\left[3\left(\frac{\phi}{T}\right)^2_{\rm crit} - \frac{v^2}{T_c^2}\right] + h} - \sqrt{-\frac{M_H^2}{2v^2}\frac{v^2}{T_c^2} + h}\right.$$
$$\left. + \sqrt{\frac{M_H^2}{2v^2}\left[\left(\frac{\phi}{T}\right)^2_{\rm crit} - \frac{v^2}{T_c^2}\right] + h} - \sqrt{-\frac{M_H^2}{2v^2}\frac{v^2}{T_c^2} + h}\right\} .$$

T_c and $(\phi/T)_{\rm crit}$ are shown as functions of M_H in Figures 5.11 and 5.12. Again we observe that ring improvement considerably reduces the strength of first-order behavior compared to that at one loop; Figures 5.13 and 5.14 compare the results for T_c and $(\phi/T)_{\rm crit}$ at one loop and with ring improvement. Notice that the corresponding mass bound on the Higgs boson of $M_H \lesssim 50$ GeV is little changed from that obtained in the previous section, where scalar loops were neglected.

5.5 Discussion

The effects of ring improvement on the Standard Model with light and heavy scalars are compared in Figures 5.15 and 5.16, which display the critical temperature and $(\phi/T)_{\rm crit}$ as functions of the Higgs mass, with the top mass fixed at the phenomenologically favored value of 130 GeV [42]. The Higgs mass bounds for each case, obtained by requiring $(\phi/T)_{\rm crit} \gtrsim 1$, are shown as functions of the top mass in Figure 5.17.

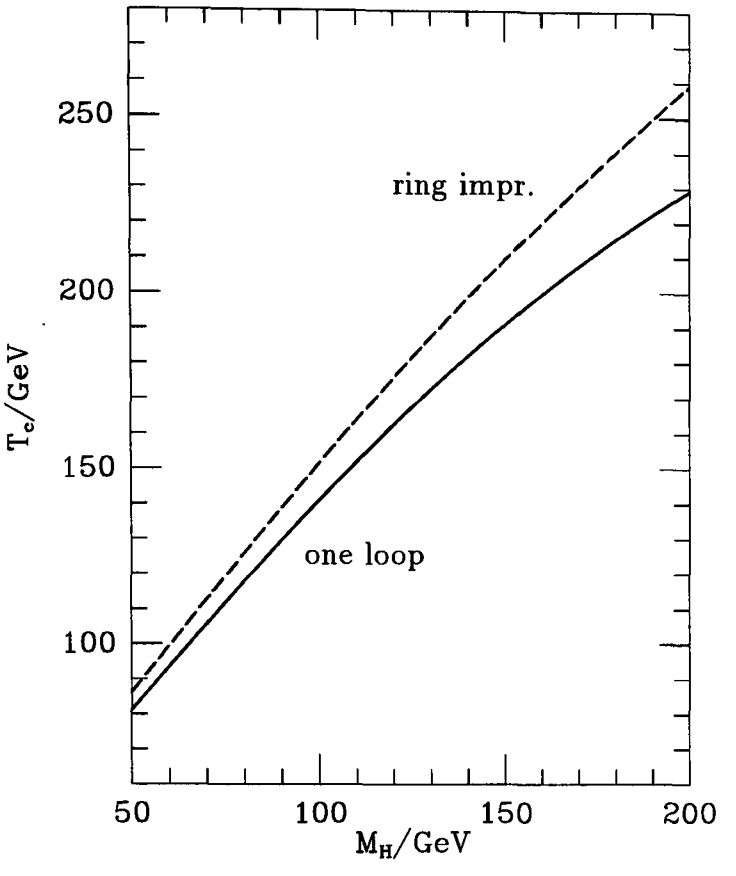

Figure 5.13: The critical temperature at one loop and with ring improvement in the Standard Model with heavy scalars; $M_t = 130$ GeV.

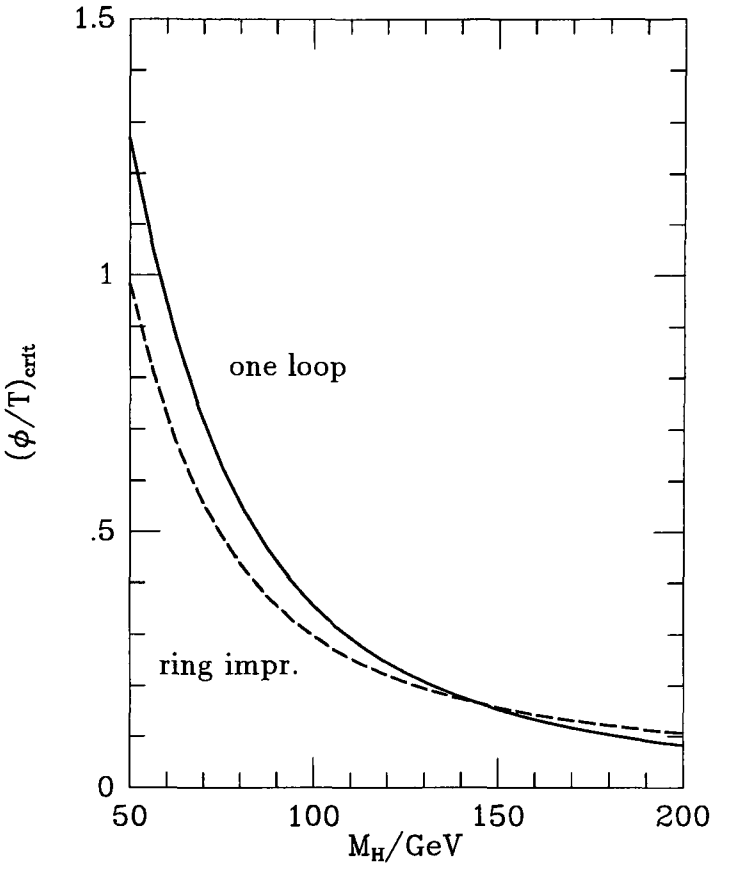

Figure 5.14: The critical point at one loop and with ring improvement in the Standard Model with heavy scalars; $M_t = 130$ GeV.

The sharp downturn at large M_t is due to the dominance of a heavy top mass in the one-loop effective potential at zero temperature, and is related to the question of vacuum stability. It is evident that the effects of ring-improvement are quite significant, reducing the bounds on M_H by up to 20%.

It is also apparent that first-order behavior is strongest for $M_H \lesssim M_W$. Thus the approximation of neglecting scalar loops in V^T is a valid one for the purpose of obtaining the baryogenesis bound on the Higgs boson mass, as we can see from Figure 5.17, where the one-loop and ring-improved curves are virtually indistinguishable. Values of T_c and $(\phi/T)_{\rm crit}$ are significantly different between the two cases of light and heavy scalar modes only for $M_H \gtrsim M_W$, in the region where the phase transition displays very weakly first-order behavior. While it has been claimed previously in the literature that the Standard Model with a heavy Higgs boson undergoes a second-order phase transition [30, 21], it is satisfying to see explicitly how the inclusion of scalar loops weakens the first-order nature of the phase transition and to observe the passage between the two regimes. In this description, it is the gauge loops that drive the phase transition and determine the strength of first-order behavior.

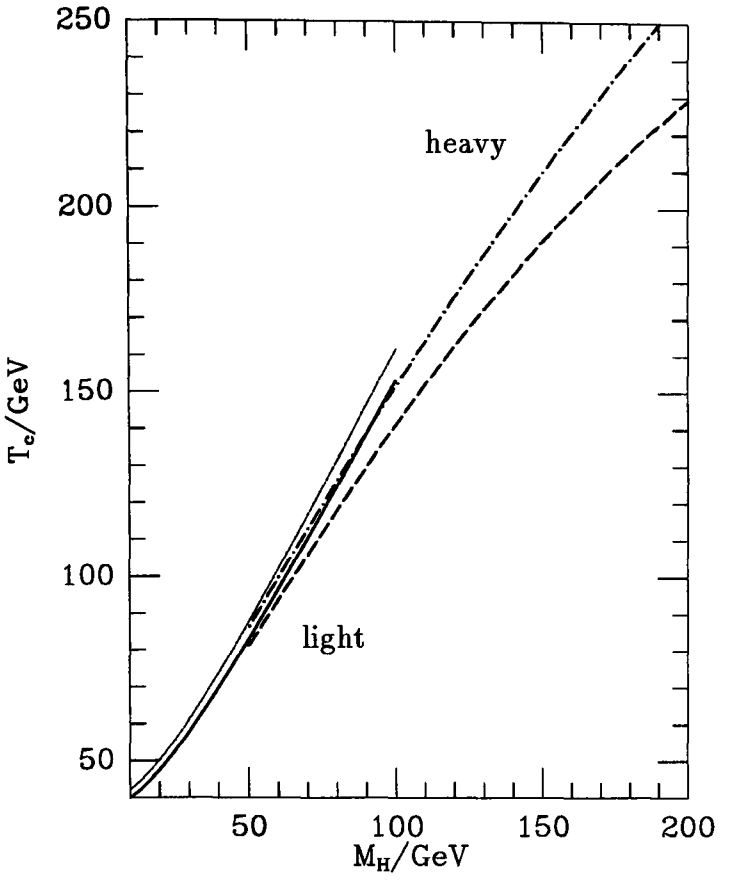

Figure 5.15: Comparison of the critical temperatures in the Standard Model with light and heavy scalars, at one loop (solid and dashed lines respectively) and with ring improvement (dotted and dash-dotted lines respectively); $M_t = 130$ GeV.

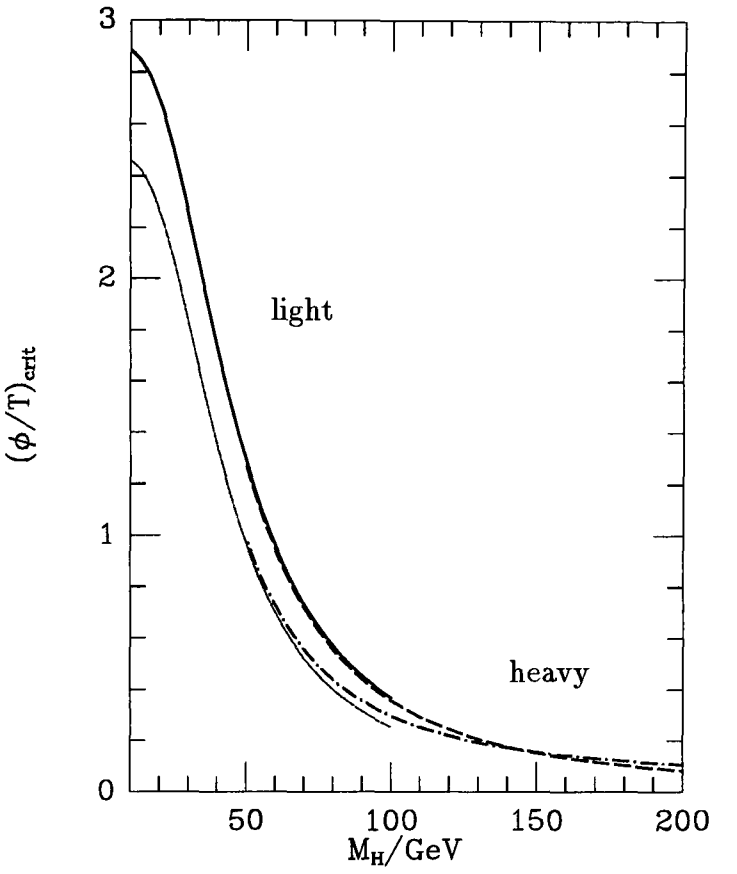

Figure 5.16: Comparison of the critical points in the Standard Model with light and heavy scalars, at one loop and with ring improvement (lines are designated as in the previous figure); $M_t = 130$ GeV.

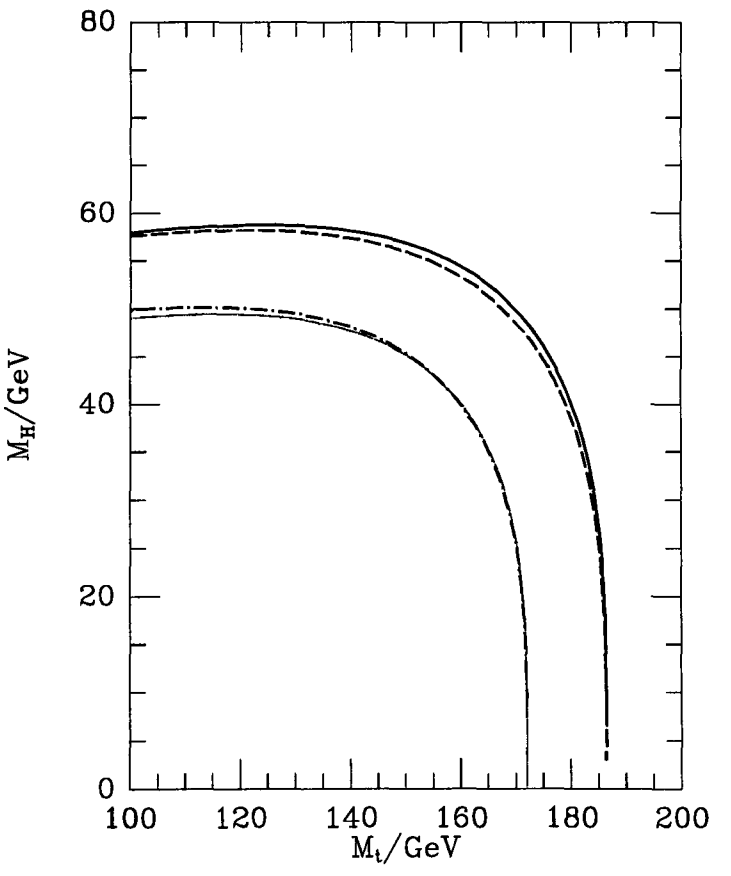

Figure 5.17: Comparison of the mass bounds on the Higgs boson in the Standard Model with light and heavy scalars, at one loop and with ring improvement (lines are designated as in the previous figure).

Chapter 6

The Singlet Extension of the Standard Model

In the last chapter, it was shown how the requirement that anomalous baryon violation not be in equilibrium, following the phase transition, places an upper bound on the mass of the Standard Model Higgs boson which is barely consistent with the experimental lower bound from LEP [42]. A possible way to avert this stringent mass bound is to extend the Standard Model. As we have seen in the one-loop description, first-order behavior derives from the negative cubic term: $(\phi/T)_{\rm crit} \sim E/\lambda_{T_c}$. The addition of an extra boson field to the Standard Model would augment the cubic contributions, hence strengthening first-order behavior and relaxing the mass bound on the Higgs boson. Thus motivated, Anderson and Hall [20] considered the simplest extension of the Standard Model, the addition of a gauge singlet field. In their one-loop analysis, these authors demonstrated that successful baryogenesis may be possible in a modest extension of the Standard Model, consistent with all other phenomenology.

This chapter demonstrates that the inclusion of ring diagrams alters the arguments of Anderson and Hall [20] for strengthening the first-order nature of the phase transition in their proposed extension of the Standard Model. The material of this chapter is drawn primarily from original work previously published [44]. We begin by analyzing the effective potential at one loop to determine the nature of the phase transition, as a function of the Higgs mass. Since first-order behavior in the minimal Standard Model is driven by gauge (rather than scalar) loops, as seen in Chapter 5, we will neglect Higgs contributions to $V^T(\phi)$, which are negligible compared to the singlet contribution. We then consider the summation of singlet and gauge ring diagrams and their effect on the nature of the phase transition. While the one-loop analysis relaxes the Higgs mass bound up to 115 GeV, the effect of ring improvement is to restrict this bound further; we find that the addition of a light singlet ($m_S(\phi) \lesssim M_W$, T_c) weakens the Higgs mass bound only by $\sim 50\%$, up to ~ 80 GeV. The analysis for a heavy singlet ($m_S(\phi) \gtrsim M_W$, T_c) remains unchanged by ring improvement, however, and may yield a more generous bound on the Higgs mass.

6.1 Effective Potential at One Loop

In the context of the one-loop analysis, Anderson and Hall [20] suggested increasing E/λ_T by adding a gauge-singlet g_S-multiplet field S to the Standard Model, with dynamics governed by

$$\mathcal{L}_S = \partial_\mu S^\dagger \partial^\mu S - \mu_S^2 S^\dagger S - \lambda_S (S^\dagger S)^2 - 2\zeta^2 S^\dagger S \cdot \Phi^\dagger \Phi \; . \tag{6.1}$$

Requiring both μ_S^2 and ζ^2 to be positive ensures that only the Higgs field Φ determines electroweak symmetry-breaking (that is, $\langle S \rangle = 0$ at all temperatures). Upon spontaneous symmetry-breaking, $\langle \Phi \rangle = \frac{1}{\sqrt{2}} \begin{pmatrix} 0 \\ \phi \end{pmatrix}$, S acquires the mass $m_S^2(\phi) = \mu_S^2 + \zeta^2 \phi^2$. At the one-loop level, the S contribution to the effective potential may be calculated analogously to the pure scalar theory (see (3.18) and (3.15)).

Anderson and Hall considered the two possibilities of a heavy and a light singlet. In the first case where S is extremely heavy, its thermal contribution is Boltzmann suppressed, and only the zero-temperature part contributes at one loop. Although E remains the same as in the Standard Model, λ_T receives a negative piece due to the S mass; hence $(\phi/T)_{\rm crit} \sim E/\lambda_{T_c}$ is larger than in the Standard Model. In addition, the argument is unaffected by ring diagrams, since for large enough mass, the S ring diagrams are irrelevant. Consequently, up through ring diagrams, a heavy singlet may indeed strengthen the first-order phase transition and evade the experimental Higgs bound.

As for the light singlet, we may use the high-temperature approximation (Appendix B), given by

$$\Delta V^T_{\rm S,\,1\ loop}(\phi) = 2g_S \left\{ \left(\frac{M_S^2}{32\pi^2} + \frac{T^2}{24} \right) m_S^2(\phi) - \frac{T}{12\pi} m_S^3(\phi) - \frac{m_S^4(\phi)}{64\pi^2} \log \left(\frac{M_S^2}{a_B T^2} \right) \right\} . \tag{6.2}$$

The effective potential for the Standard Model then becomes

$$V^T_{1\ \rm loop}(\phi) = \tilde{D} \left(T^2 - \tilde{T}_0^2 \right) \phi^2 - \tilde{E} T \phi^3 - \frac{g_S T}{6\pi} m_S^3(\phi) + \frac{\tilde{\lambda}_T}{4} \phi^4 \; , \tag{6.3}$$

where

$$\begin{aligned} \tilde{D} &= D + \frac{g_S \zeta^2}{12} \\ \tilde{T}_0^2 &= \frac{1}{\tilde{D}} \left[D T_0^2 - \frac{g_S \zeta^2 M_S^2}{16\pi^2} + \frac{g_S \zeta^2 \mu_S^2}{16\pi^2} \log \left(\frac{M_S^2}{a_B T^2} \right) \right] \\ \tilde{\lambda}_T &= \lambda_T - \frac{g_S \zeta^4}{8\pi^2} \log \left(\frac{M_S^2}{a_B T^2} \right) \; . \end{aligned} \tag{6.4}$$

If we assume, for the purpose of illustration, that S is light enough that $\mu_S^2 \ll \zeta^2 \phi^2$ at the asymmetric minimum during the phase transition, the coefficient of the negative

cubic term is increased to $\widetilde{E} = E + g_S\zeta^3/(6\pi)$; consequently $(\phi/T)_{\rm crit} \sim \widetilde{E}/\widetilde{\lambda}_{\widetilde{T}_0} > E/\lambda_{T_0}$, thus strengthening first-order behavior and suppressing baryon washout. More generally, in the absence of prejudice toward the singlet mass, [1] the critical point occurs at

Critical temperature: (6.5)

$$\widetilde{D}T_c^2 - \frac{g_S\zeta^2\mu_S}{4\pi}T_c = \frac{M_H^2}{4} - 2Bv^2 - \frac{g_S\zeta^2 M_S^2}{16\pi^2} + \frac{g_S\zeta^2\mu_S^2}{16\pi^2}\log\left(\frac{M_S^2}{a_B T_c^2}\right)$$

Asymmetric minimum: (6.6)

$$\widetilde{\lambda}_{T_c}\left(\frac{\phi}{T}\right)_{\rm crit} - 3E = \frac{g_S\zeta^2}{2\pi\left(\frac{\phi}{T}\right)_{\rm crit}}\left[\sqrt{\zeta^2\left(\frac{\phi}{T}\right)^2_{\rm crit} + \frac{\mu_S^2}{T_c^2}} - \sqrt{\frac{\mu_S^2}{T_c^2}}\right] .$$

Hence in the one-loop analysis, adding a light singlet yields a more generous bound on the Higgs mass, as shown in Figures 6.1 and 6.2 (compare to Figures 5.1 and 5.2 for the minimal Standard Model). In these figures, T_c and $(\phi/T)_{\rm crit}$ were computed for

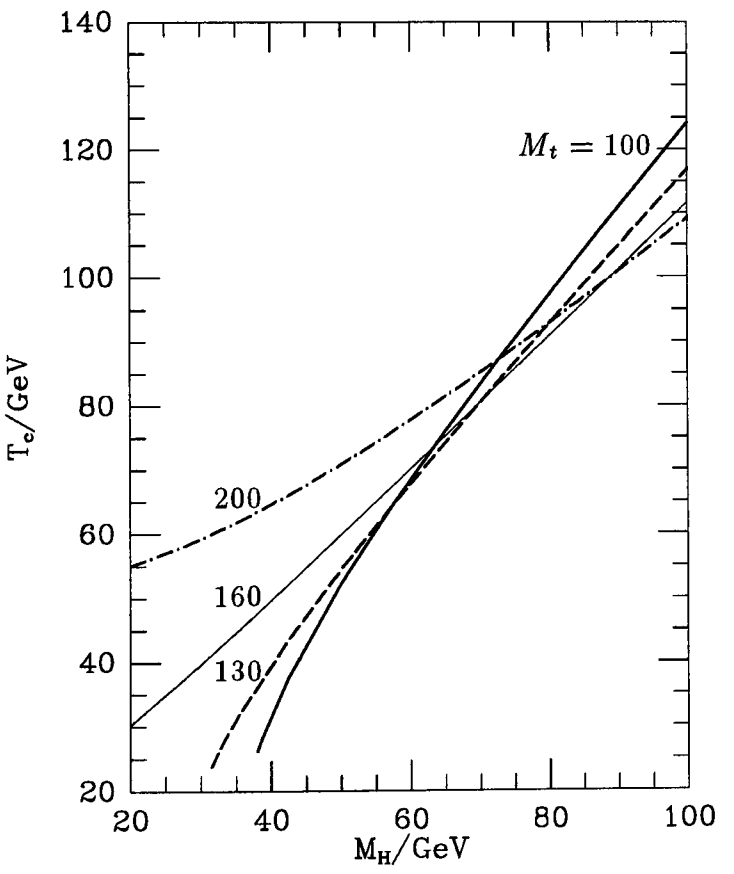

Figure 6.1: The critical temperature at one loop in the singlet extension of the Standard Model; the top mass in GeV labels the lines.

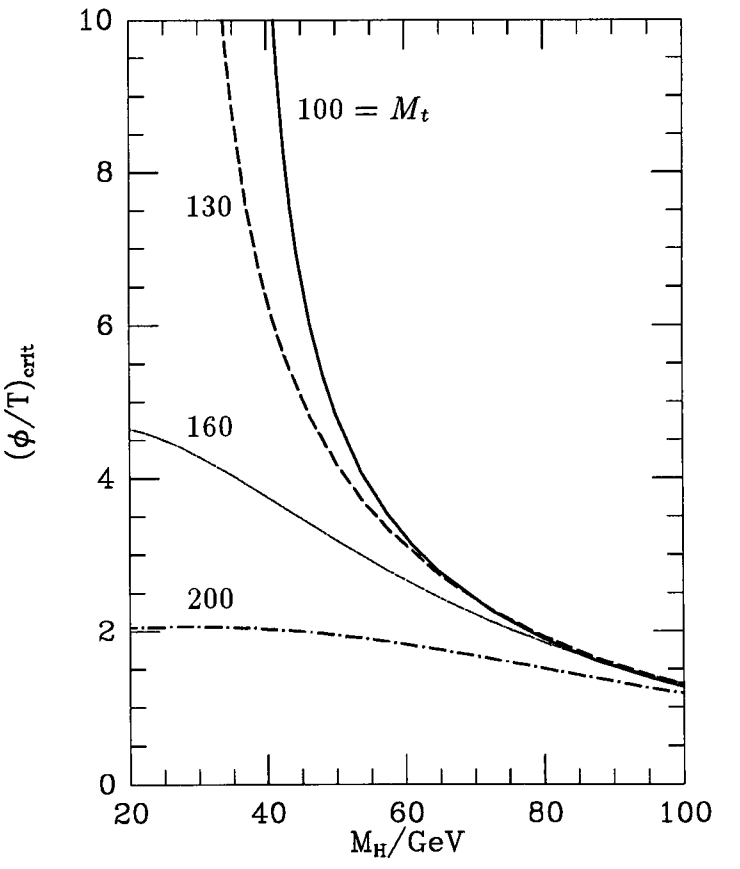

Figure 6.2: The critical point at one loop in the singlet extension of the Standard Model.

$g_S = \zeta = \lambda_S = 1$ and $\mu_S = 50$ GeV, without the assumption $M_S^2 \ll \zeta^2\phi_{\rm min}^2$.

[1] We assume only that S is light enough for the high-temperature approximation to be valid during the phase transition.

6.2 Effective Potential with Ring Improvement

Taking ring diagrams into account, the presence of S affects the analysis of the Standard Model in two ways. First, the appearance of virtual S-loops increases the scalar self-energies ($\propto T^2$), thus changing the scalar ring diagrams. [2] Secondly, S must be ring-improved since it contributes to V^T at one loop. As found earlier (Section 3.3 or Appendix B) when discussing the scalar phase transition, the S-ring diagrams sum to

$$-\frac{g_S T}{6\pi}\left\{\left[m_S^2(\phi)+\Pi_S(0)\right]^{3/2}-m_S^3(\phi)\right\}\ . \tag{6.7}$$

The self-energy is computed from the Feynman graphs of Figure 6.3 (recall that only

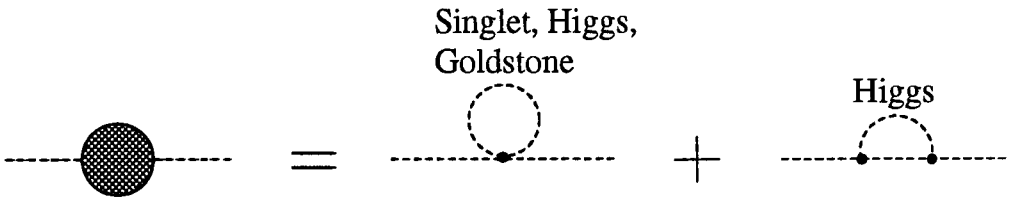

Figure 6.3: The singlet self-energy at one loop.

the quadratically-divergent first graph is relevant), which give the leading temperature dependence $\Pi_S(0)=\frac{1}{3}(\zeta^2+\lambda_S)T^2$. The result is the ring-improved effective potential:

$$\begin{aligned} V^T_{\rm ring}(\phi) &= \widetilde{D}\left(T^2-\widetilde{T}_0^2\right)\phi^2-\frac{2}{3}ET\phi^3+\frac{\widetilde{\lambda}_T}{4}\phi^4 \\ &\quad -\frac{T}{12\pi}\left\{2\left[m_W^2(\phi)+\Pi_W^{00}(0)\right]^{3/2}+\left[m_Z^2(\phi)+\Pi_Z^{00}(0)\right]^{3/2}\right. \\ &\quad \left.+2g_S\left[m_S^2(\phi)+\Pi_S(0)\right]^{3/2}\right\}\ . \end{aligned} \tag{6.8}$$

Parametrizing the self-energies as $\Pi_W^{00}(0)=wT^2$, $\Pi_Z^{00}(0)=zT^2$, and $\Pi_S(0)=sT^2$, the critical point is characterized by

Critical temperature: (6.9)

$$\begin{aligned} &\left(\widetilde{D}-\frac{1}{8\pi}\left[2\frac{g^2}{4}\sqrt{w}+\frac{g^2}{4\cos^2\theta_{\rm W}}\sqrt{z}\right]\right)T_{\rm c}^2-\frac{g_S\zeta^2}{4\pi}T_{\rm c}\sqrt{\mu_S^2+sT_{\rm c}^2} \\ &\qquad =\frac{M_H^2}{4}-2Bv^2-\frac{g_S\zeta^2M_S^2}{16\pi^2}+\frac{g_S\zeta^2\mu_S^2}{16\pi^2}\log\left(\frac{M_S^2}{a_BT_{\rm c}^2}\right) \end{aligned}$$

[2] Although we have so far neglected scalar masses, one may also want to consider the case where $m_{\rm scalar}/T\sim m_t/T, m_{W,Z}/T$ (see Chapter 5). In this case the Higgs and Goldstone fields contribute at one loop, and hence require ring-improvement in the usual manner. In the Standard Model, the scalar self-energies at one loop receive pieces from gauge, fermion, and scalar loops; in the singlet extension, they also receive a piece from S loops. This augments their self-energies by $\Delta\Pi^S(0)=\frac{g_S\zeta^2T^2}{6}$.

Asymmetric minimum: (6.10)

$$\widetilde{\lambda}_{T_c}\left(\frac{\phi}{T}\right)_{\rm crit} - 2E = \frac{1}{4\pi\left(\frac{\phi}{T}\right)_{\rm crit}}\left\{2\frac{g^2}{4}\left(\sqrt{\frac{g^2}{4}\left(\frac{\phi}{T}\right)^2_{\rm crit}+w}-\sqrt{w}\right)\right.$$
$$+\frac{g^2}{4\cos^2\theta_{\rm W}}\left(\sqrt{\frac{g^2}{4\cos^2\theta_{\rm W}}\left(\frac{\phi}{T}\right)^2_{\rm crit}+z}-\sqrt{z}\right)$$
$$\left.+2g_S\zeta^2\left(\sqrt{\zeta^2\left(\frac{\phi}{T}\right)^2_{\rm crit}+\frac{\mu_S^2}{T_c^2}+s}-\sqrt{\frac{\mu_S^2}{T_c^2}+s}\right)\right\}.$$

Because the negative cubic term is *reduced* by ring-improvement, we see that the effects of the gauge singlet on the strength of the phase transition and suppression of baryon washout are much less than expected on the basis of the one-loop analysis. To take the example given by Anderson and Hall, a Higgs mass as high as 100 GeV (with $M_t = 125$ GeV) may be accommodated by taking $g_S = \zeta = \lambda_S = 1$, which safely gives $(\phi/T)_{\rm crit} \approx 1.2$ in the one-loop calculation. With ring-improvement, however, the Higgs mass bound is relaxed only up to ~ 80 GeV (for $(\phi/T)_{\rm crit} \gtrsim 1$), as seen in Figures 6.4 and 6.5 (compare to Figures 5.4 and 5.5 for the minimal Standard Model).

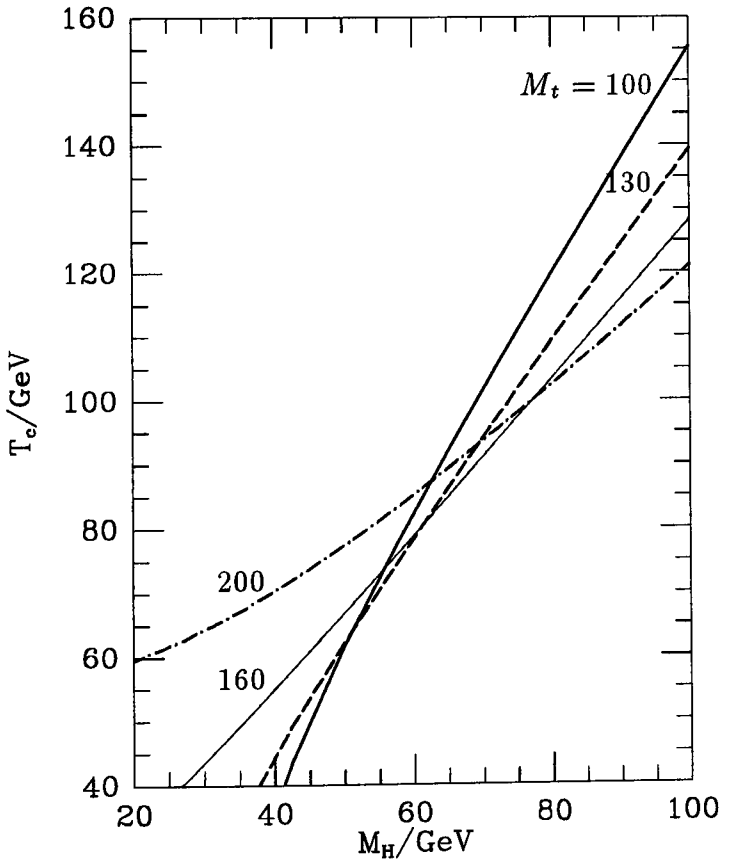

Figure 6.4: The critical temperature with ring improvement in the singlet extension of the Standard Model; the top mass in GeV labels the lines.

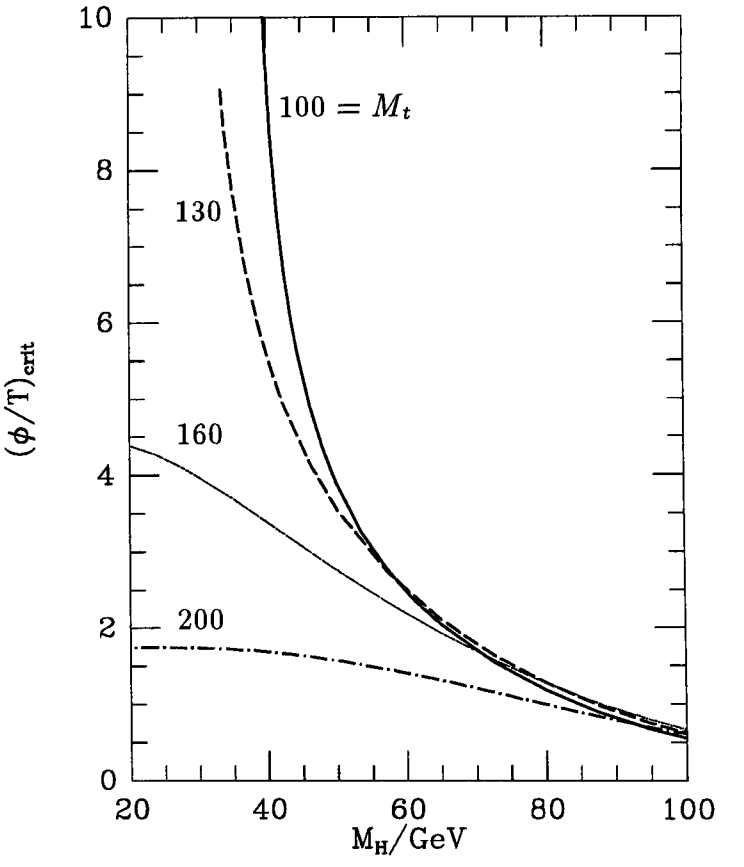

Figure 6.5: The critical point with ring improvement in the singlet extension of the Standard Model.

6.3 Discussion

The effects of ring-improvement on the Standard Model and its singlet extension are compared in Figures 6.6 and 6.7, which display the critical temperature and $(\phi/T)_{\rm crit}$

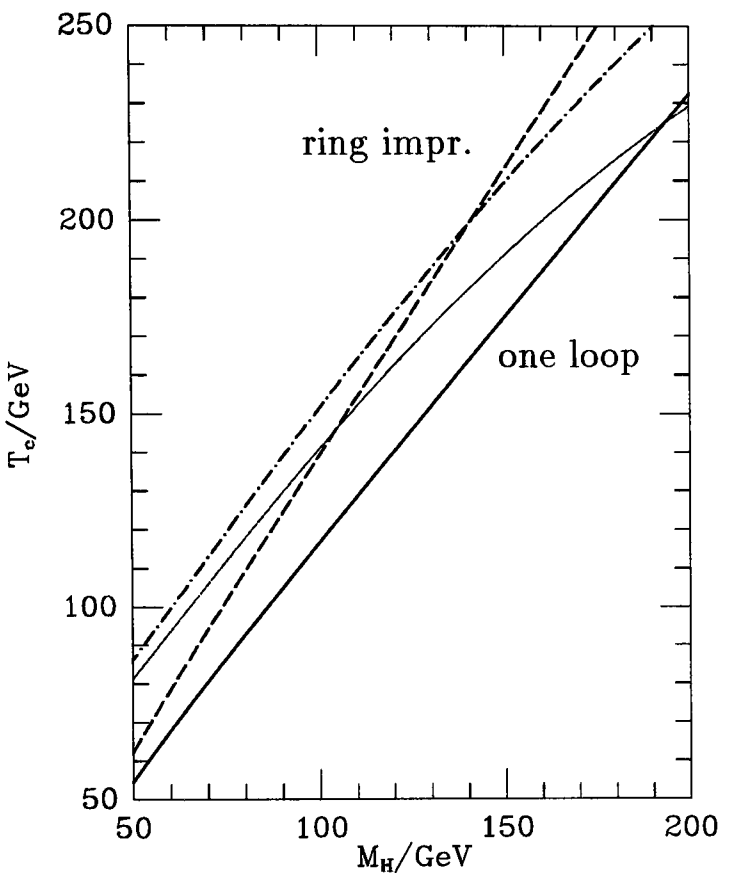

Figure 6.6: Comparison of the critical temperatures, at one loop and with ring improvement, in the Standard Model (dotted and dash-dotted lines respectively) and its singlet extension (solid and dashed lines respectively); $M_t = 130$ GeV.

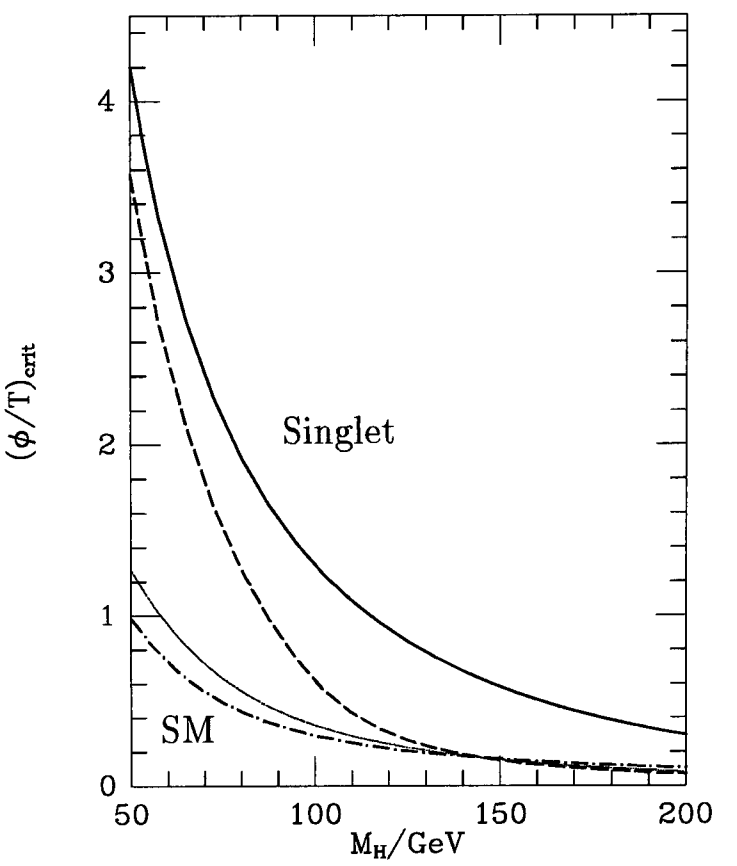

Figure 6.7: Comparison of the critical points, at one loop and with ring improvement, in the Standard Model and its singlet extension (lines are designated as in the previous figure); $M_t = 130$ GeV.

as functions of the Higgs mass, with the top mass fixed at the phenomenologically favored value of 130 GeV [42]. The Higgs mass bounds for each case, obtained by requiring $(\phi/T)_{\rm crit} \gtrsim 1$, are shown as functions of the top mass in Figure 6.8. The sharp downturn at large M_t is due to the dominance of a heavy top mass in the one-loop effective potential at zero temperature, and is related to the question of vacuum stability. It is evident that the effects of ring-improvement are quite significant, reducing the bounds on M_H by up to 30%.

One may ask to what extent these results are dependent on our choice of parameters ζ, λ_S, and μ_S ($\zeta = \lambda_S = 1$ and $\mu_S = 50$ GeV were chosen above). One finds, as expected, that the phase transition is strengthened for increasing ζ (greater interaction between the thermal baths of Higgs and singlet particles), decreasing λ_S (diminishing effect of the singlet ring diagrams), and decreasing μ_S (greater sensitivity of $m_S^2(\phi)$ to the Higgs VEV near the phase transition, and hence a larger contribution to the negative cubic term in the effective potential). Our results are robust in the sense that they changed by less than 10% when the parameters were varied over the following natural

ranges: $0.01 \leq \zeta \leq 1$ (the validity of the high temperature expansion, $m_S^2(\phi)/T^2 \lesssim 1$, requires that $\zeta \leq 1$ to avoid baryon washout), $0.01 \leq \lambda_S \leq 1$, and 10 GeV $\leq \mu_S \leq$ 100 GeV (our results are insensitive to smaller values of λ_S and μ_S). Of course, they are quite sensitive to g_S (setting $g_S = 2$ increases the bound by 25%), as shown in Figure 6.9 for $g_S = 1$ to 4, so that one may still weaken the upper bound on the Higgs

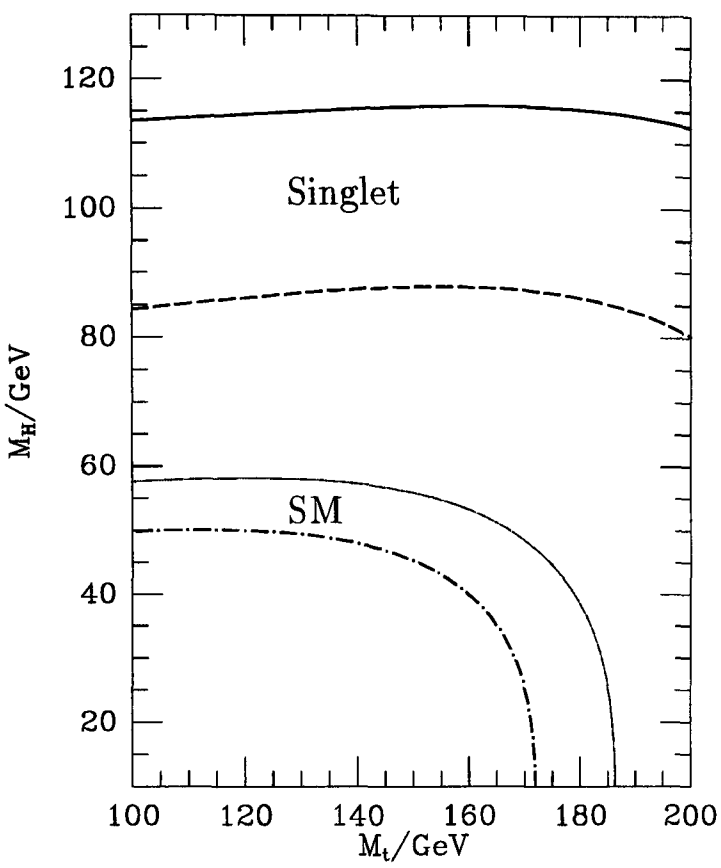

Figure 6.8: Comparison of the mass bounds on the Higgs boson, at one loop and with ring improvement, in the Standard Model (dotted and dash-dotted lines respectively) and its singlet extension (solid and dashed lines respectively).

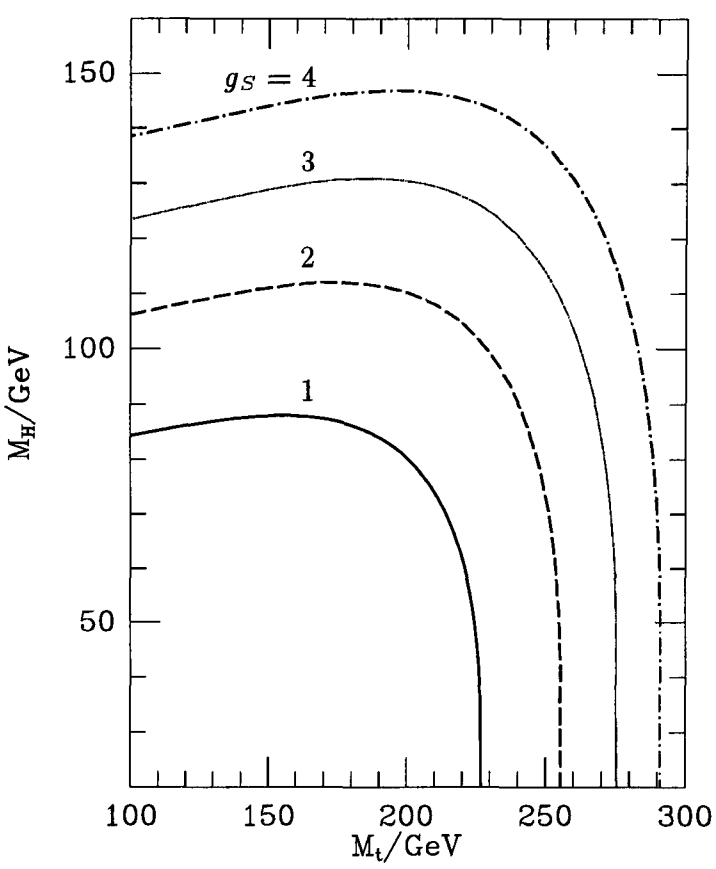

Figure 6.9: Comparison of the mass bounds on the Higgs boson (with ring improvement) in the singlet extension of the Standard Model, for various values of g_S.

mass simply by increasing the number of singlet fields.

6.4 Conclusion

We have shown that ring-improvement of the effective potential — as required for perturbative consistency — modifies the argument favoring the addition of a light singlet to the Standard Model to ensure successful baryogenesis. The Higgs mass bound is relaxed only up to $\sim$ 80 GeV, for reasonable ranges of the singlet parameters ($g_S = 1$, $\zeta \leq 1$, $\lambda_S \leq 1$, and $\mu_S \leq 100$ GeV). Such a Higgs will be found (or excluded) at LEP 200 [42]. This bound, however, may be further relaxed by enlarging the multiplet of singlet fields.

Anderson and Hall [20] also suggested an alternative way to increase $(\phi/T)_{\text{crit}} \propto E/\lambda_{T_c}$ by adding a gauge singlet: instead of increasing E with a light singlet, one can

decrease λ_{T_c} with a sufficiently heavy one. In this case, the thermal contribution of S is exponentially suppressed, and the ring diagrams negligible. Since only the zero-temperature part is involved, this possibility remains viable.

Chapter 7

The Two-Doublet Model

In this chapter we consider the phase transition in the two-doublet model. The analysis of this model is considerably more difficult than that of the Standard Model in Chapter 5 (or its singlet extension in Chapter 6). Unlike the previous cases, this model possesses a multiplicity of unconstrained parameters, which does not readily permit any definitive conclusions. To simplify the analysis, we consider only the case of light scalars.

7.1 Notation

The two-doublet model is defined by the Lagrangian

$$\mathcal{L} = \mathcal{L}_{\text{gauge}} + \mathcal{L}_{\text{fermion}} + \mathcal{L}_{\text{Higgs}} + \mathcal{L}_{\text{Yukawa}} + \mathcal{L}_{\text{gauge-fixing}} + \mathcal{L}_{\text{ghost}} + \mathcal{L}_{\text{c.t.}} \ . \tag{7.1}$$

It respects the gauge symmetry $SU(2)_L \otimes U(1)_Y$, and at zero temperature, undergoes spontaneous symmetry breaking to $U(1)_{\text{EM}}$. Because the addition of a second scalar doublet does not modify the gauge symmetry or its fermion representations, $\mathcal{L}_{\text{gauge}}$ and $\mathcal{L}_{\text{fermion}}$ remain unchanged from the Standard Model (refer to Eqns. (5.2) and (5.3)).

$\mathcal{L}_{\text{Higgs}}$ describes the dynamics of the two Higgs doublets, and is given by

$$\mathcal{L}_{\text{Higgs}} = (D_\mu \Phi_1)^\dagger (D^\mu \Phi_1) + (D_\mu \Phi_2)^\dagger (D^\mu \Phi_2) - U(\Phi_1, \Phi_2) \ . \tag{7.2}$$

Φ_1 and Φ_2 are both complex $SU(2)_L$ doublets, with weak hypercharge $Y/2 = 1/2$, so that the covariant derivative is

$$D_\mu \Phi_j = \left(\partial_\mu + ig \frac{\tau^k}{2} W_\mu^k + i \frac{g'}{2} B_\mu \right) \Phi_j \ .$$

The classical potential is

$$U(\Phi_1, \Phi_2) \ = \ \lambda_1 \left(\Phi_1^\dagger \Phi_1 - \frac{v_1^2}{2} \right)^2 + \lambda_2 \left(\Phi_2^\dagger \Phi_2 - \frac{v_2^2}{2} \right)^2$$

$$
\begin{aligned}
&+\lambda_3\left[\left(\Phi_1^\dagger\Phi_1-\frac{v_1^2}{2}\right)+\left(\Phi_2^\dagger\Phi_2-\frac{v_2^2}{2}\right)\right]^2\\
&+\lambda_4\left[\left(\Phi_1^\dagger\Phi_1\right)\left(\Phi_2^\dagger\Phi_2\right)-\left(\Phi_1^\dagger\Phi_2\right)\left(\Phi_2^\dagger\Phi_1\right)\right]\\
&+\lambda_5\left[\mathcal{R}e\left(\Phi_1^\dagger\Phi_2\right)-\frac{v_1v_2}{2}\cos\xi\right]^2+\lambda_6\left[\mathcal{I}m\left(\Phi_1^\dagger\Phi_2\right)-\frac{v_1v_2}{2}\sin\xi\right]^2 .
\end{aligned}
$$

$U(\Phi_1,\Phi_2)$ is the most general form of the potential that guarantees the desired pattern of spontaneous symmetry breaking, $SU(2)_L\otimes U(1)_Y\rightarrow U(1)_{\rm EM}$, and which is invariant under gauge transformations and the discrete symmetry $\Phi_2\rightarrow-\Phi_2$ (which is broken only softly, i.e., by terms of dimension two). The discrete symmetry is imposed on the Lagrangian to eliminate Higgs-mediated flavor-changing neutral currents, as we will see below when discussing $\mathcal{L}_{\rm Yukawa}$. The phase ξ is a measure of CP violation in the scalar sector; in analogy to the minimal supersymmetric standard model, we will assume CP invariance in the scalar couplings, so that $\xi=0$: [1]

$$
\begin{aligned}
U\left(\Phi_1,\Phi_2\right) \;=\; &\lambda_1\left(\Phi_1^\dagger\Phi_1-\frac{v_1^2}{2}\right)^2+\lambda_2\left(\Phi_2^\dagger\Phi_2-\frac{v_2^2}{2}\right)^2\\
&+\lambda_3\left[\left(\Phi_1^\dagger\Phi_1-\frac{v_1^2}{2}\right)+\left(\Phi_2^\dagger\Phi_2-\frac{v_2^2}{2}\right)\right]^2\\
&+\lambda_4\left[\left(\Phi_1^\dagger\Phi_1\right)\left(\Phi_2^\dagger\Phi_2\right)-\left(\Phi_1^\dagger\Phi_2\right)\left(\Phi_2^\dagger\Phi_1\right)\right]\\
&+\lambda_5\left[\mathcal{R}e\left(\Phi_1^\dagger\Phi_2\right)-\frac{v_1v_2}{2}\right]^2+\lambda_6\left[\mathcal{I}m\left(\Phi_1^\dagger\Phi_2\right)\right]^2 . \qquad (7.3)
\end{aligned}
$$

At zero temperature, the minimum of $U(\Phi_1,\Phi_2)$ occurs at $|\Phi_1|=v_1/\sqrt{2}$, $|\Phi_2|=v_2/\sqrt{2}$, such that $v_1^2+v_2^2=(246\text{GeV})^2$. At finite temperature, we denote the thermal average by

$$
\langle\Phi_1\rangle=\begin{pmatrix}0\\ \frac{1}{\sqrt{2}}\phi_1\end{pmatrix}, \qquad \langle\Phi_2\rangle=\begin{pmatrix}0\\ \frac{1}{\sqrt{2}}\phi_2\end{pmatrix}, \qquad (7.4)
$$

where it has been assumed that the evolution of the universe respects CP invariance and conserves electric charge. Expanding the fields about the thermal background, [2]

$$
\Phi_1 \;=\; \langle\Phi_1\rangle+\begin{pmatrix}\chi_1^+\\ H_1\end{pmatrix}=\begin{pmatrix}0\\ \frac{1}{\sqrt{2}}\phi_1\end{pmatrix}+\begin{pmatrix}\chi_1^+\\ \frac{1}{\sqrt{2}}(\chi_1+i\sigma_1)\end{pmatrix}
$$

[1] Of course, we know that for successful baryogenesis, an adequate source of CP violation (whether in the scalar or fermionic sectors) must operate during the epoch of baryon production. However, since we focus here on the phase transition and the attendant cosmological mass bound on the Higgs boson, rather than a specific mechanism of baryogenesis, the source of CP violation will be immaterial to our analysis. Hence we set $\xi=0$, without loss of generality.

[2] Note that in our analysis of the Standard Model, Chapter 5, subscripts on scalar fields specify the components of the Higgs doublet; here, they refer to either of the Higgs doublets, but *not* to the individual components.

$$\Phi_2 = \langle\Phi_2\rangle + \begin{pmatrix} \chi_2^+ \\ H_2 \end{pmatrix} = \begin{pmatrix} 0 \\ \frac{1}{\sqrt{2}}\phi_2 \end{pmatrix} + \begin{pmatrix} \chi_2^+ \\ \frac{1}{\sqrt{2}}(\chi_2 + i\sigma_2) \end{pmatrix} . \tag{7.5}$$

Under this shift, terms from $|D_\mu\langle\Phi_1\rangle|^2 + |D_\mu\langle\Phi_2\rangle|^2$ generate masses for the W and Z gauge bosons:

$$m_W^2(\phi_1,\phi_2) = \frac{g^2}{4}\left(\phi_1^2+\phi_2^2\right) \tag{7.6}$$

$$m_Z^2(\phi_1,\phi_2) = \frac{g^2+g'^2}{4}\left(\phi_1^2+\phi_2^2\right) . \tag{7.7}$$

Let us denote by m_{Wj}^2 the separate contributions of ϕ_j to m_W^2, so that $m_W^2(\phi_1,\phi_2) = m_{W1}^2(\phi_1)+m_{W2}^2(\phi_2)$, and similarly for m_Z^2; $m_{Wj}^2(\phi_j) = g^2\phi_j^2/4$, etc. Because the second doublet shares the same quantum numbers as the first, the gauge interactions of Φ_2, generated by $|D_\mu\Phi_2|^2$, simply replicate those of Φ_1 (cf. (5.20) and (7.27)).

Shifting by (7.5) in $\mathcal{L}_{\text{Higgs}}$ also results in masses for the scalar modes. The scalar boson mass-squared matrix decomposes into a charged sector, a CP-odd neutral (pseudoscalar) sector, and a CP-even neutral (scalar) sector, each of which may be diagonalized with distinct mixing angles. Using the notation of Gunion, Haber, Kane, and Dawson [45], the charged sector contains the charged physical Higgs and Goldstone bosons,

$$\begin{aligned} H^\pm &= -\sin\beta^\pm\chi_1^\pm + \cos\beta^\pm\chi_2^\pm \\ G^\pm &= \cos\beta^\pm\chi_1^\pm + \sin\beta^\pm\chi_2^\pm , \end{aligned} \tag{7.8}$$

with masses

$$m_{H^\pm,G^\pm}^2(\phi_1,\phi_2) = \frac{1}{2}\left[\mathcal{M}_{11}^\pm + \mathcal{M}_{22}^\pm \pm \sqrt{(\mathcal{M}_{11}^\pm - \mathcal{M}_{22}^\pm)^2 + 4\left(\mathcal{M}_{12}^\pm\right)^2}\right] , \tag{7.9}$$

where the mass-squared matrix and mixing angle are

$$\mathcal{M}^\pm = \begin{pmatrix} \lambda_1(\phi_1^2 - v_1^2) + \lambda_3(\phi^2 - v^2) + \frac{1}{2}\lambda_4\phi_2^2 & -\frac{1}{2}\lambda_4\phi_1\phi_2 + \frac{1}{2}\lambda_5(\phi_1\phi_2 - v_1v_2) \\ -\frac{1}{2}\lambda_4\phi_1\phi_2 + \frac{1}{2}\lambda_5(\phi_1\phi_2 - v_1v_2) & \lambda_2(\phi_2^2 - v_2^2) + \lambda_3(\phi^2 - v^2) + \frac{1}{2}\lambda_4\phi_1^2 \end{pmatrix} \tag{7.10}$$

and

$$\tan\beta^\pm = \frac{\mathcal{M}_{11}^\pm - \mathcal{M}_{22}^\pm + \sqrt{(\mathcal{M}_{11}^\pm - \mathcal{M}_{22}^\pm)^2 + 4\left(\mathcal{M}_{12}^\pm\right)^2}}{-2\mathcal{M}_{12}^\pm} . \tag{7.11}$$

The pseudoscalar sector includes the neutral physical and Goldstone modes,

$$\begin{aligned} A^0 &= -\sin\beta^0\sigma_1 + \cos\beta^0\sigma_2 \\ G^0 &= \cos\beta^0\sigma_1 + \sin\beta^0\sigma_2 , \end{aligned} \tag{7.12}$$

with masses

$$m^2_{A^0,G^0}(\phi_1,\phi_2) = \frac{1}{2}\left[\mathcal{M}^{\rm p}_{11} + \mathcal{M}^{\rm p}_{22} \pm \sqrt{(\mathcal{M}^{\rm p}_{11} - \mathcal{M}^{\rm p}_{22})^2 + 4\,(\mathcal{M}^{\rm p}_{12})^2}\right] , \tag{7.13}$$

mass-squared matrix

$$\mathcal{M}^{\rm p} = \begin{pmatrix} \lambda_1(\phi_1^2 - v_1^2) + \lambda_3(\phi^2 - v^2) + \frac{1}{2}\lambda_6\phi_2^2 & \frac{1}{2}\lambda_5(\phi_1\phi_2 - v_1v_2) - \frac{1}{2}\lambda_6\phi_1\phi_2 \\ \frac{1}{2}\lambda_5(\phi_1\phi_2 - v_1v_2) - \frac{1}{2}\lambda_6\phi_1\phi_2 & \lambda_2(\phi_2^2 - v_2^2) + \lambda_3(\phi^2 - v^2) + \frac{1}{2}\lambda_6\phi_1^2 \end{pmatrix} , \tag{7.14}$$

and mixing angle

$$\tan\beta^0 = \frac{\mathcal{M}^{\rm p}_{11} - \mathcal{M}^{\rm p}_{22} + \sqrt{(\mathcal{M}^{\rm p}_{11} - \mathcal{M}^{\rm p}_{22})^2 + 4\,(\mathcal{M}^{\rm p}_{12})^2}}{-2\mathcal{M}^{\rm p}_{12}} . \tag{7.15}$$

The scalar sector contains the two neutral physical Higgs states,

$$\begin{aligned} h^0 &= -\sin\alpha\chi_1 + \cos\alpha\chi_2 \\ H^0 &= \cos\alpha\chi_1 + \sin\alpha\chi_2 , \end{aligned} \tag{7.16}$$

with masses

$$m^2_{H^0,h^0}(\phi_1,\phi_2) = \frac{1}{2}\left[\mathcal{M}^{\rm s}_{11} + \mathcal{M}^{\rm s}_{22} \pm \sqrt{(\mathcal{M}^{\rm s}_{11} - \mathcal{M}^{\rm s}_{22})^2 + 4\,(\mathcal{M}^{\rm s}_{12})^2}\right] , \tag{7.17}$$

where

$$\mathcal{M}^{\rm s} = \begin{pmatrix} \lambda_1(3\phi_1^2 - v_1^2) + \lambda_3(3\phi_1^2 + \phi_2^2 - v^2) + \frac{1}{2}\lambda_5\phi_2^2 & 2\lambda_3\phi_1\phi_2 + \frac{1}{2}\lambda_5(2\phi_1\phi_2 - v_1v_2) \\ 2\lambda_3\phi_1\phi_2 + \frac{1}{2}\lambda_5(2\phi_1\phi_2 - v_1v_2) & \lambda_2(3\phi_2^2 - v_2^2) + \lambda_3(\phi_1^2 + 3\phi_2^2 - v^2) + \frac{1}{2}\lambda_5\phi_1^2 \end{pmatrix} \tag{7.18}$$

$$\tan\alpha = \frac{\mathcal{M}^{\rm s}_{11} - \mathcal{M}^{\rm s}_{22} - \sqrt{(\mathcal{M}^{\rm s}_{11} - \mathcal{M}^{\rm s}_{22})^2 + 4\,(\mathcal{M}^{\rm s}_{12})^2}}{-2\mathcal{M}^{\rm s}_{12}} . \tag{7.19}$$

At zero temperature, these reduce to $\tan\beta^\pm = \tan\beta^0 = v_2/v_1$, $M^2_{H^\pm} = \frac{1}{2}\lambda_4 v^2$, $M^2_{A^0} = \frac{1}{2}\lambda_6 v^2$, and $M^2_{G^\pm} = 0 = M^2_{G^0}$. Note there are only two mixing angles at zero temperature, which we denote by $\tan\alpha_0$ and $\tan\beta$.

In summary, the scalar sector possesses the following mass eigenstates: five physical scalar bosons, including the charged $H^\pm$, the neutral CP-odd A^0, and the neutral CP-even H^0 and h^0; and three Goldstone bosons, including the charged $G^\pm$ and the neutral CP-odd G^0. $M_{h^0} < M_{H^0}$, so that h^0 corresponds to the lightest Higgs boson. $\beta^\pm$ rotates the charged, β^0 the neutral CP-odd, and α the neutral CP-even scalars into their respective mass eigenstates, and note that these rotation angles are all functions of (ϕ_1,ϕ_2). Whereas the Standard Model has only one free parameter, this model has seven: $\lambda_1,\ldots,\lambda_6$, and $\tan\beta \equiv v_2/v_1$ (we have set $\xi = 0$ and v^2 is fixed by the W mass).

These may be transformed into the more convenient set $M^2_{H^\pm}$, $M^2_{A^0}$, $M^2_{H^0}$, $M^2_{h^0}$, λ_5, [3] $\tan\alpha_0$, and $\tan\beta$.

The Yukawa Lagrangian prescribes the coupling of the Higgs doublets to fermions. The structure of $\mathcal{L}_{\text{Yukawa}}$ is constrained by the need to prevent Higgs-mediated flavor-changing neutral currents, which may be ensured by imposing one of the following discrete symmetries:

$$\Phi_1 \to -\Phi_1 \,, \qquad\qquad d'^a_R \to -d'^a_R \,,$$

or

$$\Phi_1 \to -\Phi_1 \,.$$

The net effect of either of these symmetries is to force all quarks of the same charge to couple to only one scalar doublet, which is necessary and sufficient to guarantee the absence, at tree level, of flavor-changing neutral currents induced by Higgs exchange. The first symmetry implies that all up-type fermions couple only to Φ_2 while down-type fermions couple only to Φ_1; the second symmetry implies that all fermions couple only to Φ_2. In the approximation that we adopt, where all fermion masses except m_t vanish, the choice of symmetry is irrelevant:

$$\mathcal{L}_{\text{Yukawa}} = -g_t\,\overline{(t,b')}_L\,\widetilde{\Phi}_2 t_R + \text{h.c.}\,, \tag{7.20}$$

with $\widetilde{\Phi}_2 = i\tau_2\Phi_2^*$. Upon spontaneous symmetry breaking, the top quark gains a mass $m_t^2(\phi_2) = g_t^2\phi_2^2/2$.

The gauge is fixed in the R_ξ-class of renormalizable gauges, which eliminates mixing of the Goldstone and gauge fields in $\mathcal{L}_{\text{Higgs}}$; mixing arises from the kinetic cross terms $im_{Wj}(\phi_j)\left[\partial^\mu\chi_j^- W_\mu^+ - \partial^\mu\chi_j^+ W_\mu^-\right] - m_{Zj}(\phi_j)\partial^\mu\sigma_j Z_\mu$ (implied summation over $j = 1, 2$). The gauge-fixing Lagrangian is

$$\begin{aligned}\mathcal{L}_{\text{gauge-fixing}} \;=\; & -\frac{1}{2\xi}\left(\partial^\mu W_\mu^1 - \frac{g\xi}{\sqrt{2}}\mathcal{I}m\left[\phi_j\chi_j^+\right]\right)^2 - \frac{1}{2\xi}\left(\partial^\mu W_\mu^2 - \frac{g\xi}{\sqrt{2}}\mathcal{R}e\left[\phi_j\chi_j^+\right]\right)^2 \\ & - \frac{1}{2\xi}\left(\partial^\mu W_\mu^3 + \frac{g\xi}{2}\left[\phi_j\sigma_j\right]\right)^2 - \frac{1}{2\xi}\left(\partial^\mu B_\mu - \frac{g'\xi}{2}\left[\phi_j\sigma_j\right]\right)^2 .\end{aligned}$$

We choose to work in Landau gauge, $\xi \to 0$, so that

$$\begin{aligned}\mathcal{L}_{\text{gauge-fixing}} \;=\; & -\frac{1}{\xi}\left|\partial^\mu W_\mu^+\right|^2 - \frac{1}{2\xi}(\partial^\mu Z_\mu)^2 - \frac{1}{2\xi}(\partial^\mu A_\mu)^2 \\ & + im_{Wj}(\phi_j)\left[\chi_j^-\partial^\mu W_\mu^+ - \chi_j^+\partial^\mu W_\mu^-\right] - m_{Zj}(\phi_j)\sigma_j\partial^\mu Z_\mu \,,\end{aligned} \tag{7.21}$$

and the cross terms in the second line combine with those from $|D_\mu\Phi_1|^2 + |D_\mu\Phi_2|^2$ in $\mathcal{L}_{\text{Higgs}}$ to produce a total divergence, which vanishes upon integration. In this gauge ghost fields are massless and couple only to the gauge bosons; hence they do not

[3] Any one of λ_1, λ_2, or λ_3 may be chosen instead of λ_5, since $M^2_{H^0}$, $M^2_{h^0}$, and $\tan\alpha_0$ only specify three of these parameters. λ_5 is chosen since it determines an additional mass scale of the theory, $M_5^2 \equiv \frac{1}{2}\lambda_5 v^2$, to be encountered in the next section.

Field		Mass	
Gauge	$W^{\pm}$	$m_W^2 = \frac{1}{4}g^2(\phi_1^2+\phi_2^2)$	
	Z	$m_Z^2 = \frac{1}{4}(g^2+g'^2)(\phi_1^2+\phi_2^2)$	
	A	$m_A^2 = 0$	
Ghost	ω_j, ζ	$m^2 = 0$	
Fermion	t	$m_t^2 = \frac{1}{2}g_t^2\phi_2^2$	
	other quarks	$m^2 = 0$	
	leptons	$m^2 = 0$	
Scalar	h^0, H^0	$m^2_{h^0,H^0}$	(7.17)
	A^0, G^0	$m^2_{A^0,G^0}$	(7.13)
	$H^{\pm}$, $G^{\pm}$	$m^2_{H^{\pm},G^{\pm}}$	(7.9)

Table 7.1: Summary of the fields and masses in the two-doublet model, as approximated in this chapter.

contribute to the effective potential at one loop. Because ghost fields do not interact with the scalar sector in this gauge, $\mathcal{L}_{\text{ghost}}$ remains unchanged from the Standard Model, (5.14). Finally, we take the counter-term Lagrangian

$$\begin{aligned}
\mathcal{L}_{\text{c.t.}} &= A(\partial_\mu\Phi_1)^\dagger(\partial^\mu\Phi_1) + B(\partial_\mu\Phi_2)^\dagger(\partial^\mu\Phi_2) \\
&\quad + C\left(\Phi_1^\dagger\Phi_1 - \frac{v_1^2}{2}\right)^2 + D\left(\Phi_2^\dagger\Phi_2 - \frac{v_2^2}{2}\right)^2 \\
&\quad + E\left[\left(\Phi_1^\dagger\Phi_1 - \frac{v_1^2}{2}\right) + \left(\Phi_2^\dagger\Phi_2 - \frac{v_2^2}{2}\right)\right]^2 \\
&\quad + F\left[\left(\Phi_1^\dagger\Phi_1\right)\left(\Phi_2^\dagger\Phi_2\right) - \left(\Phi_1^\dagger\Phi_2\right)\left(\Phi_2^\dagger\Phi_1\right)\right] \\
&\quad + G\left[\mathcal{R}e\left(\Phi_1^\dagger\Phi_2\right) - \frac{v_1v_2}{2}\right]^2 + H\left[\mathcal{I}m\left(\Phi_1^\dagger\Phi_2\right)\right]^2 + I\,, \qquad (7.22)
\end{aligned}$$

to renormalize the effective potential $V^T(\phi_1,\phi_2)$.

As Φ_1 and Φ_2 gain thermal averages (7.5) in the spontaneously broken theory, the two-doublet model gives mass to the gauge bosons, fermions, and scalars, and yet remains renormalizable. The degrees of freedom in our two-doublet model are summarized in Table 7.1. Neglecting constants and total divergences, the Lagrangian may be expressed as a kinetic part plus an interacting part:

$$\mathcal{L} = \mathcal{L}_0 + \mathcal{L}^{\text{I}}_{\text{gauge}} + \mathcal{L}^{\text{I}}_{\text{fermion}} + \mathcal{L}^{\text{I}}_{\text{Higgs}} + \mathcal{L}^{\text{I}}_{\text{Yukawa}} + \mathcal{L}_{\text{c.t.}}\,, \qquad (7.23)$$

where

$$\begin{aligned}
\mathcal{L}_0 &= -W_\mu^+\left[g^{\mu\nu}\left(-\partial^2 - m_W^2(\phi)\right) + (1-1/\xi)\,\partial^\mu\partial^\nu\right]W_\nu^- \\
&\quad - \frac{1}{2}Z_\mu\left[g^{\mu\nu}\left(-\partial^2 - m_Z^2(\phi)\right) + (1-1/\xi)\,\partial^\mu\partial^\nu\right]Z_\nu \\
&\quad - \frac{1}{2}A_\mu\left[-g^{\mu\nu}\partial^2 + (1-1/\xi)\,\partial^\mu\partial^\nu\right]A_\nu
\end{aligned}$$

$$
\begin{aligned}
&- \overline{\omega}_j \partial^2 \omega_j - \overline{\zeta} \partial^2 \zeta \\
&+ \sum_a \left(\overline{u}^a \, i\partial\!\!\!/ u^a + \overline{d}^a \, i\partial\!\!\!/ d^a + \overline{\nu}^a \, i\partial\!\!\!/ \nu^a + \overline{e}^a \, i\partial\!\!\!/ e^a \right) - m_t(\phi_2)\, \bar{t}\, t \\
&+ \frac{1}{2} h^0 \left(-\partial^2 - m^2_{h^0}(\phi_1, \phi_2) \right) h^0 + \frac{1}{2} H^0 \left(-\partial^2 - m^2_{H^0}(\phi_1, \phi_2) \right) H^0 \\
&+ \frac{1}{2} A^0 \left(-\partial^2 - m^2_{A^0}(\phi_1, \phi_2) \right) A^0 + \frac{1}{2} G^0 \left(-\partial^2 - m^2_{G^0}(\phi_1, \phi_2) \right) G^0 \\
&+ H^+ \left(-\partial^2 - m^2_{H^\pm}(\phi_1, \phi_2) \right) H^- + G^+ \left(-\partial^2 - m^2_{G^\pm}(\phi_1, \phi_2) \right) G^- \, . \qquad (7.24)
\end{aligned}
$$

We list for reference the following interaction terms (note $\phi^2 \equiv \phi_1^2 + \phi_2^2$ and likewise for v^2):

$$
\begin{aligned}
\mathcal{L}^{\mathrm{I}}_{\mathrm{gauge}} &= g\varepsilon^{jkl} \left(\partial_\mu W^j_\nu \right) W^\mu_k W^\nu_l + g^2 \left(\delta_{km}\delta_{ln} - \delta_{kn}\delta_{lm} \right) W^k_\mu W^l_\nu W^\mu_m W^\nu_n \\
&\quad + g\varepsilon^{jkl} (\partial_\mu \overline{\omega}_j) \omega_k W^\mu_l \qquad (7.25) \\
\mathcal{L}^{\mathrm{I}}_{\mathrm{fermion}} &= \sum_a -\frac{g}{2\sqrt{2}} W^+_\mu \left[\overline{u}\gamma^\mu (1-\gamma_5)\, d' + \overline{\nu}\gamma^\mu (1-\gamma_5)\, e \right] \\
&\quad - \frac{g}{2\sqrt{2}} W^-_\mu \left[\overline{d'}\gamma^\mu (1-\gamma_5)\, u + \overline{e}\gamma^\mu (1-\gamma_5)\, \nu \right] \\
&\quad + \frac{g}{4} W^3_\mu \left[-\overline{u}\gamma^\mu (1-\gamma_5)\, u + \overline{d}\gamma^\mu (1-\gamma_5)\, d \right. \\
&\qquad \left. - \overline{\nu}\gamma^\mu (1-\gamma_5)\, \nu + \overline{e}\gamma^\mu (1-\gamma_5)\, e \right] \\
&\quad + \frac{g'}{4} B_\mu \left[-\overline{u}\gamma^\mu \left(\frac{5}{3} + \gamma_5 \right) u + \overline{d}\gamma^\mu \left(\frac{1}{3} + \gamma_5 \right) d \right. \\
&\qquad \left. - \overline{\nu}\gamma^\mu (-1+\gamma_5)\, \nu + \overline{e}\gamma^\mu (3+\gamma_5)\, e \right] \qquad (7.26) \\
\mathcal{L}^{\mathrm{I}}_{\mathrm{Higgs}} &= \lambda_1 \phi_1 (\phi_1^2 - v_1^2) \chi_1 + \lambda_2 \phi_2 (\phi_2^2 - v_2^2) \chi_2 \\
&\quad + \lambda_3 (\phi^2 - v^2) (\phi_1 \chi_1 + \phi_2 \chi_2) + \frac{\lambda_5}{2} (\phi_1\phi_2 - v_1 v_2) (\phi_2 \chi_1 + \phi_1 \chi_2) \\
&\quad + 2\lambda_1 \phi_1 \chi_1 \left[\chi_1^+ \chi_1^- + H_1^\dagger H_1 \right] + 2\lambda_2 \phi_2 \chi_2 \left[\chi_2^+ \chi_2^- + H_2^\dagger H_2 \right] \\
&\quad + 2\lambda_3 (\phi_1 \chi_1 + \phi_2 \chi_2) \left[\chi_1^+ \chi_1^- + H_1^\dagger H_1 + \chi_2^+ \chi_2^- + H_2^\dagger H_2 \right] \\
&\quad + \lambda_4 \left[\phi_1 \chi_1 \chi_2^+ \chi_2^- + \phi_2 \chi_1^+ \chi_1^- \chi_2 \right. \\
&\qquad \left. - \frac{\phi_1}{\sqrt{2}} \left(\chi_1^+ H_2 \chi_2^- + \chi_1^- H_2^\dagger \chi_2^+ \right) - \frac{\phi_2}{\sqrt{2}} \left(H_1 \chi_1^- \chi_2^+ + H_1^\dagger \chi_1^+ \chi_2^- \right) \right] \\
&\quad + \lambda_5 (\phi_2 \chi_1 + \phi_1 \chi_2) \left[\mathcal{R}e \left(\chi_1^- \chi_2^+ \right) + \frac{1}{2} (\chi_1 \chi_2 + \sigma_1 \sigma_2) \right] \\
&\quad + \lambda_6 (-\phi_2 \sigma_1 + \phi_1 \sigma_2) \left[\mathcal{I}m \left(\chi_1^- \chi_2^+ \right) + \frac{1}{2} (\chi_1 \sigma_2 - \sigma_1 \chi_2) \right] \\
&\quad + \lambda_1 \left[\chi_1^+ \chi_1^- + H_1^\dagger H_1 \right]^2 + \lambda_2 \left[\chi_2^+ \chi_2^- + H_2^\dagger H_2 \right]^2 \\
&\quad + \lambda_3 \left[\chi_1^+ \chi_1^- + H_1^\dagger H_1 + \chi_2^+ \chi_2^- + H_2^\dagger H_2 \right]^2 \\
&\quad + \lambda_4 \left[\chi_1^+ \chi_1^- H_2^\dagger H_2 + H_1^\dagger H_1 \chi_2^+ \chi_2^- - H_1 \chi_1^- H_2^\dagger \chi_2^+ - H_1^\dagger \chi_1^+ H_2 \chi_2^- \right]
\end{aligned}
$$

$$
\begin{aligned}
&+\lambda_5\left[\frac{1}{2}\left(\chi_1\chi_2+\sigma_1\sigma_2\right)+\mathcal{R}e(\chi_1^-\chi_2^+)\right]^2\\
&+\lambda_6\left[\frac{1}{2}\left(\chi_1\sigma_2-\sigma_1\chi_2\right)+\mathcal{I}m(\chi_1^-\chi_2^+)\right]^2\\
&+\sum_j\; g m_{Wj}(\phi_j)\,\chi_j W_\mu^+ W^{-\mu}+\frac{g}{2\cos\theta}\,m_{Zj}(\phi_j)\chi_j Z_\mu Z^\mu\\
&\qquad+\left(\chi_j^- W_\mu^++\chi_j^+ W_\mu^-\right)\left[e m_{Wj}(\phi_j)\,A^\mu-g m_{Zj}(\phi_j)\sin^2\theta\,Z^\mu\right]\\
&\qquad+\frac{g^2}{2}\left(H_j^\dagger H_j+\chi_j^+\chi_j^-\right)W_\mu^+W^{-\mu}+\frac{g^2}{4\cos^2\theta}H_j^\dagger H_j Z_\mu Z^\mu\\
&\qquad+\frac{g^2}{4\cos^2\theta}\,\chi_j^+\chi_j^-\left[\sin^2 2\theta\,A_\mu A^\mu+\cos^2 2\theta\,Z_\mu Z^\mu+\sin 4\theta\,A_\mu Z^\mu\right]\\
&\qquad+\frac{ge}{\sqrt{2}}\left[H_j\chi_j^- W_\mu^+ + H_j^\dagger\chi_j^+ W_\mu^-\right]\left[A^\mu-\tan\theta\,Z^\mu\right]\\
&\qquad+\frac{g}{\cos\theta}\frac{1}{2i}\left(H_j\partial_\mu H_j^\dagger-H_j^\dagger\partial_\mu H_j\right)Z^\mu\\
&\qquad+\frac{g}{\cos\theta}\frac{1}{2i}\left(\chi_j^-\partial_\mu\chi_j^+-\chi_j^+\partial_\mu\chi_j^-\right)\left[\cos 2\theta\,Z^\mu+\sin 2\theta\,A^\mu\right]\\
&\qquad+\frac{ig}{\sqrt{2}}\Big[H_j\partial^\mu\chi_j^- W_\mu^+-H_j^\dagger\partial^\mu\chi_j^+ W_\mu^-\\
&\qquad\qquad-\partial^\mu H_j\chi_j^- W_\mu^+ +\partial^\mu H_j^\dagger\chi_j^+ W_\mu^-\Big] \qquad (7.27)
\end{aligned}
$$

$$
\begin{aligned}
\mathcal{L}^{\mathrm{I}}_{\mathrm{Yukawa}} &= -\frac{g_t}{\sqrt{2}}\left(\chi_2\,\bar{t}\,t-i\,\sigma_2\,\bar{t}\,\gamma_5 t\right)\\
&\quad+\frac{g_t}{2}\left(\chi_2^-\,\overline{b'}(1+\gamma_5)\,t+\chi_2^+\,\bar{t}\,(1-\gamma_5)\,b'\right)\;. \qquad (7.28)
\end{aligned}
$$

We will compute the effective potential $V^T(\phi_1,\phi_2)$ by the tadpole method, which may be derived as in the one doublet case. By comparing the expansions for the effection potential ($\widetilde{\Gamma}^{(i,j)}$ denotes the proper $(i+j)$-vertex with i χ_1-legs and j χ_2-legs) about the symmetric point,

$$
V^T(\psi_1,\psi_2)=-\sum_{n=1}^{\infty}\frac{1}{n!}\sum_{m=0}^{n}\binom{n}{m}\,\widetilde{\Gamma}^{(n-m,m)}(0)\;\psi_1^{n-m}\psi_2^m\;,
$$

and about (ϕ_1,ϕ_2),

$$
V^T(\psi_1,\psi_2)=-\sum_{n=1}^{\infty}\frac{1}{n!}\sum_{m=0}^{n}\binom{n}{m}\,\widetilde{\Gamma}_\phi^{(n-m,m)}(0)\;(\psi_1-\phi_1)^{n-m}(\psi_2-\phi_2)^m\;,
$$

and then taking first derivatives, it is clear that

$$
\begin{aligned}
\widetilde{\Gamma}_\phi^{(1,0)}(0) &= -\frac{\partial V^T}{\partial\phi_1}(\phi_1,\phi_2)\\
\widetilde{\Gamma}_\phi^{(0,1)}(0) &= -\frac{\partial V^T}{\partial\phi_2}(\phi_1,\phi_2)\;. \qquad (7.29)
\end{aligned}
$$

Integration of the tadpole graphs thus yields the effective potential. As before, the

scalar self-energies at zero momentum may be computed from

$$\begin{aligned}
\frac{\partial^2 V^T}{\partial \phi_1^2}(\phi_1,\phi_2) &= -\widetilde{\Gamma}_{\phi}^{(2,0)}(0) \\
\frac{\partial^2 V^T}{\partial \phi_2^2}(\phi_1,\phi_2) &= -\widetilde{\Gamma}_{\phi}^{(0,2)}(0) \\
\frac{\partial^2 V^T}{\partial \phi_1 \partial \phi_2}(\phi_1,\phi_2) &= -\widetilde{\Gamma}_{\phi}^{(1,1)}(0)\,. \qquad (7.30)
\end{aligned}$$

7.2 Effective Potential

Having established notation, we turn now to computing the effective potential and deriving the baryogenesis bound on the Higgs boson mass. In analogy to the standard expressions derived in Appendix B, we sum over the various particle species to obtain the effective potential $V^T = V^0 + \Delta V^T$ for the two-doublet model at one loop, subject to the specified renormalization prescription:

$$\begin{aligned}
V^0_{1\,\mathrm{loop}}(\phi) &= V(\phi) + \sum_{j=B,F} \frac{\pm g_j}{64\pi^2}\left[m_j^4(\phi)\log\left(\frac{m_j^2(\phi)}{M_j^2}\right) - \frac{3}{2}m_j^4(\phi) + 2M_j^2 m_j^2(\phi)\right] \\
\Delta V^T_{1\,\mathrm{loop}}(\phi) &= T^4 \sum_B g_B I_B\left(\frac{m_B(\phi)}{T}\right) + T^4 \sum_F g_F I_F\left(\frac{m_F(\phi)}{T}\right)\,, \qquad (7.31)
\end{aligned}$$

where $V(\phi)$ may be expressed as

$$\begin{aligned}
V(\phi) &= \frac{M_{H^0}^2}{8}\left(\frac{v^2}{v_1^2 v_2^2}\right)\left[\cos\alpha_0 \sin\beta\left(\phi_1^2 - v_1^2\right) + \sin\alpha_0\cos\beta\left(\phi_2^2 - v_2^2\right)\right]^2 \\
&\quad + \frac{M_{h^0}^2}{8}\left(\frac{v^2}{v_1^2 v_2^2}\right)\left[\sin\alpha_0 \sin\beta\left(\phi_1^2 - v_1^2\right) - \cos\alpha_0\cos\beta\left(\phi_2^2 - v_2^2\right)\right]^2 \\
&\quad + \frac{M_5^2}{8}\left(\frac{v^2}{v_1^2 v_2^2}\right)(\sin\beta\phi_1 - \cos\beta\phi_2)^2 \\
&\qquad \cdot\left(4v_1 v_2 \sin\beta\cos\beta - [\sin\beta\phi_1 + \cos\beta\phi_2]^2\right)\,. \qquad (7.32)
\end{aligned}$$

g_j counts the degrees of freedom, $\pm$ is for bosons or fermions, and the temperature integrals $I_{B,F}$ are given in (B.5) and (B.6). The renormalization conditions

$$\begin{aligned}
\left.\frac{\partial V^0}{\partial \phi_j}\right|_{\phi=v} &= 0 \qquad (7.33) \\
\left.\left(\frac{\partial^2 V^0}{\partial\phi_j\partial\phi_k}\right)\right|_{\phi=v} &= \begin{pmatrix} \cos\alpha_0 & -\sin\alpha_0 \\ \sin\alpha_0 & \cos\alpha_0 \end{pmatrix}\begin{pmatrix} M_{H^0}^2 & 0 \\ 0 & M_{h^0}^2 \end{pmatrix}\begin{pmatrix} \cos\alpha_0 & \sin\alpha_0 \\ -\sin\alpha_0 & \cos\alpha_0 \end{pmatrix}
\end{aligned}$$

preserve (at one loop) the tree-level expressions for the zero-temperature vacuum and the corresponding masses and rotation angle for the neutral scalar sector. M_5 is an additional mass scale allowed by the tree-level potential, and is fixed by a final renor-

malization condition, whose exact form is irrelevant for our purposes. [4] Thus V^0 is expressed in terms of the fixed parameters M_{H^0}, M_{h^0}, M_5, $\tan\alpha_0$, and $\tan\beta$. Approximating the integrals $I_{B,F}$ by their high-temperature expansions, (B.9) and (B.10), yields the following expression:

$$\begin{aligned} V^T_{1\,\mathrm{loop}}(\phi) &= V(\phi) \\ &\quad + \sum_B g_B \left\{ \left(\frac{M_B^2}{32\pi^2} + \frac{T^2}{24} \right) m_B^2(\phi) - \frac{T}{12\pi} m_B^3(\phi) - \frac{m_B^4(\phi)}{64\pi^2} \log\left(\frac{M_B^2}{a_B T^2} \right) \right\} \\ &\quad - \sum_F g_F \left\{ \left(\frac{M_F^2}{32\pi^2} - \frac{T^2}{48} \right) m_F^2(\phi) - \frac{m_F^4(\phi)}{64\pi^2} \log\left(\frac{M_F^2}{a_F T^2} \right) \right\} . \end{aligned} \tag{7.34}$$

As in the Standard Model, the analysis may be divided into two cases, depending on the relative masses of the scalar and gauge bosons. In the case of light scalars, $M_{\mathrm{scalar}} \lesssim M_W$, scalar loops may be neglected from the one-loop effective potential, and the analysis is greatly simplified. For heavy scalars, $M_{\mathrm{scalar}} \gtrsim M_W$, scalar loops must be included.

As we have seen in Chapter 3, an accurate analysis demands that we sum the ring diagrams to account for the leading infrared effects, which contribute to the cubic term in V^T at the same order as the one-loop graphs. Fermion ring diagrams need not be considered since they do not contribute to the cubic terms $\sim T m_j^3(\phi)$. The scalar modes all receive cubic contributions from the ring summation, while only the longitudinal components do so for the massive gauge fields:

$$\begin{aligned} \Delta V^T_{\mathrm{ring}}(\phi) &= -\frac{T}{12\pi} \sum_{j=\mathrm{scalar}} \left\{ \left[m_j^2(\phi) + \Pi_j(0) \right]^{3/2} - m_j^3(\phi) \right\} \\ &\quad -\frac{T}{12\pi} \sum_{\substack{j=\mathrm{long.} \\ \mathrm{gauge}}} \left\{ \left[m_j^2(\phi) + \Pi_j^{00}(0) \right]^{3/2} - m_j^3(\phi) \right\} . \end{aligned} \tag{7.35}$$

$\Pi(0)$ and $\Pi^{00}(0)$ are the scalar self-energy and longitudinal component of the polarization tensor at zero momentum.

To preview the calculation in the following sections, we start with the effective potential $V^T(\phi)$ in the high-temperature approximation. We aim to derive bounds on $M_{h^0}^2$ by requiring

$$\left. \frac{\sqrt{\phi_1^2 + \phi_2^2}}{T} \right|_{\mathrm{crit}} \gtrsim 1$$

to avoid baryon washout. So first we will compute the critical temperature T_c by the

[4] This new mass scale is usually neglected in the literature. Likewise, we will take $M_5 = 0$ in the sequel.

condition

$$\det\left(\frac{\partial^2 V^T}{\partial\phi_j\partial\phi_k}\right)\Bigg|_{\phi=0} = 0\,,$$

and then determine the order paramater at the critical point $(\phi_1/T, \phi_2/T)_{\rm crit}$, by

$$\left.\frac{\partial V^T}{\partial\phi_1}\right|_{T_c} = 0 = \left.\frac{\partial V^T}{\partial\phi_2}\right|_{T_c}\,.$$

The nature of the phase transition thus will be described as functions of the parameters M_{H^0}, M_{h^0}, M_5, $\tan\alpha_0$, and $\tan\beta$. By requiring that sphaleron-mediated effects not be in equilibrium at the end of the phase transition, in order for a net baryon number to survive, we will obtain a cosmological mass bound on the Higgs boson.

Finally, a word about the parameters. The full classical potential $U(\phi)$ (7.3) is parametrized by seven quantities: $\lambda_1, \ldots, \lambda_6$, and $\tan\beta$. For the effective potential $V^T(\phi)$, λ_4 and λ_6 are irrelevant and are fixed by $m^2_{H^\pm} = \lambda_4 v^2/2$ and $m^2_{A^0} = \lambda_6 v^2/2$. So before diagonalization and renormalization, $V^T(\phi)$ is parametrized by λ_1, λ_2, λ_3, λ_5, and $\tan\beta$. Afterward, the new parameters are $M^2_{H^0}$, $M^2_{h^0}$, M^2_5, $\tan\alpha_0$, and $\tan\beta$.

Because the two-doublet model possesses so many free parameters, a general analysis is difficult and any definitive conclusion elusive. Therefore we simplify the aims of this chapter. We intend to demonstrate that the case of light scalars is essentially unchanged from that of the SM, and leads to an identical Higgs mass bound, both at one loop and with ring improvement. The case of heavy scalars, however, is potentially different, and may yield a more generous Higgs mass bound. We do not address this question here. To ensure a tractable analysis, we set the mass scale $M^2_5 = 0$. [5] This could substantially change our conclusion for the case of light scalars. In our discussion, we will attempt to indicate the general effect of a non-vanishing M^2_5.

7.3 Light Scalars

First we assume light scalar modes, $M_{\rm scalar} \lesssim M_W$, and neglect scalar loops in the effective potential. This case has been analyzed at one loop by Bochkarev, Kuzmin, and Shaposhnikov in [21]. We give below the details of the calculation at one loop, and then we determine the effect of ring improvement.

One Loop

The one-loop effective potential is given by (7.34), with $B = W^\pm, Z$ and $F = t$. The result may be written at high temperature in the form

$$V^T_{1\,\rm loop}(\phi) \;=\; V(\phi)$$

[5] As was done implicitly in previous analyses at one loop [21, 46].

$$
\begin{aligned}
&+ \left(\phi_1^2 + \phi_2^2\right)\left[D_1 T^2 + \frac{6M_W^4 + 3M_Z^4}{32\pi^2 v^2}\right] + \phi_2^2\left[D_2 T^2 - \frac{12M_t^4}{32\pi^2 v_2^2}\right] \\
&- ET\left(\phi_1^2 + \phi_2^2\right)^{3/2} \\
&- \frac{(\phi_1^2 + \phi_2^2)^2}{64\pi^2 v^4}\left[6M_W^4 \log\left(\frac{M_W^2}{a_B T^2}\right) + 3M_Z^4 \log\left(\frac{M_Z^2}{a_B T^2}\right)\right] \\
&+ \frac{\phi_2^4}{64\pi^2 v_2^4} 12 M_t^4 \log\left(\frac{M_t^2}{a_F T^2}\right) , \qquad (7.36)
\end{aligned}
$$

where

$$
\begin{aligned}
D_1 &= \frac{1}{24v^2}\left(6M_W^2 + 3M_Z^2\right) \\
D_2 &= \frac{1}{48v_2^2} 12 M_t^2 . \qquad (7.37)
\end{aligned}
$$

The critical temperature is determined by the condition

$$
\det\left(\frac{\partial^2 V^T}{\partial\phi_j \partial\phi_k}\right)\Bigg|_{\phi=0} = 0 , \qquad (7.38)
$$

with the mass squared matrix

$$
\begin{aligned}
\left.\frac{\partial^2 V^T}{\partial\phi_1^2}\right|_{\phi=0} &= -\frac{M_{H^0}^2}{2}\left(\frac{v^2}{v_1^2 v_2^2}\right)\cos\alpha\sin\beta\left(\cos\alpha\sin\beta v_1^2 + \sin\alpha\cos\beta v_2^2\right) \\
&\quad - \frac{M_{h^0}^2}{2}\left(\frac{v^2}{v_1^2 v_2^2}\right)\sin\alpha\sin\beta\left(\sin\alpha\sin\beta v_1^2 - \cos\alpha\cos\beta v_2^2\right) \\
&\quad + M_5^2\sin^2\beta + 2\left[D_1 T^2 + \frac{6M_W^4 + 3M_Z^4}{32\pi^2 v^2}\right] \qquad (7.39) \\
\left.\frac{\partial^2 V^T}{\partial\phi_2^2}\right|_{\phi=0} &= -\frac{M_{H^0}^2}{2}\left(\frac{v^2}{v_1^2 v_2^2}\right)\sin\alpha\cos\beta\left(\cos\alpha\sin\beta v_1^2 + \sin\alpha\cos\beta v_2^2\right) \\
&\quad - \frac{M_{h^0}^2}{2}\left(\frac{v^2}{v_1^2 v_2^2}\right)\cos\alpha\cos\beta\left(-\sin\alpha\sin\beta v_1^2 + \cos\alpha\cos\beta v_2^2\right) \\
&\quad + M_5^2\cos^2\beta + 2\left[(D_1 + D_2)T^2 + \frac{1}{32\pi^2}\left\{\frac{6M_W^4 + 3M_Z^4}{v^2} - \frac{12M_t^4}{v_2^2}\right\}\right] \qquad (7.40) \\
\left.\frac{\partial^2 V^T}{\partial\phi_1\partial\phi_2}\right|_{\phi=0} &= -M_5^2\sin\beta\cos\beta . \qquad (7.41)
\end{aligned}
$$

First we set $M_5^2 = 0$ for simplicity, and later consider the consequences of the case

$M_5^2 \neq 0$. Then the critical temperature is determined by

$$\left.\frac{\partial^2 V^T}{\partial \phi_1^2} \cdot \frac{\partial^2 V^T}{\partial \phi_2^2}\right|_{\phi=0} = 0 \,. \tag{7.42}$$

This means that the curvature at the origin must vanish in some direction, which, following Bochkarev, Kuzmin, Shaposhnikov, we suppose to be in the ϕ_1-direction: [6]

$$\begin{aligned} \left.\frac{\partial^2 V^T}{\partial \phi_1^2}\right|_{\phi=0} &= 0 \\ \left.\frac{\partial^2 V^T}{\partial \phi_2^2}\right|_{\phi=0} &\geq 0 \,. \end{aligned} \tag{7.43}$$

In this case we have a one-dimensional problem, nearly identical to that considered in the Standard Model of Chapter 5. The critical temperature, critical point, and Higgs mass bound may be computed and give identical results.

Thus, at one loop, first-order behavior is observed at the phase transition, provided that $M_H \lesssim 55$ GeV. However, for the reasons enumerated in our analysis of the scalar and Higgs models in Section 3.3, we must now include the ring diagrams.

Ring Improvement

The process of ring-improvement is analogous to that considered for the Standard Model. Since we only consider the case of light scalars, only the gauge polarization tensors Π^{00}_{gauge} need be computed. Because the two-doublet model retains the gauge structure of the Standard Model, the gauge and fermi contributions to Π^{00}_{gauge} are identical to those computed in Section 5.3. The scalar contributions are simply multiplied by a factor of two, as may be seen by explicit calculation of the graphs in Figure 5.3; this reflects the addition of the second Higgs doublet, since it shares identical gauge interactions with the first. The critical temperature, critical point, and Higgs mass bound may computed analogously to those computed in Section 5.3, and are virtually indistinguishable from the results in the Standard Model. We compare the mass bounds on the Higgs boson in Figure 7.1. In the same manner as observed in the Standard Model, ring improvement weakens the first-order nature of the phase transition and relaxes the mass bound on the Higgs boson.

7.4 Discussion

In our analysis we have taken $M_5 = 0$. What are the possible effects of a non-zero value of M_5? To begin with, we would have to diagonalize the mass matrix (7.39,7.40,7.41).

[6] If we choose the ϕ_2-direction, a similar result follows.

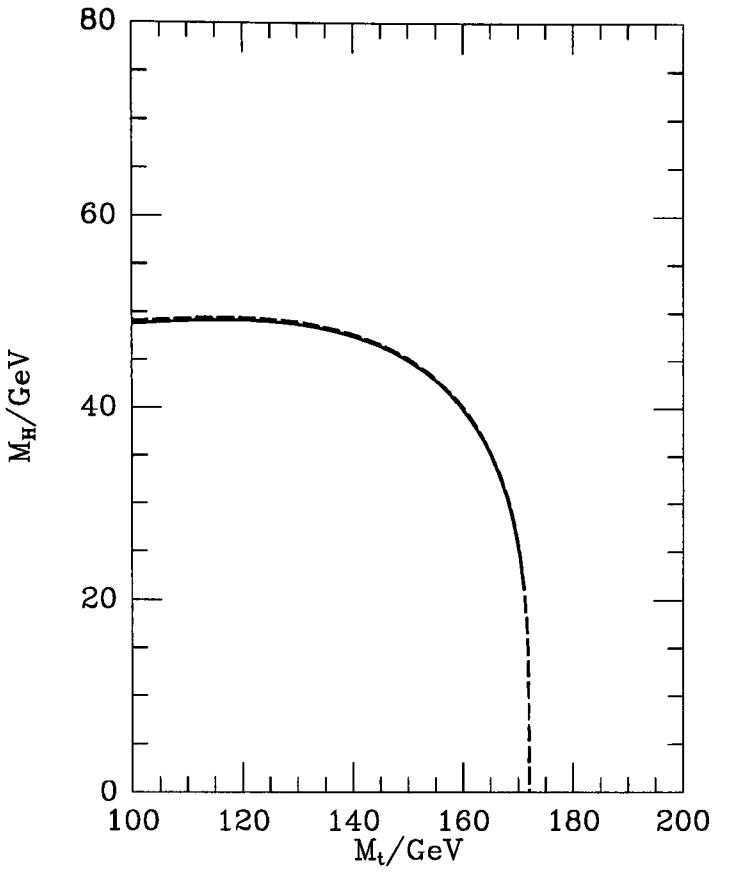

Figure 7.1: Comparison of the mass bounds on the Higgs boson, with ring improvement, in the Standard Model and two-doublet model both with light scalars.

For small M_5, this has the effect of rotating the direction of the phase transition in ϕ_1-ϕ_2 space. For larger values, the situation is unclear and depends on the relations among the various mass scales. An interesting possibility may arise with the appearance of several minima, in which case the phase transition may proceed in several steps.

Chapter 8

Electroweak Processing of a Primordial Asymmetry

In the preceding chapters we addressed the first topic of this thesis, the nature of the electroweak phase transition as described by the effective potential at finite temperature. We also considered the implications for the Higgs sector of sufficiently strong first-order behavior. The present chapter progresses to the second topic: the possibility that an asymmetry created at the GUT scale (where CP violation resides) results in baryogenesis at the weak scale. [1]

8.1 Introduction

Electroweak theory contains the means for anomalous violation of fermion number via non-perturbative effects, in the form of instantons at zero temperature [35] and sphalerons at high temperature [7]. The vacuum structure of electroweak theory admits both quantum and thermal tunneling between inequivalent vacua by such configurations. As the Adler-Bell-Jackiw-Bardeen anomaly violates B, L, and $B+L$ but conserves $B-L$, so do the sphaleron configurations, which are in equilibrium at high temperatures (see Chapter 4).

Rapid fermion number violation at high temperature raises the possibility of baryogenesis at the electroweak scale [40]. Numerous mechanisms for electroweak baryogenesis have appeared in the literature, but the most widely researched ones may be broadly classified into the following categories:

- Topological fluctuations (Turok and Zadrozny [10]): The CP-violating coupling of an axion-like Higgs phase to the gauge fields biases topological fluctuations, and hence baryon production, near the bubble walls. This requires an extension of the Standard Model with CP violation in the scalar sector.

[1] This work was done in collaboration with Dr. S. Abel.

- Spontaneous baryogenesis (Cohen, Kaplan, and Nelson [11, 12]): An adiabatic regime in thick, slow-moving bubble walls (characteristic of a weakly first-order phase transition) induces a (CP-violating) effective interaction term of the form

$$\partial_\mu \theta \cdot j_B^\mu \sim \partial_0 \theta \cdot n_B + \cdots .$$

  This term arises in CP-violating extensions of the Standard Model, and acts as a chemical (or charge) potential to bias baryon production.

- Charge transport (Nelson, Kaplan, and Cohen [13, 14]): In the presence of thin, fast-moving bubble walls (as would occur in a strongly first-order phase transition), the CP-violating reflection of fermions off the bubble walls produces a net charge flux into the symmetric phase, thus biasing baryon production. CP violation occurs in the scalar (e.g., the two-doublet model) or leptonic (e.g. Majorana neutrino masses) sectors of the extended Standard Model.

There are two severe problems for baryogenesis within the minimal Standard Model: (a) the electroweak phase transition, for a Higgs mass in the experimentally allowed range $M_H \gtrsim 55$ GeV, is not strongly enough first-order to yield an efficient scheme of baryon production (see Chapter 5); and (b) the parameter that characterizes CP violation in the Standard Model is $\delta_{\rm CP} \sim 10^{-20}$, whereas efficient baryogenesis appears to require it to be of $\mathcal{O}(10^{-8})$ [47]. Hence the above mechanisms typically employ extensions of the Standard Model to circumvent these difficulties.

Very recently, Farrar and Shaposhnikov [16] analyzed baryogenesis occurring through a charge transport mechanism in the Standard Model, and suggested that an acceptable value of n_B/s could be attained (thus obviating the need to resort to extensions of the electroweak theory for richer sources of CP violation), *provided* that the Standard Model undergoes a robust first-order phase transition. However, their analysis suffers uncertainties of unknown magnitude from the simplifying assumptions made:

- the major contribution to scattering off the bubble wall was assumed to occur at low momentum, $p \ll M$;

- the bubble wall was taken to be slow-moving, $v \ll 1$;

- the calculation was done in one spatial dimension, and it is unknown what relationship the scattering problem in one dimension bears to that in three dimensions.

On the other hand, if significant baryon production does not occur at the electroweak phase transition, rapid fermion number violation leads to the potential depletion of any baryon number generated at higher energy scales (at a prior epoch). This would happen unless such baryon number were protected by some symmetry, that is, some mode that does not equilibrate with the thermal plasma.

This prospect raises the possibility of encoding the asymmetry in a conserved global quantum number that is set primordially, which by subsequent processing at the electroweak phase transition, is converted into the presently observed baryon number. The simplest example is to have a non-zero value of $B - L$ driving baryogenesis, as first considered by Fukugita and Yanagida [48]. They reasoned that $B - L$ is untouched by the sphalerons and only the orthogonal $B+L$-projection equilibrates to zero. Therefore the baryon number that survives the electroweak phase transition is

$$B = \frac{1}{2}(B - L)_{\rm init} + \frac{1}{2}(B + L)_{\rm init}\, e^{-\gamma \Delta t} \approx -\frac{1}{2} L_{\rm init} \ ,$$

for the case in which $B_{\rm init} = 0$ and there exists a primordial L-asymmetry, such as might be produced by the out-of-equilibrium decays of massive neutrinos; Δt is the time interval that sphalerons operate in equilibrium with an interaction rate γ (assumed to be large).

Harvey and Turner [49], however, showed that the $B + L$ mode does not necessarily equilibrate to zero in the presence of rapid fermion number violation, because of the need to conserve electric and color charge. Rather,

$$B, L, B + L \ \propto \ B - L \ ,$$

for both $T \gtrsim T_{\rm c}$ and $T_{\rm c} \gtrsim T \gtrsim M_W$. A primordial asymmetry for $B - L$ ensures that a net B survives the epoch of anomalous B-violation, whereas $B - L = 0$ ensures the absence of baryon number today. However, this conclusion was based on the assumption that all particle species were relativistic, i.e., mass effects were neglected. As was demonstrated in later work [50, 51], mass effects can modify these relations: if $m_j^2/T^2 \neq 0$, then B, L, and $B + L$ need not vanish, even if $B = L$.

Because the simplest GUTs of interest conserve $B - L$ [52], one is lead to consider scenarios in which the primordial asymmetry satisfies $B = L$. Fortunately this condition admits the possibility of individual flavor asymmetries,

$$L_i - B/N \neq 0 \ ,$$

which may then encode a primordial lepton asymmetry. Such asymmetries might be produced by lepto-quarks, for example, by generational differences in their out-of-equilibrium decays. Thus lepton flavor asymmetries may bias anomalous $B + L$-processing to result in the observed B, even if $B_{\rm init} = 0$. It may be possible, therefore, to take individual flavor asymmetries $L_i - B/N \neq 0$, rather than total $B - L \neq 0$, as the driving force behind baryogenesis.

Kuzmin, Rubakov, and Shaposhnikov [50] explicitly realized this idea in the context of lepto-quark theories, which could naturally produce such asymmetries, and identified the role played by lepton mass effects. They required: (i) the absence of flavor-mixing

after the lepto-quark decays; [2] (ii) large flavor asymmetry and CP violation in the lepto-quark decays; and (iii) a large Higgs mass, $M_H \gtrsim 55$ GeV. The first two conditions prevent the symmetric case $L_1 - B/N = \cdots = L_N - B/N = 0$, while the last guarantees the equilibrium of anomalous baryon violation after the phase transition, when the leptons gain non-zero masses. This results in a baryon-to-photon ratio of

$$\frac{n_B}{n_\gamma} = -\frac{4}{13\pi^2} \sum_{i=1}^{N} \frac{m_{l_i}^2(T_*)}{T_*^2} \cdot \frac{L_i - B/N}{n_\gamma} ,$$

where T_* is the temperature at which sphaleron-mediated processes freeze out and the $L_i - B/N$ are the primordial asymmetries produced during the era of lepto-quark decays.

Dreiner and Ross [51] elaborated on the role of mass effects using chemical potentials, which easily incorporate symmetries as constraints. They noted that for $T > T_c$, B, L, $B+L$ are still proportional to $B-L$; and although $B-L=0$ implies that $L=0$, the individual lepton chemical potentials μ_i do not necessarily all vanish. For $T < T_c$, however, B, L, and $B+L$ are no longer proportional to $B-L$; here $B-L=0$ implies that

$$B = L = \frac{1}{2}(B+L) \propto \Delta\mu ,$$

where, in their notation,

$$\Delta\mu = \sum_i \mu_i \left[1 - \alpha\left(\frac{m_{l_i}^2}{T^2}\right)\right] \propto \sum_i \mu_i \frac{m_{l_i}^2}{T^2} .$$

If the primordial lepton asymmetry allows some $L_i \neq 0$, as might occur in leptogenesis that is not family-symmetric, then some μ_i is non-vanishing. Such μ_i determines the extent to which the initial L_i asymmetry is converted into the final B asymmetry; thus B and L need not vanish even if $B-L$ is conserved.

Campbell, Davidson, Ellis, and Olive [53] carried these ideas further and demonstrated how to avoid the m^2/T^2 suppression through lepton-violating interactions. Provided that some — but not all — lepton flavors are violated by $\Delta L \neq 0$ interactions in equilibrium, B may be regenerated without the m^2/T^2 lepton mass effects. Instead B depends only on the initial asymmetry of the non-equilibrating modes. For example, if lepton-violating interactions equilibrate $L_1 - B/3$ and $L_2 - B/3$ to zero, then the non-zero $L_3 - B/3$ biases baryon production via sphalerons:

$$B \propto B - L = B/3 - L_3 \neq 0 ,$$

without mass effects.

These analyses considered the processing of primordial asymmetries by rapid fermion

[2] More precisely, the requirement is that flavor mixing should be out of equilibrium: $\Gamma_{\text{mixing}} \ll H(T)$ for $T < T_{\text{decay}}$.

number violation *in equilibrium* and thus implicitly assumed second-order behavior at the phase transition to preserve such equilibrium. What happens if the thermal plasma undergoes a departure from equilibrium of anomalous $B + L$-violation? This occurs if the universe undergoes a first-order phase transition, as lattice studies of the Standard Model and analytical work on some extensions of the Standard Model seem to suggest. Then one must study the rate equation that describes the approach of B to its equilibrium value, as we do later.

This chapter proposes and studies a mechanism to convert a primordial lepton asymmetry into the observed baryon asymmetry at a first-order electroweak phase transition. It combines the ideas of Nelson, Kaplan, and Cohen for the enhancing effect of charge transport via fermion reflection off the expanding bubble walls, and the methods of Farrar and Shaposhnikov for describing the fermionic collective modes of a relativistic plasma. This mechanism yields a baryon number proportional to the initial lepton asymmetry L, which may be consistent with the observed value of $B \sim 10^{-10}$ for $L/s \sim 2 \cdot 10^{-5}$, without requiring any assumption about enhanced (or maximal) CP violation in the dynamics (which plays no role in our mechanism [3]). Put concisely, the mechanism we analyze operates under the following assumptions:

- the universe undergoes an electroweak phase transition that is strongly first-order, with thin bubble walls and a departure from equilibrium of anomalous baryon violation;
- the lepton sector conserves CP;
- $B - L = 0$, although $L_i - B/3 \neq 0$ encodes the primordial lepton asymmetry.

At high temperature or density, the fundamental excitations may not coincide with the elementary particles; as a result, perturbation theory in terms of the bare fields may be inadequate to describe effects essentially due to the ambient plasma. In order to proceed in a valid perturbative calculation, we first determine the quasiparticle modes that exist in a relativistic plasma at high temperature. Using these modes, we compute the reflection coefficients and then the lepton flux reflected off the expanding bubble wall. Because the reflected flux $\propto M_l/T$, where M_l is the lepton flavor mass and $T \sim 100$ GeV is the critical temperature of the phase transition, the τ-lepton flux will predominate. The thermal scattering length of the leptonic quasiparticles will then be computed, to give an indication of how long the reflected leptons remain in the unbroken phase before being absorbed by the advancing front of broken phase. During its time in the unbroken phase, the τ-lepton flux biases anomalous baryon violation, which is assumed to be in equilibrium outside the bubble (the region of $\phi = 0$). The sphaleron processes thus produce baryons, which are swallowed into the broken phase and survive to the present. We then estimate the generated baryon number and find

[3] CP violation is of course evident in the initial condition of a primordial L-asymmetry; and CP violation in the particle dynamics would have been required for its generation at the GUT scale, as we know from the Sakharov conditions.

that $B \sim 10^{-10}$ can be accommodated in this scenario, provided that the primordial τ-asymmetry is $L_\tau/s \sim 2 \cdot 10^{-5}$, or scaling by the lepton number density,

$$\frac{n_l - n_{\bar{l}}}{n_l + n_{\bar{l}}} \sim 0.002 \, .$$

Our primary sources are the papers by Nelson, Kaplan, and Cohen [13] and by Farrar and Shaposhnikov [16], denoted NKC and FS respectively. The starting point of our analysis is the rate equation (4.7) describing the approach of baryon number to equilibrium:

$$\dot{\rho}_B = -\frac{3\Gamma_B}{T}\frac{\partial F}{\partial B} \, . \tag{8.1}$$

The partial derivative of the free energy is taken with all conserved quantum numbers held fixed, and as we will compute later, is simply proportional to the hypercharge:

$$\frac{\partial F}{\partial B} = \xi \frac{\rho_Y}{T^2} \, , \tag{8.2}$$

where the parameter ξ depends on the model under consideration and may be determined by explicit computation with chemical potentials. Integrating the rate equation ahead of the advancing bubble wall,

$$\begin{aligned} \rho_B &= -\frac{3\Gamma_B}{T}\int dt \, \frac{\partial F}{\partial B} = -\frac{3\xi\Gamma_B}{T^3}\int_{-\infty}^{z/u} dt \, \rho_Y(z-ut) \\ &= -\frac{3\xi\Gamma_B f_Y \tau_T}{uT^3} \, , \end{aligned} \tag{8.3}$$

where f_Y is the reflected hypercharge flux and τ_T the thermal transport time ($\sim$ thermal scattering length). Scaling by the entropy density and recalling the rate for anomalous baryon violation in the symmetric phase (see (4.6)),

$$\Gamma_B = 3\kappa\alpha_W^4 T^4 \, , \tag{8.4}$$

we arrive at our final expression for the observed baryon number:

$$\frac{\rho_B}{s} = -\frac{9\alpha_W^4 \kappa\xi}{u}\left(\frac{f_Y \tau_T T}{s}\right) \, . \tag{8.5}$$

We take $\kappa \sim 1$, $u \sim 0.1$, and are left to compute ξ, f_Y, and τ_T, which we do in the following sections.

8.2 Quasiparticle Excitations in a Relativistic Plasma at High Temperature

We determine the leptonic modes in the thermal plasma (which is characterized by the four-velocity u^α) and obtain the quasiparticle solutions for left and right chiralities, which have different interactions and hence develop different thermal masses. This section summarizes basic results; more complete treatments may be found in Weldon and Lebedev [54].

Thermal Lepton Masses

The lepton thermal self-energy at one loop is given by the graphs of Figure 8.1:

$$\Sigma(P) = iA\int\frac{d^4k}{(2\pi)^4}\,D_{\mu\nu}(k)\gamma^\mu S(k+P)\gamma^\nu + iB\int\frac{d^4k}{(2\pi)^4}\,D(k)S(k+P) \tag{8.6}$$

$$\equiv -a(\omega,p)\,\not{P} - b(\omega,p)\,\not{u}\,, \tag{8.7}$$

where a and b are functions of the Lorentz invariants

$$\omega \equiv P\cdot u \tag{8.8}$$

$$p \equiv \sqrt{(P\cdot u)^2 - P^2}\,, \tag{8.9}$$

such that $\omega^2 - p^2 = P^2$. a and b are computed in [54]:

$$a(\omega,p) = \frac{\Omega^2}{p^2}\left[1 - \frac{\omega}{2p}\log\left(\frac{\omega+p}{\omega-p}\right)\right] \tag{8.10}$$

$$b(\omega,p) = \frac{\Omega^2}{p}\left[-\frac{\omega}{p} + \frac{1}{2}\left(\frac{\omega^2}{p^2}-1\right)\log\left(\frac{\omega+p}{\omega-p}\right)\right] \tag{8.11}$$

$$\Omega^2 = (A+\frac{1}{2}B)\frac{T^2}{8}\,. \tag{8.12}$$

The constants A and B depend on the lepton chirality and the model under consider-

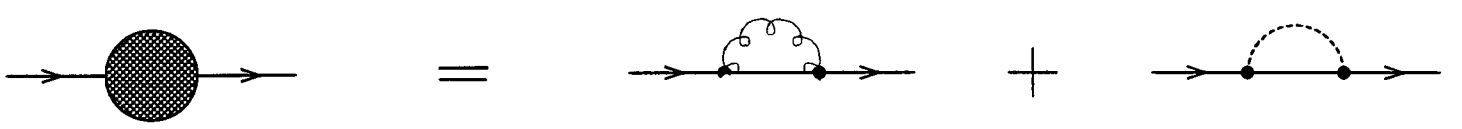

Figure 8.1: The fermion self-energy at one loop.

ation. For the minimal Standard Model and the two-doublet model, one can easily see that

$$\begin{array}{lll} A_L = \frac{3}{4}g^2 + \frac{1}{4}g'^2 & ; & B_L = g_\tau^2 \\ A_R = g'^2 & ; & B_R = 2g_\tau^2 \end{array}\,, \tag{8.13}$$

where the Yukawa contributions are identical for both models, since in either case, the lepton couples to only one scalar doublet. This yields the following thermal lepton

masses:

$$\Omega_L^2 = \frac{1}{8v^2}\left(2M_W^2 + M_Z^2 + M_\tau^2\right)T^2 \approx (0.209\,T)^2 \tag{8.14}$$

$$\Omega_R^2 = \frac{1}{4v^2}\left(2\tan^2\theta_{\rm W}\,M_W^2 + M_\tau^2\right)T^2 \approx (0.127\,T)^2\,. \tag{8.15}$$

Note that $\Omega_L > \Omega_R$; this is true for all leptons l, provided that $M_l < 116$ GeV. Also, this result is gauge invariant.

Dispersion Relations

The self-energy (8.7) leads to the following fermion propagator:

$$S(P) = \left[(1+a)\not{p} + b\not{u}\right]^{-1} = \left[(1+a)\not{p} + b\not{u}\right]/Z\,, \tag{8.16}$$

where the denominator is

$$Z(\omega,p) = (1+a)^2P^2 + 2(1+a)b\,P\cdot u + b^2 = \left[\omega(1+a)+b\right]^2 - \left[p(1+a)\right]^2\,. \tag{8.17}$$

The poles of the propagator occur at the zeros of $Z(\omega,p)$:

$$\omega(1+a) + b = \pm p(1+a)\,, \tag{8.18}$$

which includes both positive- and negative-energy solutions (note that $(1+a)$ is even, and b odd, under $\omega \to -\omega$); given a positive-energy solution $\omega(p)$, the corresponding negative-energy solution is $-\omega(p)$. So it suffices to find only the positive-energy solutions.

The dispersion relation is given by

$$\begin{aligned}\omega \mp p &= -a(\omega,p)(\omega \mp p) - b(\omega,p) \\ &= \frac{\Omega^2}{p}\left[\pm 1 + \frac{1}{2}\left(1 \mp \frac{\omega}{p}\right)\log\left(\frac{\omega+p}{\omega-p}\right)\right]\,.\end{aligned} \tag{8.19}$$

Each chirality has two distinct modes, shown in Figure 8.2, which we label normal ($\omega_+(p)$) and abnormal ($\omega_-(p)$). The abnormal mode is actually unstable for $p \gtrsim \Omega$ [54]. The dispersion relations may be approximated for small and large p as

$$\frac{\omega_+(p)}{\Omega} \approx \begin{cases} 1 + \frac{1}{3}\frac{p}{\Omega} + \frac{1}{3}\left(\frac{p}{\Omega}\right)^2 & : p \lesssim \Omega \\ \sqrt{2 + \left(\frac{p}{\Omega}\right)^2} & : p \gtrsim \Omega \end{cases} \tag{8.20}$$

$$\frac{\omega_-(p)}{\Omega} \approx \begin{cases} 1 - \frac{1}{3}\frac{p}{\Omega} + \frac{1}{3}\left(\frac{p}{\Omega}\right)^2 & : p \lesssim \Omega \\ \frac{p}{\Omega}\left[1 + 2\exp\left(-2\left(\frac{p}{\Omega}\right)^2 - 2\right)\right] & : p \gtrsim \Omega \end{cases}\,. \tag{8.21}$$

We plot the dispersion relations in Figure 8.3 for left and right chiralities of the τ-lepton.

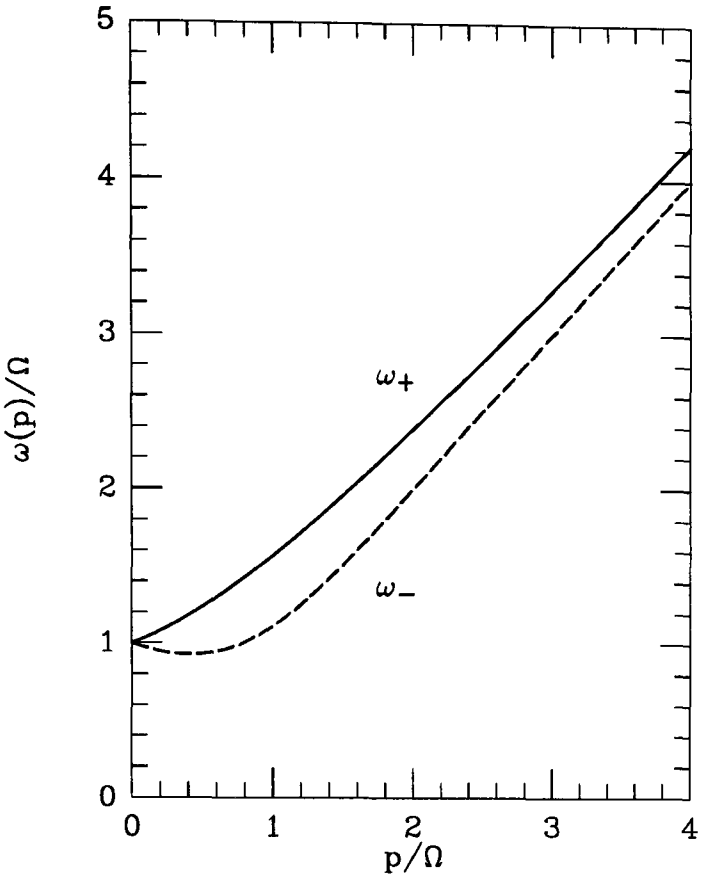

Figure 8.2: The dispersion relations for normal and abnormal plasma modes in the symmetric phase.

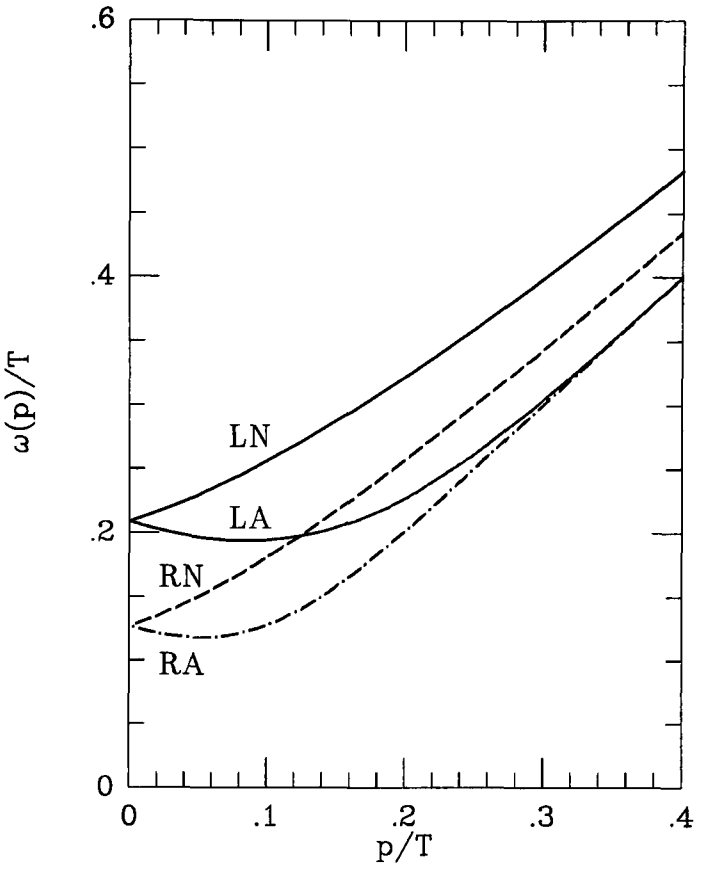

Figure 8.3: The dispersion relations for left and right chiralities of the τ-lepton in the symmetric phase of the Standard Model and two-doublet model.

Modified Dirac Equation and Effective Lagrangian

In the **symmetric phase**, the effective Lagrangian may be written as

$$\mathcal{L}_{\text{eff}} = L^\dagger \left(\Sigma_L^0 + \Sigma_L^{\text{s}}\right) L + R^\dagger \left(\Sigma_R^0 + \Sigma_R^{\text{s}}\right) R \; ; \tag{8.22}$$

the tree-level Dirac operator and thermal corrections are

$$\Sigma_{L,R}^0 = \omega \pm \vec{\sigma}\cdot\vec{p} \tag{8.23}$$

$$\Sigma_{L,R}^{\text{s}} = \Omega_{L,R}^2 \left(\pm\frac{\vec{\sigma}\cdot\vec{p}}{p^2}\left[1 - F\left(\frac{\omega}{p}\right)\right] - \frac{1}{\omega}F\left(\frac{\omega}{p}\right)\right) \; , \tag{8.24}$$

where

$$F(x) = \frac{x}{2}\log\left(\frac{x+1}{x-1}\right) \; . \tag{8.25}$$

At small momenta, $p \lesssim \Omega$ and $\omega - \Omega \ll \Omega$, we may linearize the effective Lagrangian as

$$\mathcal{L}_{\text{eff}} = 2iL^\dagger \left(\partial_0 - \frac{1}{3}\vec{\sigma}\cdot\vec{\partial} + i\Omega_L\right) L + 2iR^\dagger \left(\partial_0 + \frac{1}{3}\vec{\sigma}\cdot\vec{\partial} + i\Omega_R\right) R \; , \tag{8.26}$$

leading to the dispersion relation $\omega_\pm(p) = \Omega \pm \frac{1}{3}|\vec{p}|$. The group velocities of the various modes are approximately

$$v = \frac{\partial \omega_\pm}{\partial p} \approx \begin{cases} \pm\frac{1}{3}\frac{\vec{p}}{|p|} & : p \lesssim \Omega \\ 1 & : p \gtrsim \Omega \end{cases} . \tag{8.27}$$

In the **broken phase**, the Dirac operator is

$$\begin{pmatrix} \Sigma_L^0 + \Sigma_L^{\rm b} & M \\ M^\dagger & \Sigma_R^0 + \Sigma_R^{\rm b} \end{pmatrix} , \tag{8.28}$$

where the thermal piece includes a contribution due to mass corrections in the broken theory:

$$\Sigma_{L,R}^{\rm b} = \Sigma_{L,R}^{\rm s} + \delta\Sigma_{L,R} . \tag{8.29}$$

We then obtain the dispersion relation from

$$\det \begin{pmatrix} \Sigma_L^0 + \Sigma_L^{\rm b} & M \\ M^\dagger & \Sigma_R^0 + \Sigma_R^{\rm b} \end{pmatrix} = 0 . \tag{8.30}$$

Again, we may linearize for $p \ll \Omega_{L,R}$:

$$\begin{aligned} \mathcal{L}_{\rm eff} &= 2iL^\dagger \left(\partial_0 - \frac{1}{3}\vec{\sigma}\cdot\vec{\partial} + i\Omega_L\right) L + 2iR^\dagger \left(\partial_0 + \frac{1}{3}\vec{\sigma}\cdot\vec{\partial} + i\Omega_R\right) R \\ &\quad + L^\dagger M R + R^\dagger M^\dagger L , \end{aligned} \tag{8.31}$$

yielding the dispersion relation

$$\omega(p) = \frac{\Omega_L + \Omega_R}{2} \pm \sqrt{\frac{M^2}{4} + \left(\frac{\Omega_L - \Omega_R}{2} \pm \frac{|\vec{p}|}{3}\right)^2} , \tag{8.32}$$

where the first $\pm$ is for L, R and the second for normal or abnormal, respectively; the solutions $\omega(p)$ are shown in Figures 8.4 and 8.5. Notice that the left abnormal and right normal lines do not intersect (as they do in the symmetric phase), but instead are separated by an energy interval $\Delta\omega = M_\tau$ about the point $\omega_0 = (\Omega_L + \Omega_R)/2$. This interval is the region of total reflection, as we will see below when we consider the scattering of fermions off the bubble wall.

The full effective Lagrangian is then

$$\mathcal{L}_{\rm eff} = L^\dagger \left(\Sigma_L^0 + \Sigma_L^{\rm b}(x)\right) L + R^\dagger \left(\Sigma_R^0 + \Sigma_R^{\rm b}(x)\right) R + \mathcal{L}_{\rm Yukawa}(x) , \tag{8.33}$$

which reflects the spacetime dependence of the interactions in different phases of the plasma. Because the left and right chiralities interact differently with the domain wall, there exists the possibility of separating C- and CP-odd currents that reflect off the wall (weak hypercharge, for instance).

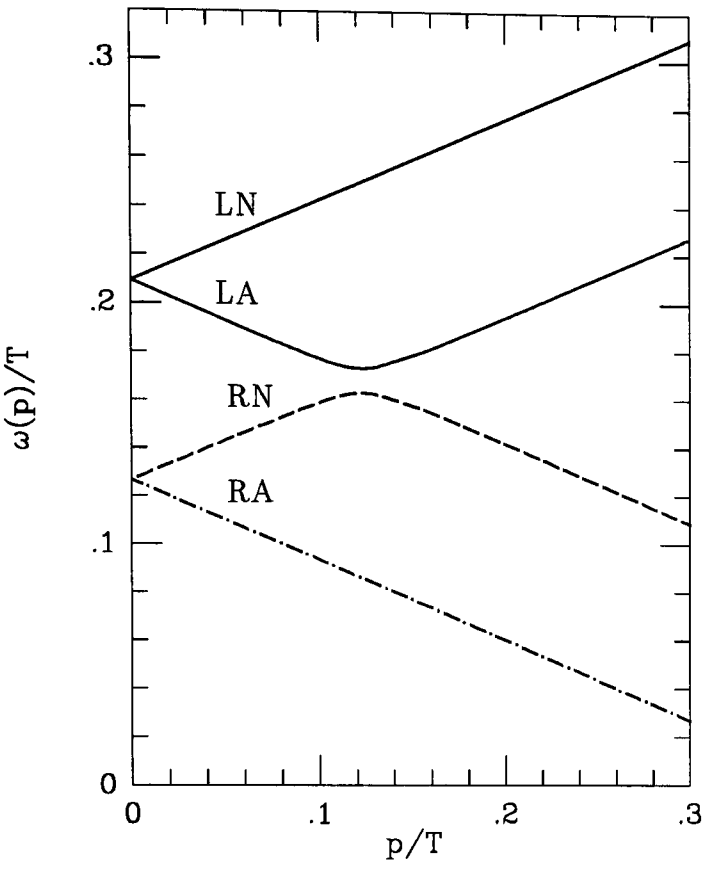

Figure 8.4: The dispersion relations, at low momenta in the broken phase, for normal and abnormal modes of left and right chiralities of the τ-lepton in the Standard Model and two-doublet model.

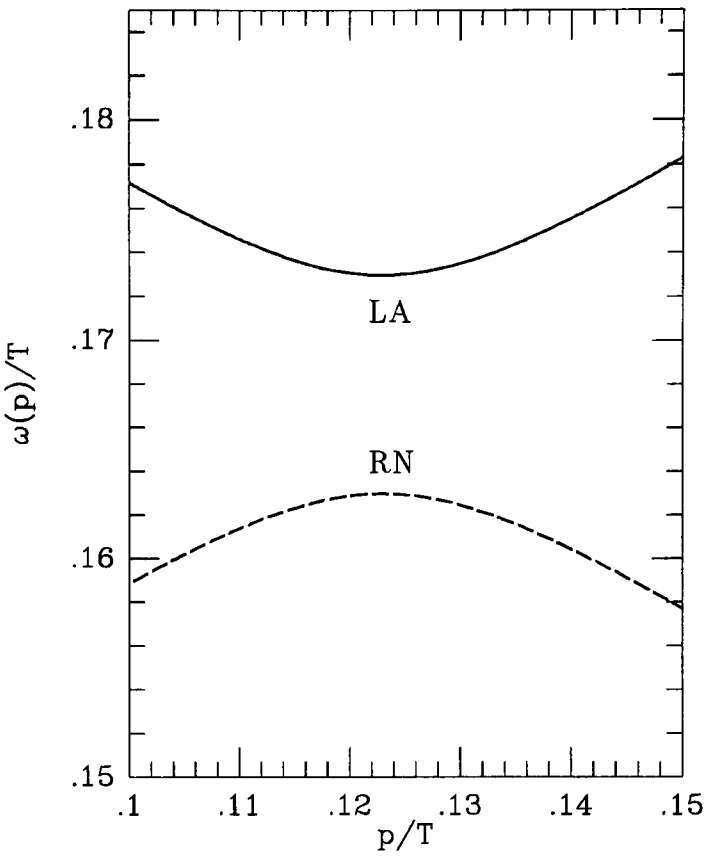

Figure 8.5: Close-up of the previous figure, magnifying the separation between the left abnormal and right normal lines.

8.3 Reflection Coefficients

We start from the Dirac equation:

$$\begin{pmatrix} \Sigma_L^0 + \Sigma_L^{\rm s} + \delta\Sigma_L & \mathcal{M} \\ \mathcal{M}^\dagger & \Sigma_R^0 + \Sigma_R^{\rm s} + \delta\Sigma_R \end{pmatrix} \begin{pmatrix} L \\ R \end{pmatrix} = 0 \,, \tag{8.34}$$

where $\mathcal{M}(x)$ is the position-dependent mass and embodies the details of the bubble wall profile; in the broken phase $\Sigma^{\rm b} = \Sigma^{\rm s} + \delta\Sigma$ and $\mathcal{M} = M$, while in the symmetric phase $\delta\Sigma = 0 = \mathcal{M}$.

As a first approximation, set $\Sigma^{\rm b} \approx \Sigma^{\rm s}$ or $\delta\Sigma \approx 0$, which is plausible since for leptons $M/T \ll 1$; $\delta\Sigma$ includes mass corrections in the one-loop graphs via the propagator $[\not{p} + M]^{-1}$, where the momentum integrals are dominated by the region $p \sim T$. Using the limit $F(x) \stackrel{x\to\infty}{\longrightarrow} 1 + \frac{1}{3x^2}$, we may linearize the Dirac equation at low momenta, $p \ll \Omega$:

$$\begin{pmatrix} \omega\left(1 + \tilde{\alpha}_L + \tilde{\beta}_L\right) + i\vec{\sigma}\cdot\vec{\partial}(1 + \tilde{\alpha}_L) & \mathcal{M} \\ \mathcal{M}^\dagger & \omega\left(1 + \tilde{\alpha}_R + \tilde{\beta}_R\right) - i\vec{\sigma}\cdot\vec{\partial}(1 + \tilde{\alpha}_R) \end{pmatrix} \begin{pmatrix} L \\ R \end{pmatrix} = 0 \,. \tag{8.35}$$

This may be written as

$$\begin{pmatrix} \sigma^j & 0 \\ 0 & -\sigma^j \end{pmatrix} \frac{\partial \Psi}{\partial x^j} = iUR\Psi \ , \tag{8.36}$$

where

$$U = \begin{pmatrix} \omega\left(1+\tilde{\alpha}_L+\tilde{\beta}_L\right) & \mathcal{M} \\ \mathcal{M}^\dagger & \omega\left(1+\tilde{\alpha}_R+\tilde{\beta}_R\right) \end{pmatrix} \tag{8.37}$$

$$R = \begin{pmatrix} (1+\tilde{\alpha}_L)^{-1} & 0 \\ 0 & (1+\tilde{\alpha}_R)^{-1} \end{pmatrix} \tag{8.38}$$

$$\Psi = R^{-1} \begin{pmatrix} L \\ R \end{pmatrix} \tag{8.39}$$

$$\tilde{\alpha}_L = -\frac{1}{3}\frac{\Omega_L^2}{\omega^2}\left(1-3u-2u^2\right)(1-u) \quad ; \quad \tilde{\beta}_L = -\frac{2}{3}\frac{\Omega_L^2}{\omega^2}(1+u)^2(1-u) \tag{8.40}$$

$$\tilde{\alpha}_R = -\frac{1}{3}\frac{\Omega_R^2}{\omega^2}\left(1+3u-2u^2\right)(1+u) \quad ; \quad \tilde{\beta}_R = -\frac{2}{3}\frac{\Omega_R^2}{\omega^2}(1-u)^2(1+u) \tag{8.41}$$

A Lorentz transformation from the fluid frame to the wall frame (with velocity u) has been performed in the small u limit; the u-dependence of $\tilde{\alpha}$ and $\tilde{\beta}$ reflect the spinor transformation. Because we are working in the wall frame, the energy and momentum parallel to the wall are conserved: $i\frac{d}{dt} = \omega$, $i\frac{\partial}{\partial x_{||}} = p_{||}$. We have also taken the limit $|p|^2 \ll \omega^2$ above in the approximation for $F(\omega/p)$, which is not quite accurate since we may have comparable contributions from small $p_\perp$ (component of momentum perpendicular to the wall) but large $p_{||}$.

Because the reflection coefficient depends strongly only on $p_\perp$ (taken to be p_z), we set $p_{||} = 0$:

$$\begin{pmatrix} \sigma^3 & 0 \\ 0 & -\sigma^3 \end{pmatrix} \frac{\partial \Psi}{\partial z} = iUR\Psi \ , \tag{8.42}$$

which decomposes into

$$\frac{\partial}{\partial z}\begin{pmatrix} \psi_1 \\ \psi_3 \end{pmatrix} = i\begin{pmatrix} \omega\left(\frac{1+\tilde{\alpha}_L+\tilde{\beta}_L}{1+\tilde{\alpha}_L}\right) & \mathcal{M}\left(\frac{1}{1+\tilde{\alpha}_R}\right) \\ -\mathcal{M}^\dagger\left(\frac{1}{1+\tilde{\alpha}_L}\right) & -\omega\left(\frac{1+\tilde{\alpha}_R+\tilde{\beta}_R}{1+\tilde{\alpha}_R}\right) \end{pmatrix}\begin{pmatrix} \psi_1 \\ \psi_3 \end{pmatrix} \tag{8.43}$$

$$\frac{\partial}{\partial z}\begin{pmatrix} \psi_4 \\ \psi_2 \end{pmatrix} = i\begin{pmatrix} \omega\left(\frac{1+\tilde{\alpha}_R+\tilde{\beta}_R}{1+\tilde{\alpha}_R}\right) & \mathcal{M}^\dagger\left(\frac{1}{1+\tilde{\alpha}_L}\right) \\ -\mathcal{M}\left(\frac{1}{1+\tilde{\alpha}_R}\right) & -\omega\left(\frac{1+\tilde{\alpha}_L+\tilde{\beta}_L}{1+\tilde{\alpha}_L}\right) \end{pmatrix}\begin{pmatrix} \psi_4 \\ \psi_2 \end{pmatrix} . \tag{8.44}$$

This describes reflection and transmission perpendicular to the wall.

In analogy to the method of NKC, we write the solution as a path-ordered integral:

$$\begin{pmatrix} \psi_1 \\ \psi_3 \end{pmatrix}(z,t) = e^{-i\omega t}\,\Omega(z)\begin{pmatrix} \psi_1 \\ \psi_3 \end{pmatrix}_0 \tag{8.45}$$

$$\begin{pmatrix} \psi_4 \\ \psi_2 \end{pmatrix}(z,t) = e^{-i\omega t}\,\overline{\Omega}(z)\begin{pmatrix} \psi_4 \\ \psi_2 \end{pmatrix}_0 , \tag{8.46}$$

where

$$\Omega(z) = \mathcal{P}\exp i\int_{-z_0}^{z} dx \begin{pmatrix} \omega\left(\frac{1+\tilde{\alpha}_L+\tilde{\beta}_L}{1+\tilde{\alpha}_L}\right) & \mathcal{M}\left(\frac{1}{1+\tilde{\alpha}_R}\right) \\ -\mathcal{M}^\dagger\left(\frac{1}{1+\tilde{\alpha}_L}\right) & -\omega\left(\frac{1+\tilde{\alpha}_R+\tilde{\beta}_R}{1+\tilde{\alpha}_R}\right) \end{pmatrix} \tag{8.47}$$

$$\overline{\Omega}(z) = \mathcal{P}\exp i\int_{-z_0}^{z} dx \begin{pmatrix} \omega\left(\frac{1+\tilde{\alpha}_R+\tilde{\beta}_R}{1+\tilde{\alpha}_R}\right) & \mathcal{M}^\dagger\left(\frac{1}{1+\tilde{\alpha}_L}\right) \\ -\mathcal{M}\left(\frac{1}{1+\tilde{\alpha}_R}\right) & -\omega\left(\frac{1+\tilde{\alpha}_L+\tilde{\beta}_L}{1+\tilde{\alpha}_L}\right) \end{pmatrix} . \tag{8.48}$$

We denote the path-ordered exponentials by

$$\Omega(z) = \mathcal{P}\exp i\int_{-z_0}^{z} dx\, Q(x) \tag{8.49}$$

$$\overline{\Omega}(z) = \mathcal{P}\exp i\int_{-z_0}^{z} dx\, \overline{Q}(x)\,; \tag{8.50}$$

note that Ω and $\overline{\Omega}$ satisfy the differential equations $\frac{d\Omega}{dz} = iQ$ and $\frac{d\overline{\Omega}}{dz} = i\overline{Q}$. Ω describes $L \to R$ reflection and $R \to R$ transmission, while $\overline{\Omega}$ describes $R \to L$ reflection and $L \to L$ transmission.

As a first approximation, we take the wall profile to be described by a step-function:

$$\mathcal{M} = \begin{cases} M & : z > 0 \\ 0 & : z < 0 \end{cases} . \tag{8.51}$$

Then in the symmetric phase,

$$\Omega(z<0) = \begin{pmatrix} \exp i\omega\left(\frac{1+\tilde{\alpha}_L+\tilde{\beta}_L}{1+\tilde{\alpha}_L}\right) z & 0 \\ 0 & \exp -i\omega\left(\frac{1+\tilde{\alpha}_R+\tilde{\beta}_R}{1+\tilde{\alpha}_R}\right) z \end{pmatrix} \equiv \begin{pmatrix} \exp ip_L^{\rm s} z & 0 \\ 0 & \exp -ip_R^{\rm s} z \end{pmatrix} , \tag{8.52}$$

while in the broken phase, Ω may be diagonalized as

$$\Omega(z>0) = D^{-1}\begin{pmatrix} \exp ip_L^{\rm b} z & 0 \\ 0 & \exp -ip_R^{\rm b} z \end{pmatrix} D\,, \tag{8.53}$$

where the momenta in the broken phase are

$$\pm\, p_{L,R}^{\rm b} = \frac{p_L^{\rm s} - p_R^{\rm s}}{2} \pm \sqrt{\left(\frac{p_L^{\rm s} + p_R^{\rm s}}{2}\right)^2 - \frac{M^2}{(1+\tilde{\alpha}_L)(1+\tilde{\alpha}_R)}}\,. \tag{8.54}$$

Then

$$D\begin{pmatrix} \psi_1 \\ \psi_3 \end{pmatrix}(z>0) = \begin{pmatrix} \exp ip_L^{\rm b} z & 0 \\ 0 & \exp -ip_R^{\rm b} z \end{pmatrix} D\begin{pmatrix} \psi_1 \\ \psi_3 \end{pmatrix}(0)\,, \tag{8.55}$$

with the diagonalization matrix given by

$$D = \begin{pmatrix} \frac{1}{Y}(\overline{\omega} + \sqrt{B}) & \frac{1}{Y}\left(\frac{M}{1+\tilde{\alpha}_R}\right) \\ \frac{1}{X}\left(\frac{M}{1+\tilde{\alpha}_L}\right) & \frac{1}{X}\left(\overline{\omega} + \sqrt{B}\right) \end{pmatrix} , \tag{8.56}$$

where

$$\overline{\omega} = \frac{p_L^s + p_R^s}{2} \tag{8.57}$$

$$B = \overline{\omega}^2 - \frac{M^2}{(1+\tilde{\alpha}_L)(1+\tilde{\alpha}_R)} \tag{8.58}$$

and X and Y are just normalization constants. The reflection coefficient comes from the condition

$$\begin{pmatrix} T \\ 0 \end{pmatrix} = D \begin{pmatrix} 1 \\ R \end{pmatrix} , \tag{8.59}$$

yielding

$$\mathcal{R}_{L\to R} = |R|^2_{L\to R} = \left|\frac{1+\tilde{\alpha}_R}{1+\tilde{\alpha}_L}\right| \left|\frac{\overline{\omega} - \sqrt{B}}{\overline{\omega} + \sqrt{B}}\right| . \tag{8.60}$$

Similarly, the right-to-left reflection coefficient may be found from the Dirac equation (8.44) for ψ_2 and ψ_4, with the result

$$\mathcal{R}_{R\to L} = \left|\frac{1+\tilde{\alpha}_L}{1+\tilde{\alpha}_R}\right| \left|\frac{\overline{\omega} - \sqrt{B}}{\overline{\omega} + \sqrt{B}}\right| . \tag{8.61}$$

Note that $\mathcal{R}_{L\to R} \approx \mathcal{R}_{R\to L} \approx 1$ if $\sqrt{B}$ is imaginary; that is, if

$$\overline{\omega}^2 < \frac{M^2}{(1+\tilde{\alpha}_L)(1+\tilde{\alpha}_R)} , \tag{8.62}$$

we get *total reflection.* In physical terms, an imaginary contribution to the momentum (8.54) implies an evanescent (decaying exponential) transmission amplitude in the broken phase.

Although the step-function wall profile may produce spurious effects due to its discontinuity, Farrar and Shaposhnikov considered the smooth profile

$$\mathcal{M}^2 = \frac{M^2}{1+e^{-az}} , \tag{8.63}$$

and found the reflection coefficients

$$\begin{aligned} \mathcal{R}_{L\to R} &= \left|\frac{1+\tilde{\alpha}_R}{1+\tilde{\alpha}_L}\right| \left|\frac{\sinh\frac{\pi}{a}(\overline{\omega} - \sqrt{B})}{\sinh\frac{\pi}{a}(\overline{\omega} + \sqrt{B})}\right| \\ \mathcal{R}_{R\to L} &= \left|\frac{1+\tilde{\alpha}_L}{1+\tilde{\alpha}_R}\right| \left|\frac{\sinh\frac{\pi}{a}(\overline{\omega} - \sqrt{B})}{\sinh\frac{\pi}{a}(\overline{\omega} + \sqrt{B})}\right| . \end{aligned} \tag{8.64}$$

Notice that total reflection again appears for $\overline{\omega}^2 < M^2/(1+\tilde{\alpha}_L)(1+\tilde{\alpha}_R)$. We will take this as a general condition for total reflection (like the condition $\omega < M$ for the zero-temperature case). The region of total reflection is shown in Figure 8.6. As expected by

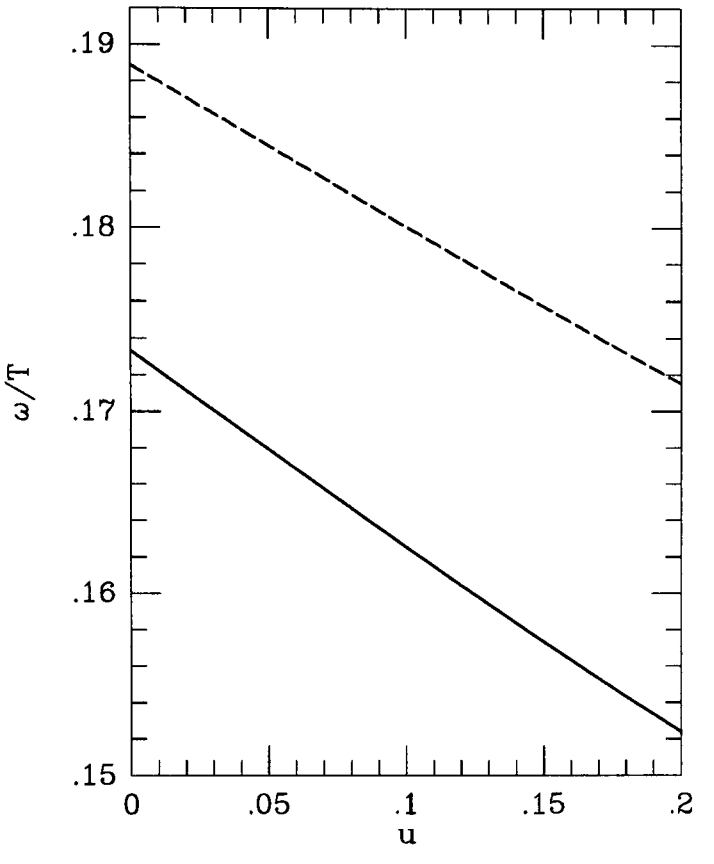

Figure 8.6: The region of total reflection (bounded by the curves plotted) for the τ-lepton in the Standard Model and two-doublet model, as a function of the wall velocity; the temperature is taken to be $T = 100$ GeV.

comparison to the dispersion relations in the broken phase (Figure 8.5), total reflection occurs in the energy interval of width $\Delta\omega \sim M$ about $\omega_0 \sim (\Omega_L + \Omega_R)/2$; the deviation results from the dependence of the reflection coefficients on the wall velocity u.

8.4 Reflected Hypercharge Flux

In this section we compute the hypercharge flux reflected off the bubble wall. We neglect quarks, since we assume that the primordial baryon asymmetry vanishes and that CP violation in the CKM matrix is inadequate to produce the observed baryon number. We want to calculate

$$\begin{aligned} f_Y &= -\frac{1}{2}f_{\tau_L} + \frac{1}{2}f_{\bar{\tau}_R} - f_{\tau_R} + f_{\bar{\tau}_L} - \frac{1}{2}f_{\nu_\tau} + \frac{1}{2}f_{\bar{\nu}_\tau} \\ &\quad + (\mu\text{-contribution}) + (e\text{-contribution})\,. \end{aligned} \tag{8.65}$$

Because $M_\tau \gg M_\mu, M_e$, the interactions of the muon and electron families with the bubble wall are negligible compared to those of the tau family, and hence their contributions to the reflected flux may be ignored. In this section, f_{τ_L} denotes the τ_L particle flux in the fluid frame, while $f_L^{\mathrm{s,b}}$ denotes the τ_L number density distributions in the

wall frame, for the symmetric and broken phases; and similarly for the other species.

To find f_j, the particle flux in the thermal (fluid) frame, we compute the flux γf_j in the wall frame ($\gamma = 1/\sqrt{1-u^2}$, where u is the wall velocity):

$$\gamma f_{\tau_L} = \int \frac{d^3k}{(2\pi)^3} \left[f_R^{\rm s}(k_L, k_T) \cdot \mathcal{R}_{R\to L}(\omega) + f_L^{\rm b}(-k_L, k_T) \cdot \mathcal{T}_L(\omega) \right] \tag{8.66}$$

$$\gamma f_{\bar{\tau}_R} = \int \frac{d^3k}{(2\pi)^3} \left[f_{\bar{L}}^{\rm s}(k_L, k_T) \cdot \mathcal{R}_{L\to R}(\omega) + f_{\bar{R}}^{\rm b}(-k_L, k_T) \cdot \mathcal{T}_R(\omega) \right] . \tag{8.67}$$

The integrals are taken over particle momenta in the wall frame and have separate contributions due to reflection from the symmetric phase and transmission from the broken phase; by CPT and Lorentz invariance, $\mathcal{R}_{\bar{L}\to\bar{R}} = \mathcal{R}_{L\to R}$ and $\mathcal{T}_{\bar{R}} = \mathcal{T}_R$, etc. The difference of these integrals may be written as

$$\begin{aligned} f_{\tau_L} - f_{\bar{\tau}_R} = \frac{1}{\gamma} \int \frac{d^3k}{(2\pi)^3} \Big[& f_R^{\rm s} (\mathcal{R}_{R\to L} - \mathcal{R}_{L\to R}) + (f_R^{\rm s} - f_{\bar{L}}^{\rm s})\, \mathcal{R}_{L\to R} \\ & + f_L^{\rm b} \mathcal{T}_L - f_{\bar{R}}^{\rm b} \mathcal{T}_R \Big] . \end{aligned} \tag{8.68}$$

We *assume* that the major contribution comes from total reflection in the second piece, i.e., from the term $(f_R^{\rm s} - f_{\bar{L}}^{\rm s}) \cdot \mathcal{R}_{L\to R}$ when $\mathcal{R}_{L\to R} \approx 1$, as in the analysis of FS. How do we justify this assumption?

- First, transmission from the broken phase is comparatively unimportant since it is assumed that the broken phase — like the symmetric phase — has zero net hypercharge. This assumption, together with the absence of total reflection off the symmetric phase (the dispersion curves for left-abnormal and right-normal modes intersect in the symmetric phase; see Figure 8.3), implies that the transmitted hypercharge flux is negligible when summed over all particle species. Thus reflection yields the only substantial hypercharge flux, and in particular, the contribution from total reflection predominates.

- $f_R^{\rm s} \cdot (\mathcal{R}_{R\to L} - \mathcal{R}_{L\to R})$ is likely small since this difference in reflection coefficients results from the difference in the left and right thermal masses, and is typically much smaller than $\mathcal{R}$. For instance, this term is less than 15% of $(f_R^{\rm s} - f_{\bar{L}}^{\rm s}) \cdot \mathcal{R}_{L\to R}$ in the region of total reflection, for the parameter range of interest.

Under this assumption,

$$f_{\tau_L} - f_{\bar{\tau}_R} \approx \frac{1}{\gamma} \int \frac{d^3k}{(2\pi)^3} \, (f_R^{\rm s} - f_{\bar{L}}^{\rm s}) \cdot \mathcal{R}_{L\to R} \, , \tag{8.69}$$

and similarly for the difference

$$f_{\tau_R} - f_{\bar{\tau}_L} \approx \frac{1}{\gamma} \int \frac{d^3k}{(2\pi)^3} \, (f_L^{\rm s} - f_{\bar{R}}^{\rm s}) \cdot \mathcal{R}_{R\to L} \, . \tag{8.70}$$

These integrals are dominated by the region of total reflection, $\mathcal{R} \approx 1$, which (as we have seen above) occurs for $B < 0$ or

$$\overline{\omega}^2 < \frac{M^2}{(1+\tilde{\alpha}_L)(1+\tilde{\alpha}_R)} \,. \tag{8.71}$$

We neglect the neutrino contribution, since for ν_τ, $M^2 = 0$ and $B \geq 0$. Then the hypercharge flux is

$$\begin{aligned} f_Y &\approx -\frac{1}{2}\left(f_{\tau_L} - f_{\bar{\tau}_R}\right) - \left(f_{\tau_R} - f_{\bar{\tau}_L}\right) \\ &\approx -\frac{1}{\gamma}\int \frac{d^3k}{(2\pi)^3}\left\{\frac{1}{2}\left(f^{\rm s}_R - f^{\rm s}_{\bar{L}}\right)\cdot\mathcal{R}_{L\to R} + \left(f^{\rm s}_L - f^{\rm s}_{\bar{R}}\right)\cdot\mathcal{R}_{R\to L}\right\} \\ &\approx -\frac{1}{\gamma}\int_{B<0} \frac{d^3k}{(2\pi)^3}\left\{\frac{1}{2}\left(f^{\rm s}_R - f^{\rm s}_{\bar{L}}\right) + \left(f^{\rm s}_L - f^{\rm s}_{\bar{R}}\right)\right\} \,. \end{aligned} \tag{8.72}$$

The flux distributions are taken in the wall frame:

$$f^{\rm s}_j = \frac{\partial\omega_j}{\partial k_z}\cdot n_F\left(\gamma\left[\omega_j - uP^z_j\right] \mp \mu_j\right) \,, \tag{8.73}$$

where the group momentum and fermion particle distribution (in the thermal frame) are

$$P^z_j = \omega_j \frac{\partial\omega_j}{\partial k_z} \tag{8.74}$$

$$n_F(\omega \mp \mu) = \frac{1}{e^{(\omega\mp\mu)/T}+1} \,. \tag{8.75}$$

Then

$$\begin{aligned} f_Y \approx -\frac{1}{\gamma}\int_{B<0} \frac{d^3k}{(2\pi)^3}\Bigg\{&\frac{1}{2}\frac{\partial\omega_R}{\partial k_z}\left[n_F\left(\gamma[\omega_R - uP^z_R] - \mu_{\tau_R}\right) - n_F\left(\gamma[\omega_R - uP^z_R] + \mu_{\tau_R}\right)\right] \\ &+ \frac{\partial\omega_L}{\partial k_z}\left[n_F\left(\gamma[\omega_L - uP^z_L] - \mu_{\tau_L}\right) - n_F\left(\gamma[\omega_L - uP^z_L] + \mu_{\tau_L}\right)\right]\Bigg\} \,. \end{aligned} \tag{8.76}$$

As a conservative estimate, we truncate the region of phase space where $B < 0$ to the region where $k_{||} \lesssim \frac{3}{2}(\Omega_L - \Omega_R)$ and $\partial\omega_{L,R}/\partial k_{||} \approx 0$ (cf. FS); then the $k_{||}$- and k_z-integrals separate, giving the result

$$\begin{aligned} f_Y \approx -\frac{1}{\gamma}\cdot\frac{1}{4\pi}&\left(\frac{3}{2}\left[\Omega_L - \Omega_R\right]\right)^2 \\ &\cdot\left\{\frac{1}{2}\int_{B<0}\frac{d\omega_R}{2\pi}\left[n_F\left(\gamma\left[\omega_R - uP^z_R\right] - \mu_{\tau_R}\right) - n_F\left(\gamma\left[\omega_R - uP^z_R\right] + \mu_{\tau_R}\right)\right]\right. \end{aligned}$$

$$+ \int_{B<0} \frac{d\omega_L}{2\pi} \left[n_F \left(\gamma \left[\omega_L - u P_L^z \right] - \mu_{\tau_L} \right) - n_F \left(\gamma \left[\omega_L - u P_L^z \right] + \mu_{\tau_L} \right) \right] \Bigg\}$$

$$\approx -\frac{9}{16\pi\gamma} \Delta\omega \left(\Omega_L - \Omega_R \right)^2 \left\{ \frac{1}{2} \Delta n_F \left(\gamma \left[\omega_0 - u P_R^z \right] \mp \mu_{\tau_R} \right) + \Delta n_F \left(\gamma \left[\omega_0 - u P_L^z \right] \mp \mu_{\tau_L} \right) \right\} , \tag{8.77}$$

where the region of total reflection is centered about ω_0 with spread $\Delta\omega$. To lowest order in the chemical potentials $\mu_{\tau_L,\tau_R}/T$,

$$\Delta n_F \left(\gamma \left[\omega_0 - u P_j^z \right] \mp \mu_j \right) = n_F \left(\gamma \left[\omega_0 - u P_j^z \right] - \mu_j \right) - n_F \left(\gamma \left[\omega_0 - u P_j^z \right] + \mu_j \right)$$

$$\approx \frac{\mu_j / T}{1 + \cosh \left(\frac{\gamma(\omega_0 - u P_j^z)}{T} \right)} , \tag{8.78}$$

and in the limit of small u and $k_{||}$,

$$P^z \approx \frac{\omega_0}{3} (1 + 2u/3) . \tag{8.79}$$

Hence

$$\frac{1}{2} \Delta n_F \left(\gamma \left[\omega_0 - u P_R^z \right] \mp \mu_{\tau_R} \right) + \Delta n_F \left(\gamma \left[\omega_0 - u P_L^z \right] \mp \mu_{\tau_L} \right) \approx \frac{1}{2} \cdot \frac{(\mu_{\tau_R} + 2\mu_{\tau_L})/T}{1 + \cosh \left(\frac{\omega_0}{T} (1 - u/3) \right)} ; \tag{8.80}$$

noticing that $L_\tau = (\mu_{\tau_R} + 2\mu_{\tau_L}) T^2/6$ (refer to Section 8.5), we find that f_Y is simply proportional to the primordial lepton asymmetry. Our final result for the reflected hypercharge flux is then

$$f_Y \approx -\frac{27}{16\pi} \cdot \frac{(\Omega_L - \Omega_R)^2 \Delta\omega}{T^3} \cdot \frac{L_\tau}{1 + \cosh \left(\frac{\omega_0}{T} (1 - u/3) \right)} . \tag{8.81}$$

Recall the assumptions made in our derivation:

- the hypercharge flux is dominated by the contribution from total reflection;
- $k_{||} \ll \omega_0$ may be taken in the flux integrals;
- $u \ll 1$.

We believe this expression to be a conservative lower bound, since we have truncated the flux integral (8.77) in the region of total reflection and we have neglected the contribution of $k_{||} \sim \omega_0$.

8.5 Partial Derivative of the Free Energy with Respect to Baryon Number

We now compute $\partial F/\partial B$, the partial derivative of the free energy with all conserved quantum numbers held fixed. We cannot simply adopt the result of NKC, since their analysis implies not only $B = L = 0$, but also $B_j = L_j = 0$ for the individual generations. Since we are interested in the case of generational differences in lepton asymmetries, we redo the analysis.

$\partial F/\partial B$ depends on the interactions and species in equilibrium. We assume that on the timescale τ_T,

- $SU(3)_C \otimes SU(2)_L \otimes U(1)_Y$ interactions are in equilibrium (including quark mixing and light-fermion Yukawa interactions, which are assumed to be out of equilibrium in the NKC analysis);
- only anomalous $B + L$-violation is not in equilibrium.

Then the (approximately) conserved quantum numbers and their associated chemical potentials are

$$\begin{aligned} B/3 - L_j &\leftrightarrow \mu_j \\ B &\leftrightarrow \mu_B \\ Y/2 &\leftrightarrow \mu_Y \\ T_3 &\leftrightarrow \mu_T \ . \end{aligned}$$

This implies that on the timescale of interest, Q, L_j, and $B \pm L$ are also conserved. In contrast NKC had $B_1 = B_2$ and B_3 separately conserved, and $L_j = L/3$; when the constraints $B = 0 = L$ and $B_1 = B_2 = 0$ were imposed, one obtained $B_j = 0 = L_j$. In our case we have L_j conserved and $B_j = B/3$, and the constraints we impose are $B = 0 = L$, so that $B_j = 0$ although $L_j \neq 0$ is allowed.

The net particle number densities are

$$\begin{aligned}
\rho_{t_L} &= 3\left[\frac{1}{9}(\mu_1+\mu_2+\mu_3)+\frac{1}{3}\mu_B+\frac{1}{6}\mu_Y+\frac{1}{2}\mu_T\right]\frac{T^2}{6} \\
\rho_{b_L} &= 3\left[\frac{1}{9}(\mu_1+\mu_2+\mu_3)+\frac{1}{3}\mu_B+\frac{1}{6}\mu_Y-\frac{1}{2}\mu_T\right]\frac{T^2}{6} \\
\rho_{t_R} &= 3\left[\frac{1}{9}(\mu_1+\mu_2+\mu_3)+\frac{1}{3}\mu_B+\frac{2}{3}\mu_Y\right]\frac{T^2}{6} \\
\rho_{b_R} &= 3\left[\frac{1}{9}(\mu_1+\mu_2+\mu_3)+\frac{1}{3}\mu_B-\frac{1}{3}\mu_Y\right]\frac{T^2}{6} \\
\rho_{c_L} &= \rho_{u_L} = \rho_{t_L} \quad ; \quad \rho_{s_L} = \rho_{d_L} = \rho_{b_L} \\
\rho_{c_R} &= \rho_{u_R} = \rho_{t_R} \quad ; \quad \rho_{s_R} = \rho_{d_R} = \rho_{b_R} \\
\rho_{e_L} &= \left(-\mu_1-\frac{1}{2}\mu_Y-\frac{1}{2}\mu_T\right)\frac{T^2}{6} \quad ; \quad \rho_{\nu_e} = \left(-\mu_1-\frac{1}{2}\mu_Y+\frac{1}{2}\mu_T\right)\frac{T^2}{6}
\end{aligned}$$

$$
\begin{aligned}
\rho_{\mu_L} &= \left(-\mu_2 - \frac{1}{2}\mu_Y - \frac{1}{2}\mu_T\right)\frac{T^2}{6} \quad ; \quad \rho_{\nu_\mu} = \left(-\mu_2 - \frac{1}{2}\mu_Y + \frac{1}{2}\mu_T\right)\frac{T^2}{6} \\
\rho_{\tau_L} &= \left(-\mu_3 - \frac{1}{2}\mu_Y - \frac{1}{2}\mu_T\right)\frac{T^2}{6} \quad ; \quad \rho_{\nu_\tau} = \left(-\mu_3 - \frac{1}{2}\mu_Y + \frac{1}{2}\mu_T\right)\frac{T^2}{6} \\
\rho_{e_R} &= (-\mu_1 - \mu_Y)\frac{T^2}{6} \quad ; \quad \rho_{\mu_R} = (-\mu_2 - \mu_Y)\frac{T^2}{6} \quad ; \quad \rho_{\tau_R} = (-\mu_3 - \mu_Y)\frac{T^2}{6} \\
\rho_{\phi^+} &= n(\mu_Y + \mu_T)\frac{T^2}{6} \quad ; \quad \rho_{\phi^0} = n(\mu_Y - \mu_T)\frac{T^2}{6} \\
\rho_{W^+} &= 4\mu_T\frac{T^2}{6} \, .
\end{aligned}
$$

n above denotes the number of scalar doublets in equilibrium. Then

$$
\begin{aligned}
B &= 3 \cdot \frac{1}{3}(\rho_{t_L} + \rho_{b_L} + \rho_{t_R} + \rho_{b_R}) \\
&= \left[\frac{4}{3}(\mu_1 + \mu_2 + \mu_3) + 4\mu_B + 2\mu_Y\right]\frac{T^2}{6} \\
L &= \rho_{e_L} + \rho_{\mu_L} + \rho_{\tau_L} + \rho_{\nu_e} + \rho_{\nu_\mu} + \rho_{\nu_\tau} + \rho_{e_R} + \rho_{\mu_R} + \rho_{\tau_R} \\
&= \left[-3(\mu_1 + \mu_2 + \mu_3) - 6\mu_Y\right]\frac{T^2}{6} \\
\frac{Y}{2} &= 3 \cdot \frac{1}{6}(\rho_{t_L} + \rho_{b_L}) + 3 \cdot \frac{2}{3}\rho_{t_R} - 3 \cdot \frac{1}{3}\rho_{b_R} \\
&\quad - \frac{1}{2}(\rho_{e_L} + \rho_{\mu_L} + \rho_{\tau_L} + \rho_{\nu_e} + \rho_{\nu_\mu} + \rho_{\nu_\tau}) \\
&\quad - (\rho_{e_R} + \rho_{\mu_R} + \rho_{\tau_R}) + \frac{1}{2}\left(\rho_{\phi^+} + \rho_{\phi^0}\right) \\
&= \left[\frac{8}{3}(\mu_1 + \mu_2 + \mu_3) + 2\mu_B + (10 + n)\mu_Y\right]\frac{T^2}{6} \\
T_3 &= (10 + n)\mu_T\frac{T^2}{6} \, .
\end{aligned}
$$

Imposing the conditions $B = 0 = L$, we find

$$
\begin{aligned}
\mu_Y &= 6\mu_B \\
\mu_1 + \mu_2 + \mu_3 &= -12\mu_B \, ,
\end{aligned}
$$

in which case

$$
\frac{\partial F}{\partial B} = \mu_B = \frac{\rho_Y}{(5 + n)T^2} \equiv \frac{\xi\rho_Y}{T^2} \, . \tag{8.82}
$$

Note that

$$
L_j = (-3\mu_j - 2\mu_Y)\frac{T^2}{6} = \left[-3\mu_j + (\mu_1 + \mu_2 + \mu_3)\right]\frac{T^2}{6} \, . \tag{8.83}
$$

8.6 Thermal Transport Time

After rebounding off the bubble wall, the reflected lepton flux travels in the symmetric phase until the advancing front of broken phase captures it, during which time the

corresponding hypercharge current biases baryon production via anomalous processes. We now compute the thermal transport time τ_T, defined as the average time that a reflected τ-lepton spends in the plasma prior to absorption by the bubble of broken phase. Consider diffusion away from the wall of a particle with velocity v and mean free path l; capture occurs when the wall intercepts the randomly walking particle (N here is the number of collisions):

$$u\tau_T = \left\langle l\sqrt{N} \right\rangle = \left\langle l\sqrt{\frac{v\tau_T}{l}} \right\rangle ,$$

or

$$\tau_T = \left\langle \frac{lv}{u^2} \right\rangle . \tag{8.84}$$

We now calculate the thermal average

$$\langle lv \rangle = \frac{\langle v \rangle_1}{\langle n\sigma \rangle_2} ,$$

where the subscripts 1 and 2 refer to thermal averages taken over the rebounding particles and particles in the plasma, respectively; n is the particle number density and σ the thermally averaged cross section. The inverse mean free path is

$$\langle n\sigma \rangle_2 = \sum_2 \frac{g_1 g_2}{\langle n \rangle_1} \int \frac{d^3\vec{p}_1\, d^3\vec{p}_2}{(2\pi)^6} \frac{\sigma_{12}(\vec{p}_1, \vec{p}_2)}{(e^{E_1/T}+1)(e^{E_2/T}+1)} ,$$

where the sum is taken over all interactions of particle 1 with the heat bath and g_j counts the spin degrees of freedom. For ease of computation, [4] we consider only the leading contributions from tree-level scattering on mass shell; numerical calculation confirms that other contributions are indeed less significant. In this case, the transition probabilities sum to

$$\begin{aligned} \sum |T|^2 \;\approx\; & \frac{e^2}{\sin^2\theta_{\rm W}} \left(\Omega_W^2 - \Omega_\tau^2\right) \\ & + \frac{e^2}{\sin^2\theta_{\rm W}\,\cos^2\theta_{\rm W}} \Big(4\sin^4\theta_{\rm W}\,\Omega_W^2 + 8\sin^4\theta_{\rm W}\,\Omega_\tau^2 - 2\sin^2\theta_{\rm W}\,\Omega_W^2 \\ & \qquad - 4\sin^2\theta_{\rm W}\,\Omega_\tau^2 + \Omega_W^2 - \Omega_\tau^2\Big) \\ & + 4e^2\left(\Omega_\gamma^2 + \Omega_\tau^2\right) , \end{aligned}$$

where we respectively list the contributions of W, Z, and γ scattering in the plasma; we neglect Higgs scattering since it is suppressed by the small Yukawa coupling g_τ^2. Ω_j is the thermal mass of particle species j, and we approximate $\Omega_\gamma \approx \Omega_W$ and $\Omega_{\nu_\tau} \approx \Omega_\tau$.

[4] Complications arise from the infinite bremsstrahlung contributions of two-vertex graphs.

The mean free path then evaluates to

$$\langle n\sigma \rangle_2 \sim \frac{T}{100} \,. \tag{8.85}$$

Computing $\langle v \rangle = \langle nv \rangle / \langle n \rangle \approx 1$, we find that $v \approx 1$ for most leptons in the plasma, which implies that the reflected current thermalizes quickly. The thermal transport time is then

$$\tau_T \equiv \frac{x}{u^2 T} \sim \frac{100}{u^2 T} \,. \tag{8.86}$$

8.7 Discussion

We take the expression (8.5) for the final baryon number and put in the pieces (8.81), (8.82), and (8.86) for the reflected hypercharge flux, the partial derivative of the free energy with respect to baryon number, and the thermal transport time, to arrive at

$$\begin{aligned}
\frac{\rho_B}{s} &\approx \frac{243}{16\pi} \cdot \frac{\kappa \alpha_{\rm W}^4}{(5+n)u^3} \cdot \frac{x \left(\Omega_L - \Omega_R\right)^2 \Delta\omega}{T^3 \left[1 + \cosh \frac{\omega_0}{T}(1 - u/3)\right]} \cdot \left(\frac{L_\tau}{s}\right) \\
&\approx 6.3 \cdot 10^{-6} \cdot \frac{\kappa x}{(5+n)u^3 \left[1 + \cosh \frac{\omega_0}{T}(1 - u/3)\right]} \cdot \frac{\left(\Omega_L - \Omega_R\right)^2 M_\tau}{T^3} \cdot \left(\frac{L_\tau}{s}\right) \\
&\approx 6.3 \cdot 10^{-6} \cdot \kappa \left(\frac{6}{5+n}\right) \left(\frac{0.1}{u}\right)^3 \left(\frac{100\,\mathrm{GeV}}{T}\right) \left(\frac{2}{1 + \cosh \frac{\omega_0}{T}(1 - u/3)}\right) \left(\frac{x}{100}\right) \cdot \left(\frac{L_\tau}{s}\right) \,,
\end{aligned} \tag{8.87}$$

where the various parameters have been scaled by their typical values. We believe (8.87) to be a conservative lower bound on the effect of this mechanism, since we have underestimated the flux integrals and the thermal scattering length. By requiring the observed baryon number of $B \sim 10^{-10}$ to be generated in this manner, we obtain an estimate for the primordial lepton asymmetry (for the above parameter values):

$$\frac{L_\tau}{s} \sim 2 \cdot 10^{-5} \,, \tag{8.88}$$

corresponding to

$$\frac{n_l - n_{\bar{l}}}{n_l + n_{\bar{l}}} \sim 0.002 \,. \tag{8.89}$$

It is of interest to compare this constraint with that obtained from equilibrium scenarios for lepton-to-baryon conversion. As a generic example, we consider the analysis of Kuzmin, Rubakov, and Shaposhnikov [50] as summarized in (8.1). Taking the requisite large Higgs mass to be $M_H \sim 100$ GeV, and consequently the sphaleron freeze-out temperature (approximately the critical temperature) to be $T_* \sim 150$ GeV (refer to Figure 5.11), we estimate the generated baryon asymmetry as

$$\frac{n_B}{s} \approx -\frac{4}{13\pi^2} \frac{m_\tau^2}{T_*^2} \cdot \left(\frac{L_\tau}{s}\right) \approx -4.4 \cdot 10^{-6} \cdot \left(\frac{L_\tau}{s}\right) \,. \tag{8.90}$$

Hence the observed baryon asymmetry may be accounted for in this scheme for a primordial lepton asymmetry of $L_\tau/s \sim 2 \cdot 10^{-5}$, which is identical to our value found above despite the m_τ^2/T^2 suppression. This is not surprising since, as we have emphasized, the assumption that baryon violation is in equilibrium (on the timescale of interest) is an overly optimistic one.

8.8 Conclusion

We have considered two possible methods to transform a primordial lepton asymmetry into the observed baryon asymmetry. First, if the thermal plasma maintains equilibrium, anomalous processes may convert generational lepton asymmetries into baryon number, whose final value depends on the primordial asymmetry. The effectiveness of this scenario is determined by the extent to which anomalous baryon violation remains in equilibrium, as expressed by the suppression factor $M_l^2(T_*)/T_*^2$ at sphaleron freeze-out. Second, for a departure from equilibrium such as might occur during a first-order phase transition, lepton reflection off the phase separation boundary may radiate a net hypercharge flux, which then triggers baryon production as described by the rate equation (8.1). The effectiveness of this charge transport mechanism is determined by the strength of the lepton Yukawa interactions with the bubble wall, through the factor M_l/T. Both mechanisms work most efficiently for the τ-lepton. Although a comparison between the two depends on the choice of parameter values, there is a clear trade-off between opposing tendencies: anomalous baryon violation in equilibrium generates greater net B, but risks suppression by lepton mass effects.

In this chapter we have pursued the second line of reasoning and have investigated this mechanism in some detail. We have made several assumptions in deriving the final baryon number, which we summarize:

- the reflected hypercharge flux is dominated by the contribution due to total reflection;
- the linearized (low-momentum) Lagrangian is valid in the region of total reflection;
- the wall velocity is non-relativistic (implying that the hypercharge current rapidly thermalizes).

We have found that the observed baryon number of $B \sim 10^{-10}$ may be generated by our mechanism, if the primordial lepton asymmetry is as high as $L_\tau/s \sim \mathcal{O}(10^{-5})$. This is also true in the alternative approach where sphaleron transitions are assumed to be in equilibrium throughout; however, as discussed in Chapter 4, this assumption is not justified.

With the inclusion of scalar leptons in supersymmetry, we note that the τ-slepton may play a similar role to the τ-lepton above. After finding the quasiparticle modes

and dispersion relations by diagonalizing the mass matrices in both the symmetric and broken phases, one may analyze the scattering of sleptons off the bubble wall in the fashion described above. On physical grounds we expect a region of total reflection of width $\Delta\omega \sim M_\tau$, which yields an M_τ/T-suppressed contribution to the reflected hypercharge flux, in the manner demonstrated. This is in contrast to the mechanism considered by Dreiner and Ross [51], where the minimal supersymmetric extension of the Standard Model produces a much greater enhancement due to the large mass splittings of right and left sleptons.

More generally, we emphasize that potential scenarios of baryogenesis need not satisfy the Sakharov conditions [3] in the same process at the same spacetime point; in fact, separation of these processes may yield more efficient baryogenesis. In this chapter we have demonstrated a mechanism in which these conditions are satisfied separately: CP violation at the GUT scale, baryon violation at the electroweak scale (in the symmetric phase), and a departure from equilibrium at the electroweak phase transition (at the phase separation boundary), may generate the baryon number we observe today.

Chapter 9

Conclusion

Baryogenesis is one of the outstanding problems at the interface between particle physics and cosmology. In this thesis we have considered several aspects of baryogenesis occurring at the cosmological electroweak phase transition. We used the effective potential at finite temperature to analyze the phase transition in the minimal Standard Model, and derived the critical temperature and order parameter, as functions of the Higgs and top masses. By requiring that $(\phi/T)_{\rm crit} \gtrsim 1$ for efficient baryogenesis and avoiding sphaleron erasure following the phase transition, we obtained a cosmological upper bound on the Higgs boson mass as a function of the top mass. This was done first at one loop and then with ring improvement. We then considered the two simplest extensions of the Standard Model, the addition of a gauge singlet and a second Higgs doublet, as a direct way of relaxing the Higgs mass bound. Again $T_{\rm c}$, $(\phi/T)_{\rm crit}$, and the associated Higgs mass bounds were computed as functions of the parameters. Finally we analyzed a charge transport mechanism, in the context of a strongly first-order electroweak phase transition, which enhances the electroweak processing of a primordial asymmetry into the observed baryon number.

9.1 Directions for Future Work

A serious criticism of the work in this thesis concerns the general approach of using the effective potential to analyze the electroweak phase transition. Various authors have questioned the suitability of the effective potential for describing the essentially infrared phenomena that occur at a phase transition driven by radiative corrections (like the electroweak phase transition). Some advocate a renormalization group treatment to analyze such phase transitions [56] more accurately. This may be achieved through the use of a scale-dependent coarse-grained effective action, whose scale k acts as an infrared cut-off; couplings, for instance, then run as $\lambda(k,T)$. One may therefore use the renormalization group evolution equations or the $4-\varepsilon$ expansion as a means of describing the phase transition, while maintaining rigid control over infrared divergences.

A straightforward way to extend the work of this thesis is to consider more complex extensions of the Standard Model within the context of our analysis. As we have discussed, extensions of the Standard Model allow richer sources of CP violation and more strongly first-order phase transitions. The most natural direction would be to include supersymmetry, and some of the results of our two-doublet analysis (with ring-improvement) could be adapted. First one would have to include the effect of heavy scalars, which we neglected in our analysis of Chapter 7; however, this is more amenable in supersymmetric models than in the general two-doublet model per se, since supersymmetry imposes constraints on the various parameters. One may also be interested in studying the effect of including supersymmetry in our mechanism for converting a primordial lepton asymmetry into the observed baryon asymmetry. In this case, the scalar sleptons may play a similar role to that of the τ-lepton.

Appendix A

Conventions

In this thesis we use natural units, $c = \hbar = k_B = 1$, and the flat metric $g_{00} = 1$, $g_{jj} = -1$. In all Feynman diagrams, curly lines represent weak gauge boson (rather than gluon) lines.

A.1 Equilibrium Thermodynamics

Basic results of equilibrium thermodynamics are tabulated here for convenience [57, 55]. The distribution function of a particle species is given by

$$f(\vec{k}) = \frac{1}{e^{(E-\mu)/T} \pm 1}\,, \tag{A.1}$$

where $E = \sqrt{|\vec{k}|^2 + m^2}$ and $\pm$ is for Fermi-Dirac or Bose-Einstein species. The number density n, energy density ρ, and pressure p are then

$$n = g \int \frac{d^3\vec{k}}{(2\pi)^3} f(\vec{k}) \tag{A.2}$$

$$\rho = g \int \frac{d^3\vec{k}}{(2\pi)^3} f(\vec{k}) E(\vec{k}) \tag{A.3}$$

$$p = g \int \frac{d^3\vec{k}}{(2\pi)^3} f(\vec{k}) \frac{|\vec{k}|^2}{3E(\vec{k})}\,, \tag{A.4}$$

where the particle species is assumed to be an ideal — that is, dilute and weakly-interacting — gas, with g internal degrees of freedom.

In the relativistic ($T \gg m$) and non-degenerate ($\mu \ll T$) limit,

$$n \approx \begin{cases} (\zeta(3)/\pi^2) g T^3 & \text{Bose} \\ (3/4)(\zeta(3)/\pi^2) g T^3 & \text{Fermi} \end{cases} \tag{A.5}$$

$$\rho \approx \begin{cases} (\pi^2/30) g T^4 & \text{Bose} \\ (7/8)(\pi^2/30) g T^4 & \text{Fermi} \end{cases} \tag{A.6}$$

$$p \approx \rho/3 , \tag{A.7}$$

where $\zeta(3) \approx 1.20206$. In the non-relativistic limit, these quantities are all exponentially suppressed by the Boltzmann factor, while the degenerate limit is irrelevant to the work in this thesis. The entropy density is

$$s = \frac{\rho + p}{T} , \tag{A.8}$$

and since the relativistic contribution predominates over the non-relativistic, it may be approximated as

$$s \approx \frac{2\pi^2}{45} g_* T^3 , \tag{A.9}$$

where

$$g_* = \sum_B g_B \left(\frac{T_B}{T}\right)^3 + \frac{7}{8} \sum_F g_F \left(\frac{T_F}{T}\right)^3 . \tag{A.10}$$

g_* counts the relativistic degrees of freedom, and in the case that all relativistic particle species share a common temperature, it reduces to

$$g_* = \sum_B g_B + \frac{7}{8} \sum_F g_F . \tag{A.11}$$

The particle asymmetry of a species may be expressed in terms of the chemical potential μ, assuming that the species is in chemical equilibrium (so that $\mu_+ = -\mu_-$). In the relativistic non-degenerate limit,

$$n_+ - n_- = g \int \frac{d^3\vec{k}}{(2\pi)^3} \left[\frac{1}{e^{(E-\mu)/T} \pm 1} - \frac{1}{e^{(E+\mu)/T} \pm 1} \right] \tag{A.12}$$

$$\approx \begin{cases} \frac{gT^2}{3}\mu + \mathcal{O}(\mu^3) & \text{Bose} \\ \frac{gT^2}{6}\mu + \mathcal{O}(\mu^3) & \text{Fermi} \end{cases} . \tag{A.13}$$

Appendix B

The Effective Potential at One Loop and with Ring Improvement

This appendix derives the boson and fermion contributions to the effective potential at one loop, and gives the expansion valid at high temperature. It then gives the contribution due to the summation of ring diagrams.

B.1 High-Temperature Expansion for the Effective Potential at One Loop

The tadpole method (see Figure B.1) may be easily employed to derive the standard

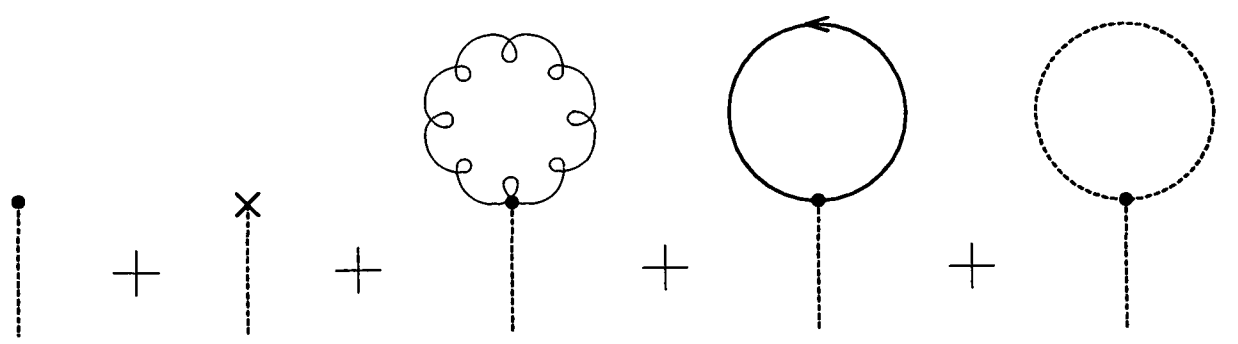

Figure B.1: The gauge, fermion, and scalar tadpole graphs for the effective potential at one loop.

expression for the one-loop effective potential [58]:

$$V_{1\text{ loop}}(\phi) = U(\phi) + \sum_{j=B,F} \frac{\pm g_j}{2} \int \frac{d^4k}{(2\pi)^4} \log\left(k^2 + m_j^2(\phi)\right) + V_{\text{c.t.}} \,. \qquad \text{(B.1)}$$

At finite temperature, the vacuum and thermal pieces separate, and the effective potential becomes

$$V_{1\,\mathrm{loop}}^{T}(\phi) = V_{1\,\mathrm{loop}}^{0}(\phi) + \Delta V_{1\,\mathrm{loop}}^{T}(\phi)\,, \tag{B.2}$$

where

$$V_{1\,\mathrm{loop}}^{0}(\phi) = U(\phi) + \sum_{j=B,F} \frac{\pm g_j}{2} \int \frac{d^4k_E}{(2\pi)^4} \log\left(k_E^2 + m_j^2(\phi)\right) + V_{\mathrm{c.t.}}\,, \tag{B.3}$$

and

$$\Delta V_{1\,\mathrm{loop}}^{T}(\phi) = T^4 \sum_B g_B I_B\left(\frac{m_B(\phi)}{T}\right) + T^4 \sum_F g_F I_F\left(\frac{m_F(\phi)}{T}\right)\,. \tag{B.4}$$

The convergent integrals I_B and I_F embody the thermal effects at one loop of the ambient boson and fermion fields:

$$I_B(y) = \frac{1}{2\pi^2}\int_0^\infty dx\ x^2 \log\left(1 - \exp\left(-\sqrt{x^2+y^2}\right)\right) \tag{B.5}$$

$$I_F(y) = -\frac{1}{2\pi^2}\int_0^\infty dx\ x^2 \log\left(1 + \exp\left(-\sqrt{x^2+y^2}\right)\right)\,. \tag{B.6}$$

Our renormalization prescription for $V_{1\,\mathrm{loop}}^{0}$ preserves the tree-level relations for the minimum and the related mass:

$$\left.\frac{dV^0}{d\phi}\right|_{\phi=v} = 0$$

$$\left.\frac{d^2V^0}{d\phi^2}\right|_{\phi=v} = M_H^2\,, \tag{B.7}$$

and renormalization results in the expression

$$V_{1\,\mathrm{loop}}^{0}(\phi) = U(\phi) + \sum_{j=B,F} \frac{\pm g_j}{64\pi^2}\left[m_j^4(\phi)\log\left(\frac{m_j^2(\phi)}{M_j^2}\right) - \frac{3}{2}m_j^4(\phi) + 2M_j^2 m_j^2(\phi)\right]\,. \tag{B.8}$$

The integrals I_B and I_F possess the high-temperature expansions

$$I_B(y) \approx \text{constant} + \frac{y^2}{24} - \frac{y^3}{12\pi} - \frac{y^4}{64\pi^2}\log\left(\frac{y^2}{c_B}\right) + \mathcal{O}(y^6, y^6\log y) \tag{B.9}$$

$$I_F(y) \approx \text{constant} + \frac{y^2}{48} + \frac{y^4}{64\pi^2}\log\left(\frac{y^2}{c_F}\right) + \mathcal{O}(y^6, y^6\log y)\,, \tag{B.10}$$

where $\log c_B = \frac{3}{2} + 2\log 4\pi - 2\gamma \approx 5.41$ and $\log c_F = \frac{3}{2} + 2\log\pi - 2\gamma \approx 2.64$. Although formally a function of y^2, notice that $I_B(y)$ is non-analytic in y^2; hence the cubic term in the expansion (B.9). This cubic term is crucial to the first-order behavior of the phase transition, and it derives directly from the zero mode in the one-loop graph. Thus infrared effects will be important to the first-order nature of the phase transition.

The fermi contribution (B.6) lacks this non-analyticity, and plays no role in the infrared behavior of the theory. Approximations valid at low temperature may also be derived [20], and the integrals themselves may be evaluated numerically; but for $y < 2$, the high-temperature expansion is valid to within 10%.

The final expression for the one-loop effective potential at high temperature reads

$$\begin{aligned} V^T_{1\,\mathrm{loop}}(\phi) &= U(\phi) \\ &\quad + \sum_B g_B \left\{ \left(\frac{M_B^2}{32\pi^2} + \frac{T^2}{24} \right) m_B^2(\phi) - \frac{T}{12\pi} m_B^3(\phi) - \frac{m_B^4(\phi)}{64\pi^2} \log\left(\frac{M_B^2}{a_B T^2} \right) \right\} \\ &\quad - \sum_F g_F \left\{ \left(\frac{M_F^2}{32\pi^2} - \frac{T^2}{48} \right) m_F^2(\phi) - \frac{m_F^4(\phi)}{64\pi^2} \log\left(\frac{M_F^2}{a_F T^2} \right) \right\} . \end{aligned} \tag{B.11}$$

Notice the cancelation of the $m_j^4 \log m_j^2$ terms. In the cases considered in this thesis, $T \sim v = \mu/\sqrt{\lambda}$ near the phase transition, and the high-temperature expansion gives a valid approximation to the effective potential (e.g. (3.19) and (3.59)).

B.2 Summation of Ring Diagrams

As we have seen in Section 3.3, an accurate computation of the effective potential demands that we sum the ring diagrams, in order to account for the leading infrared contributions to the cubic terms $\sim T m_j^3(\phi)$. Fermion ring diagrams, with Matsubara frequencies $\omega_n = (2n+1)\pi T$, need not be considered since they lack a zero mode and hence do not contribute to the cubic term.

The ring diagrams may be computed easily by means of the tadpole method. The result for a particular mode is

$$-\frac{T}{12\pi} \left\{ \left[m_j^2(\phi) + \Pi_j(0) \right]^{3/2} - m_j^3(\phi) \right\} ,$$

where $\Pi_j(0)$ is the self-energy at zero momentum. In general, the infrared self-energy may be computed at one loop to determine its leading (quadratic) temperature dependence: $\Pi_j(0) \sim \lambda T^2, g^2 T^2$. For massive gauge fields, however, only the (three-dimensionally) longitudinal component of the polarization tensor is non-zero at one loop; the transverse components vanish until two loops, where the leading temperature dependence is $\Pi_j^{kk}(0) \sim \lambda^2 T^2, g^4 T^2$. Therefore at one loop, the summation of ring diagrams yields

$$\begin{aligned} \Delta V^T_{\mathrm{ring}}(\phi) &= -\frac{T}{12\pi} \sum_{j=\mathrm{scalar}} \left\{ \left[m_j^2(\phi) + \Pi_j(0) \right]^{3/2} - m_j^3(\phi) \right\} \\ &\quad -\frac{T}{12\pi} \sum_{\substack{j=\mathrm{long.} \\ \mathrm{gauge}}} \left\{ \left[m_j^2(\phi) + \Pi_j^{00}(0) \right]^{3/2} - m_j^3(\phi) \right\} . \end{aligned} \tag{B.12}$$

$\Pi(0)$ and $\Pi^{00}(0)$ are the scalar self-energy and longitudinal component of the gauge polarization tensor at zero momentum ($\omega_n = 0$, $\vec{k} \to 0$).

Appendix C

Loop Integrals at High Temperature

This appendix computes one-loop integrals for bosons and fermions, which are used when calculating the leading temperature dependence of scalar self-energies and gauge polarization tensors. The one-loop computation involves loop integrals $\int d^4k$ which become $T\sum_n \int d^3\vec{k}$ at finite temperature, where the sum is over discrete frequencies $\omega_n = 2n\pi T$ for Bose loops and $\omega_n = (2n+1)\pi T$ for Fermi loops. These loops may be evaluated in two steps: first performing the sum by contour integration (refer to the contours C_B and C_F of Figure 2.1), and then integrating over spatial momenta.

C.1 Bose Integrals

The Bose loops involve the following sums:

$$\begin{aligned}
T\sum_{n=-\infty}^{\infty} \frac{1}{\omega_n^2 + \vec{k}^2} &= \int \frac{dk_E^0}{2\pi} \frac{1}{k_E^2} + \frac{1}{|\vec{k}|\left(\exp(\beta|\vec{k}|) - 1\right)} \\
T\sum_{n=-\infty}^{\infty} \frac{1}{\left(\omega_n^2 + \vec{k}^2\right)^2} &= \int \frac{dk_E^0}{2\pi} \frac{1}{k_E^4} + \frac{1}{2}\left[\frac{1}{|\vec{k}|^3\left(\exp(\beta|\vec{k}|) - 1\right)} + \frac{\beta\exp(\beta|\vec{k}|)}{\vec{k}^2\left(\exp(\beta|\vec{k}|) - 1\right)^2}\right] \\
T\sum_{n=-\infty}^{\infty} \frac{\omega_n^2}{\left(\omega_n^2 + \vec{k}^2\right)^2} &= \int \frac{dk_E^0}{2\pi} \frac{\left(k_E^0\right)^2}{k_E^4} + \frac{1}{2}\left[\frac{1}{\vec{k}^2\left(\exp(\beta|\vec{k}|) - 1\right)} - \frac{\beta\exp(\beta|\vec{k}|)}{\left(\exp(\beta|\vec{k}|) - 1\right)^2}\right],
\end{aligned} \tag{C.1}$$

where $\beta = T^{-1}$. The first sum is evaluated by contour integration (see Figure 2.1):

$$T\sum_n f(k^0 = i2n\pi T) = \frac{T}{2\pi i}\oint_{C_B} dk^0\, f(k^0)\,\frac{1}{2T}\coth(\frac{k^0}{2T})$$

$$= \int_{-\infty}^{\infty} \frac{dk^0}{2\pi} f(ik^0) + \frac{1}{2\pi i} \int_{-i\infty+\epsilon}^{i\infty+\epsilon} dk^0 \frac{2f(k^0)}{e^{k^0/T}-1} . \qquad \text{(C.2)}$$

The second sum is obtained by differentiation of the first sum, and the third is obtained from the first two. Integrating, we obtain the desired integrals:

$$\begin{aligned}
\int \frac{d^3\vec{k}}{(2\pi)^3} T \sum_{n=-\infty}^{\infty} \frac{1}{\omega_n^2 + \vec{k}^2} &= \int \frac{d^4k_E}{(2\pi)^4} \frac{1}{k_E^2} + \frac{T^2}{2\pi^2} \int_0^{\infty} dx \frac{x}{e^x - 1} \\
\int \frac{d^3\vec{k}}{(2\pi)^3} T \sum_{n=-\infty}^{\infty} \frac{1}{\left(\omega_n^2 + \vec{k}^2\right)^2} &= \int \frac{d^4k_E}{(2\pi)^4} \frac{1}{k_E^4} + \frac{1}{4\pi^2} \int_0^{\infty} dx \frac{1}{x(e^x - 1)} + \frac{e^x}{(e^x - 1)^2} \\
\int \frac{d^3\vec{k}}{(2\pi)^3} T \sum_{n=-\infty}^{\infty} \frac{\vec{k}^2}{\left(\omega_n^2 + \vec{k}^2\right)^2} &= \int \frac{d^4k_E}{(2\pi)^4} \frac{\vec{k}^2}{k_E^4} + \frac{T^2}{4\pi^2} \int_0^{\infty} dx \frac{x}{e^x - 1} + \frac{x^2 e^x}{(e^x - 1)^2} \\
\int \frac{d^3\vec{k}}{(2\pi)^3} T \sum_{n=-\infty}^{\infty} \frac{\omega_n^2}{\left(\omega_n^2 + \vec{k}^2\right)^2} &= \int \frac{d^4k_E}{(2\pi)^4} \frac{(k_E^0)^2}{k_E^4} + \frac{T^2}{4\pi^2} \int_0^{\infty} dx \frac{x}{e^x - 1} - \frac{x^2 e^x}{(e^x - 1)^2} .
\end{aligned} \qquad \text{(C.3)}$$

Consulting Gradshteyn and Rhyzik [59],

$$\begin{aligned}
\int_0^{\infty} dx \frac{x}{e^x - 1} &= \zeta(2) = \pi^2/6 \\
\int_0^{\infty} dx \frac{x^2 e^x}{(e^x - 1)^2} &= 2\zeta(2) = \pi^2/3 .
\end{aligned}$$

Our final results for Bose integrals are

$$\begin{aligned}
\int \frac{d^3\vec{k}}{(2\pi)^3} T \sum_{n=-\infty}^{\infty} \frac{1}{\omega_n^2 + \vec{k}^2} &= \int \frac{d^4k_E}{(2\pi)^4} \frac{1}{k_E^2} + \frac{T^2}{12} \\
\int \frac{d^3\vec{k}}{(2\pi)^3} T \sum_{n=-\infty}^{\infty} \frac{\vec{k}^2}{\left(\omega_n^2 + \vec{k}^2\right)^2} &= \int \frac{d^4k_E}{(2\pi)^4} \frac{\vec{k}^2}{k_E^4} + \frac{T^2}{8} \\
\int \frac{d^3\vec{k}}{(2\pi)^3} T \sum_{n=-\infty}^{\infty} \frac{\omega_n^2}{\left(\omega_n^2 + \vec{k}^2\right)^2} &= \int \frac{d^4k_E}{(2\pi)^4} \frac{(k_E^0)^2}{k_E^4} - \frac{T^2}{24} .
\end{aligned} \qquad \text{(C.4)}$$

C.2 Fermi Integrals

The corresponding Fermi integrals may be evaluated in a similar manner, which may be outlined as follows:

$$
\begin{aligned}
T\sum_{n=-\infty}^{\infty}\frac{1}{\omega_n^2+\vec{p}^2} &= \int\frac{dp_E^0}{2\pi}\frac{1}{p_E^2}-\frac{1}{|\vec{p}|\,(\exp(\beta|\vec{p}|)+1)} \\
T\sum_{n=-\infty}^{\infty}\frac{1}{(\omega_n^2+\vec{p}^2)^2} &= \int\frac{dp_E^0}{2\pi}\frac{1}{p_E^4}-\frac{1}{2}\left[\frac{1}{|\vec{p}|^3\,(\exp(\beta|\vec{p}|)+1)}+\frac{\beta\exp(\beta|\vec{p}|)}{\vec{p}^2\,(\exp(\beta|\vec{p}|)+1)^2}\right] \\
T\sum_{n=-\infty}^{\infty}\frac{\omega_n^2}{(\omega_n^2+\vec{p}^2)^2} &= \int\frac{dp_E^0}{2\pi}\frac{(p_E^0)^2}{p_E^4}+\frac{1}{2}\left[-\frac{1}{\vec{p}^2\,(\exp(\beta|\vec{p}|)+1)}+\frac{\beta\exp(\beta|\vec{p}|)}{(\exp(\beta|\vec{p}|)+1)^2}\right],
\end{aligned}
\tag{C.5}
$$

The contour integral (see Figure 2.1) for the first sum is

$$
\begin{aligned}
T\sum_n g(p^0=i(2n+1)\pi T) &= \frac{T}{2\pi i}\oint_{C_F}dp^0\;g(p^0)\,\frac{1}{2T}\tanh(\frac{p^0}{2T}) \\
&= \int_{-\infty}^{\infty}\frac{dp^0}{2\pi}\,g(ip^0)-\frac{1}{2\pi i}\int_{-i\infty+\epsilon}^{i\infty+\epsilon}dp^0\,\frac{2g(p^0)}{e^{p^0/T}+1}\,.
\end{aligned}
\tag{C.6}
$$

Then

$$
\begin{aligned}
\int\frac{d^3\vec{p}}{(2\pi)^3}T\sum_{n=-\infty}^{\infty}\frac{1}{\omega_n^2+\vec{p}^2} &= \int\frac{d^4p_E}{(2\pi)^4}\frac{1}{p_E^2}-\frac{T^2}{2\pi^2}\int_0^{\infty}dx\,\frac{x}{e^x+1} \\
\int\frac{d^3\vec{p}}{(2\pi)^3}T\sum_{n=-\infty}^{\infty}\frac{1}{(\omega_n^2+\vec{p}^2)^2} &= \int\frac{d^4p_E}{(2\pi)^4}\frac{1}{p_E^4}-\frac{1}{4\pi^2}\int_0^{\infty}dx\,\frac{1}{x(e^x+1)}+\frac{e^x}{(e^x+1)^2} \\
\int\frac{d^3\vec{p}}{(2\pi)^3}T\sum_{n=-\infty}^{\infty}\frac{\vec{p}^2}{(\omega_n^2+\vec{p}^2)^2} &= \int\frac{d^4p_E}{(2\pi)^4}\frac{\vec{p}^2}{p_E^4}-\frac{T^2}{4\pi^2}\int_0^{\infty}dx\,\frac{x}{e^x+1}+\frac{x^2e^x}{(e^x+1)^2} \\
\int\frac{d^3\vec{p}}{(2\pi)^3}T\sum_{n=-\infty}^{\infty}\frac{\omega_n^2}{(\omega_n^2+\vec{p}^2)^2} &= \int\frac{d^4p_E}{(2\pi)^4}\frac{(p_E^0)^2}{p_E^4}-\frac{T^2}{4\pi^2}\int_0^{\infty}dx\,\frac{x}{e^x+1}-\frac{x^2e^x}{(e^x+1)^2}\,.
\end{aligned}
\tag{C.7}
$$

From Gradshteyn and Ryzhik [59],

$$
\begin{aligned}
\int_0^{\infty}dx\,\frac{x}{e^x+1} &= \zeta(2)/2=\pi^2/12 \\
\int_0^{\infty}dx\,\frac{x^2e^x}{(e^x+1)^2} &= \zeta(2)=\pi^2/6\,.
\end{aligned}
$$

Hence, for Fermi loops,

$$\begin{aligned}
\int \frac{d^3\vec{p}}{(2\pi)^3} T \sum_{n=-\infty}^{\infty} \frac{1}{\omega_n^2 + \vec{p}^2} &= \int \frac{d^4p_E}{(2\pi)^4} \frac{1}{p_E^2} - \frac{T^2}{24} \\
\int \frac{d^3\vec{p}}{(2\pi)^3} T \sum_{n=-\infty}^{\infty} \frac{\vec{p}^2}{(\omega_n^2 + \vec{p}^2)^2} &= \int \frac{d^4p_E}{(2\pi)^4} \frac{\vec{p}^2}{p_E^4} - \frac{T^2}{16} \\
\int \frac{d^3\vec{p}}{(2\pi)^3} T \sum_{n=-\infty}^{\infty} \frac{\omega_n^2}{(\omega_n^2 + \vec{p}^2)^2} &= \int \frac{d^4p_E}{(2\pi)^4} \frac{(p_E^0)^2}{p_E^4} + \frac{T^2}{48} \,. \qquad \text{(C.8)}
\end{aligned}$$

It should be noted that the four-dimensional Euclidean integral (the first piece), for both the Bose and Fermi cases, is a temperature-independent loop integral, and may be renormalized perturbatively in the usual zero-temperature fashion. Hence, at high temperature, its effects may be neglected relative to the quadratic temperature dependence of the second piece.

Bibliography

[1] E.L. Wright, J.C. Mather, D.J. Fixsen, et. al., Report No. NASA-GSFC 93-03.

[2] G. Steigman, *Ann. Rev. Astron. Astrophys.* **14**, 339 (1976).

[3] A.D. Sakharov, *JETP Lett.* **5**, 24 (1967).

[4] E.W. Kolb and M.S. Turner, *Ann. Rev. Nuc. Part. Sci.* **33**, 645 (1983).

[5] A.G. Cohen, D.B. Kaplan, and A.E. Nelson, *Ann. Rev. Nucl. Part. Sci.* **43** (1993).

[6] A.D. Linde, *Phys. Lett.* **70B**, 306 (1977); S. Dimopoulos and L. Susskind, *Phys. Rev.* **D18**, 4500 (1978).

[7] N.S. Manton, *Phys. Rev.* **D28**, 2019 (1983); F.R. Klinkhamer and N.S. Manton, *Phys. Rev.* **D30**, 2212 (1984).

[8] V.A. Kuzmin, V.A. Rubakov, and M.E. Shaposhnikov, *Phys. Lett.* **155B**, 36 (1985).

[9] P. Arnold and L. McLerran, *Phys. Rev.* **D36**, 581 (1987); *Phys. Rev.* **D37**, 1020 (1988); L. Carson, X. Li, L. McLerran, and R.T. Wang, *Phys. Rev.* **D42**, 2127 (1990).

[10] N. Turok and J. Zadrozny, *Phys. Rev. Lett.* **65**, 2331 (1990); *Nuc. Phys.* **B358**, 471 (1991); L. McLerran, M. Shaposhnikov, N. Turok, and M. Voloshin, *Phys. Lett.* **256B**, 451 (1991).

[11] A.G. Cohen and D.B. Kaplan, *Phys. Lett.* **B199**, 251 (1987); *Nucl. Phys.* **B308**, 913 (1988); A.G. Cohen, D.B. Kaplan, and A.E. Nelson, *Phys. Lett.* **B263**, 86 (1991); S.A. Abel, W.N. Cottingham, and I.B. Whittingham, Report No. RAL-93-002.

[12] A.G. Cohen and A.E. Nelson, *Phys. Lett.* **297B**, 111 (1992).

[13] A.E. Nelson, D.B. Kaplan, and A.G. Cohen, *Nucl. Phys.* **B373**, 453 (1992).

[14] A.G. Cohen, D.B. Kaplan, and A.E. Nelson, *Nucl. Phys.* **B349**, 727 (1991).

[15] M.E. Shaposhnikov, *Nucl. Phys.* **B299**, 797 (1988).

[16] G.R. Farrar and M.E. Shaposhnikov, Report No. CERN-TH.6732/93.

[17] D.J. Gross, R.D. Pisarski, and L.G. Yaffe, *Rev. Mod. Phys.* **53**, 43 (1981).

[18] M. Dine, R.G. Leigh, P. Huet, A. Linde, and D. Linde, *Phys. Rev.* **D46**, 550 (1992).

[19] M.E. Carrington, *Phys. Rev.* **D45**, 2933 (1992).

[20] G.W. Anderson and L.J. Hall, *Phys. Rev.* **D45**, 2685 (1992).

[21] A.I. Bochkarev, S.V. Kuzmin, and M.E. Shaposhnikov, *Phys. Lett.* **B244**, 275 (1990); *Phys. Rev.* **D43**, 369 (1991).

[22] J.I. Kapusta, *Finite-Temperature Field Theory*, Cambridge University Press (1989).

[23] L. Dolan and R. Jackiw, *Phys. Rev.* **D9**, 3320 (1974).

[24] C.W. Bernard, *Phys. Rev.* **D9**, 3312 (1974).

[25] S. Weinberg, *Phys. Rev.* **D9**, 3357 (1974).

[26] E.J. Weinberg and A. Wu, *Phys. Rev.* **D36**, 2474 (1987).

[27] S. Coleman, *Phys. Rev.* **D15**, 2929 (1977).

[28] A. Linde, *Nucl. Phys.* **B216**, 421 (1983).

[29] D.E. Brahm and S.D.H. Hsu, Report No. HUTP-91-A063.

[30] D.A. Kirzhnits and A.D. Linde, *Ann. Phys.* **101**, 195 (1976); A.D. Linde, *Rep. Prog. Phys.* **42**, 25 (1979).

[31] P. Fendley, *Phys. Lett.* **B196**, 175 (1987).

[32] E. Braaten and R.D. Pisarski, *Nucl. Phys.* **B337**, 569 (1990).

[33] R.G. Leigh, in *Baryon Number Violation at the Electroweak Scale*, eds. L.M Krauss and S-J. Rey, World Scientific (1992).

[34] S. Adler, *Phys. Rev.* **177**, 2426 (1969); J.S. Bell and R. Jackiw, *Nuovo Cimento* **51**, 47 (1969); W. Bardeen, *Phys. Rev.* **184**, 1841 (1969).

[35] G. 't Hooft, *Phys. Rev. Lett.* **37**, 8 (1976).

[36] A.A. Belavin, A.M. Polyakov, A.S. Schwartz, and Yu.S. Tyupkin, *Phys. Lett.* **B59**, 85 (1975).

[37] B. Kastening, R.D. Peccei, and X. Zhang, *Phys. Lett.* **B266**, 413 (1991).

[38] M. Dine, O. Lechtenfeld, B. Sakita, W. Fischler, and J. Polchinski, *Nucl. Phys.* **B342**, 381 (1990).

[39] J. Ambjorn, T. Askaard, H. Porter, and M.E. Shaposhnikov, *Nucl. Phys.* **B353**, 346 (1991); J. Ambjorn and K. Farakos, *Phys. Lett.* **294B**, 248 (1992).

[40] For recent reviews, see M.E. Shaposhnikov, Report No. CERN-TH.6497/92; A.G. Cohen, D.B. Kaplan, and A.E. Nelson, Report No. BUHEP-93-4.

[41] J.I. Kapusta, *Finite Temperature Field Theory*, Cambridge University Press (1989); A.D. Linde, *Particle Physics and Inflationary Cosmology*, Harwood (1990).

[42] For recent reviews, see L. Rolandi, Report No. CERN-PPE-92-175; P. Langacker, Report No. UPR-0512-T.

[43] M. Sher, *Phys. Rep.* **179**, 273 (1989).

[44] K.E.C. Benson, *Phys. Rev.* **D48**, 2456 (1993).

[45] J.F. Gunion, H.E. Haber, G.L. Kane, and S. Dawson, *The Higgs Hunters Guide*, Addison Wesley (1989).

[46] N. Turok and J. Zadrozny, *Nuc. Phys.* **B369**, 729 (1992).

[47] M.E. Shaposhnikov, *JETP Lett.* **44**, 465 (1986).

[48] M. Fukugita and T. Yanagida, *Phys. Lett.* **B174**, 45 (1986).

[49] J.A. Harvey and M.S. Turner, *Phys. Rev.* **D42**, 3344 (1990).

[50] V.A. Kuzmin, V.A. Rubakov, and M.E. Shaposhnikov, *Phys. Lett.* **B191**, 171 (1987).

[51] H. Dreiner and G.G. Ross, Report No. OUTP-92-08P.

[52] G.G. Ross, *Grand Unified Theories*, Benjamin/Cummings (1984).

[53] B.A. Campbell, S. Davidson, J. Ellis, and K.A. Olive, *Phys. Lett.* **B297**, 118 (1992).

[54] H.A. Weldon, *Phys. Rev.* **D26**, 1394 (1982); *Phys. Rev.* **D26**, 2789 (1982). See also V.V. Lebedev and A.V. Smilga, *Ann. Phys.* **202**, 229 (1990).

[55] E.W. Kolb and M.S. Turner, *The Early Universe*, Addison-Wesley (1990).

[56] M. Alford and J. March-Russell, Report No. LBL-34573; N. Tetradis and C. Wetterich, Report No. DESY 92-093.

[57] S. Weinberg, *Gravitation and Cosmology*, Wiley (1972).

[58] S. Coleman and E. Weinberg, *Phys. Rev.* **D7**, 1888 (1973).

[59] I.S. Gradshteyn and I.M. Rhyzik, *Table of Integrals, Series, and Products*, Academic Press (1980).